Cardiac Structural and Functional Consequences of the Desmin p.R406W Mutation

Michelle Geryk

COLLEGE DOCTORAL PAYS DE LA LOIRE ED BIOLOGIE SANTE

Nantes Université

THESE DE DOCTORAT

NANTES UNIVERSITE

ECOLE DOCTORALE N° 605
Biologie-Santé
Spécialité : Physiologie, Physiopathologie, Biologie Systémique Médicale

Par

Michelle GERYK

Cardiac Structural and Functional Consequences of the Desmin p.R406W Mutation

Thèse présentée et soutenue à Nantes, le 10 avril 2024

Unité de recherche : L'institut du Thorax (INSERM UMR 1087 / CNRS UMR 6291)

Rapporteurs avant soutenance :

Hendrik MILTING	Professor, Heart and Diabetes Center NRW, Erich & Hanna Klessmann-Institute, Bad Oeynhausen, Germany
Albano MELI	Chargé de recherche, INSERM, PhyMedExp, Montpellier

Composition du Jury :

Présidente :	Isabelle BARO	Directrice de recherche, INSERM, L'institut du Thorax, Nantes
Examinatrices :	Kirstine CALLØ	Associate professor, Dept. of Veterinary and Animal Sciences, Faculty of Health and Medical Sciences, University of Copenhagen
	Ana-Maria GOMEZ	Directrice de recherche, INSERM, Laboratoire de Signalisation et Physiopathologies Cardiovasculaire, Université Paris-Saclay
Dir. de thèse :	Flavien CHARPENTIER	Directeur de recherche, INSERM, L'institut du Thorax, Nantes

To my L

Acknowledgements

I would like to start off by thanking Dr. Hendrik Milting and Dr. Albano Meli for accepting to take part in my jury. Thank you for taking the time to read and evaluate my manuscript and for your feedback.

Thank you, Dr. Ana-Maria Gomez, for being part of my jury, and also for being on my thesis committee throughout the past three years. I am grateful for your insight and guidance during my research journey.

I am very grateful to Dr. Kirstine Callø for teaching me how to patch and being my first ever supervisor. Thank you for introducing me to the world of electrophysiology and different animal hearts (especially the elephant). Your continuous support throughout my research career has led to me to this day. Thank you for your expert advice during my thesis committee meetings and for accepting the role as an examiner for my defense.

A big thank you to Dr. Isabelle Baro for not only being a member of my jury, but for your support, advice, and great guidance throughout my time in the lab. You have taught me everything I know about the dynamic clamp and have always helped me with my never-ending set-up problems but also answered all my questions. Thank you for taking the time to talk about patch, my results, and everything in between. I am very grateful to have had you as one of my mentors.

I would particularly like to thank the person who answered my email asking for a PhD and entrusting me with this project; my supervisor Dr. Flavien Charpentier. Thank you for your constant support with all my project ideas and making all of them happen. I appreciate that you always took the time to discuss my results and the project, for teaching me and providing me with excellent advice and insight to push me to think more critically (and be more patient). I have especially enjoyed our scientific discussions but also our conversations during very long and frustrating EHT patch days. Thank you for believing in me and motivating me to continue my scientific career.

I would also like to thank Jerome Montnach for taking the time to try optical mapping experiments and being patient and willing to test out all my ideas. Thank you for also writing (and constantly modifying) the R scripts that made AP analysis that much easier. To Gildas, thank you for always fixing my patch set-up and discussing electrophysiology. Your expertise has taught me a lot!

Thank you to the members of Team 1, especially Julien, Pierre, Estelle and Jean-Jacques, for sharing your knowledge and expertise with me and guiding me through the WGS process.Thank you to my collaborators Francois Guillonneau for taking on the task of performing proteomic studies on my EHTs; Rodolphe Perrot for TEM imaging of my EHTs; and to the GenoA and BiRD platform for performing the 3’RNA sequencing experiments.

Thank you to all the secretaries for your help throughout the years and helping me navigate the very complex French system.

Thank you, Diane, for teaching me about iPS, the rules in the lab and including me in the not-so-healthy Wednesday lunch group and introducing me to goûter time. Your support and our

conversations made it easier for me to integrate into the lab and not be so lonely during Covid restrictions.

I would also like to thank the iPS team, for taking care of my endless plates of cells and EHTs over the weekend so I can go visit my family. To Virginie V., Marine, and Amandine for our lovely conversations during long culture days and to Virginie F. for helping me with my CRISPR. To Lise, thank you for always being available to help me (especially the very dreaded cell line paper), for taking the time to listen to me complain about my cells (among other things), for our including me in the Wednesday outings, and for making coffee in my office (excellent excuse for a nice little break for me). And to Auroooooreee for answering my LONG list of daily questions and sharing your lab expertise with me. You have always helped me with my lab problems and have guided me through many of my experiments (and RNA extractions).

To all of Team 2, thank you for putting up with my English presentations and for helping me integrate into the team! Thank you, Nathalie, for our iPS discussions, to Agnes T. for taking care of my mice and showing me different techniques, to Anne for performing immuno experiments.

Thank you to the Tuesday evening Koh-lanta group, for inviting me come along to watch the show! I have very fond memories of the snacks, the stories, but mostly of all your pets! These evenings were always a very nice break from the lab and a nice introduction to apero. Thank you all for integrating me into your group and always making me feel at home and welcome.

To my lemon sister, Salam, thank you for your kindness and patience in the lab. You always took the time to listen to me and guided me throughout my writing process. I loved getting to know you in the iPS room during our long, evening culture days. You too have taught me to be more patient and to be confident in my work.

To my office neighbor, CJ the DJ, thank you for putting up with me all these years, for teaching me how to do Western blots, for making coffee in the morning, for listening to me (especially my complaining), and for helping me with French administration ;)

To my besties for life, Bastienko, Manonka and Robinek, honestly, thank you for putting up with me and letting me be part of the bestie group! You made life here a lot more fun with our outings (RIP random uber drivers' car), our dinner parties, our fat Wednesdays, our coffee breaks and our trips (TORONTO 2024!!). I really enjoyed my time in Nantes mainly because of you :D Robinek, aka Robbie Bobbie, thank you for all your expert CRISPR advice, for your humour, for sharing you Nante enthusiasm, for your excellent rap playlists and for being supportive. Bastien, thank you for coming back to analyze my results. The heat-maps are great.

To my favourite colleague, Manon, thank you for helping with all my # phone calls, for your excellent humour that always ended in you crying, for our little tea time sessions, for taking care of my car, for inviting me to your wedding, and for your overall everyday support in the lab but also outside. You really are the best colleague ever!

Kidding Bastien! Thank you for watering my plants, for all your very bad jokes and puns, for taking the time to explain your analysis (as painful as it was), for picking me up from the airport, and for "teaching" me how to make EHTs. Thank you for being patient with me these last few months and motivating me (more like stressing me out) to finish. Thank you for sharing your passion for Nantes and Bretagne and for trying to teach me about French culture.

My dear Dr. Lubka, we were having coffee together when I got the email about this job and you have supported me every step of the way. Thank you for putting-up with all my crazy ideas from the very beginning (Marche days), making time for coffee every time I visit, and I can't wait to finally be neighbours! To Dr. Kubo, Marketka and Roman, thank you for taking me in and for our lovely dinners and chats.

Mare, my twin, thank you for believing in me from the very beginning.

To my dear Claudia, thank you for standing by me all these years and cheering me on from afar. I appreciate all the love and support. I think all our late night Parklawn "study" sessions prepared me for the past three years. Thank you for always checking on me and for the coffee machine of course!

Thank you to my first lab partner, Leo Mogus, for your constant support and for believing in me. Thank you for being so sophisticated and for your humour (and the laugh that comes with it, of course). Thank you for always checking up on me and being there for me even from far away. I hope I can finally visit you! To my study buddy, Marissa, thank you for your kindness and support over the years.

Mr. & Mrs. G, thank you for always taking care of me when I came to visit, for all the gluten-free snacks, and for fixing my little car! Katka and Libor, thank you for your kindness and for the coffee supply ;)

Thank you, Niki and Luki, for your support from across the pond and gifts in the mail and to Misko (my favourite brother) for your letters. Thank you to teta Helena and ujo Roman for your love and support and for always making sure I'm ok :)

A big thank you goes to Kubik and Zuzka for always having my back during all my moves, for always picking me up from the airport and taking me in (thanks for the sofa bed ;)), for always making me a cup of coffee...or three, for our FT chats and our travels together. Your kindness and support have made all of this easier. To Theo and Ellie, thank you for your cuteness and sassiness that always helped lightened my mood.

Thank you to the greatest Moooooooom and daaaaaad. I could not have done any of this without your love and support. No amount of words can express how grateful I am to you for everything you have done, and continue to do for me; you really are the world's greatest parents <3. Thank you for giving me my love for travel and adventure and for the courage and support to go out on my own. I am very greatful you put me into extended French in grade 5 (who would've thought ;)) and for teaching us so many languages growing up. Thank you for our weekly calls that helped me get through all of this.

To my dearest husband L,
For the first time, I think I am at a loss for words. Nothing I write will ever be enough to express my eternal gratitude. Thank you for being by my side throughout this journey, for all your sacrifices that made all of this possible, for the hours and hours we spent on the phone every day and for believing in me. Thank you for the love and respect you showed me and for being there through the good and the bad <3. I promise I'm coming home now.

Love always,
M

Table of Contents

List of Abbreviations

3

3'SRP – 3'Sequencing RNA Profiling

A

ACM – arrhythmogenic cardiomyopathy

AP – action potential

APD – action potential duration

ARVD/C – arrhythmogenic right ventricular dysplasia/cardiomyopathy

ATAC-Seq – assay for transposase accessible chromatin with sequencing

AV node – atrioventricular node

B

BrS – Brugada Syndrome

C

CHO – Chinese hamster ovary cells

CM - cardiomyocyte

CRISPR/Cas9 – cluster regularly interspaced palindromic repeats (coupled to nuclease 9)

Cx40 – connexin 40

Cx43 – connexin 43

Cx45 – connexin 45

D

DCM – dilated cardiomyopathy

DES – human desmin gene

Des – mouse desmin gene

dV/dt_{max} – maximum rate of change

E

ECG – electrocardiogram

ECM – extracellular matrix

ECMO – extracorporeal membrane oxygenation

EHT – engineered heart tissue

G

GFAP – glial fibrillary acidic protein

gRNA – guide RNA

H

HCM – hypertrophic cardiomyopathy

HEK – human embryonic kidney cells

hiPSC – human induced pluripotent stem cells

hiPSC-CM – human induced pluripotent stem cell derived cardiomyocyte

I

ICD – implantable cardiac defibrillator

IC-R406 – isogenic control CRISPR/Cas9 generated hiPSC line

ID – intercalated disc

IF – intermediate filament

IM-R406W – isogenic mutant CRISPR/Cas9 generated hiPSC line

L

LBB – left bundle branch

LBBB – left bundle branch block

LINC complex – linker of the nucleoskeleton and cytoskeleton

LV – left ventricle

LVNC – left ventricular non-compaction

M

MDP – maximum diastolic potential

N

$Na_V1.5$ – voltage gated sodium channel

NCX – Na^+/Ca^{2+} exchanger

NF – neurofilament

P

PBMC – peripheral blood mononuclear cells

PCA – principal component analysis

PCL – pacing cycle length

PTM – post-translational modification

PT-R406W – patient hiPSC line

R

RBB – right bundle branch

RBBB- right bundle branch block

RCM – restrictive cardiomyopathy

RMP – resting membrane potential

RyR – ryanodine receptor

S

SA node – sinoatrial node

SCD – sudden cardiac death

SERCA pump – SR Ca-ATPase pump

SR – sarcoplasmic reticulum

STDS – ST-segment depression syndrome

T

TEM – transmission electron microscopy

U

ULF – unit length filament

W

WGS – whole genome sequencing

List of Figures

List of Tables

Preface

The research work was performed at *l'institut du thorax*, Nantes, France, in the "Ion Channels and Cardiopathies" team, led by Flavien Charpentier and Michel De Waard. This project is centered around a patient case of desminopathy with a severe cardiac phenotype, that started long before I joined the lab. Desmin mutations can lead to skeletal and/or cardiac disease, and we chose to focus on the cardiac effects caused by the desmin p.R406W mutation. The idea behind this work was to use the patient's hiPSCs to study the cardiac phenotype. We focused on deciphering any consequences the desmin p.R406W mutation may have on the action potential of cardiomyocytes. We employed electrophysiological approaches to study the mutation in a 2D and 3D model. Furthermore, using proteomic and transcriptomic techniques allowed us to identify several downstream ramifications of the mutation in a 3D model.

Chapter I
Introduction

When deciphering the role of an organ in the body, we must consider its structure; the anatomy of the organ as a whole, but also the individual components and layers that compose it. By investigating an organ's composition, shape, and form, it can give us insight into its function; or its physiology. The idea of structure-function relationships has been an important focus in research that undertakes the role of trying to understand the human body and its contributing parts. Oftentimes, we can see the function, for example, the beating of the heart, and by understanding the role of a single contracting cardiomyocyte, can we then begin to understand how the individual cells contribute to the functionality of the heart. The structure of the human body is organized hierarchically. When considering the body as a whole, we can recognize that it is made up of many different systems such as the digestive and circulatory systems, for example. These are in turn composed of specialized organs and layers of tissue. Going further down the chain, we know that cells make up organs, but the cells themselves are a composition of organelles. Finally, one such organelle, the nucleus, holds the DNA that in turn, gives rise to components that make up the systems and ultimately results in the formation of the human body (Alcocer-Cuarón et al., 2014) creating an integrated chain (Figure 1). Understanding the fundamental building blocks of a structure can elucidate its function.

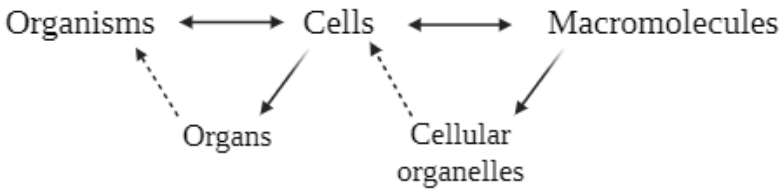

Figure 1. A representative scheme of the hierarchy that exists within multicellular organisms.
Double-ended arrows depict the continuity of organization; from the basic structural units that give rise to a complex organism. Solid arrows represent increased complexity as well as differentiation whereas dotted arrows show interactions that result in a structural unit with increased intricacy (adapted and modified from (Alcocer-Cuarón et al., 2014)).

When inspecting the heart, we can likewise categorize it in a hierarchical manner (Figure 2). We recognize that DNA gives rise to the intracellular components of the cardiomyocyte, such as different proteins, that allow for an abundance of functions. Cells have the ability to attach to neighboring cells, thanks to several protein interactions, and can therefore communicate with one another. Ultimately, these cell-cell interactions build a structurally and functionally intact heart. Cardiomyocytes have been at the heart of research for centuries. It became evident very early on that there is a very intricate structure and function relationship

between the different components of the heart which are still being studied to the present day. Over the years, as our knowledge of genetics developed and became of high interest and importance, a new objective to decipher genotype-phenotype relationships emerged. Many diseases have been attributed to genetic causes, yet the genotype-phenotype relationship is not always evident.

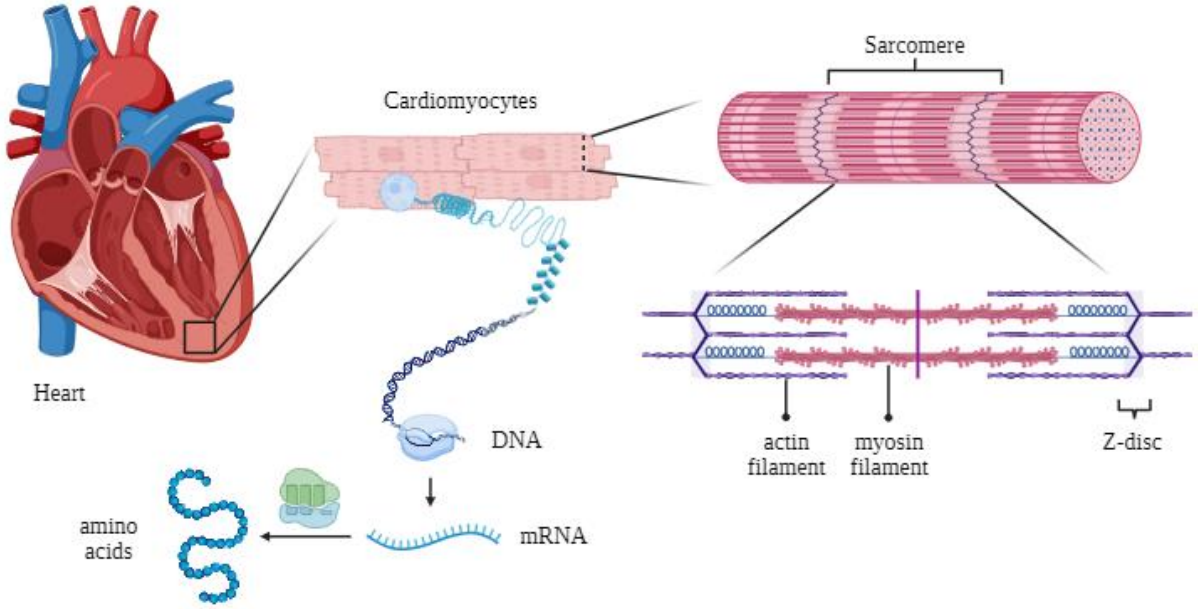

Figure 2. Hierarchical organization of the heart.
The heart is composed of multiple cell types, including cardiomyocytes that contract. Every cardiomyocyte contains myofibrils that are formed from sarcomere repeats. The sarcomere's relaxation and contraction is due to its structural composition of thin actin filaments that attach to the Z-discs and crosslink with thick myosin filaments. During development, all structures arise from DNA that is transcribed into mRNA and translated into amino acids that undergo structural modifications and folding. Complex interactions of many proteins ultimately give rise to the heart and its structural components (images created using BioRender.com and adapted from (Ahmed et al., 2022)).

Structure and function as well as genotype and phenotype relationships are the central themes of this thesis. The introduction will give insight into how the heart beats under normal, physiological conditions. Next, the inter- and intracellular connections that allow for this function will be explored. Furthermore, a point mutation in a gene that leads to cardiac disease will be examined through different experimental methods. This will allow us to get a deeper understanding of the structure and function relationships of the heart and their importance in health and disease.

1.1 Cardiac Physiology

Herophilus established that the heart is composed of four chambers and it was postulated by Erasistratus of Chios that this organ functions like a pump, while Claudius Galen described the shape of the heart and the positioning of vessels (Roberts et al., 2019). Cardiomyocytes must contract in an organized fashion to make sure enough blood is pumped throughout the body to all the organs and tissues. The first step is to ensure that a proper heart is formed during development so that it can perform this difficult task. Damage that occurs during the stages of development or later in life can have detrimental effects on a person's life and result in disease or even death (Table 1).

Table 1. **List of cardiomyopathies and their respective descriptions.**

Cardiomyopathy	Description
Dilated Cardiomyopathy (DCM)	Dilatation of the left and/or right ventricle and systolic dysfunction while maintaining normal wall thickness. It is one of the leading causes of heart failure (Burkett & Hershberger, 2005; Dellefave & McNally, 2010; Eldemire et al., 2023; Maron et al., 2006). There are three categories of DCM: nonsyndromic, syndromic, and acquired (Hershberger & Jordan, 2022). Hereditary DCM is largely due to mutations in cytoskeletal proteins (Perriard et al., 2003).
Hypertrophic Cardiomyopathy (HCM)	Hypertrophy of ventricular walls, thus increasing the risk of heart failure, atrial fibrillation, and myocardial ischemia. HCM is the most common cause of sudden cardiac death (SCD) in young patients (Liew et al., 2017; Maron et al., 2006). Mutations in sarcomeric genes are responsible for the majority of genetic HCM cases (Y. Wang et al., 2023).
Restrictive Cardiomyopathy (RCM)	Myocardial stiffness results in impaired muscle relaxation leading to diastolic dysfunction and restricted filling of ventricles (Y. Wang et al., 2023). Diastolic dysfunction can lead to left atrial or biatrial enlargement and in certain cases, ventricle chamber size may be altered (Chintanaphol et al., 2022; P. Elliott et al., 2008).
Left Ventricular Non-Compaction (LVNC)	Deep intertrabecular recesses mostly in the apical part of the left ventricle with a thin layer of compacted myocardium (Femia et al., 2020; Maron et al., 2006). The congenital phenotype is likely due to compaction problems that occur during heart development (Mirza et al., 2022).
Arrhythmogenic Cardiomyopathy (ACM)	Progressive replacement of the myocardium with fibrofatty tissue from the epi- to endocardium leads to ventricular systolic dysfunction and thinning of walls with SCD being one of the first symptoms (Corrado et al., 2017). This genetic disorder can affect the left or right ventricle and increases risk of ventricular arrhythmias (Mestroni & Sbaizero, 2018). Majority of ACM causing mutations are found in desmosomal proteins (Mestroni & Sbaizero, 2018).

1.1.1 Development of the Heart

The developing embryo grows rapidly and the need for sufficient nutrient delivery throughout the organism, as well as waste removal, increases the demand for the circulatory system. The first organ that develops within an embryo is the heart (Woodcock & Matkovich, 2005). The cardiomyocytes derived from the mesoderm form into a heart tube that undergoes rightward looping and elongation giving rise to the initial structure. Further morphogenesis leads to the formation of the chambers and valves that separate the systemic and pulmonary circulation (Figure 3) (Miquerol & Kelly, 2013; Woodcock & Matkovich, 2005). During morphogenesis, cells organize into the different compartments of the heart and interconnect among themselves. The next step of cardiac development requires changes on both the cellular and tissue level that will create an organ capable of performing the demanding function (Guo & Pu, 2020).

Throughout the stages of development, cardiomyocytes mature in terms of their structure, electrophysiological properties, and metabolism to meet the needs of the developing embryo and eventually life after birth (Guo & Pu, 2020). Early signs of the sinoatrial (SA) node appear when the heart is still in tubular form (Figure 3). The SA node initiates spontaneous beating thanks to its pacemaker activity (Miquerol & Kelly, 2013). Cells are capable of differentiation from precursors, but also new cardiomyocytes can arise from the division of existing ones (Foglia & Poss, 2016). The structural changes that occur throughout these stages prepare the heart for its lifelong function.

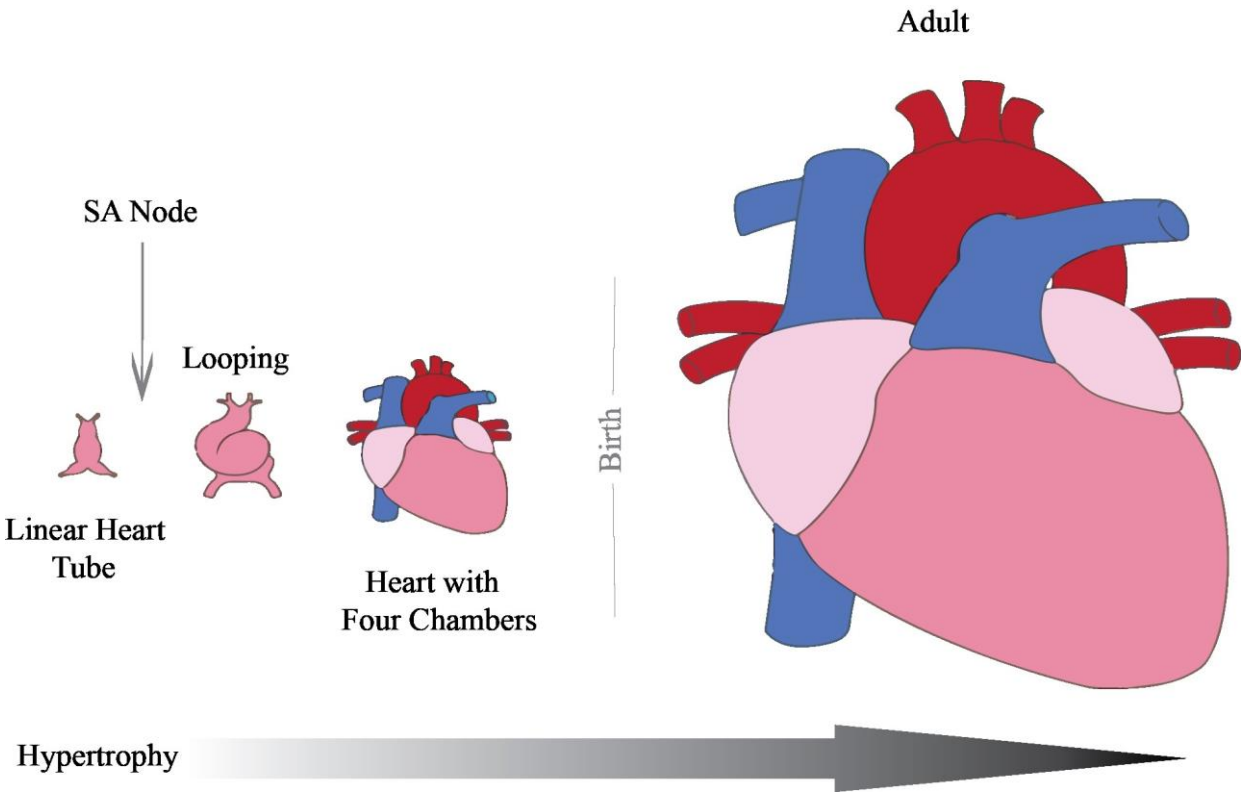

Figure 3. Schematic representation of the developing heart.
The initial cardiac crescent continues to proliferate and differentiate and subsequently transforms into a linear heart tube (left) that loops to the right and increases in length. The tubular heart shows signs of pacemaker activity and during heart tube elongation, the posterior left part forms the sinoatrial (SA) node. After birth, cardiac cells increase in size; hypertrophy, without significant cellular proliferation, giving rise to the adult-sized heart (right) ((Miquerol & Kelly, 2013; van Eif et al., 2018; Woodcock & Matkovich, 2005), figure modified from (Guo & Pu, 2020)).

The ongoing cardiac formation and maturation changes during gestation eventually result in near-mature cardiomyocytes that contract in a synchronized manner. During ongoing maturation, myofibril expansion occurs longitudinally rather than laterally, and Z-disc alignment allows for proper organization that leads to an increased force of contraction (Bishop et al., 2022). There is less automaticity in mature cardiomyocytes and the resting membrane potential (RMP) becomes more negative. The number of mitochondria increases to keep up with the energy demands of the evolving heart and cristae become more apparent (Guo & Pu, 2020). After birth, cardiomyocytes increase in size (hypertrophy; Figure 3) rather than in number (Woodcock & Matkovich, 2005). Therefore, the renewal of cardiac cells is almost none (Foglia & Poss, 2016) highlighting why proper formation during development is important to avoid congenital heart defects.

1.2 The Contracting Heart

The synchronized cardiac contraction and relaxation is an interplay between electrical signals and the mechanical function of cardiomyocytes. The spontaneous firing of pacemaker cells in the SA node, located at the junction between the right atrium and the superior vena cava, starts the chain of electrical events that pass through both atria and into the atrioventricular (AV) node (Figure 4) (Nerbonne & Kass, 2005; D. S. Park & Fishman, 2017; Pérez-Pomares et al., 2018). Here, both left and right atria contract (D. S. Park & Fishman, 2017). Slowing of the signal at the AV node, before propagating onwards, allows for proper atrial contraction and proper filling of the ventricles (D. S. Park & Fishman, 2017; Pérez-Pomares et al., 2018). From there, the bundle of His starts off the ventricular conduction system that rapidly propagates the electrical signal through the right bundle branch (RBB) and two left bundle branches (LBB) and into the distal network of Purkinje fibers (Figure 4) (D. S. Park & Fishman, 2017; Pérez-Pomares et al., 2018). The electrical signal is dispersed throughout the entirety of the ventricles allowing for contraction from the apex to the base of the heart but also relaxation of the atria at this time (Pérez-Pomares et al., 2018). The synchronized movement of the heart, coupled with the electrical activity, occurs about 100, 000 times per day in a healthy human (Schmitt et al., 2014).

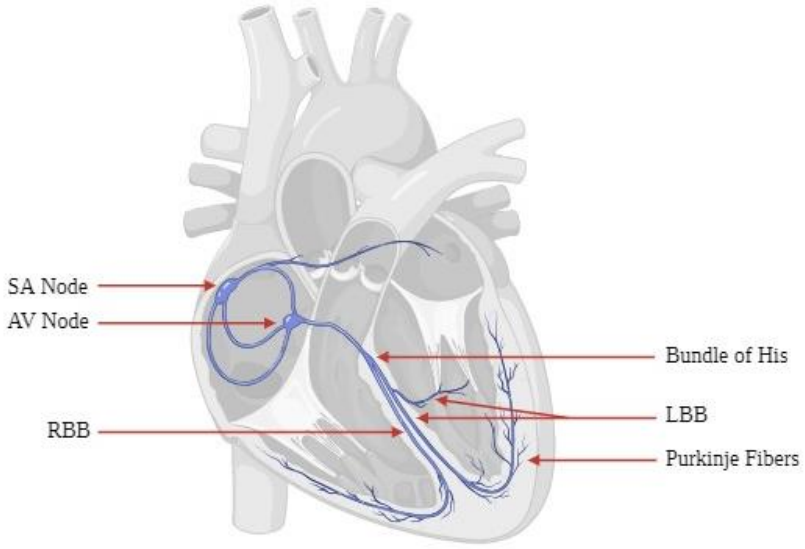

Figure 4. The cardiac conduction system.
The spontaneous pacemaker activity of the sinoatrial (SA) node propagates the signal into the atrioventricular (AV) node. Next, the bundle of His propagates the electrical signal into the right bundle branch (RBB) and the two left bundle branches (LBB) that extend into Purkinje fibers (images created using BioRender.com and adapted from (Ashley & Niebauer, 2004)).

The cardiac muscle is not solely composed of cardiomyocytes. The heterogeneity of the muscle adds to its health, but also disease. A recent study used a transcriptomic approach to demonstrate that only about 35.9% of the cells in the adult human heart are cardiomyocytes (Tucker et al., 2020) but their volume contribution is between 65% to 80% (Hall et al., 2021). The combination of fibroblasts, endothelial cells, macrophages, adipocytes, neurons, and other cell types all contribute to the organ's composition and functionality (Litviňuková et al., 2020). In healthy adult human tissue, about 32.4% of cells are fibroblasts (Tucker et al., 2020) but the number can change over time as a person ages or due to disease and injury, such as myocardial infarction (Hall et al., 2021). Fibroblasts have been shown to play a role as a structural support system of the heart where they are responsible for establishing the extracellular matrix (ECM) allowing for cardiomyocytes to organize properly (Nicin et al., 2022). Fibroblasts contribute to heart remodeling in disease by triggering the production of the ECM after injury but also their decreased capacity to regenerate over time and increased fibrosis during aging impede proper heart function (Gomes et al., 2021). Increased fibrosis throughout disease progression can result in cardiac stiffening and in turn lead to decreased cardiac function (Frangogiannis, 2021).

The electrical signals passing through the heart are reflected on an electrocardiogram (ECG), which records the heart's activity from electrodes placed on a person's chest (Figure 5A) (Kennedy et al., 2016). The ECG trace starts at the isoelectric line and reaches the first deflection called the P wave, which depicts atrial depolarization. Next, the QRS complex outlines the ventricular muscle cell depolarization and ends in a final deflection termed the T wave, which corresponds to ventricular repolarization (Figure 5B). The ST segment represents a time when ventricular cardiomyocytes are equally polarized and reach the plateau of the action potential (AP) (Ashley & Niebauer, 2004; Klabunde, 2017). At the end of the T wave, the trace returns to the isoelectric line before commencing the cycle again (Figure 5) (Becker, 2006). It is important to note that there are some observable sex-related differences on the ECG, such as longer QT intervals in females than in males. These sex-related differences are also age-dependent since a majority of the distinctions begin at puberty but diminish around the seventh decade of life (Prajapati et al., 2022). Defects during the development of the conduction system are an underlying cause of cardiomyopathies and arrhythmias (Miquerol & Kelly, 2013).

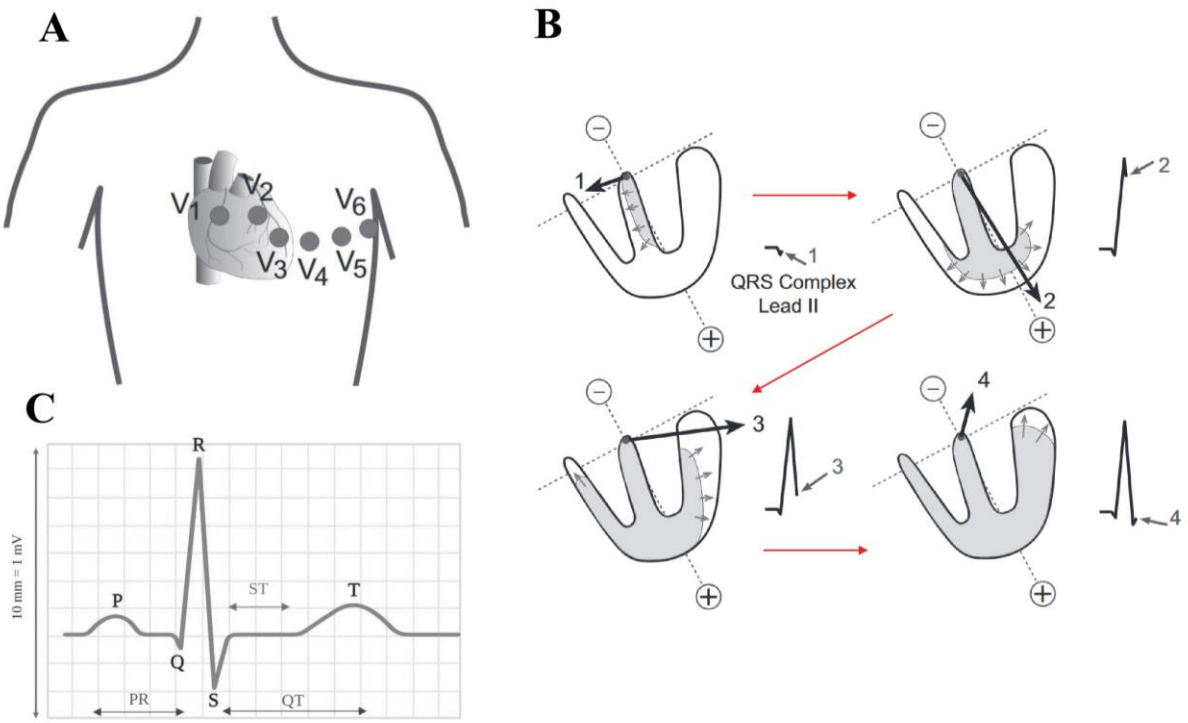

Figure 5. Representative illustration of an electrocardiogram.
Six chest leads are placed on the surface of the body (A) where they record waves based on the electrical activity of the heart (B) and result in waves, segments, and intervals (C) (figure modified from (Klabunde, 2017)).

The observable patterns on the ECG are based on the heart as a whole. To appreciate the functioning heart, it is important to recognize the structure and function of individual cardiomyocytes during cardiac contraction.

1.3 Action Potentials and Signal Propagation

Electrical excitation of individual cardiomyocytes leads to their contraction and results in the contraction of the heart at a rate of about 60 beats/minute (Schmitt et al., 2014). This process is called excitation-contraction coupling (Bers, 2002). Cardiac excitation is governed by APs generated by individual cells and diffusion of the signal from one cell to the next via gap junctions (Kléber & Rudy, 2004). The AP is separated into five distinct phases that is a result of dynamic changes in sodium (Na^+), calcium (Ca^{2+}), chloride (Cl^-), and potassium (K^+) ion concentrations. During this process, the cell lipid bilayer acts as the capacitator separating the ionic charges and concentration differences between the inside and outside of the cell (Kléber & Rudy, 2004). The RMP of working myocardial cells is around -90 mV (Grant, 2009), due to a strong K^+ conductance carried by the inward rectifier current, I_{K1} (Kir2.x channels).

Once there is a change of membrane potential to less negative values that reach a threshold of around -55 mV, voltage-gated sodium channels, $Na_V1.5$, are activated, open, and depolarize the cell. The rapid inward sodium current (I_{Na}) is responsible for the depolarizing phase 0 of the AP (Figures 6 & 7) (Schmitt et al., 2014). This is facilitated by the strong decrease of I_{K1} during the depolarization process. Atrial and ventricular cells can reach a maximal voltage between +20 mV and +40 mV, respectively, and a 200-400 V/s maximum rate of change (dV/dt_{max}) of membrane potential during phase 0 (J. Liu et al., 2016). The subsequent phase 1 rapid repolarization is due to $Na_V1.5$ inactivation and transient voltage-gated outward potassium current (I_{to}) activation at membrane potentials of -30 mV (Nerbonne & Kass, 2005; Schmitt et al., 2014). Depolarizing L-type calcium current ($I_{Ca,L}$, $Ca_V1.2$ channels), repolarizing Ca^{2+}-activated chloride (Cl^-) current, and the Na^+/Ca^{2+} exchanger (NCX) current also contributes to phase 1 (J. Liu et al., 2016). The NCX generates an outward repolarizing current by transporting one Ca^{2+} ion in and three Na^+ ions outside the cell, whereas the opposite happens throughout most of the cardiac cycle (J. Liu et al., 2016). In phase 2, also known as the plateau phase, a depolarizing current is generated by Ca^{2+} entry via the $I_{Ca,L}$, while the delayed potassium rectifying currents I_{Kr} ($K_V11.1$) and I_{Ks} ($K_V7.1$) have a repolarizing effect and start the shift towards the RMP (Kléber & Rudy, 2004; Nerbonne & Kass, 2005; Woodcock & Matkovich, 2005). Here, the NCX does the opposite and releases three Na^+ ions in and one Ca^{2+} ion out of the cell (J. Liu et al., 2016). Phase 3 repolarization is initiated by K^+ movement out of the cell when I_{Kr} and I_{Ks} exceed the $I_{Ca,L}$ (that inactivates) and the NCX depolarizing current (Kléber & Rudy, 2004; J. Liu et al., 2016). Eventually, the RMP is restored in phase 4 due to the I_{K1} progressively increasing towards the end of phase 3, in addition to I_{Kr} and I_{Ks}, and its continued activity during phase 4 (Figure 6 & 7) (Anumonwo & Lopatin, 2010; Grant, 2009; J. Liu et al., 2016; Schmitt et al., 2014).

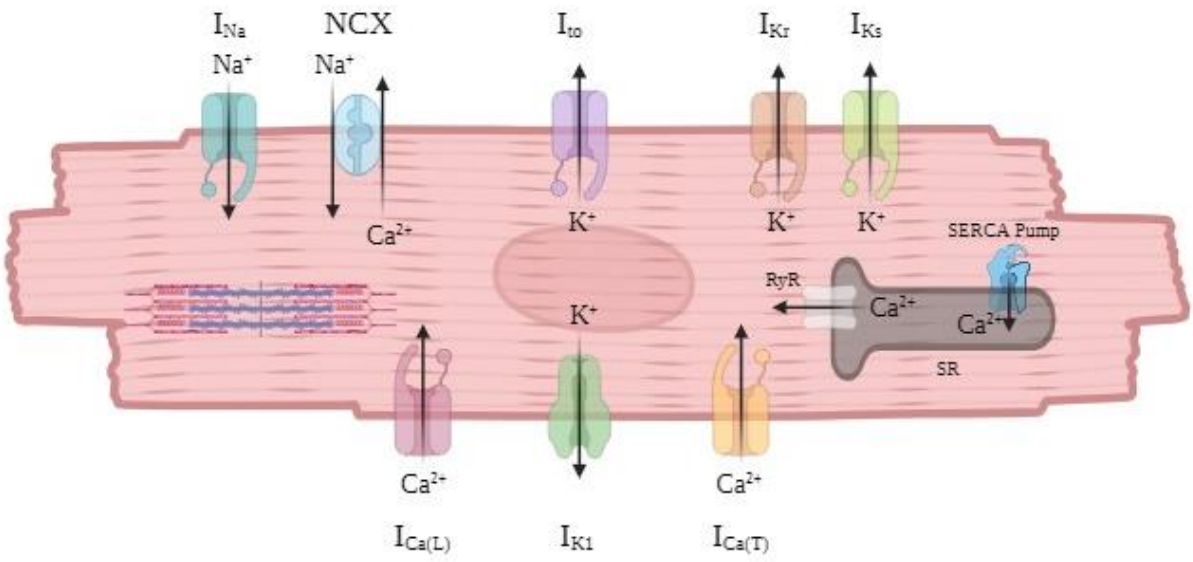

Figure 6. Diagram of the dynamic changes of ion channels in a cardiac cell.
The action potential stems from dynamic changes in Na^+, Ca^{2+}, Cl^-, and K^+ ion concentrations. These ions pass through specific ion channels during the different phases of the action potential (image created using BioRender.com and adapted from (Kléber & Rudy, 2004))

The electrochemical gradient that depolarizes and repolarizes the cells differs between cells since ion channel expression depends on cell type and thus yields different AP parameters (Figure 7) (Grant, 2009; Nerbonne & Kass, 2005). One prominent difference is the rate of depolarization (dV/dt_{max}) during phase 0 in the atria and the ventricles versus SA and AV nodes since they have a higher I_{Na} compared to the nodes that have almost no $Na_V1.5$. The phase 0 in nodal cells is due to $I_{Ca,L}$ activation. In these cells, the diastolic depolarization, which is responsible for automatic activity, is primarily governed by the pacemaker current (I_f) activated by hyperpolarization (HCN channels), the T-type Ca^{2+} current ($I_{Ca,T}$; $Ca_V3.1$), the NCX current and low voltage-activated L-type Ca^{2+} current carried by $Ca_V1.3$ channels, giving them their automaticity (Cingolani et al., 2018; Grant, 2009; Mangoni & Nargeot, 2008; Nerbonne & Kass, 2005; D. S. Park & Fishman, 2017). The characteristic automaticity of the SA node can be suppressed if the rate of firing is faster than the spontaneous one, a phenomenon known as overdrive suppression (Wolk et al., 1999). The membrane potential during phase 4 in SA and AV nodes is around -50 to -65 mV, respectively, which is more depolarized than the -80 to -90 mV in the remainder of the heart. With the lack of I_{Na} in the nodes, the onset of phase 0 is slow (Figure 7) (Grant, 2009; J. Liu et al., 2016). Similarly, I_{K1} is larger in ventricles, adding to the negative membrane potential. The lack of this I_{K1} current renders the diastolic membrane potential less negative in the nodes (Anumonwo & Lopatin, 2010).

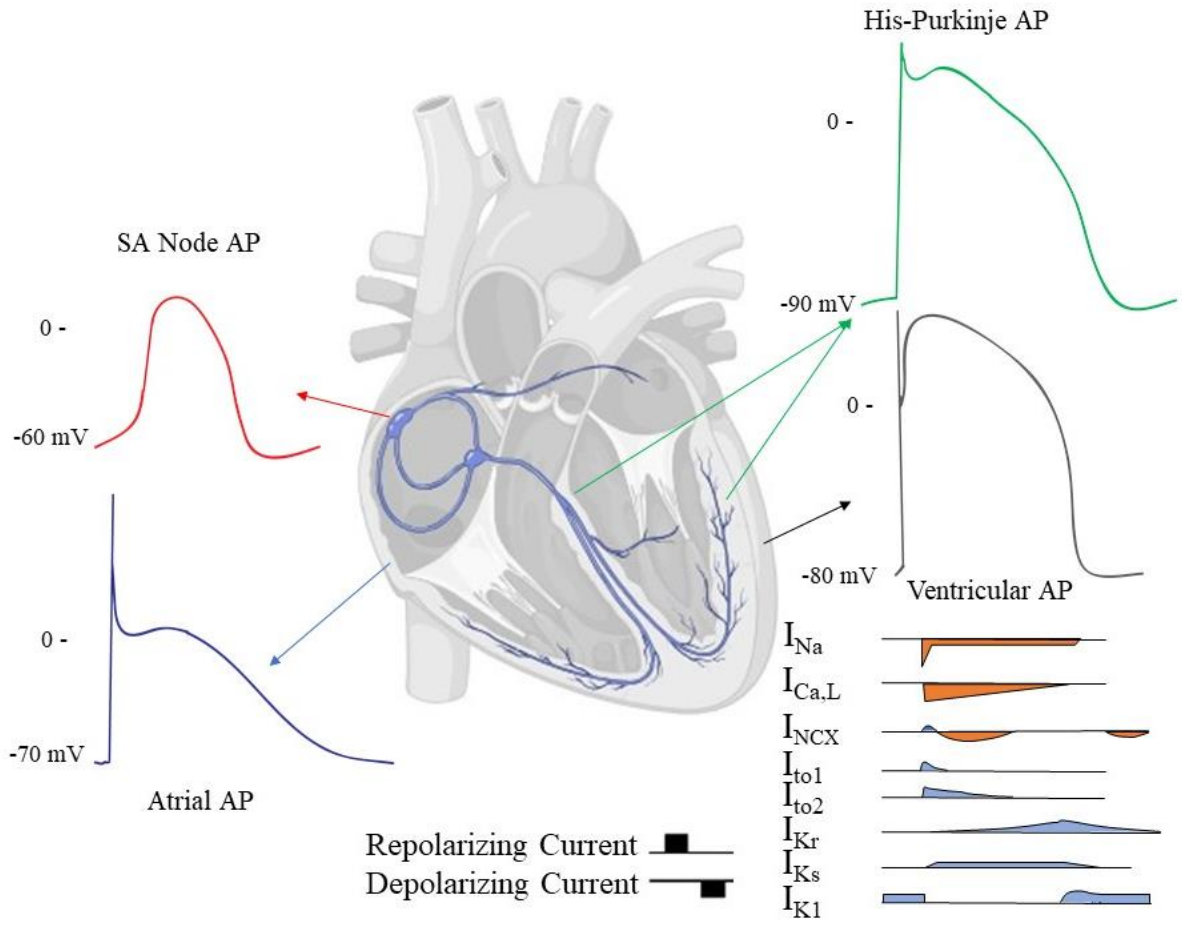

Figure 7. Electrophysiology of the heart.
Representative images of action potentials (APs) found in different parts of the heart. The APs vary in length and amplitude. Negative resting membrane potential is found in the ventricles and Purkinje fibers as opposed to the SA node and the atria, where their resting membrane potential is less negative (image created using BioRender.com and adapted from (J. Liu et al., 2016; Nerbonne & Kass, 2005; Schmitt et al., 2014)).

The structure-function relationship in cardiomyocytes is closely related to the function of ion channels and the contractile apparatus. The influx of Ca^{2+} into the cell is one of the key contributors to regulating the contractile function. The electrical activity of cells, as described above, leads to their excitation that results in cardiomyocyte, but also cardiac contraction. The Ca^{2+} channels are located in the T-tubules of cardiomyocytes which are in close proximity to the sarcoplasmic reticulum (SR) (Eisner et al., 2017; Schmitt et al., 2014). The influx of $I_{Ca,L}$ during phase 2 of the AP allows Ca^{2+}-dependent Ca^{2+} release from ryanodine receptors (RyR) found in the SR membrane (Schmitt et al., 2014). Next, Ca^{2+} binds to troponin, leading to actin and myosin sliding towards the Z-disc and shortening of the filaments thus resulting in contraction of the cell (Bers, 2002; Eisner et al., 2017). The relaxation step is achieved by Ca^{2+}

removal from the intracellular space via the SR Ca-ATPase (SERCA) pump and the NCX (Figure 6 & 8) (Eisner et al., 2017; Woodcock & Matkovich, 2005) down its concentration gradient and thus pushing the AP into phase 3 by creating a less positive environment (Nerbonne & Kass, 2005).

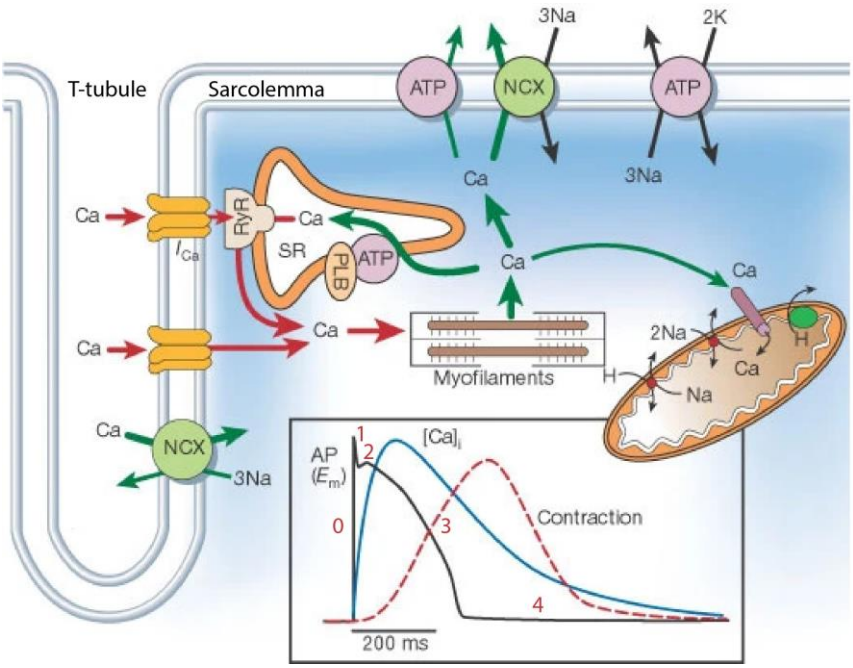

Figure 8. Excitation-contraction coupling.
Calcium contributes to the contraction of the cardiomyocyte by binding to troponin resulting in a shortening of the myofilaments i.e. contraction of the cell. The calcium influx likewise contributes to phase 2 of the AP (modified from (Bers, 2002)).

Changes in calcium handling of cardiomyocytes has several downstream effects and contributes to diseases that can result in heart failure (Benitah et al., 2021). Incorrect calcium handing by the SR is a prime contributor to this problem (Marks, 2013) and may have two consequences: decreased contractility and occurrence of arrhythmias. Concerning contractility, increased calcium leak from the SR through the RyR due to CaMKII phosphorylation can deplete SR calcium stores (Benitah et al., 2021) and decrease calcium transient (Marks, 2013). Another contributing factor is the compromised activity of the SERCA pump in heart failure that has a lower uptake which results in lower calcium stores (Benitah et al., 2021; Marks, 2013). Consequently, decreased levels of calcium hinder excitation-contraction coupling (Sutanto et al., 2020). Subsequently, mutations in RyR have also been found to cause calcium leak (Sleiman et al., 2021). The RyRs are typically in close proximity to calcium channels that are anchored in T-tubules. Remodeling of the tubules in disease causes a greater distance between the RyR and the calcium channel which can cause an inconsistent calcium release

within the cell (Chakraborty et al., 2023). A decrease in calcium transient during systole due to lowered calcium availability of the SR has shown to decrease cell contraction in heart failure (Marks, 2013).

But abnormal calcium handling will also have electrophysiological and arrhythmic consequences. An increase of RyR sensitivity or their phosphorylation can result in open RyRs even at rest, thus leading to calcium leak during diastole that may raise membrane potential and transiently increase NCX activity, thus leading to a transient inward current at the origin of delayed afterdepolarizations. If sufficient calcium is released, the AP threshold can be reached, thus triggering an AP (Chakraborty et al., 2023; Lerman et al., 2024) that can generate an extrasystole and ventricular tachycardia (Chakraborty et al., 2023). In correctly functioning cardiac tissue, a delayed afterdepolarization of one or few cells is typically not enough to spark changes to neighboring cells and to the rest of the heart. In diseased tissue, cell-to-cell connections can be compromised due to fibrosis, for example. If that is the case, fewer cells might be required to trigger arrhythmias (Lerman et al., 2024). Early afterdepolarizations can also occur if the potassium current is decreased which in turn would allow for the calcium channels switch from inactivated to activated state causing a calcium influx. But abnormal calcium handling during prolonged action potential can increase NCX current which will also contribute to formation of early afterdepolarizations (Chakraborty et al., 2023). The electrical activity allows for the mechanical activity, and for synchronization of these two activities to occur, the cells must be interconnected. The structure and function of intercalated discs add another layer of complexity to cell function.

1.4 Intercalated Discs

Transverse lines that couple individual cells in the cardiac muscle are known as intercalated discs (ID) (Estigoy et al., 2009). These structures connect cells physically during forceful contractions to create a continuum capable of dynamic cellular functions, mainly electrical homeostasis. The ID hosts gap junctions, desmosomes, and adherens junctions (Figure 9) (Nielsen et al., 2023). An abundance of proteins are found within each of the ID compartments and add to its functionality.

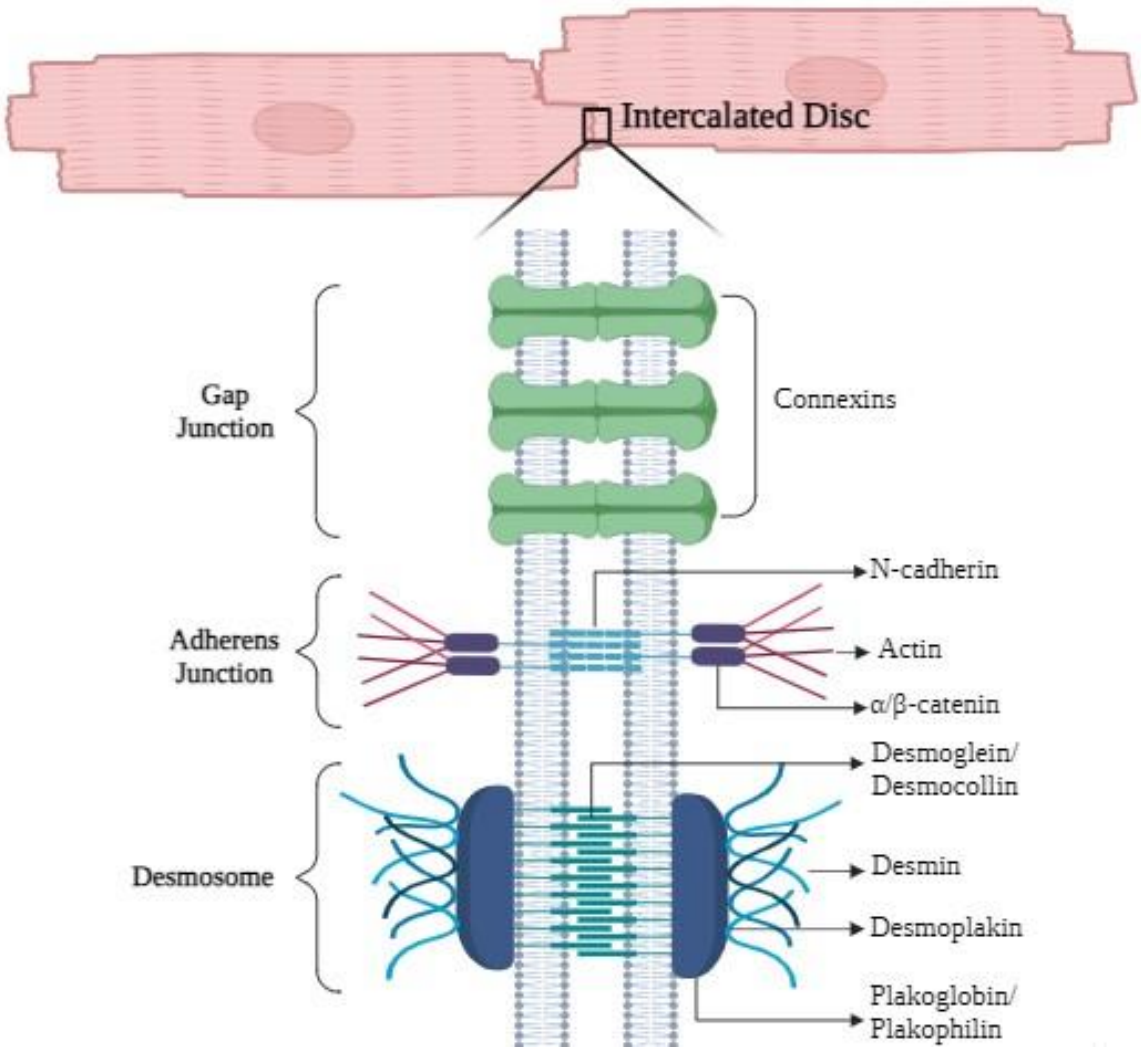

Figure 9. The intercalated disc.
Cardiomyocytes are joined together via intercalated discs (ID). The ID is made up of gap junctions, adherens junctions, and desmosomes. Multiple proteins are anchored at the sarcolemma and allow for the connection between the neighboring cells as well as intracellular proteins such as actin and intermediate filaments (desmin) (image created using BioRender.com and adapted from (Nielsen et al., 2023; Vermij et al., 2017)).

1.4.1 Gap Junctions

The AP propagates thanks to an orchestrated flow of current in and out of cells. In order for full muscle contraction to happen, the AP must propagate from one cell to the next. Electrical communication occurs thanks to gap junctions in the ID that form low-resistance pathways (Kléber & Rudy, 2004). Six proteins, connexins, join together to form a connexon (hemichannel) and reside in the transmembrane space of cells, where they link together with the connexons from neighboring cells to form a channel (Nielsen et al., 2023). There are 21 different connexins identified in humans and named according to their molecular weight

(Nielsen et al., 2023). They are located in multiple organs such as the liver, skin, and of interest – the heart (Kléber & Jin, 2021). The main connexin proteins found in the heart are connexin 40 (Cx40), connexin 43 (Cx43), and connexin 45 (Cx45). These connexins are dispersed throughout different parts of the heart (Figure 10). In the ventricles, Cx43 prevails, while Cx40 is primarily expressed in the Purkinje system (Kléber & Jin, 2021; Monteiro et al., 2017). Cx45 is most notably detected in the SA and AV nodes (Severs et al., 2008). The structure of these channels reflects their functional properties. Channels from opposing cells must be juxtaposed to form a functional channel, but the channel permeability is controlled by their open and closed states (Contreras et al., 2003).

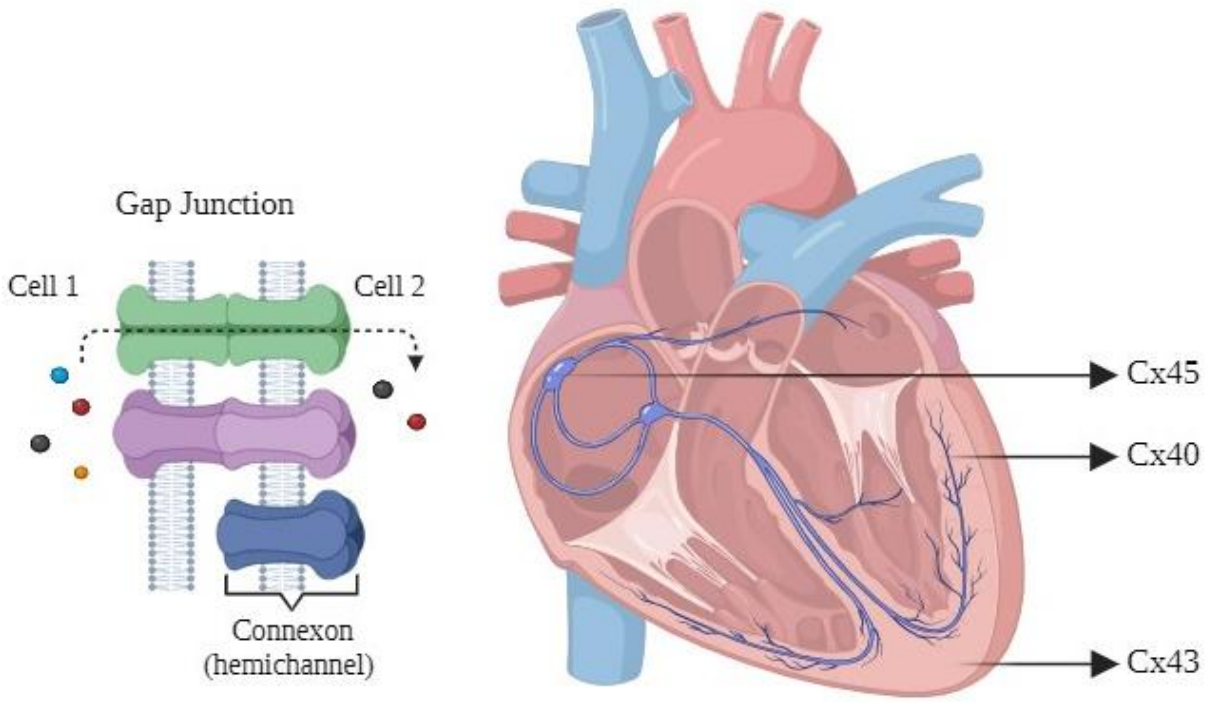

Figure 10. Gap junctions connect cells via connexins.
Different types of connexins are found throughout the heart depending on their location. Connexin 45 (Cx45) prevails in the nodes while connexin 40 (Cx40) is primarily found in the Purkinje system. Connexin 43 (Cx43) is located in the ventricles. Hemichannels from neighboring cells connect to create a connexin channel that is capable of passing ions from one cell to the other (image created using BioRender.com and adapted from (Kléber & Jin, 2021; Nielsen et al., 2023)).

The fluctuating ions during an AP must be propelled from one cell into the next and pass through the whole organ to reach synchronized contraction and pump blood throughout the body. Connexins have such a role since these intercellular connections are rather unselective and pass most ions (Ca^{2+}, Na^{+}, K^{+}, Cl^{-}) and other molecules (such as ATP) from one cell to the next (Rodríguez-Sinovas et al., 2021). The current that travels via gap junctions leads to the depolarization of downstream cardiomyocytes. There is an increased density level of I_{Na} at the ID. Co-immunoprecipitation studies have demonstrated that $Na_V1.5$ channels are in close proximity to Cx43, thus demonstrating the preferential location of sodium channels at the ID (Veeraraghavan et al., 2014). The positioning of the $Na_V1.5$ channels at the perinexus is thought to augment electrotonic coupling between cells and increase the success of AP propagation throughout the heart (Kléber & Rudy, 2004; Pfeiffer et al., 2014). It is therefore not surprising that Cx43 knock-out mice are more susceptible to arrhythmias but interestingly enough, the absence of Cx43 also leads to $Na_V1.5$ channel absence resulting in decreased sodium current (Jansen et al., 2012). The mechanism of AP propagation and conduction between cells has been challenged by research over the years.

1.4.1.1 Ephaptic Coupling

Another school of thought about electrical communication between cells infers that the colocalization of the $Na_V1.5$ channel and connexins at the perinexus of the gap junction is of little importance. The theory of ephaptic coupling suggests that depolarization of cells does not rely on gap junctions (Lin & Keener, 2013), but rather the extracellular space as the main means of cell-cell communication (Lin & Keener, 2010). Since Na^{+} accumulates between cells, this difference in potential between the intra- and extracellular space causes one cell to depolarize the next (Kucera et al., 2002). Although this theory is plausible, the lack of direct and experimental evidence leaves the discussion open-ended.

1.4.2 Adherens junction

The adherens junction is a complex, multiprotein structure, spanning the intra- and extracellular spaces between neighboring cells. Changes in cell tension can be sensed at this junction and allow for continuity of force generated by contraction (Nielsen et al., 2023; Pruna & Ehler, 2020). The major transmembrane protein of the adherens junction is N-cadherin, which forms a homodimer in the extracellular space with N-cadherins from adjacent cells (Vermij et al., 2017). β-catenin binds N-cadherin at the intracellular side. Actin filaments preserve the brick-like architecture of cardiomyocytes by anchoring to α-catenin and vinculin

which are both bound to β-catenin (Figure 11) (Estigoy et al., 2009; Pruna & Ehler, 2020; Vermij et al., 2017). It is understood that the interaction of N-cadherin and β-catenin stabilizes myofibrils, but cadherin's primary role is to form strong cell-cell interactions since its deletion in murine models resulted in the death of embryos that demonstrated a lack of observable IDs (Kostetskii et al., 2005). Deletion of N-cadherin impairs the mechanical coupling and structural integrity of cardiomyocytes which consequently alters the mechanical functionality of the heart (Chopra et al., 2011). Furthermore, β-catenin plays a role in the Wnt signaling pathway during early development (before gastrulation) where activation of the pathway induces the formation of the heart and formation of the mesoderm (one of the three layers from which the heart stems) (Q. Wang et al., 2012). Additionally, Wnt signaling promotes the expression of Cx43 (Ai et al., 2000).

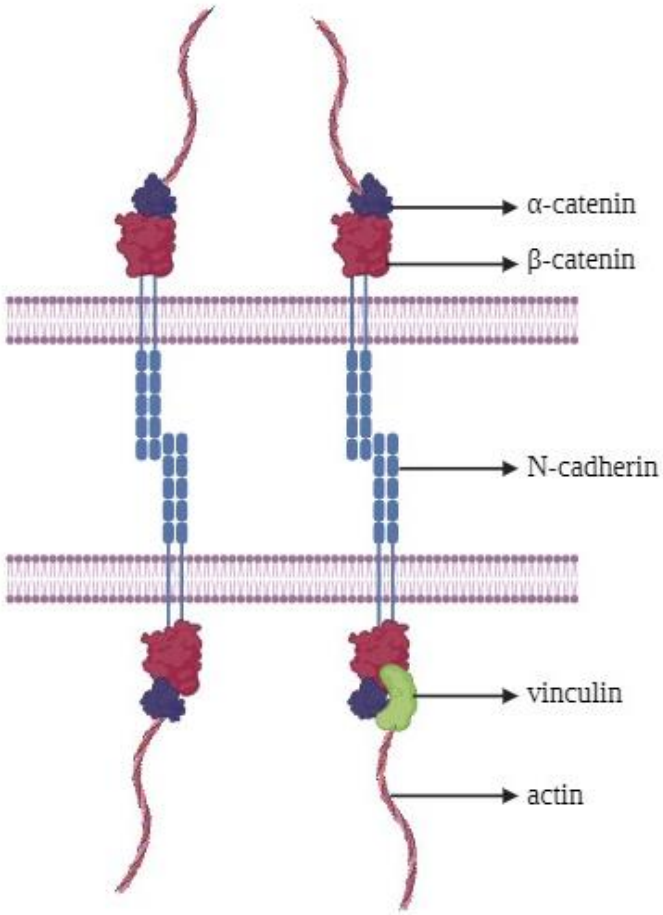

Figure 11. The adherens junction.
N-cadherin forms homodimers with N-cadherin from adjacent cells in the extracellular space while attaching to vinculin, α- and β-catenin that further attach to actin to provide stability for myofibrils (image created using BioRender.com and adapted from (Nielsen et al., 2023)).

1.4.3 Desmosomes

In the working myocardium, desmosomes are structural bridges between individual cells. They provide structural and mechanical support for the cell. Located in the ID, desmosomes form a mosaic composed of assorted proteins. The two main desmosomal cadherin proteins in the myocardium are desmoglein-2 and desmocollin-2 (Patel & Green, 2014). They span the sarcolemma and have an intracellular C-terminal tail while the N-terminus is located on the extracellular side (Nielsen et al., 2023). In the extracellular space between cells, these two proteins form a bond with one another, that helps maintain the structural integrity of the myocardium (Figure 12) (Moazzen et al., 2023). Plakoglobin and plakophilin-2 are two armadillo proteins that act as linkers in the desmosome. The two cadherins are located on the cytoplasmic side and attach to desmoplakin (Noorman et al., 2009; Patel & Green, 2014).

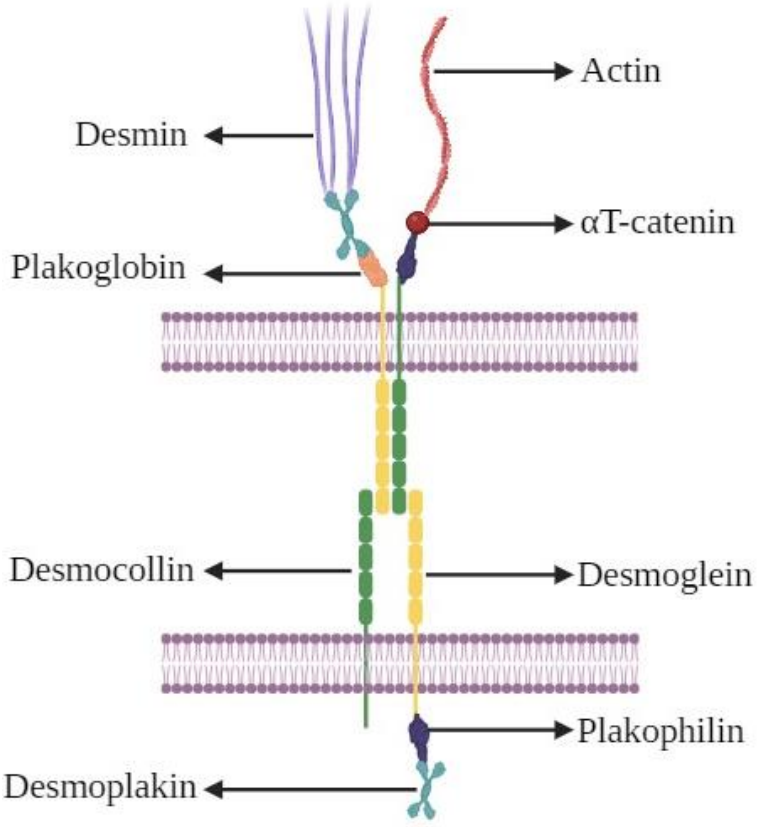

Figure 12. Illustration of desmosomes and their associated proteins.
Desmosomes are composed of multiple proteins where some span the plasma membrane, such as desmoglein and desmocollin, while others are located on the intracellular side (image created using BioRender.com and adapted from (Patel & Green, 2014)).

It has been shown that 90% of the ID is composed of three intracellular proteins: plakoglobin, plakophilin-2, and desmoplakin (Pieperhoff & Franke, 2007). Studies revealed that the above-discussed adherens junctions and desmosomes are distinct, individual protein clusters and can be distinguished during the development of mammalian hearts. Postnatally, they merge and form the *areae compositae* (Pieperhoff & Franke, 2007). The maturation of cardiomyocytes happens after birth and depends on the formation of tight connections in the *areae compositae* to ensure better mechanical and structural organization resulting in a heart that can handle the force of every contraction. It is no surprise that mutations in plakoglobin have been linked to Naxos disease whereas Carvajal syndrome results from desmoplakin mutations, both having cardiomyopathy as a hallmark of the disease (Patel & Green, 2014). Mutations of these proteins most notably lead to arrhythmogenic right ventricular cardiomyopathy (ARVC) (Alcalai et al., 2003; McKoy et al., 2000). Furthermore, not only does desmoplakin connect to plakoglobin or plakophilin-2 in the cytoplasm, but it also connects the desmosome to intermediate filaments (Patel & Green, 2014).

Chapter II
Intermediate Filaments

Cells rely on different types of filaments to perform their function. These filaments are grouped into three types: microtubules, actin microfilaments, and intermediate filaments (IFs). The type of filaments and their function strongly depend on cell type and localization within the body (Caporizzo & Prosser, 2022). Cardiac microtubules form straight and stiff cytoskeletal filaments from αβ-tubulin heterodimers that attach to one another from end to end (MacTaggart & Kashina, 2021). The microtubule network is capable of growing with the addition of new heterodimers or shortening if dimers detach in order to accommodate the cell's needs (Grimes et al., 2019). Microtubules are essential for maintaining proper cell structure and provide support during contraction by utilizing force and tension resistance but also for trafficking of membrane proteins (Warner et al., 2022). The growth of the cytoskeletal microtubule network can also backfire since an increase in tubulin synthesis contributes to diseases such as HCM (Warner et al., 2022).

Actin microfilaments are part of the contractile apparatus. In the cardiac sarcomere, they interact with troponin and tropomyosin forming the thin filament of the sarcomere that interacts with myosin (thick filament) during contraction (Martin & Kirk, 2020). Of the six isoforms found in the human body, α-actin is predominantly located in cardiomyocytes (MacTaggart & Kashina, 2021). The thin actin filaments attach to Z-discs located throughout the sarcomeres. During contraction when Ca^{2+} becomes available in the cells, the distance from one Z-disc to the other is reduced due to the sliding of thin and thick filaments (Frank & Frey, 2011; Mason et al., 2022). Both HCM and DCM have been associated with mutations of actin filaments and their binding partners, typically impairing their connection to the Z-disc (Murphy & Young, 2015).

Intermediate filaments get their name from the size of their diameter: 25 nm for microtubules, 7-10 nm for actin filaments, and 10-12 nm for IFs (Strelkov et al., 2003). Various IFs have been identified in humans and are subdivided into six groups according to amino acid sequence similarities (Table 2) (Tsikitis et al., 2018). All IFs share the basic structure composed of an N-terminal head, an α-helical rod domain that is highly conserved, and a C-terminal tail (Eriksson et al., 2009). There are different types of IFs found in the heart: type IV (nestin and synemin), type V (lamins), and type III (vimentin, desmin, and syncoilin) (Tsikitis et al., 2018). Desmin is the most expressed and abundant IF in the heart (Tsikitis et al., 2018) and will be the primary focus throughout the rest of this thesis.

Table 2. Classification of intermediate filament proteins.
There are six different types of IFs that are grouped together depending on the similarity of their amino acid sequence. Different types of intermediate filaments are found in different parts of the body and have varying molecular weights (kDa).

Type	Protein(s)	Location	Molecular Weight	References
I	Keratin (Acidic)	Epithelial cells	~40-57 kDa	(Daly et al., 1998; Jacob et al., 2018; Szeverenyi et al., 2008)
II	Keratin (Basic)	Epithelial cells	~50-70 kDa	(Daly et al., 1998; Jacob et al., 2018; Szeverenyi et al., 2008)
III	Vimentin	Mesenchyme derived cells	55 kDa	(Daly et al., 1998; Hol & Capetanaki, 2017; Strelkov et al., 2003; Szeverenyi et al., 2008; Viedma-Poyatos et al., 2020)
	Peripherin	Neurons	58 kDa	
	Glial Fibrillary Acidic Protein (GFAP)	Glial cells, astrocytes	53 kDa	
	Syncoilin	Muscle cells	~8-55 kDa	
	Desmin	Muscle cells	52 kDa	
IV	Neurofilaments (NF: NF-L, NF-H, NF-M)	Muscle cells, neurons	~60-200 kDa,	(Daly et al., 1998; Galou et al., 1997; Homberg & Magin, 2014; Szeverenyi et al., 2008; Uhlén et al., 2015)
	Nestin		~177 kDa	
	α-internexin		~55 kDa	
	Synemin		140-173 kDa	
V	Lamins (A, B, C)	All tissues (nuclear membrane)	60-70 kDa	(Daly et al., 1998; Szeverenyi et al., 2008)
VI	Filensin	Eye lens	~58-75 kDa	(Daly et al., 1998; Szeverenyi et al., 2008; Uhlén et al., 2015)
	Phakinin		~46 kDa	

2.1 Desmin

In 1976, Elias Lazarides and Bruce Hubbard isolated and characterized an intermediate-sized protein from chicken gizzards and gave it the name desmin, which stems from a Greek word that means bond or link (Lazarides & Hubbard, 1976). It was purified for the first time in the following year by the same group (Izant & Lazarides, 1977) and the nucleotide sequence was deciphered a few years later in 1989 (Li et al., 1989). Desmin makes up for ~2% of the proteins located in the cardiac muscle cells (Paulin & Li, 2004). The importance of desmin became evident when mutations in the gene led to changes in the protein structure and caused mild or severe myopathies. Although desmin is also found in skeletal and smooth muscles, the primary focus of this thesis will be on its structure and function in the heart.

2.1.1 From Gene to Protein

A single gene located on chromosome 2q35 (Viegas-Pequignot et al., 1989) codes for desmin's nine exons and eight introns (Li et al., 1989). Desmin consists of 470 amino acids (Costa et al., 2004). The N-terminal head precedes the α-helical rod domain and a C-terminal tail follows on the other end. The central α-helical domain is divided into four segments (1A, 1B, 2A, and 2B), that are connected by linkers L1, L12, and L2 (Figure 13). Each of the four segments is highly conserved among vertebrates (Bär et al., 2004). Desmin assembles into long filaments in the following step-by-step process (Figure 13):

- Two monomers align in parallel to one another and form a coiled-coil structure between their α-helical domains (Clemen et al., 2013)
- Next, a tetramer is formed from two dimers that associate in an anti-parallel and half-staggered manner (Bär et al., 2004). The N-terminal head interacts with the rod domain at specific locations that are important for IF assembly (Brodehl et al., 2018; Godsel et al., 2008)
- Eight tetramers are then capable of spontaneously assembling laterally and in parallel into filaments that are 60 nm in length. These fragments are called unit-length filaments (ULF) (Agnetti et al., 2022; Clemen et al., 2013)
- Longitudinal annealing of ULFs results in filament formation (Herrmann & Aebi, 2004)
- The final step of this process is referred to as radial compaction, where the filament diameter decreases from about 15 nm to 10 nm (Agnetti et al., 2022; Herrmann & Aebi, 2004)

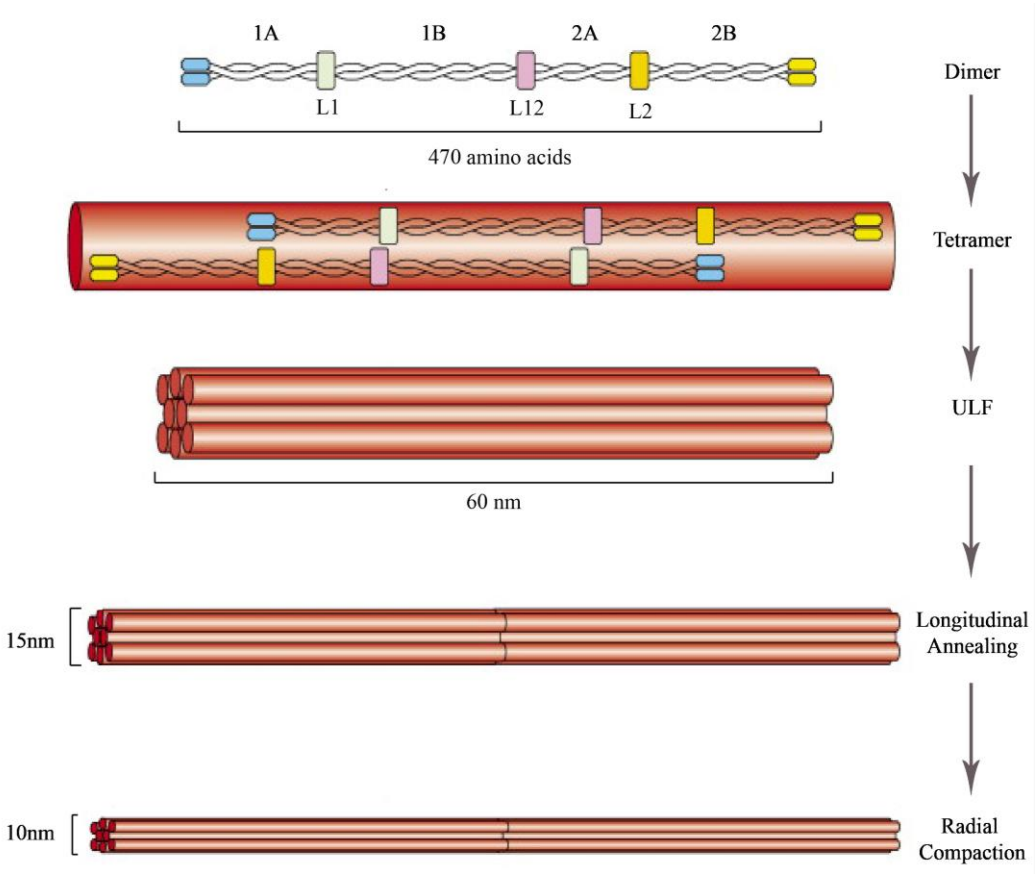

Figure 13. Desmin assembly process from dimer to the compacted filament.
Desmin intermediate filaments follow a step-by-step process to form a proper filament that is 10 nm in diameter (modified from (Godsel et al., 2008)).

The assembly process of IFs must be executed correctly in order to produce compacted filaments, as mentioned above. Several parts of the segments and non-helical domains of the protein play a vital role in higher-level structural organization of individual monomers into fully formed, cell-spanning filaments. Deletions and point mutations within the 470 amino acids can have serious consequences on desmin IF assembly and can lead to disease.

2.1.2 Post-Translational Modifications

Post-translational modifications (PTM) are important for regulating desmin filament assembly or disassembly and are critical in health and disease. In the case of abnormal filament formation, PTMs can help discard the protein by tagging it for degradation. The PTMs at play are ubiquitination, ADP-ribosylation, phosphorylation, and nonenzymatic modifications such as oxidation, nitration, and glycation (Snider & Omary, 2014; Tsikitis et al., 2018; D. L. Winter et al., 2014). There are many enzymes that can modify desmin, such as PKC, PKA, and Rho-associated kinase, to name a few (Table 3) (D. L. Winter et al., 2014). A large number of PTMs

are located in the N-terminal head, which is known to be important for filament assembly. Modifications in this part of the protein can determine the fate of desmin (D. L. Winter et al., 2014). Therefore, incorrectly assembled IFs must be discarded (Omary, 2009) for the preservation of the structural and functional integrity of the cell.

A majority of the PTMs have a role in dismantling desmin or lead to its degradation through ubiquitination (del Monte & Agnetti, 2014; Tsikitis et al., 2018). The homeostasis and turnover rate of desmin is therefore highly dependent on PTMs, which can lead to disease if the modifications are not strictly controlled. For example, GSK-3β kinase biphosphorylates desmin and by doing so, the filament can incorporate itself into the Z-disc (Bouvet et al., 2021; Tsikitis et al., 2018). If the GSK-3β kinase activity is inhibited in diseased tissue, as was observed in some cases of heart failure, desmin will be found primarily in a monophosphorylated state and its integration into the Z-disc can be hindered. Consequently aggregates will form (Agnetti et al., 2014; Rainer et al., 2018). The inhibition of GSK-3β in mice demonstrated that phosphorylation of desmin was halted and that the IF could not depolymerize (Aweida et al., 2018), providing further evidence that PTMs are important for desmin dynamics. Without proper regulation of desmin via PTMs, the filaments lose their ability to provide the necessary structural support within the cells and cannot bind to the relevant organelles and sarcolemma in order to regulate proper force and tension within the cell during contraction, if they are clustered together. Changes to PTMs can thus be the driving force of some diseases since unusual PTM of desmin result in its aggregation.

Table 3. List of enzymes that are known to modify desmin.
Post-translational modifications of the desmin intermediate filament and the processes they might be or are implicated in (table adapted from (D. L. Winter et al., 2014)).

Enzyme	Abbreviation	Modification	Activity
Protein kinase A	PKA	Phosphorylation	Myoblast fusion
Protein kinase C	PKC	Phosphorylation	Desminopathies
Cyclin-dependent kinase 1	CDK1	Phosphorylation	Desminopathies
p21-activated kinase	PAK	Phosphorylation	Muscle contraction; cardiac excitation and contraction
Rho-associated kinase	Rho-kinase	Phosphorylation	Muscle contraction; cell division
Aurora kinase B	Aurora-B	Phosphorylation	Cell division
Ca^{2+}/calmodulin-dependent protein kinase II	CaMKII	Phosphorylation	Heart failure
Mono-ADP-ribosyltransferase	ART1	Mono-ADP-ribosylation	Myoblast differentiation
E3 ubiquitin-protein ligase TRIM32	TRIM32	Ubiquitylation	Muscle atrophy
ADP-ribosylarginine hydrolase	ADPRH	Removes mono-ADP-ribosylation	Unknown
Type 1 protein phosphatase	PP1	Removes phosphorylation	Cell division

2.1.3 The Three-Part Protein Structure

Understanding the role of each of the three parts of IFs; the non-helical head and tail and the α-helical central rod domain, during IF assembly can help decipher the genotype-phenotype relationships. Over the years, various experiments, mainly in vitro studies, have demonstrated the structural consequences that arise when we mutate IF genes. Vimentin is another type III filament (Table 2), often used in in vitro experiments since there is a high sequence homology between desmin and vimentin. Both form coiled-coil dimers so they can be used to study assembly properties of IFs with mutations/deletions (Bär et al., 2004). The N-terminal head contains amino acids that can interact with amino acids of the rod domain, which in turn allows for IF assembly (Tsikitis et al., 2018). This domain is thought to be necessary for instigating the formation of tetramer complexes by creating stable connections between dimers (Figure 14A) (Bär et al., 2004). Indeed, the creation of "headless" vimentin IFs demonstrated the importance of the N-terminal domain in building IFs, since these headless filaments halted the assembly following dimer formation (Herrmann et al., 1996). Similarly, removing both non-helical terminal ends resulted in a lack of filament formation, implying that the central rod domain is not enough to initiate IF assembly since not even aggregate formation could be observed (Herrmann et al., 1996). Nevertheless, small deletions in segment 1A have consequences on the final form of the IF, even if the head and tail are intact. Segment 1A contains a preserved, 26-residue sequence, of which eight residues are highly conserved among different IF types (Strelkov et al., 2002). Crystal structures of this segment revealed the importance of the α-helical shape in segment 1A, as it allows for coiled-coil formation during dimerization (Strelkov et al., 2002). The coiled-coil form of segment 2B unwinds at a heptad stutter located at residue Phe351 (Figure 14B), while maintaining α-helices parallel to one another, to better orient the relevant residues of the N-terminal head and C-terminal tail during IF assembly (Figure 14 A) (Strelkov et al., 2003). The accurate formation of a filament highly depends on all three parts of the protein, and any modifications result in deleterious effects.

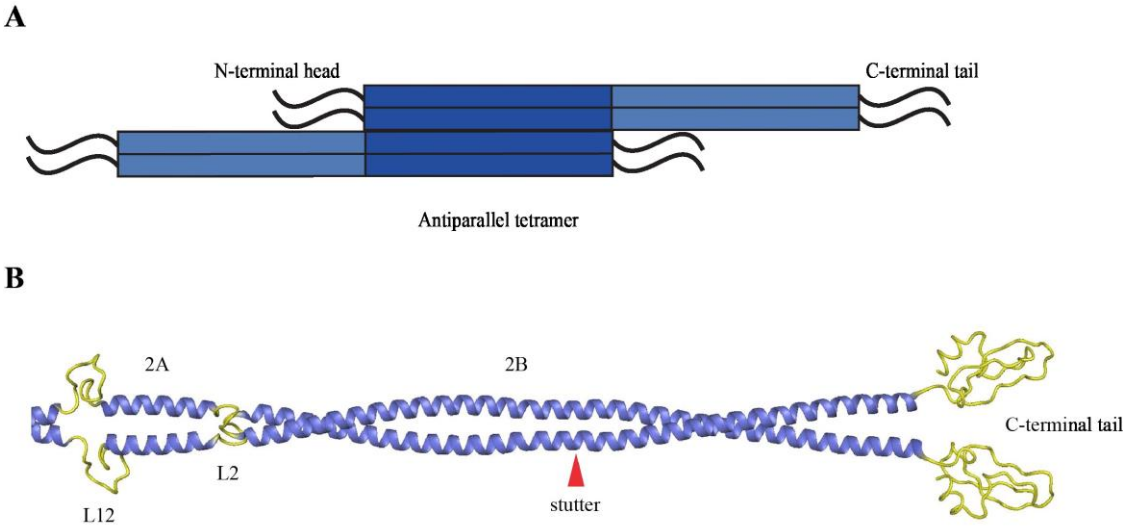

Figure 14. Desmins head, rod, and tail domains are important for proper filament formation.
The interaction of the N-terminal head with the rod domain allows for proper tetramer formation (A) while the stutter in segment 2B is necessary for filament assembly by correctly orienting the terminal ends (B) (image modified from (Agnetti et al., 2022; Bär et al., 2004)).

SW13 cells are naturally vimentin-free and have proven to be a useful tool in deciphering the structural consequences of various mutations within the desmin gene (Dalakas et al., 2000; Goudeau et al., 2001). An in-frame deletion p.Q113_L115del from a patient with LVNC was transfected into SW13 cells. The functional experiments revealed desmin aggregate formation as opposed to the typical filaments that were observed in control cells (Marakhonov et al., 2019). Many other mutations in the desmin gene result in the same observable phenotype of desmin aggregates. This phenotype has become a hallmark of desmin mutations that is thought to be implicated in cardiac and/or skeletal myopathy (Kaminska et al., 2004). Desmin aggregates are not only observed experimentally in transfection studies but also in muscle biopsies of patients with desminopathy, although transfection studies are still used today to confirm the structural consequences of given desmin mutations (Kaminska et al., 2004).

The sequence motif, “TYRKLLEGEESRI”, is located in the terminal end of desmin in segment 2B. Most IFs contain this motif and it is highly conserved among species (Bär et al., 2004; Herrmann et al., 2000). Its importance during desmin assembly was investigated by Herrmann and colleagues who isolated proteins from bacteria that expressed plasmids with a truncated form of the motif ending at position 402, thus excluding the YRKLLEGEE segment of the motif and the C-terminal tail. In vitro experiments led to the observation of short and uncompacted filaments alongside others that were longer and compacted. Overall, they did not

elongate compared to control filaments. The truncated desmin did not form into the classical tetramers and filaments were larger in size due to increased numbers of dimers. They concluded that the YRKLLEGEE motif was responsible for correct tetramer formation and assembly of the proper number of subunits in each cross-section of the filament. Consequently, it did not fully impair filament formation, although it was incorrect (Herrmann et al., 2000). The C-terminal tail mainly contributes to the association of filaments laterally as opposed to longitudinally, and has been shown to be important during the compaction of the filaments (Bär et al., 2004), similar to the results obtained from deleting the sequence motif. Mutations within the terminal end of segment 2B result in many cardiac disorders such as those found in Table 1, and have been reviewed in Chapter III: Review. Desmin mutations have been located throughout different parts of the protein and can contribute to myopathy with different levels of severity.

2.2 Desmin Expression During Development

Desmin is expressed early on during development and is thus known as a myogenic marker for cardiac but also skeletal muscles. In mice, for example, desmin appears 8.25 days post coitum in the neuroectoderm. At this stage, it is expressed transiently with other IFs such as keratin, nestin, and vimentin. Desmin is detected in the early developing heart (8.5 days post coitum) and by day 9 post coitum, desmin is expressed together with vimentin and nestin in the somites (Milner et al., 1996). Vimentin is predominantly expressed in myoblasts but is later downregulated and no longer detected in adult mice, whereas the opposite holds true for desmin (Capetanaki et al., 2007; Clemen et al., 2013). The early expression of desmin suggests that it may have a role in the differentiation of muscle cells during development, but as mentioned above, desmin null mice are still viable and can reproduce. Cardiomyocyte structural organization is typically lacking during development, yet it has been suggested that in rat hearts, a transient increase in smooth muscle proteins alongside desmin allows for myofibrillar organization (Ya et al., 1997). Before the proper intracellular organization of cardiomyocytes, desmin has been located together with sarcomeres at the periphery of cardiac cells. The observed proximity of desmin to the Z-discs in correctly organized cells has therefore implied that IFs are important for Z-disc alignment and proper sarcomere formation and organization (Moorman et al., 1998; Ya et al., 1997). The close association and interaction of desmin with the contractile apparatus can explain cardiomyocyte structural organization.

In the human fetal heart, desmin is observed as early as 9 weeks of gestation (Yamamoto et al., 2011). The distribution of desmin during fetal development is time and space-dependent as it has been noted to be in the atria at 9 weeks and appear in the ventricles at 18 weeks of gestation (Yamamoto et al., 2011). Interestingly, it has been demonstrated that mutated desmin can disrupt cardiogenesis by damaging certain cardiogenic regulators during development (Hol & Capetanaki, 2017; Tsikitis et al., 2018). It was shown that desmin expression during normal development resulted in an upregulation of Nkx2.5 and brachyury, which are key regulators of cardiac development, but cardiomyocytes that lack desmin express lower levels of these genes (Hofner et al., 2007). Phosphorylation of the N-terminal end of desmin helps with the cardiomyogenic commitment of cells and obstructing this PTM can lead to the downregulation of several genes including Mef2C, which is involved in cardiac morphogenesis, goosecoid, brachyury, and Nkx2.5 (Höllrigl et al., 2007). These cardiomyocytes also lacked myofibrils further suggesting that desmin is also needed for cardiomyocyte differentiation (Höllrigl et al., 2002, 2007). Furthermore, desmin expression has been identified in the developing SA and AV nodes as well as bundle branches (H.-X. Liu et al., 2020), strongly implicating that this IF has a role in the conduction system and proper development. Patients with mutations in *DES* are likely to develop cardiac conduction problems such as arrhythmias and bundle branch blocks (Chapter III: Review) pointing to the importance of IFs in the conduction system during development but also throughout one's life. Interestingly, in patients with DCM, vimentin, which is typically only expressed during development, can be observed together with other fetal genes (Singh et al., 2020), further implying that IFs are important for maintaining proper cardiac function.

Mice are commonly used to model diseases/disorders and have shown to be useful when trying to get insight into functional as well as structural consequences. Desminopathies are no exception to this as desmin knock-out mice have been used in multiple studies. Interestingly, these mice are fertile and can develop normally without observable defects (Paulin & Li, 2004) suggesting that desmin is not essential for development. Consequently, defects appear only after birth in desmin-expressing cells, meaning in smooth, skeletal, and cardiac muscles (Hnia et al., 2015). Some of the cardiac consequences of this deletion on a cellular level include increased and improper localization of mitochondria with altered structure, lack of organization and degeneration of cardiac myofibers, disruption of intercalated discs, and increased fibrosis and calcifications, to mention a few (Hnia et al., 2015). Furthermore, the desmin knock-out mice develop DCM and HCM with observable ventricular wall remodeling (Paulin & Li, 2004).

These consequences are not surprising since desmin is flexible and functions as a spring during contraction to dampen the strain while also forming an extensive network within cardiomyocytes (Figure 15). Overall, desmin has been shown to be an integral part of cells to maintain the health of the cardiac muscle.

2.3 Localization of Desmin and its Cellular Interactions

Desmin filaments form a cell-spanning web that throughout cardiomyocytes that interacts with over 15 different proteins (Figure 15). One of its roles, as the most abundant IF, is to provide mechanical support to maintain cellular structural and functional integrity. However, models with desmin mutations or with a complete knock-out of the gene have suggested a more extensive role such as organelle function and positioning, and transduction of mechanochemical signals (Tsikitis et al., 2018). The interactome helps in regulating cardiomyocyte function by sensing and adapting to the environment. Much of what we know and understand about desmin IFs has been learned through desmin knock-out mouse models. Understanding the functional and structural support that desmin provides throughout the lifetime of an organism has become a critical aspect of understanding the genotype-phenotype relationships at play, especially in patients with desmin mutations, since disease onset varies from patient to patient. The architecture of individual cardiomyocytes contributes to the heart's functionality.

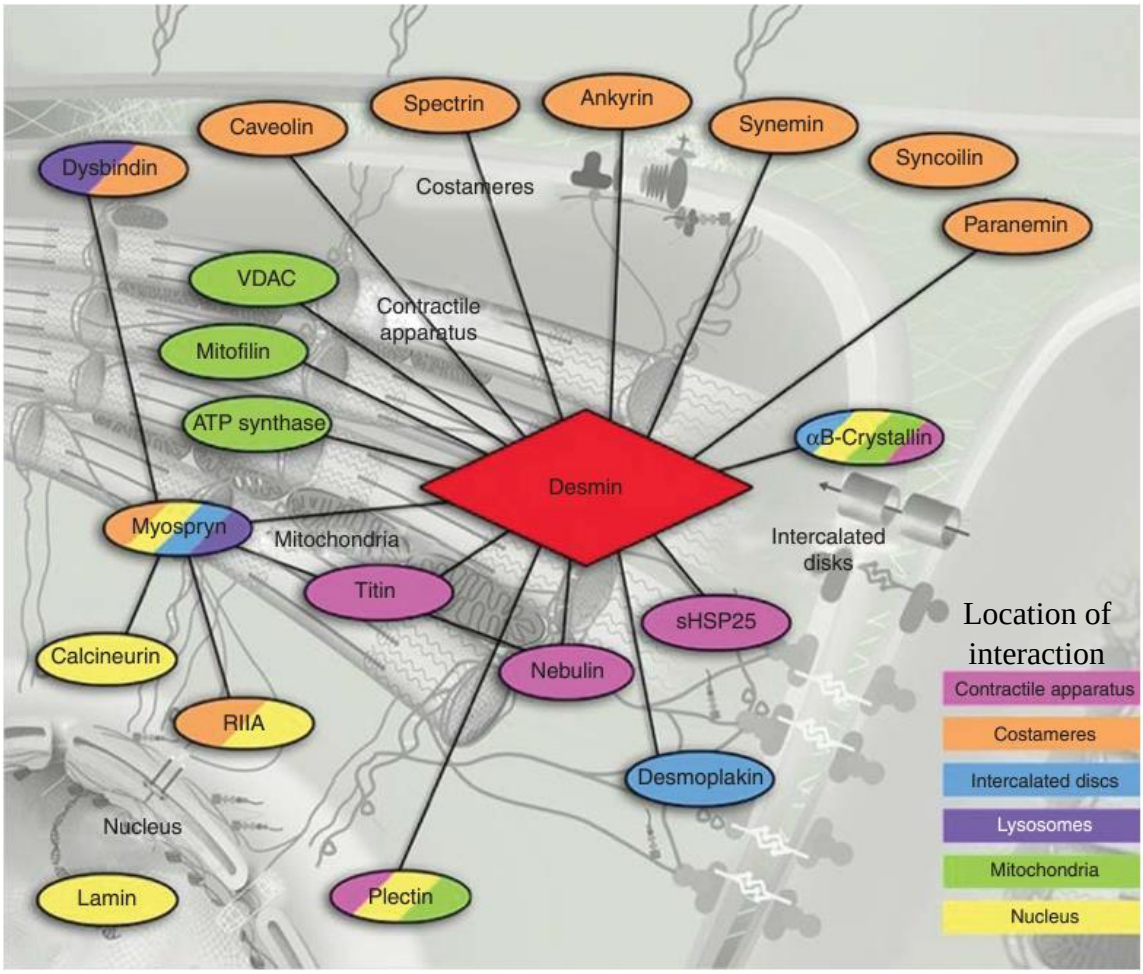

Figure 15. Desmin forms a cell-spanning web that interacts with different structures and proteins.
(colour legend: bottom right; image modified from (Hol & Capetanaki, 2017)).

The structural scaffold formed by desmin filaments traverses the cells and therefore, the interactions that are created have specific roles in maintaining the cells structural and functional integrity. Desmin binds to the nucleus, sarcolemma, mitochondria, the SR, and the Z-discs (Figure 16) (Agnetti et al., 2022; Capetanaki et al., 2007; Tsikitis et al., 2018). The IF network facilitates crosstalk within cells between different organelles and is thought to be a mechanotransducer and sensor since it can sense stress and strain of the cell and respond accordingly. The interacting partners that allow for desmin to bind indirectly to organelles are also necessary in maintaining cardiac health.

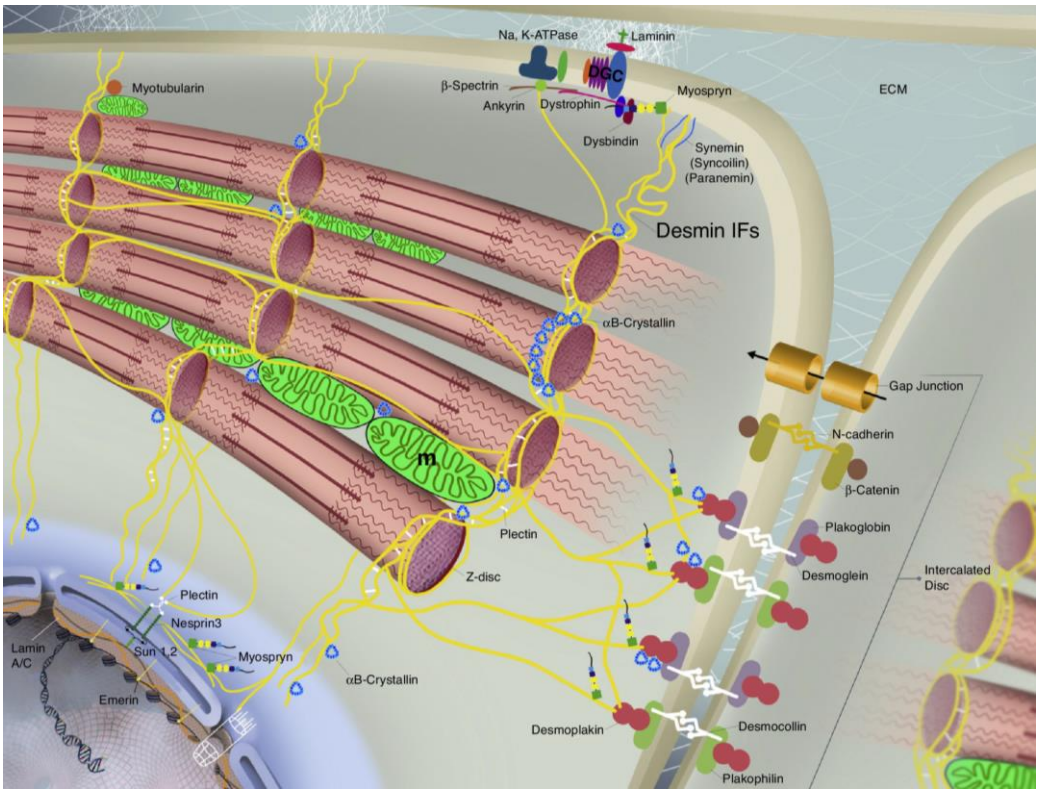

Figure 16. Desmin binds to the sarcolemma and multiple organelles in cardiomyocytes. (image modified from (Capetanaki et al., 2015)).

2.3.1 The Nucleus

Desmin filaments bind indirectly to the nucleus via plectin and the linker of the nucleoskeleton and cytoskeleton (LINC) complex protein nesprin-3 where its role is thought to maintain proper shape and size of the nucleus, and structure of the nuclear lamina (Brayson & Shanahan, 2017; Heffler et al., 2020). Reducing the amount of desmin in rat cardiomyocytes with shRNAs resulted in a decrease of nuclear volume, demonstrating the importance and need for filaments to provide structural support and for maintaining the size of the nucleus (Heffler et al., 2020). A decrease in desmin also results in altered nuclear morphology, such as inward folding of the nuclear lamina that may result in the collapsing of the nucleus due to the altered connection between desmin and the LINC complex (Heffler et al., 2020; Nikolova et al., 2004). Changes to the nucleus in cardiomyocytes can also result in a disorganization of the genome (Heffler et al., 2020). Consequently, the knocking down of desmin in rat cardiomyocytes has been shown to change the transcription of genes that are important for calcium handling, such as the RyR and SERCA pump. Indeed, these cardiomyocytes displayed reduced contractility

and changes in the calcium transient (short and rapid decay of current). Such changes can cause DCM in patients (Brayson & Shanahan, 2017; Heffler et al., 2020; Ramspacher et al., 2015).

Furthermore, desmin has been suggested to take part in mechanochemical signaling. Desmin connects the nucleus with the contractile apparatus that can lead to changes in signaling and possibly cell remodeling (Hol & Capetanaki, 2017) depending on the signal that is transmitted from the ECM down to the nucleus. Desmins interaction with myospryn, a calcineurin modulator, allows for myospryn localization at the perinuclear space. Desmins binding to myospryn has also been shown to regulate the positioning of lysosomes (Kouloumenta et al., 2007; Tsoupri & Capetanaki, 2013). Without desmin, myospryn is no longer found at the perinuclear space and the distribution of lysosomes in the cytoplasm is lost (Capetanaki et al., 2007). Overall, desmin is necessary for protecting the nucleus against structural damage that can have a severe impact on the downstream functions of the organelle.

2.3.2 The Contractile Apparatus

In order for individual cardiomyocytes to sense and respond to mechanical stretch and force, the connection between the contractile apparatus and the sarcolemma (and ECM) is necessary. Synemin mediates desmins interactions with the contractile apparatus since synemin binds to α-actinin at the Z-disc and with desmin, linking them together. Synemin is also the middle man between the costamers of the sarcolemma, where it associates with dystrobrevin, dystrophin, and vinculin, and desmin filaments (Brodehl et al., 2018; Capetanaki et al., 2007; Hnia et al., 2015). Likewise, plectin 1f and spectrin link desmin to costamers (Tsikitis et al., 2018) and ankyrin has also been proposed to act as a linker (Figure 15) (Hol & Capetanaki, 2017). These interactions allow the interconnection of organelles and structural components of the cells, but they are also key for structural organization since IFs loop around the Z-discs, leading to the subsequent alignment of the myofibrils. Indeed, desmin knock-out mice reveal a misalignment of myofibrils and a loss of attachment to the plasma membrane, making them unstable and less sensitive to mechanical changes, resulting most often in cell death (Agnetti et al., 2022). Uncoupling from the sarcolemma destabilizes the contractile apparatus. Consequently, this alters the tension of the filaments and sarcomeres, compromising the connection between neighboring cells.

2.3.3 Desmin Chaperone

The small heat shock protein, αB-crystallin, has been identified in cardiac muscle, where it acts as a chaperone for proper desmin folding. αB-crystallin binds to unfolded filaments but

also directs proteins for degradation as needed (Claeyssen et al., 2023). This chaperone is important for maintaining desmin filament homeostasis by preventing protein denaturation and aggregate formation (J. L. Elliott et al., 2013; Goldfarb & Dalakas, 2009; Nicholl & Quinlan, 1994) by untangling filaments that may be aggregated or starting to form clusters (Claeyssen et al., 2023). One of the binding sites of αB-crystallin is on the C-terminal end of desmin. If mutations occur at this site of the filament, the chaperone's activity can be compromised (Claeyssen et al., 2023). They also appear together in the mitochondria-SR contact site (Tsikitis et al., 2018). αB-crystallin can have a cardioprotective quality control against development of heart failure in desmin null mice. Indeed, if the chaperone is overexpressed, it has been shown to protect the mitochondria from undergoing structural and functional changes, and thereby keeping it functional (Diokmetzidou et al., 2016). On the other hand, mutations in αB-crystallin result in desmin aggregate formation due to improper protein folding within the tissue and metabolic abnormalities (Maloyan et al., 2005; Rajasekaran et al., 2007). The intimate relationship between desmin and its chaperone provide the basis for correct cardiomyocyte structure and function since misfolded desmin proteins caused by poor chaperone activity can be the root cause of diseases (McLendon & Robbins, 2011). Indeed, the hallmark of desmin related myopathy, or desminopathy (OMIM#:601419), is aggregate formation. The composition of these aggregates has been studied and results show that they are composed of not only desmin and αB-crystallin, but also of many other proteins including synemin, laminin, actin, plectin to name a few. Mutations in both desmin and its chaperone cause similar diseases and phenotypes (Goldfarb & Dalakas, 2009; Tsikitis et al., 2018). Correct desmin assembly and folding is necessary for maintaining proper organelle positioning, including the mitochondria.

2.3.4 Mitochondria

The contraction and relaxation of the heart is energetically demanding. To fulfill these energy needs, desmin anchors and distributes mitochondria proximally to the myofibrils (Capetanaki et al., 2007; Elsnicova et al., 2022). Desmin filaments bring the mitochondria close to the sarcomeres, where the mitochondria are often found between myofibrils, thus ensuring that the produced ATP is near the contractile structures that require and utilize it (McLendon & Robbins, 2011; Milner et al., 2000). Calcium is important for regulating the production of ATP in mitochondria but is also important for proper excitation-contraction (Figure 8). Therefore, if mitochondrial function is altered in mutant cells, they have a limited ability to generate enough energy to support the cellular function. Consequently, the increased calcium causes an ionic imbalance and can result in arrhythmias and cardiomyopathy (Smolina et al., 2014).

Furthermore, if too much calcium is present in the cells, it can lead to cell death by apoptosis and autophagy (Schwarz & Leube, 2016).

The exact way by which desmin binds/interacts with mitochondria has not been fully deciphered although studies suggest that it interacts via the cytolinker plectin 1B (L. Winter et al., 2008). Recent reports suggest a direct interaction between the desmin and mitochondria through the N-terminal head of desmin (Dayal et al., 2020). Experiments in desmin null mice demonstrated a loss of mitochondrial organization and positioning as one of the first muscular consequences of the knock-out model. Mitochondria are no longer packed into long strands between the myofibrils but are rather clumped together and can be found in the subsarcolemmal space. Mitochondria in this model have been described as swollen and enlarged in size with irregular cristae, and increased in number (Milner et al., 1996, 2000). Consequently, respiratory activity and function, as well as mitochondrial protein expression, are affected in these mice (Fountoulakis et al., 2005). These changes become more pronounced over time as the mice age, but also if they exercise and exert more physical force (Milner et al., 2000). Later in life the ventricles of the mice dilate and they develop HCM and heart failure (Milner et al., 1999).

Mutations in *DES* have been described in patients suffering from cardiac and/or skeletal disorders. Understanding how and if mitochondrial positioning and function is involved in patient specific cases is relevant in order to assess the extent to which desmin plays a role in human health and disease. Mouse models have provided evidence of structural and functional consequences in desmin knock-out and mutant models, but they are not always representative of the human condition. Altered mitochondrial functioning has been observed in patients with mutations p.S13F (McCormick et al., 2015) and p.R454W (Kubánek et al., 2020). A patient with the desmin p.S13F mutation was reported to have HCM where mitochondrial function demonstrated a deficiency in complex I (part of the respiratory chain), along with smaller mitochondrial mass, as well as a reduced mitochondrial DNA (McCormick et al., 2015). Similar results were observed in the patient with the p.R454W desmin mutation although the patient had RCM as opposed to HCM (Kubánek et al., 2020). Here, mutations on both ends of the desmin filament have shown to impact cellular function and their consequences on patient health. The results from mice and patients' studies suggest that desmin filaments are necessary for proper intracellular architecture that can affect neighboring cells and intercellular connections. Desmin provides proper anchoring of mitochondria and other cellular organelles to maintain cellular integrity and function.

2.3.5 Intercalated Disc

IDs are responsible for mechanical as well as structural support of the heart thanks to the desmosomes, gap junctions and adherens junctions, that couple neighboring cardiomyocytes (1.4 Intercalated Discs). Desmin attaches to the desmosome via desmoplakin (Figure 12) (Nielsen et al., 2023). This connection is important not only for maintaining cardiomyocyte architectural integrity during contraction and relaxation, but also for transduction of mechanical signals between cells. Patients with desmoplakin mutations develop arrhythmogenic right ventricular dysplasia/cardiomyopathy (ARVD/C) (Z. Yang et al., 2006). Mouse models with mutant desmoplakin display decreased levels of the protein at the cell membrane. This change was associated with ventricular hypertrophy resulting in decreased cardiac function, higher cardiac fibrosis, but also loss of connection with desmin filaments (Z. Yang et al., 2006). In mutant mice, the lost connection between desmin and the desmosomes ultimately result in architectural changes of the ID that can help explain the cardiac consequences and arrhythmias in patients (Z. Yang et al., 2006) since the stability of the desmosome is compromised leading to a change in cell-to-cell coupling and communication. Furthermore, overexpression of mutant desmoplakin has shown to be lethal in developing mice and led to abnormalities in cardiac development (Z. Yang et al., 2006). Alternatively, if the desmin filaments are unable to attach properly at the IDs, ventricular conduction is compromised as a result of improper electrical coupling of cardiomyocytes. It was demonstrated in a mouse model, that some desmin mutations can lead to a reduction in the number of gap junctions, and that consequently leads to a decrease of Cx43 in the gap junctions due to their inability to localize properly (Cao et al., 2021; Gard et al., 2005; Noorman et al., 2009). Plectin is another important protein whose role is to help mediate the attachment between desmin and the Z-discs and desmosomes (Herrmann et al., 2020; Konieczny et al., 2008) at the IDs in cardiomyocytes. Furthermore, the proinflammatory cytokine, TNF-α, is not normally expressed in the myocardium of healthy patients, but has can been seen in patients with heart failure. TNF-α activates caspases that cleave desmin that consequently forms aggregates. In diseased hearts, desmin cleavage destabilizes the IDs, leads to cells death, and mitochondrial defects (Hol & Capetanaki, 2017; Panagopoulou et al., 2008).

Structural modifications within the IDs can explain some cardiomyopathies associated with desmin mutations. Losing the stable connection between cells not only affects their electrical coupling, but also the structural and mechanical coupling. The creation of a gap

between cardiomyocytes can be difficult to rescue and therefore remodeling of the cardiac tissue can take place.

2.4 ST-Segment Depression Syndrome

Bundgaard and colleagues identified a 36-year-old patient with nonischemic, persistent, and deep ST-segment depressions, visible on a 12-lead ECG (Figure 17) (Bundgaard et al., 2018). The patient developed atrial fibrillation in his mid-fifties and a few years later had ventricular fibrillation that led to aborted SCD (Bundgaard et al., 2018). In their study, they also describe patients from five unrelated families that suffered from similar cardiac symptoms such as fibrillation, tachycardia, arrhythmia, and aborted SCD (Christensen et al., 2022) but most notably with the presence of the persistent ST-segment depression.

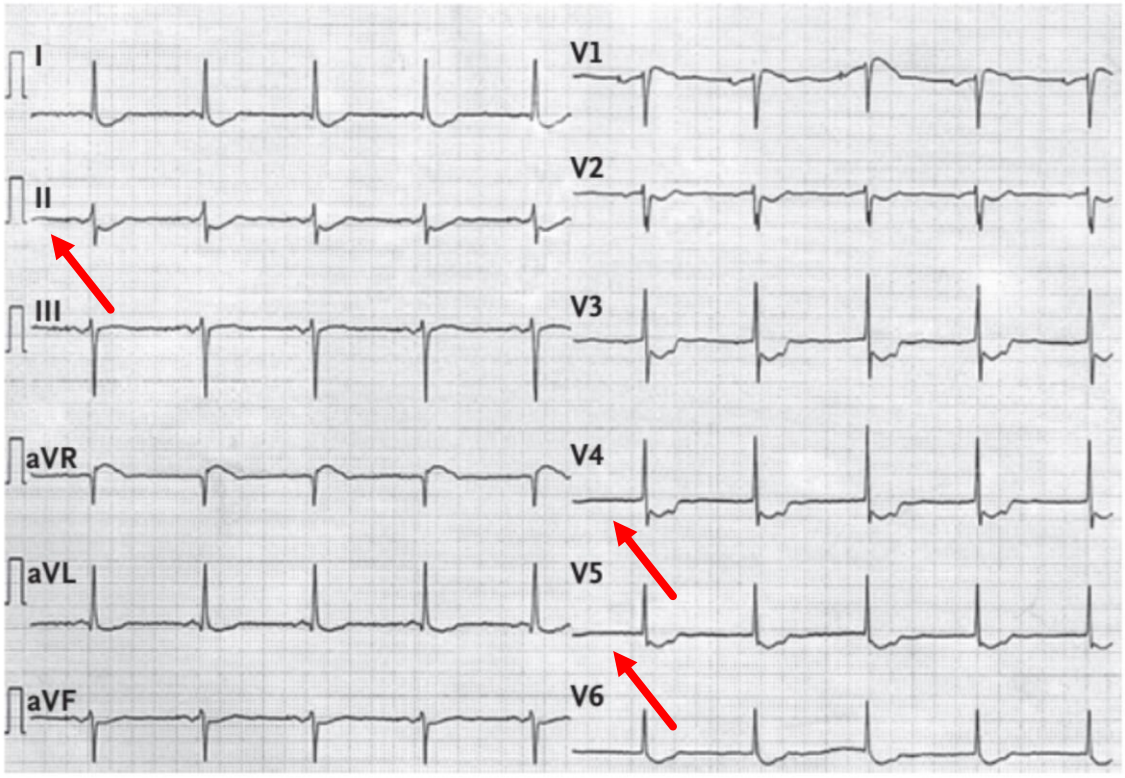

Figure 17. Electrocardiogram of patient with ST-segment depression syndrome.
Red arrows point to ECG leads where the depression of the ST-segment has been identified. This segment depression is persistent over time in patients with the syndrome (image modified from (Bundgaard et al., 2018)).

Genetic testing did not reveal mutations in genes associated with cardiac diseases, including *DES* (Bundgaard et al., 2018). The mode of inheritance was autosomal dominant

(Christensen et al., 2022). This arrhythmogenic disease was later given its name: ST-segment depression syndrome (STDS) with proposed diagnostic criteria in Table 4 (Christensen et al., 2021). Additional families have since been identified and diagnosed. Interestingly, biopsies from affected individuals demonstrated an enlargement of the nucleus and a decrease of myofibrils in the perinuclear space (Christensen et al., 2021).

Table 4. Proposed diagnostic criteria for patients with suspected ST-segment depression syndrome.
(table modified from (Christensen et al., 2022))

Probands	Relatives
Unexplained concave-upward ST-depression ≥0.1 mV in at least 4 leads (V3-V6 and I–III) 80 ms after J point	Unexplained concave-upward ST-depression ≥0.05 mV in at least 4 leads (V3–V6 and I–III) 80 ms after J point
ST-elevation ≥0.1 mV in aVR	
Common criteria for probands and relatives:	
No episodes of normalized ECG (i.e., persistent ECG pattern over time)	
Accentuation of ST depression during exercise	
Autosomal dominant pattern of inheritance	

2.5 Previous Reports of the Desmin p.R406W Mutation

The desmin p.R406W mutation is located in segment 2B and has been previously reported in patients with skeletal and/or cardiac myopathy. The primary focus will be on cardiac involvement, although skeletal muscle involvement has also reported in patients. This mutation was first described by Park and colleagues in a 24 year-old patient with AV block, with muscle biopsies that revealed aggregates (K.-Y. Park et al., 2000). Transfection studies of SW13 cells expressing this mutation confirmed formation of aggregates similar to the ones seen in the patient's muscle (Chourbagi et al., 2011; Goudeau et al., 2006; K.-Y. Park et al., 2000). Another patient in her second decade of life was reported by a different group with conduction defects and syncope with same results from muscle biopsy and SW13 transfection studies that demonstrated desmin-positive aggregates (Dalakas et al., 2000). Three new patients presenting with arrhythmia and AV block were positive for the desmin p.R406W mutation and presented

with the same muscle aggregate phenotype, and with an early onset of disease, at 15, 23, and 18 years of age (Dagvadorj et al., 2004). A protein structure predictive model showed that the mutation affects the ability of desmin to form a coiled-coil, most likely due to the change of the structural motif TY**R**KLLEGEESRI that is found in this section of segment 2B, and now changing to TY**W**KLLEGEESRI in patients (Dagvadorj et al., 2004). This change may have the ability to hinder dimer interactions between the head and tail of longitudinally assembling filaments and further impair their radial compaction (Bär et al., 2004). A salt bridge between the amino acids E401 and R406 (Figure 18) also seems to be affected by mutations and have a consequence on desmins binding ability with synemin (Chourbagi et al., 2011). In vitro assembly experiments demonstrated that longitudinal annealing of desmin p.R406W mutated filaments was impaired and they did not compact radially to the typical 10 nm diameter (Bär et al., 2005).

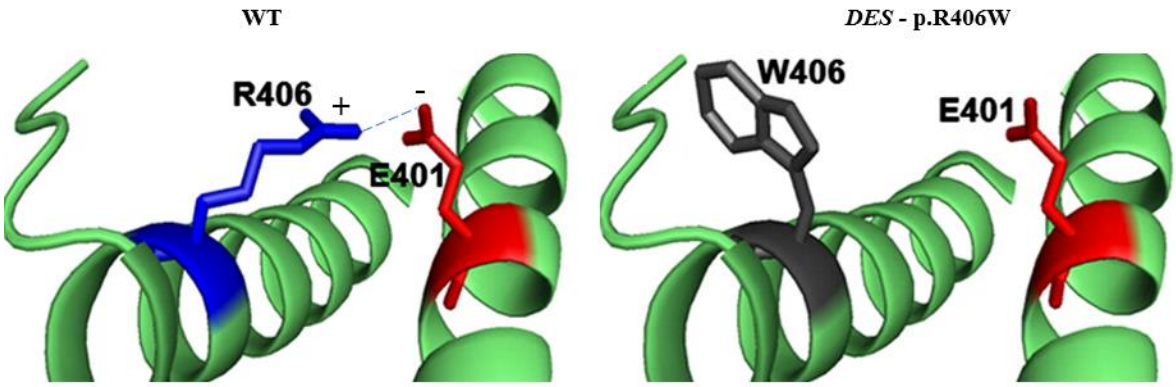

Figure 18. In silico modeling of the coiled-coil interactions in wild-type versus mutant (p.R406W) desmin filaments.
A salt bridge (left WT panel; dashed line) is created between amino acid residues E401 and R406 in segment 2B that is lost when replaced with a different amino acid residue (right panel; *DES* p.R406W) (image modified from (Chourbagi et al., 2011)).

Furthermore, a patient with disease onset at 18-years of age with the p.R406W desmin mutation was reported to have dilation of both atria with normal-sized ventricles and a slightly reduced left ventricular ejection fraction and documented sustained and non-sustained ventricular tachycardia. In this case, muscle biopsies from both ventricles were studied revealing fibrosis as well as hypertrophy of the myofibrils and skeletal muscle biopsies revealed aggregate deposits (Luethje et al., 2004). Another two patients, diagnosed at 15 and 27 years of age, were found to have right-bundle branch block (RBBB) and AV block, respectively, and

one of the patients was diagnosed with RCM (Arbustini et al., 2006). A myocardial sample obtained from one of the two patients depicted the same phenotype of aggregates in tissue (Arbustini et al., 2006).

A new case was reported of a patient with disease onset at 15 years of age with AV block, RCM, and SCD, 13 years after initial diagnosis. Aggregates were observed on biopsy samples of skeletal muscle (Olivé et al., 2004). A few other patients have been identified with this mutation including a patient diagnosed at 14 years of age and having AV block and atrial fibrillation (Wahbi et al., 2012), another with ACM (Kubánek et al., 2020), a patient with atrial fibrillation, left bundle branch block (LBBB) and RCM (Z. Chen et al., 2021), and an 8-year old patient with AV block and diagnosed with HCM (Oka et al., 2021). Overall, patients with the desmin p.R406W mutation show aggregate formation in both skeletal and cardiac muscle, early onset of disease between the first and third decade of life, and are typically diagnosed with some form of cardiomyopathy. Even though biopsies have been performed on both skeletal and cardiac tissue, a majority of the reports are from skeletal muscle biopsies due to the limited availability of cardiac samples.

The disease has also been modelled using cardiomyocytes derived from induced pluripotent stem cells (iPSC-CMs) transfected with a plasmid expressing the human desmin p.R406W variant. The study also demonstrated aggregate formation within the cells (Kubánek et al., 2020). AV block, AV and bifascicular bundle-branch block, tachycardia and RCM of a new 15-year old patient prompted Herrmann and colleagues to model the desmin disease in a p.R405W (ortholog to the human p.R406W desmin) desmin knock-in mouse model (Herrmann et al., 2020). Similar to the desmin knock-out studies, these mice were also viable and able to reproduce. Immunofluorescent staining of a LV sample from the patient revealed an absence of desmin signal at the IDs but also irregular staining of desmoplakin, which is typically where the two proteins colocalize. Furthermore, Cx43 and N-cadherin had irregular localization within the mutant heart. The observations from the mouse model recapitulated the aggregate phenotype in both cardiac and skeletal muscle samples. The most notable cardiac structural changes was the irregular distribution pattern of desmin at the Z-discs, as well as irregular IDs with irregular desmoplakin distribution. The irregular staining patterns of both desmoplakin and desmin resulted in disturbed IDs with poor cell to cell connections (Herrmann et al., 2020). This mutant specific modeling in the mouse elucidates how disturbances in the contact between cells via the desmosomes in the IDs is critical for cardiac function and that loss of this stable anchoring and scaffolding connection between organelles and the sarcolemma and extracellular

matrix can result in cardiac diseases, such as the ones found in the above-mentioned patients with the desmin p.R406W mutation. It may, in part, explain the electrical problems that can be due to changes in conduction and propagation of the electrical signal.

2.6 Models of Study

Over the years, several experimental models have been developed to study cardiac physiology and pathology, and have helped us understand the genotype-phenotype relationships. Multiple models have also been useful for testing the efficacy of pharmacological agents to provide new therapy and treatments for a multitude of diseases. Even though many cell and animal models are still successfully used today, they do not always recapitulate the precise disease phenotype, mainly due to the physiological differences between animals and humans. Researchers choose an appropriate experimental model based on the experimental question. For example, transfected human embryonic kidney (HEK) (H.-G. Wang et al., 2016) or Chinese hamster ovary (CHO) (Calloe et al., 2018) cell lines are often transfected and used to study single ion channels, such as the $Na_V1.5$ channel. Cell line models such as these provide information about activation and inactivation of a channel, to assess if a mutation causes gain or loss of function activity (Calloe et al., 2018), for example. The information gained from experiments using single cells can add to the knowledge of the cardiac phenotype found in a patient. Furthermore, pharmaceutical agents can be tested on these cells to observe their effects (Calloe et al., 2022). This kind of knowledge can also allow clinicians to propose new therapies, but it is not always possible using a single cell model.

Animal models including the fruit fly, zebrafish, rat, and dog, to name a few, have been used in studies in order to understand the pathogenic mechanisms behind cardiac diseases (Purevjav, 2019). As mentioned earlier, murine models (Herrmann et al., 2020) are helpful for understanding the structure-function relationships at play, but more on a whole animal level. Although animal models are frequently used in research today, studying diseases in the human context has necessitated the discovery and driven the research that employs the iPSC model (Yoshida & Yamanaka, 2017) that can be differentiated into cardiomyocytes (iPSC-CMs), among others (Oh et al., 2019). iPSC-CMs are versatile and can be applied to study different diseases using many techniques, including immunofluorescence (Kubánek et al., 2020) and recording action potentials (Verkerk et al., 2017). These cells have opened the door for personalized medicine since human iPSCs (hiPSCs) can be reprogrammed from patient cells and used directly for experiments (Oh et al., 2019) and therefore preserving the genetic

background. Likewise, it is possible to edit the genome of these cells with the use of CRISPR/Cas9 gene editing tools (Chun et al., 2018). These tools have created a unique opportunity to study and understand certain genotype-phenotype relationships by modelling them using specific patient samples.

The maturity of hiPSC-CMs has been disputed in the scientific community in part due to their electrical immaturity caused by the lack of I_{K1} (Bett et al., 2013; Verkerk et al., 2017) and the expression of mainly $Na_V1.5$ in its fetal isoform that results in a slower phase 0 of the AP (Figure 19) (Karbassi et al., 2020). Thus, the hiPSC-CMs immaturity is comparable to that of fetal cardiomyocytes (Wu et al., 2021). Indeed, the cells are typically round as opposed to the elongated brick-like shape of adult cardiomyocytes, they lack T-tubules, have spontaneous contractions, unorganized myofibrils, and different energy metabolism (glycolysis dependent as opposed to the fatty acids used for ATP production in mitochondria of adult cardiomyocytes) (Figure 19) (Bekhite & Schulze, 2021; Karbassi et al., 2020; Wu et al., 2021). Certain advances have been made such as adding triiodothyronine and dexamethasone into the maturation media, for example, to promote T-tubule development (L. Wang et al., 2021) or prolonging culture time. The patch clamp technique to measure APs of hiPSC-CMs has also been ameliorated through the implementation of the dynamic clamp approach that injects in silico I_{K1} in real time (Verkerk et al., 2017). This mimics the AP morphology of an adult ventricle cardiomyocyte more closely as opposed to standard methods since the maximum diastolic potential (MDP) can be set close to -90 mV, whereas the MDP is close to -60 mV in the absence of I_{K1} in hiPSC-CM (Karbassi et al., 2020; Verkerk et al., 2017). It has therefore become important to improve structural and functional maturity of hiPSC-CMs to ameliorate their properties to correctly model physiological aspects of human cardiomyocyte.

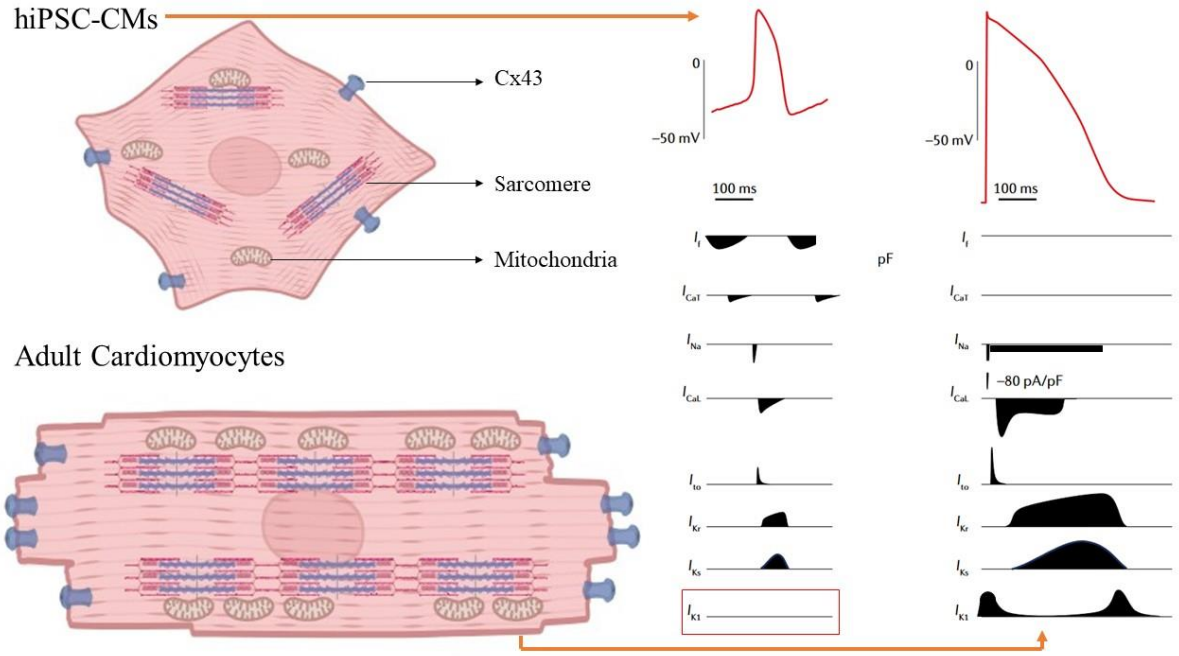

Figure 19. Differences between cardiomyocytes derived from hiPSCs and adult cardiomyocytes.
The structural properties and characteristics vary between adult cardiomyocytes and hiPSC-CMs (left panel), most notably, the sarcomere organization, number and location of mitochondria, as well as connexin 43 (Cx43) distribution. The electrophysiological characteristics are also different between the two cell types, mainly due to the lack of ion channels in hiPSC-CMs that alters the currents (right panel), such as I_{K1} highlighted in the red box (image created using BioRender.com and adapted from (Karbassi et al., 2020; Tani & Tohyama, 2022)).

Engineered heart tissues (EHTs) are created by molding hiPSC-CMs into a three-dimensional, band-like structure attached to silicone pillars on either end (Figure 20) (Eschenhagen et al., 2012). This technique was first described using neonatal rat cardiomyocytes (Zimmermann et al., 2002) and has since been applied to hiPSC-CMs in efforts to improve maturity and represent the complexity of the organ and its inter- and intracellular interactions (de Lange et al., 2021). EHTs have been used to model certain cardiomyopathies including HCM, DCM and ion channelopathies (Tani & Tohyama, 2022). They provide a novel way of studying the heart by mimicking the myocardium while keeping the desired genetic background of the patient or specific genotype according to the research question at hand. To imitate the ECM, a Matrigel matrix is often used as it contains collagen and laminin, and is mixed together with fibrinogen and thrombin which partake in the coagulation pathway (Eschenhagen et al., 2012; Mannhardt et al., 2016; Tani & Tohyama, 2022). Similar to the heart, EHTs can be a combination of specific cells containing 30% fibroblasts and around 70% hiPSC-

CMs (Tani & Tohyama, 2022), depending on the protocol. Although improvements have been made to this 3D model, one clear limitation of these tissues is the lack of vascularization.

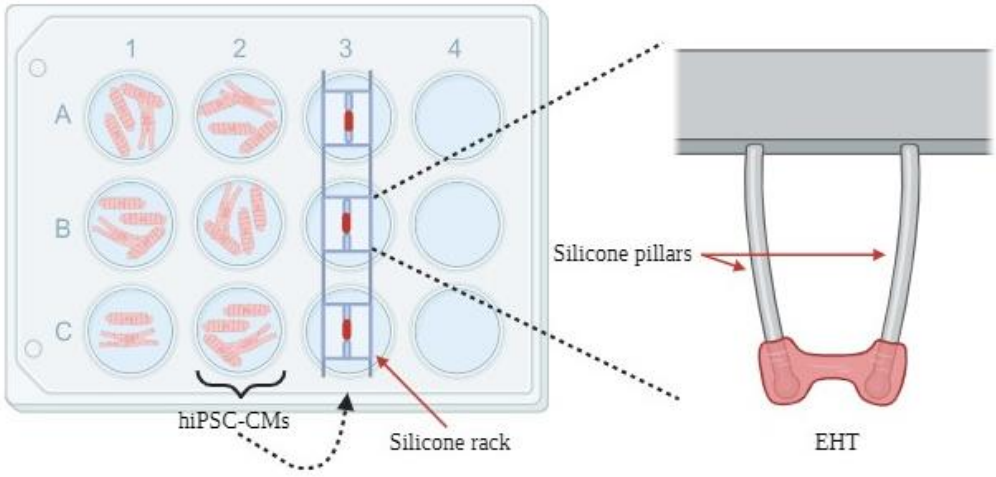

Figure 20. **Engineered heart tissue.**
Multiple three-dimensional EHTs can be created on a silicone rack using hiPSC-CMs (left panel) and molding them into a rectangular shape that is attached to silicone pillars on either end (right panel). The EHTs contract spontaneously but lack vascularization (image created using BioRender.com and adapted from (Eschenhagen et al., 2012)).

In certain aspects, 3D modeling has improved the maturity of the hiPSC-CMs to resemble the adult myocardium. Using this 3D construct, T-tubules have been shown to develop compared to the monolayer of hiPSC-CMs, as well as an improvement of Ca^{2+} handling with increased expression of RyR have been noted (de Lange et al., 2021). EHTs have improved structure and number of mitochondria which in turn mediates metabolic maturity while favoring oxidative metabolism as opposed to glycolysis that is often observed in 2D culture (Mannhardt et al., 2016; Ulmer et al., 2018). Furthermore, sarcomere alignment has been shown to be ameliorated (J. Liu et al., 2020), improved upstroke velocity of APs with increased I_{Na} density (Lemoine et al., 2017), and increased Cx43 throughout the cell membrane (Lemoine et al., 2017). Constant electrical stimulation of the EHTs with increased frequency over time (from 2 Hz to 6 Hz in the span of two weeks) demonstrated structural maturity of hiPSC-CMs in EHTs, mainly in their size that was comparable to adult-like cardiomyocytes, increased mitochondrial cristae, and improved calcium handling (Karbassi et al., 2020; Ronaldson-Bouchard et al., 2019). Although there is still a large window for improvement, 3D modeling holds great promise for modeling the heart in a human context as opposed to rodent models that are still frequently used.

Chapter III

Review

Review

Pathophysiological Mechanisms of Cardiomyopathies Induced by Desmin Gene Variants Located in the C-Terminus of Segment 2B

Michelle Geryk and Flavien Charpentier

Published in the *Journal of Cellular Physiology*

DOI: 10.1002/jcp.31254

Pathophysiological Mechanisms of Cardiomyopathies Induced by Desmin Gene Variants Located in the C-Terminus of Segment 2B

Michelle Geryk, Flavien Charpentier*

Nantes Université, CNRS, INSERM, L'institut du thorax, F-44000 Nantes, France.

ORCID: 0000-0001-9929-5192 (MG); 0000-0002-5057-0998 (FC)

Running title: Desmin Gene Variants and Cardiomyopathies

* **Correspondence:**

L'institut du thorax, Inserm UMR1087, CNRS UMR6291

IRS-UN, 8 quai Moncousu

44007 Nantes cedex 1, France

E-mail: flavien.charpentier@univ-nantes.fr

Tel. + 33 228 08 01 64

Author contributions

MG performed the literature search and drafted the manuscript. FC critically revised the manuscript. Both authors read and approved the final manuscript.

Abstract

Desmin, the most abundant intermediate filament in cardiomyocytes, plays a key role in maintaining cardiomyocyte structure by interconnecting intracellular organelles, and facilitating cardiomyocyte interactions with the extracellular matrix and neighboring cardiomyocytes. As a consequence, mutations in the desmin gene (*DES*) can lead to desminopathies, a group of diseases characterized by variable and often severe cardiomyopathies along with skeletal muscle disorders. The basic desmin intermediate filament structure is composed of four segments separated by linkers that further assemble into dimers, tetramers and eventually unit length filaments that compact radially to give the final form of the filament. Each step in this process is critical for proper filament formation and allow specific interactions within the cell. Mutations within the desmin gene can disrupt filament formation, as seen by aggregate formation, and thus have severe cardiac and skeletal outcomes, depending on the locus of the mutation. The focus of this review is to outline the cardiac molecular consequences of mutations located in the C-terminal part of segment 2B. This region is crucial for ensuring proper desmin filament formation and is a known hotspot for mutations that significantly impact cardiac function.

Key words

Desminopathy, cardiac arrhythmia, intermediate filament, cardiomyopathy

Statements and Declarations

Competing interests: the authors have no competing interests to declare that are relevant to the content of this article.

Introduction

Intermediate filaments (IFs) constitute one of the three protein networks within the cytoskeleton, alongside actin microfilaments and microtubules (Granger & Lazarides, 1979; Maggi et al., 2021). IFs play an important role in upholding the physical structure of cardiomyocytes, where they are responsible for the intricate connections between organelles, and provide mechanical strength and stability to the cell by forming a stress-resistant network (Lazarides, 1980; Tsikitis et al., 2018). The most abundant IF found in cardiomyocytes is desmin (OMIM: #125660), a muscle-specific IF whose role is to maintain the overall intracellular structure of these cells (Lazarides, 1980). Over the years, numerous genetic variants have been discovered in the desmin gene and found to affect cardiac structure and function, including electrical activity, ultimately leading to disease.

Cardiac diseases stemming from desmin mutations include arrhythmogenic cardiomyopathy (ACM) (Protonotarios et al., 2021), hypertrophic cardiomyopathy (HCM) (Harada et al., 2018; Oka et al., 2021), dilated cardiomyopathy (DCM) (Goudeau et al., 2006; Taylor et al., 2007; Zhao et al., 2015), left ventricular non-compaction (LVNC) (Miszalski-Jamka et al., 2017), and restrictive cardiomyopathy (RCM) (Arbustini et al., 2006; Chen et al., 2021; Herrmann et al., 2020; Olivé et al., 2004). These diseases are most often associated with atrial and ventricular tachyarrhythmias, as well as cardiac conduction defects such as atrioventricular block, leading to syncopal episodes or sudden cardiac death (SCD). The onset of the disease for the majority of patients is between the ages of 20-40 years (Strach et al., 2008), with some cases being diagnosed as early as the first decade of life (Oka et al., 2021). Mutation location has not been shown to be indicative of a particular cardiac disease, since different patients with the same mutation may display different symptoms and diseases, as well as different ages of onset. It is worth noting that cardiac involvement is one of the consequences of desmin mutations and patients may also have skeletal myopathy, creating a plethora of symptoms and complications (Kubánek et al., 2020; van Spaendonck-Zwarts et al., 2011). Some patients present with both skeletal and cardiac diseases, while others may have one or the other (Goldfarb et al., 2004).

In this review, we provide up-to-date insight into the pathophysiological mechanisms of cardiac diseases due to desmin mutations, with a focus on the C-terminal part of segment 2B between amino acid residues 350-406, which are a known locus for mutations linked to a wide range of cardiac disorders, although mutations have been identified in all parts of the desmin gene (Bär et al., 2007; Bär et al., 2010; Brodehl et al., 2022).

Structure and Function of Desmin Filaments

More than 73 IFs have been identified and are further divided into six groups. Desmin belongs to the type III IF group and is the most abundant IF in cardiomyocytes (Herrmann & Aebi, 2004; Tsikitis et al., 2018). In humans, a single gene (*DES*) mapped on chromosome 2 (2q35; Fig. 1a) codes for desmin and its 470 amino acids (Brodehl et al., 2018). IFs are responsible for controlling the mechanical and physical stress that is imparted onto cells, due to their demanding function, by forming an intricate three-dimensional lattice interconnecting and anchoring intracytoplasmic organelles, contractile apparatus, desmosomes and the cytoskeleton (Capetanaki et al., 2007).

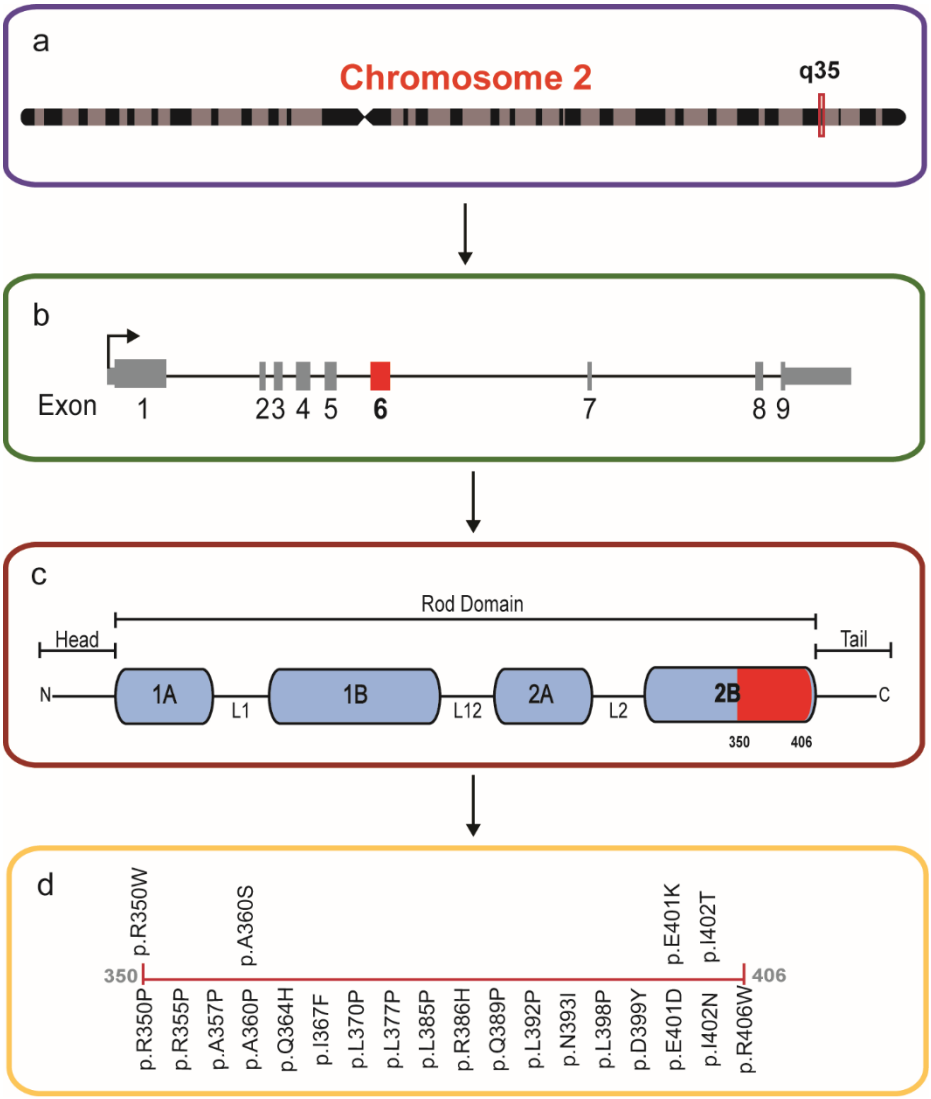

Fig. 1. The desmin gene, located on chromosome 2q35 (a), comprises 9 exons (b) that encode the final protein (c) containing a non-α-helical N-terminal head, an α-helical rod domain, and a non-α-helical C-terminal tail. The rod domain is made up of 4 segments, 1A, 1B, 2A, and segment 2B, with a significant number of disease-causing mutations identified in this region (Goudeau et al., 2006). These segments are interconnected by linkers L1, L12, and L2.

Mutations that are the focus of this article are located between amino acids 350-406, highlighted in red and listed at the bottom (d).

The central structure of desmin is an α-helical rod domain composed of four segments (coil 1A, 1B, 2A, and 2B) separated by three linkers (L1, L12, and L2). This structure is surrounded by a non-α-helical N-terminal head and a non-α-helical C-terminal tail (Fig. 1c), which are important for assembly of the filaments and organization of the IF network within the cell (Bär et al., 2010; Goudeau et al., 2001; Hnia et al., 2015; Li et al., 1989; Maggi et al., 2021; Sharma et al., 2009). There is a highly conserved YRKLLEGEE motif located on the C-terminal end of segment 2B (Herrmann et al., 2000). The tail end controls the diameter of filaments during their assembly along with the YRKLLEGEE motif that is needed for the formation of the proper coiled-coil structure of the terminal end of segment 2B (Bär et al., 2004, 2010; Eldirany et al., 2021; Herrmann et al., 2000). Correct assembly of filaments is imperative to ensure proper function. Briefly, rod domains of two monomers wrap around one another to form a coiled-coil resulting in a dimer. Two dimers then align in an antiparallel manner forming a tetramer. Eight tetramers align laterally and associate with one another forming a unit-length filament (ULF) which aligns end-to-end with other ULFs and undergoes radial compaction decreasing the diameter of the filament from 16 nm to 10 nm (Dutour-Provenzano & Etienne-Manneville, 2021; Hnia et al., 2015).

The desmin network plays a key role in structural integrity, mechano-transduction and mechano-sensation of muscle cells. It traverses the cardiomyocyte and forms interactions along the way from laterally linking and aligning myofibrils at the Z-disks (Bär et al., 2004; Granger & Lazarides, 1979; Huang et al., 2002; Noureddine & Gehmlich, 2023) to connecting the contractile apparatus to the nucleus, mitochondria, T-tubules, and the sarcolemma at the level of costamers (Bär et al., 2004; Brodehl et al., 2018; Dalakas et al., 2000; Lazarides, 1978; Spörrer et al., 2022). Desmin interacts with the desmosomes of the intercalated disks through desmoplakin which helps dampen the generated forces and tension from every cardiac contraction (Dalakas et al., 2000; Lapouge et al., 2006). The desmin network also connects to a variety of proteins such as αB-crystallin at the Z-disks, allowing desmin to provide protection against mechanical stress-induced damage (Djabali et al., 1997; Goudeau et al., 2001). Likewise, desmin interacts with synemin, a type IV intermediate filament, which links desmin filaments to costamers. Interestingly, gene variants of synemin have also been associated with DCM (Maggi et al., 2021; Paulin et al., 2020). Desmin also plays a key role in connecting the cytoskeleton to the nucleoskeleton via its binding to nesprin 3 mediated by the giant linker protein plectin. Nesprin 3, which is located in the outer nuclear membrane, is a protein of the

linker of nucleoskeleton and cytoskeleton complex (LINC) which couples cytoskeletal proteins to proteins of the nuclear lamina, such as lamin A/C (Maggi et al., 2021). The interactions between the desmin and the lamin networks not only determine the proper positioning and shape of the nucleus, but also participate to the nuclear mechanotransduction and force-dependent gene transcriptional regulation (for detailed reviews, see Coscarella et al., 2023; Lityagina & Dobreva, 2021; West et al., 2023). It is not surprising that mutations in desmin can have detrimental roles knowing that the IF network in cardiomyocytes is so extensive. To study the structural and functional consequences of those mutations, several models have been used over the years.

Mouse models have been a useful tool for understanding the role of desmin in cardiomyocytes. Desmin knock-out (*Des*$^{-/-}$) mice have been used to study the consequences of fully deleting the *Des* gene, some of them being calcifications within the heart and degeneration of myocytes (Balogh et al., 2002; Li et al., 1996). Interestingly enough, it has been shown that desmin is not necessary for muscle development since *Des*$^{-/-}$ mice are viable and can reproduce (Li et al., 1996; Milner et al., 1999) even though the hearts of these mice have structural abnormalities including lack of myofibril lateral alignment, altered mechanical stability at the intercalated disk, as well as improper positioning and organization of mitochondria and nucleus that can all possibly contribute to cardiomyocyte hypertrophy, ventricular dilatation and impaired systolic function (Mavroidis et al., 2015; Milner et al., 1999; Thornell et al., 1997). Interestingly, in baseline conditions, *Des*$^{-/-}$ mice do not exhibit the atrioventricular conduction blocks often seen in human desminopathies (Mavroidis et al., 2015, 2020; Schrickel et al., 2010), although one study showed a moderate prolongation of the PR interval (Mavroidis et al., 2020). However, atrioventricular block was observed in *Des*$^{-/-}$ mice during endurance exercising (Mavroidis et al., 2015). *Des*$^{-/-}$ mice also exhibit slightly slower conduction in the ventricles. Similar results were obtained in a transgenic mouse model of human desmin-related cardiomyopathy with cardiac specific overexpression of the p.R173_E179del mutation (Gard et al., 2005). These results are most likely explained by abnormal connexin 43 (Cx43) expression at the intercalated disks. Indeed, within intercalated disks, desmin has been shown to associate with connexin 43 (Cx43) and a decrease in Cx43 expression at the intercalated disks is observed when desmin levels are reduced, which decreases electrical coupling between cells (Cao et al., 2021; Gard et al., 2005).

Concerning ventricular tachyarrhythmias, results obtained in *Des*$^{-/-}$ mice differ between studies, with one study showing that *Des*$^{-/-}$ mice are less prone to pacing-induced ventricular

arrhythmias than wildtype mice (Schrickel et al., 2010), while other studies showed higher incidence of spontaneous ventricular premature beats in *Des*$^{-/-}$ mice (Mavroidis et al., 2015; Mavroidis et al., 2020). *Des*$^{-/-}$ mice are also more prone to spontaneous supraventricular arrhythmias (Mavroidis et al., 2015; Mavroidis et al., 2020) and pacing-induced atrial fibrillation (Schrickel et al., 2010).

In addition to cardiomyocyte structural, electrophysiological, and contractile defects, desmin deficiency also leads to metabolic disorders. Indeed, in parallel to improper localization of mitochondria, as well as ultrastructural mitochondrial defects, desmin knock-out mice are also characterized by severely impaired oxidative phosphorylation and fatty and amino acid metabolism due to severe remodeling of the expression of mitochondrial proteins (Elsnicova et al., 2022). Loss of mitochondrial spatial organization associated with decreased metabolic capacity of mitochondrial respiratory chain complexes have also been shown in patients with *DES* variants (Kubánek et al., 2020). When studying how the p.E439K desmin variant may affect mitochondria in cardiomyocytes derived from human induced pluripotent stem cells (iPSC-CMs), Hovhannisyan *et al.* concluded that not only are mitochondria physically altered but also functionally. The study demonstrated fewer cristae that could explain the decrease in the expression of COXIV, a mitochondrial respiratory chain protein (Hovhannisyan et al., 2024). Furthermore, RNA sequencing showed that iPSC-CMs with the E439K mutation show downregulation of genes that are related to mitochondria, compared to control cells (Hovhannisyan et al., 2024). Mitochondrial alterations in desmin mutant and null cells have been the focus of many studies and reviews suggesting that respiration parameters tend to decrease which can be one explanation for cardiomyocyte dysfunction and altered functionality (Alam et al., 2018; Maggi et al., 2021; Smolina et al., 2020). Consistent with a major pathogenetic role of mitochondrial dysfunction, reducing the oxidative stress (Rapti et al., 2017) or improving mitochondrial function (Diokmetzidou et al., 2016; Weisleder et al., 2004) has been shown to improve cardiac function of desmin knock-in mice.

Focusing on coil 2B, desmin knock-in mice have been employed to replicate human missense mutations including the p.R350P mutation, with the mouse ortholog being p.R349P. These mice have successfully mimicked the human pathology. Specifically, the mouse hearts exhibit the formation of protein aggregates, DCM, conduction abnormalities, higher susceptibility to atrial and ventricular tachyarrhythmias, along with skeletal muscle weakness, mirroring the clinical manifestations of the patients (Clemen et al., 2015; Stöckigt et al., 2020). Knock in mouse models carrying the p.R405W mutation, the orthologous counterpart to the

human p.R406W mutation, or the p.R349P mutation have challenged our understanding of these mutations. These models not only depicted how disruption of the IF network increases mechanical sensitivity due to myofibril disorganization, as discussed earlier, but also shed light on the impact of desmin deficiency at the intercalated disk in the entire heart, ultimately resulting in cardiomyopathy (Clemen et al., 2015; Diermeier et al., 2017; Herrmann et al., 2020). Unfortunately, to the best of our knowledge, electrocardiogram (ECG) recordings or other electrophysiological experiments were not performed on the p.R405W knock-in mice.

Overall, both knock-in and knock-out models have illustrated the importance of desmin IFs within cardiomyocytes and in both models, there were structural and functional consequences, such as altered mitochondrial shape, number and positioning in relation to myofibers (Agbulut et al., 1996; Capetanaki et al., 1997; Stöckigt et al., 2020).

In addition to mouse model, a few studies have used the zebrafish model (Vogel et al., 2009), which exhibits a desmin tissue distribution comparable to humans. These studies aimed to elucidate the role of desmin in cardiac development and function. In contrast to humans, two desmin paralogs sharing >80% similarity in protein sequences with the human gene (*desma* and *desmb*) exist in zebrafish and show differential spatiotemporal expression during zebrafish embryonic and larval development. Vogel *et al.* showed that zebrafish embryos injected with a morpholino targeting desmin mRNAs exhibited a reduced number of sarcomeric units, which were also thinner, and a widening and misalignment of Z-disks, as observed in desmin-deficient mice. Desmin-deficient zebrafish embryos also showed sinus bradycardia. Although the study showed no evidence of atrioventricular block, this result is interesting knowing that patients with desmin-related cardiomyopathies often exhibit anomalies of their cardiac conduction system (Vogel et al., 2009). More recently, Ramspacher *et al.* used genetically engineered zebrafish models to compare the effect of desmin aggregate formation and desmin loss of function. They found abnormal embryonic heart contractility in the absence of desmin and in the presence of desmin aggregates. This was at least partly explained by an altered morphology of sarcoplasmic reticulum and an abnormal localization and clustering of ryanodine receptors, leading to impaired calcium signaling (Ramspacher et al., 2015).

In the past, cellular models used for studying structural and functional consequences of desmin gene variants were limited to various cell lines such as H9C2, HT-1080 or SW-13 lines. Recently, different studies have used iPSC-CMs to elucidate the functional consequences of three novel variants located in coil 1, the p.Y122C variant associated to arrhythmogenic cardiomyopathy, the p.Y122H variant associated to RCM (Brodehl, Hakimi, et al., 2019) and

the p.L115I variant associated to biventricular ACM (Protonotarios et al., 2021), and one variant (p.A337P) located in coil 2 and associated to LVNC (Kulikova et al., 2021). It is regrettable that those studies used control iPSC-CMs in which plasmids encoding wildtype or mutant desmin were overexpressed. rather than using the full potential of the model by comparing iPSC-CMs from patients with desmin mutations and their isogenic controls (or vice versa). Yet iPSC-CMs from a patient with DCM had been used as early as 2013 (Tse et al., 2013) to investigate the effects of the p.A285V-DES variant identified in this patient. The variant was shown to induce desmin aggregation and Z-disk streaming. Nevertheless, those recent studies confirmed results obtained in SW-13 and/or HT-1080 and showed that these variants were indeed pathogenic, all leading to desmin aggregation. The same approach was used by Kubanek and co-workers to investigate the pathogenicity of 6 *DES* variants identified in 6 probands from a cohort of patients with cardiomyopathies of unexplained etiology (Kubánek et al., 2020). Desmin aggregates were observed in iPSC-CMs and HT-1080 cells transfected with the p.K43E variant, previously classified as variant of unknown significance (VUS), and the p.R406W variant, but not in cells transfected with the newly identified p.Q364H variant, consistent with observations in patient cardiac and/or muscle biopsies. However, no aggregates were observed in iPSC-CMs (and HT-1080 cells) transfected with the p.S57L, p.A210D and p.R454W variants, although they were observed in patient biopsies (Kubánek et al., 2020). This highlights some of the limitations of this model, which unfortunately has not been explored in greater depth. A deeper investigation of transfected iPSC model has been performed by Brodehl and co-workers who investigated the structural consequences of 34 VUS located in desmin 1A subdomain. This study allowed the re-classification of 14 VUS as likely pathogenic variants, which is important for the appropriate management of patients carrying these variants. Interestingly, all variants leading to abnormal desmin filaments assembly were located in the N-terminal part of coil 1A, suggesting that this region is another hot spot for pathogenic mutations (Brodehl et al., 2022). Therefore, despite limitations, this approach seems appropriate to perform large functional screening of *DES* gene VUS.

Desmin Mutations in Coil 2B and their Consequences

The structural organization and formation of desmin filaments play an instrumental role in disease onset and progression. The highly conserved filament is composed of various coils and linkers, as described above, and they all play a role in stability and function of mature filaments (Goudeau et al., 2001; Herrmann et al., 2000). It has been shown that the C-terminal end of the coil is responsible for radial compaction as well as forming links between tetramers

(Herrmann et al., 2000). A majority of the known desmin mutations are located in segment 2B, mostly with an autosomal dominant inheritance pattern (Goldfarb & Dalakas, 2009; Goudeau et al., 2006; Harada et al., 2018), which is why this is a region of high interest for many studies.

As mentioned earlier, the last 32 residues in coil 2B are highly conserved among species and play a crucial role in mediating interactions between dimers, ensure proper IF formation and compaction to attain the precise filament size (Herrmann et al., 2000; Strelkov et al., 2002). To assess the importance of these residues and the YRKLLEGEE motif, Herrmann *et al.* conducted experiments involving the removal of a part of the motif. They showed that rather than forming a filamentous network, desmin formed aggregates as well as short and thin filaments that loosely attached to nearby fibrils (Herrmann et al., 2000). In comparison to wild-type desmin, the truncated desmin IF formed thicker, less compacted filaments, resulting in a loss of flexibility and changes in the strength of interactions with intracellular organelles within the cell (Goldfarb & Dalakas, 2009; Herrmann et al., 2000; Strelkov et al., 2002). The reduced length and loss of flexibility of desmin IFs are consequential to cardiac function, impeding cardiomyocyte contraction and altering intracellular function and communication.

Over the years, more than 30 mutations, mostly missense, have been identified within the 120 amino acids that form coil 2B, and associated with various cardiac disorders (Cunningham et al., 2022). Of importance, amino acids at positions 350 to 406 of this segment are a hotspot for accumulating point mutations. This region is evolutionarily highly conserved, has been subject of extensive research over the years and is interesting to investigate because of the diversity of cardiomyopathies that can arise solely from mutations in this specific location (Fig. 2). Mutations in other parts of desmin, including hot spots, have been previously reviewed in detail (Brodehl et al., 2018, 2022; Tsikitis et al., 2018). Proline has been shown to act as an α-helix and β-sheet breaker by introducing kinks in the backbone of the helix. In addition, the inability of proline to form stabilizing hydrogen bonds contributes to lower flexibility in the coils (Bär, Fischer, et al., 2005; Li, Goto, et al., 1996; Olivé et al., 2007). A majority of the mutations found in this region involve the substitution of other amino acids with prolines (Table 1). Indeed, Goudeau *et al*. used the C2.7 cell line, MCF7 cell line, and the SW13 cell line to demonstrate that overexpression of the p.Q389P desmin IF results in aggregate formation (Goudeau et al., 2001), while Dalakas *et al.* transfected SW13 cells with the p.A360P mutant and observed the formation of "*short, thick, and kinked irregular structures*" within the cells (Dalakas et al., 2000). Muscle biopsies from a patient deemed to have a "disabling disease" and carrying the p.L392P desmin mutation were analyzed, revealing the presence of aggregates

(Olivé et al., 2007). However, not all amino acid substitutions by proline act the same, as demonstrated by *in vitro* assembly experiments involving mutations p.R350P, p.A357P, p.A360P, p.L370P, p.L385P and p.Q389P (Bär, Mucke, et al., 2005). Aggregate formation and irregular filaments were observed for all six mentioned mutations, but their structural organization varied. Desmin IFs with p.A360P and p.Q389P mutations stuck together with some observations of branching and "kink" formation, whereas desmin IFs with the p.L385P mutation could form some ULFs but radial compaction and longitudinal annealing were absent, resulting in the formation of short filament structures (Bär, Mucke, et al., 2005). The desmin p.A357P mutation has been said to generate "sticky" IFs in the way that the filaments clustered together to form large aggregates (Bär, Mucke, et al., 2005). Interestingly enough, the above mentioned mutants could form filaments to a certain extent, but mutations p.R350P and p.L370P in desmin had difficulties initiating and forming ULFs and proceeded to break apart into small aggregate clusters (Bär, Mucke, et al., 2005). The desmin mutation p.L398P has been classified as a VUS by Minoche *et al*. (Minoche et al., 2019). However, the same mutation was identified by another group in a patient with non-compaction cardiomyopathy (Van Waning et al., 2018) and *in vitro* studies have confirmed that it forms aggregates (Brodehl, Ebbinghaus, et al., 2019). Finally, a p.L377P mutation was found in a patient who showed no significant findings on the ECG yet imaging revealed myocardial lesions, and hypertrophy of the left ventricle was identified (Strach et al., 2008). To the best of our knowledge, no *in vitro* studies have been performed on this mutation to confirm its pathogenicity. Although these results demonstrate that these mutations lead to formation of desmin aggregates which are often found in patient skeletal and cardiac biopsies, the role of these aggregates has not been elucidated. It is unfortunate that many variants have not been studied in other models, for example iPSC-CMs, that could potentially describe the genotype-phenotype relationship. Furthermore, studies with cells such as the commonly used SW13 cells, rarely allow us to understand the pathophysiological significance of these genetic variants and IF contribution to the pathology and development of it.

Studying individual cells *in vitro* gives us insight into the consequences of the disorganization of a single cell, but it is unrepresentative of the heart as a whole and how cells work together. In order to better understand how a single mutation affects the heart, different models are employed to recapitulate the pathology of a patient, such as mouse models.

The p.R350P mutation has been examined in various related patients presenting with variable degrees of myopathy ranging from mild weakness of distal muscles to severe and

generalized myopathy. Surprisingly, some family members carrying the same mutation as the proband, did not present with any signs of myopathy (Bär, Fischer, et al., 2005; Strach et al., 2008). A number of patients also showed variable degrees of dyspnea. Similarly, some patients had no signs of cardiomyopathy while others exhibited cardiac hypertrophy associated with severe dyspnea and in certain cases leading to progressive or acute cardio-respiratory failure (Bär, Fischer, et al., 2005). In these patients, cardiomyopathy was sometimes associated with atrioventricular conduction disorders, as well as tachyarrhythmias (Bär, Fischer, et al., 2005). Interestingly, in the families reported by Strach and co-workers, ECGs were found to be normal although unexplored putatively affected siblings had died of SCD (Strach et al., 2008). In muscle biopsies, cell models or *in vitro* assembly studies, aggregate formation was the most observed trend. Using a knock-in mouse model carrying the equivalent p.R349P mutation, it was observed that the phenotype was more uniform: the mutation induced moderate cardiac structural changes, *i.e.*, a mild increase in myocardial fibrosis, without functional consequences but with higher susceptibility to spontaneous and induced arrhythmias. Of particular interest is that knock-in mice were more sensitive to blood pressure overload than wild-type mice, with a more severe deterioration of cardiac function, increased incidence of conduction disorders, including second degree atrioventricular block, higher susceptibility to triggered atrial fibrillation and ventricular tachycardia, and a reduced number of functional mitochondria (Stöckigt et al., 2020). Although these knock-in mice can model the consequences of the p.R350P mutation, they are limited in providing evidence for how the mutation causes these effects. Further functional studies are critical in order to provide better insight into the molecular cause of the disorders. Studying these mice during development might hint at the role of desmin in health and disease and likewise provide a better understanding of the physiological role of IFs. Three-dimensional skeletal muscle microtissues were constructed from stem cells comparing wild type desmin to p.R350P mutant concluding that the mutant tissue deteriorated and broke during tetanic stimulation with observed spontaneous contractions during non-stimulated periods (Spörrer et al., 2022). These functional studies, together with the reports on p.R350P desmin structure (Bär, Fischer, et al., 2005; Bär, Mucke, et al., 2005), elucidate that diseased cardiac tissue and the variable cardiac symptoms, arrhythmias and cardiomyopathies, can be attributed to IF aggregate formation in cardiomyocytes that no longer provide a protective structural mechanism within the cell during the highly stressful cardiac contraction, preventing the preservation of cardiomyocytes integrity.

Concerning the pathophysiological consequences of desmin p.R355P mutation, muscle biopsies uncovered desmin aggregates from a patient with progressive muscle weakness and

suffering from left atrium enlargement, sinus bradycardia and atrioventricular block, necessitating dual chamber pacemaking (Fidziańska et al., 2005), while another unrelated patient developed bifascicular block in his twenties (Wahbi et al., 2012). Similarly, patients with the p.L370P (Arias et al., 2006) or p.L392P (Olivé et al., 2007) mutations had skeletal muscle weakness as well as variable cardiac dysfunctions, most notably HCM (Olivé et al., 2007), which can likely be attributed to protein aggregates found in muscle biopsies (Arias et al., 2006; Maerkens et al., 2013; Olivé et al., 2007). Of note, aggregates are not only composed of desmin, but rather a mixture with its binding partners such as vimentin and αβ-crystallin (Maerkens et al., 2013). The interactions between desmin and its various binding partners needs be explored in further detail to potentially determine the root of the problem, mainly to determine what initiates the formation of aggregates. Furthermore, these patients also exhibited supraventricular tachyarrhythmias, atrial fibrillation (Arias et al., 2006) or atrioventricular block (Olivé et al., 2007). Interestingly, the p.L370P mutation is also associated to a high familial incidence of sudden death in young adults who, unlike the proband, have not been genotyped (Arias et al., 2006). However, the molecular mechanisms of these arrhythmias remain to be determined. Whether or not desmin mutations directly affect ion channel sarcolemmal expression and/or function is currently unknown. For instance, the impact of desmin mutations on ion channels expressed at the intercalated disks, besides connexin 43 (Cao et al., 2021), such as $Na_V1.5$ or Kir2.1, which highly contribute to cardiac conduction (Shy et al., 2013; Vermij et al., 2017), is still unknown. Alternatively, it can be hypothesized that altered nucleus mechanotransduction secondary to desmin mutations might affect the transcriptional regulation of ion channel expression but, to the best of our knowledge, this has not been investigated.

From the multiple proline substitutions at different locations within the desmin gene, we can observe a trend where aggregate formation is reported whether it is in *in vitro* cell studies or observed in muscle biopsies from patients. But proline substitutions are not the only ones that lead to these outcomes. Additionally, many other types of missense mutations have been identified in coil 2B as associated with desminopathy (Table 1).

393 **Table 1.** List of missense mutations located on the desmin gene positioned between amino-
394 acids 350-406 and reported cardiac disorders.

Mutation	Cardiac consequences, symptoms	References
p.R350P	HCM, AV conduction defects, tachyarrhythmias, dyspnea, SCD	Bär, Fischer et al., 2005; Bär, Mucke, et al., 2005; Clemen et al., 2015; Diermeier et al., 2017; Fischer et al., 2008; Spörrer et al., 2022; Stöckigt et al., 2020; Strach et al., 2008; Walter et al., 2007
p.R350W	DCM	Andreasen et al., 2013; Taylor et al., 2007
p.R355P	AV conduction defects, AF, syncope	Fidziańska et al., 2005; Hong et al., 2011; Wahbi et al., 2012
p.A357P	dyspnea	Bär, Mucke et al., 2005; Chourbagi et al., 2011; Dagvadorj et al., 2003
p.A360P	RCM, AV conduction defects, syncope, SCD	Bär, Mucke et al., 2005; Dalakas et al., 2000; Goldfarb et al., 1998; Goudeau et al., 2006; Kreplak & Bär, 2009
p.A360S	LVNC	Miszalski-Jamka et al., 2017
p.Q364H	LVNC	Kubánek et al., 2020
p.I367F	HCM, RCM, dyspnea	Fischer et al., 2008; Olivé et al., 2007; Olivé et al., 2011; Ripoll-Vera et al., 2015)
p.L370P	DCM, HCM, SVT	Arias et al., 2006; Bär, Mucke et al., 2005; Chourbagi et al., 2011; Dagvadorj et al., 2003; Olivé et al., 2011; Yu et al., 2017
p.L377P	HCM	Fischer et al., 2008; Strach et al., 2008
p.L385P	Mild ventricular dilation, AV conduction defects	Bär, Mucke et al., 2005; Sugawara et al., 2000
p.R386H	DCM	Zhao et al., 2015
p.Q389P	AV conduction defects	Bär, Mucke et al., 2005; Chourbagi et al., 2011; Goudeau et al., 2001; Kreplak & Bär, 2009
p.L392P	HCM, AV conduction defects	Maerkens et al., 2013; Olivé et al., 2007; Olivé et al., 2011
p.N393I	AV conduction defects	Bär, Mucke et al., 2005; Dalakas et al., 2000; Goldfarb et al., 1998; Goudeau et al., 2006
p.L398P	DCM, noncompaction cardiomyopathy	Brodehl, Ebbinghaus et al., 2019; Minoche et al., 2019; Van Waning et al., 2018
p.D399Y	DCM, AV conduction defects	Bär, Mucke et al., 2005; Chourbagi et al., 2011; Fischer et al., 2008; Fokstuen et al., 2016; Goudeau et al., 2006; Kreplak & Bär, 2009; Maerkens et al., 2013
p.E401D	ACM, AV conduction defects, syncope, SCD	Bermúdez-Jiménez et al., 2018; Chourbagi et al., 2011; Segura-Rodríguez et al., 2020

p.E401K	DCM, ACM, AV conduction defects, syncope	Bermúdez-Jiménez et al., 2018; Chourbagi et al., 2011; Fischer et al., 2021; Goudeau et al., 2006
p.I402N	DCM, arrhythmias, SCD	Weihl et al., 2015
p.I402T	DCM, AV conduction defects, ventricular tachyarrhythmias	B. Fischer et al., 2021
p.R406W	DCM, ACM, HCM, RCM, conduction defects, AF, VT, syncope, SCD	Arbustini et al., 2006; Bär, Mucke, et al., 2005; Chen et al., 2021; Chourbagi et al., 2011; Dagvadorj et al., 2004; Dalakas et al., 2000; Fischer et al., 2008; Goudeau et al., 2006; Herrmann et al., 2020; Kubánek et al., 2020; Luethje et al., 2004; Oka et al., 2021; Olivé et al., 2004; Park et al., 2000; Takegami et al., 2023; Wahbi et al., 2012

Abbreviations: ACM, arrhythmogenic cardiomyopathy; AF, atrial fibrillation; AV, atrioventricular; DCM, dilated cardiomyopathy; HCM, hypertrophic cardiomyopathy; RCM, restrictive cardiomyopathy; SCD, sudden cardiac death; SVT, supraventricular tachyarrhythmias; VT, ventricular tachyarrhythmias.

Among them, p.R350W, p.D399Y, p.E401K, p.E401D, p.I402T and p.R406W also lead to formation of aggregates inside the cells whereas p.N393I does not. The severity as well as the overall structure of the aggregates vary from one mutation to the next but ultimately there is a lack of proper filament formation. In addition to missense mutations, two deletions, p.E359_S361del and p.N366del, have been identified in the C-terminal part of coil 2B (Kaminska et al., 2004). The first deletion was associated with adult-onset progressive myopathy without cardiac defects, while the second one was associated with a similar myopathy but also late development of a cardiomyopathy characterized by cardiac conduction block and respiratory insufficiency. The two mutations affected the ability of desmin to form functional filaments, leading to desmin aggregates and disorganized clusters scattered throughout the cytoplasm. Finally, an indel mutation (p.M349_R355delinsG) has been identified in a Chinese family with complete atrioventricular block, without clinical signs of structural disease, and mild skeletal myopathy (Cao et al., 2013). Aggregate formation is well documented in multiple studies, yet it is still unsure how they contribute to disease. Another unexplored avenue is the distinction between skeletal and cardiac myopathy and how/why some mutations lead to one or the other, or in certain cases, to both myopathies.

Interestingly enough, all the above-mentioned missense mutations are located at the C-terminal end of segment 2B (Fig. 1c). An RCM diagnosis has been made in patients with the p.R406W mutation (Olivé et al., 2004) as well as in patients with p.L392P and p.I367F desmin mutations (Olivé et al., 2007). Mutations in desmin at position R350W can likewise lead to DCM with no skeletal involvement (Taylor et al., 2007). Rare cases of LVNC in patients with p.A360S mutation in desmin have also been observed (Miszalski-Jamka et al., 2017). Additionally, the p.E401D mutation has been found in a family with ARVC in which histological analysis on human cardiac tissue showed an increase in intercellular space and fibrillar connective tissue (Segura-Rodríguez et al., 2020). Among these, LVNC has been associated with 3 different mutations, RCM with 4, ACM with 3, and HCM with 6. DCM is the most reported cardiomyopathy among patients, associated with 9 different mutations (Fig. 2). Unfortunately, not all patient cases provided information on a specific cardiomyopathy, nor have they been assessed in cellular or animal experiments. Of note, some mutations can manifest with multiple phenotypes (Fig. 2). For example, HCM was found in a patient carrying the p.I367F desmin mutation, while a different patient with the same mutation exhibited RCM. This underlines that the location of the mutation does not necessarily predict the

cardiomyopathy or clinical outcome and that it would be important to explore the differences to potentially identify a potential treatment for patients.

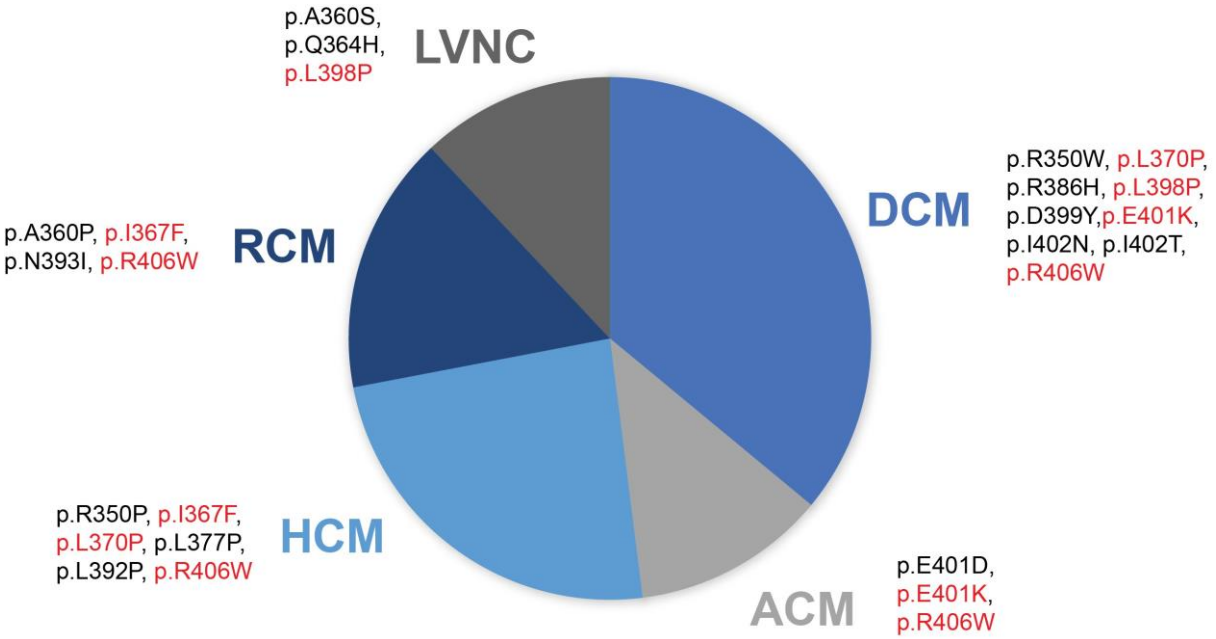

Fig. 2. Five distinct cardiomyopathies have been reported in patients with mutations located in the C-terminal end of segment 2B of the desmin gene, specifically between amino acids 350-406. Nine different mutations have been associated with dilated cardiomyopathy (DCM), three mutations with arrhythmogenic cardiomyopathy (ACM), six different mutations have been linked to hypertrophic cardiomyopathy (HCM), four to restrictive cardiomyopathy (RCM), and three to left ventricular non-compaction (LVNC). Mutations highlighted in red have been linked to more than one cardiomyopathy in different patients carrying the same mutation.

Moreover, the age of disease onset and the degree of cardiac involvement, along with skeletal involvement in some cases, differ among patients with all desmin mutations. The well characterized and studied desmin p.R406W mutation tends to manifest with an earlier onset of desminopathy, as early as 7 years of age (Oka et al., 2021), presenting with cardiac involvement followed by gradual skeletal muscle degeneration throughout life (Dagvadorj et al., 2004; Oka et al., 2021; Park et al., 2000). Almost all patients with this mutation have atrioventricular block or left/right bundle branch block (Arbustini et al., 2006; Chen et al., 2021; Dagvadorj et al., 2004; Herrmann et al., 2020; Oka et al., 2021; Olivé et al., 2004; Park et al., 2000), but while most patients are diagnosed with RCM (Arbustini et al., 2006; Chen et al., 2021; Herrmann et al., 2020; Olivé et al., 2004), cases of HCM (Oka et al., 2021; Takegami et al., 2023) and DCM (Dagvadorj et al., 2004) have also been reported (Fig. 2, p.R406W in red). The disease progression is faster in patients with this mutation, as observed in the four unrelated patients investigated by Dagvadorj *et al.*, where the onset of the disease occurred at 15, 18, 23 and 24

years of age, with severe disability or SCD occurring shortly after (Dagvadorj et al., 2004). To the best of our knowledge, aggregate formation has been consistently observed by all teams in all patients with this mutation.

Most studies that are presented in this review have illustrated similar results, that being aggregate formation, which is intriguing especially knowing that different point mutations lead to a variety of cardiomyopathies. Studying IFs during development in either mouse or iPS-CM models could elucidate the physiological role of desmin in health and disease. Of interest it would be of high value to have image-based results detecting the appearance and interlinking of IFs and its binding partners during different stages of development. Understanding when the IF scaffold starts and is completed in cells could likewise provide insight into why certain mutations have an earlier onset as opposed to others.

Conclusion and Future Perspectives

Proper cardiomyocyte function depends on the intricate relationship between structure and function. The organization of the cell plays an important role in determining signal propagation and transduction from one cardiomyocyte to another in order to attain the synchronized beating of the heart. Cardiomyocytes do not regenerate, which is most probably why the above mentioned desmin mutations have an early onset of cardiac consequences and the disease progresses rapidly and spirals out of control so quickly. Why the disease progresses faster for some mutations compared to others is not clear and the genotype/phenotype relationship is not as clean cut as it would seem. Proline substitutions seem to be abundant and predominant compared to other amino acid replacements, but it has not been uncovered as to why that is the case. On the other hand, when the C-terminal tail is truncated, desmin cannot form an interaction with desmoplakin, whereas the removal of the N-terminal head does not disturb their bond, but instead has consequences on other binding properties (Lapouge et al., 2006). In this context, the association zone should be considered and binding partners should be involved in further studies. It is obvious by now that many mutations within the desmin gene result in aggregate formation resulting in an array of diseases due to alternation of the intracellular organization in cardiomyocytes. What remains unclear is what happens to the aggregates in the cells over time and how exactly they interfere with cellular function, apart from the physical loss of connection. Mutations could be further investigated using new cell models such as iPSC-CMs from patients to shed light on current and potentially unknown

desmin interactions and better understand the function of desmin within the cell. Likewise, cardiac organoids or engineered heart tissues could possibly help us understand any compensatory mechanisms within cells containing aggregates that may exist to cope with the lack of intracellular support. Unfortunately, no known treatments exist for patients with desminopathy which is why it is important to understand the full function of desmin and its binding partners in hopes of at least slowing the progression of cardiac and skeletal symptoms of patients.

Acknowledgements.

The authors wish to thank Dr. Isabelle Baró for her critical reading of the manuscript. Michelle Geryk was supported by the *Agence Nationale de la Recherche* (ANR-19-CE14-0031-02 to FC).

Conflict of interest

The authors declare that they have no conflict of interest.

References

Agbulut, O., Li, Z., Mouly, V., & Butler-Browne, G. S. (1996). Analysis of skeletal and cardiac muscle from desmin knock-out and normal mice by high resolution separation of myosin heavy-chain isoforms. Biology of the Cell, 88(3), 131–135. https://doi.org/10.1111/j.1768-322X.1996.tb00987.x

Alam, S., Abdullah, C. S., Aishwarya, R., Miriyala, S., Panchatcharam, M., Peretik, J. M., Orr, A. W., James, J., Robbins, J., & Bhuiyan, Md. S. (2018). Aberrant Mitochondrial Fission Is Maladaptive in Desmin Mutation–Induced Cardiac Proteotoxicity. Journal of the American Heart Association: Cardiovascular and Cerebrovascular Disease, 7(14), e009289. https://doi.org/10.1161/JAHA.118.009289

Andreasen, C., Nielsen, J. B., Refsgaard, L., Holst, A. G., Christensen, A. H., Andreasen, L., Sajadieh, A., Haunsø, S., Svendsen, J. H., & Olesen, M. S. (2013). New population-based exome data are questioning the pathogenicity of previously cardiomyopathy-associated genetic variants. European Journal of Human Genetics, 21(9), 918–928. https://doi.org/10.1038/ejhg.2012.283

Arbustini, E., Pasotti, M., Pilotto, A., Pellegrini, C., Grasso, M., Previtali, S., Repetto, A., Bellini, O., Azan, G., Scaffino, M., Campana, C., Piccolo, G., Viganò, M., & Tavazzi, L. (2006). Desmin accumulation restrictive cardiomyopathy and atrioventricular block associated with desmin gene defects. European Journal of Heart Failure, 8(5), 477–483. https://doi.org/10.1016/j.ejheart.2005.11.003

Arias, M., Pardo, J., Blanco-Arias, P., Sobrido, M.-J., Arias, S., Dapena, D., Carracedo, Á., Goldfarb, L. G., & Navarro, C. (2006). Distinct phenotypic features and gender-specific disease manifestations in a Spanish family with desmin L370P mutation. Neuromuscular Disorders, 16(8), 498–503. https://doi.org/10.1016/j.nmd.2006.05.011

Balogh, J., Merisckay, M., Li, Z., Paulin, D., & Arner, A. (2002). Hearts from mice lacking desmin have a myopathy with impaired active force generation and unaltered wall compliance. Cardiovascular Research, 53(2), 439–450. https://doi.org/10.1016/S0008-6363(01)00500-4

Bär, H., Fischer, D., Goudeau, B., Kley, R. A., Clemen, C. S., Vicart, P., Herrmann, H., Vorgerd, M., & Schröder, R. (2005). Pathogenic effects of a novel heterozygous R350P desmin mutation on the assembly of desmin intermediate filaments in vivo and in vitro. Human Molecular Genetics, 14(10), 1251–1260. https://doi.org/10.1093/hmg/ddi136

Bär, H., Goudeau, B., Wälde, S., Casteras-Simon, M., Mücke, N., Shatunov, A., Goldberg, Y. P., Clarke, C., Holton, J. L., Eymard, B., Katus, H. A., Fardeau, M., Goldfarb, L., Vicart, P., & Herrmann, H. (2007). Conspicuous involvement of desmin tail mutations in diverse cardiac and skeletal myopathies. Human Mutation, 28(4), 374–386. https://doi.org/10.1002/humu.20459

Bär, H., Mucke, N., Kostareva, A., Sjoberg, G., Aebi, U., & Herrmann, H. (2005). Severe muscle disease-causing desmin mutations interfere with in vitro filament assembly at distinct stages. Proceedings of the National Academy of Sciences, 102(42), 15099–15104. https://doi.org/10.1073/pnas.0504568102

Bär, H., Schopferer, M., Sharma, S., Hochstein, B., Mücke, N., Herrmann, H., & Willenbacher, N. (2010). Mutations in Desmin's Carboxy-Terminal "Tail" Domain Severely Modify Filament

and Network Mechanics. Journal of Molecular Biology, 397(5), 1188–1198. https://doi.org/10.1016/j.jmb.2010.02.024

Bär, H., Strelkov, S. V., Sjöberg, G., Aebi, U., & Herrmann, H. (2004). The biology of desmin filaments: How do mutations affect their structure, assembly, and organisation? Journal of Structural Biology, 148(2), 137–152. https://doi.org/10.1016/j.jsb.2004.04.003

Bermúdez-Jiménez, F. J., Carriel, V., Brodehl, A., Alaminos, M., Campos, A., Schirmer, I., Milting, H., Abril, B. Á., Álvarez, M., López-Fernández, S., García-Giustiniani, D., Monserrat, L., Tercedor, L., & Jiménez-Jáimez, J. (2018). Novel Desmin Mutation p.Glu401Asp Impairs Filament Formation, Disrupts Cell Membrane Integrity, and Causes Severe Arrhythmogenic Left Ventricular Cardiomyopathy/Dysplasia. Circulation, 137(15), 1595–1610. https://doi.org/10.1161/CIRCULATIONAHA.117.028719

Brodehl, A., Ebbinghaus, H., Gaertner-Rommel, A., Stanasiuk, C., Klauke, B., & Milting, H. (2019). Functional analysis of DES-p.L398P and RBM20-p.R636C. Genetics in Medicine, 21(5), 1246–1247. https://doi.org/10.1038/s41436-018-0291-2

Brodehl, A., Gaertner-Rommel, A., & Milting, H. (2018). Molecular insights into cardiomyopathies associated with desmin (DES) mutations. Biophysical Reviews, 10(4), 983–1006. https://doi.org/10.1007/s12551-018-0429-0

Brodehl, A., Hakimi, S. A. P., Stanasiuk, C., Ratnavadivel, S., Hendig, D., Gaertner, A., Gerull, B., Gummert, J., Paluszkiewicz, L., & Milting, H. (2019). Restrictive Cardiomyopathy is Caused by a Novel Homozygous Desmin (DES) Mutation p.Y122H Leading to a Severe Filament Assembly Defect. Genes, 10(11), 918. https://doi.org/10.3390/genes10110918

Brodehl, A., Holler, S., Gummert, J., & Milting, H. (2022). The N-Terminal Part of the 1A Domain of Desmin Is a Hot Spot Region for Putative Pathogenic DES Mutations Affecting Filament Assembly. Cells. https://doi.org/10.3390/cells11233906

Cao, J., Gao, Q., Chen, H., Zhang, Q., Wang, Z., & Li, Y. (2021). Desmin Correlated with Cx43 May Facilitate Intercellular Electrical Coupling during Chronic Heart Failure. Evidence-Based Complementary and Alternative Medicine, 2021, 1–9. https://doi.org/10.1155/2021/6621132

Cao, L., Hong, D., Zhu, M., Li, X., Wan, H., & Hong, K. (2013). A novel heterozygous deletion-insertion mutation in the desmin gene causes complete atrioventricular block and mild myopathy. Clinical Neuropathology, 32(1), 9–15. https://doi.org/10.5414/NP300514

Capetanaki, Y., Bloch, R. J., Kouloumenta, A., Mavroidis, M., & Psarras, S. (2007). Muscle intermediate filaments and their links to membranes and membranous organelles. Experimental Cell Research, 313(10), 2063–2076. https://doi.org/10.1016/j.yexcr.2007.03.033

Capetanaki, Y., Milner, D. J., & Weitzer, G. (1997). Desmin in Muscle Formation and Maintenance: Knockouts and Consequences. Cell Structure and Function, 22(1), 103–116. https://doi.org/10.1247/csf.22.103

Chen, Z., Li, R., Wang, Y., Cao, L., Lin, C., Liu, F., Hu, R., Nan, J., Zhuang, X., Lu, X., Nan, G., Hu, G., Xue, J., Zhang, Y., Xiao, J., Yao, Y., Guo, S., & Lei, J. (2021). Features of myocardial injury detected by cardiac magnetic resonance in a patient with desmin-related restrictive cardiomyopathy. ESC Heart Failure, 8(6), 5560–5564. https://doi.org/10.1002/ehf2.13624

584 Chourbagi, O., Bruston, F., Carinci, M., Xue, Z., Vicart, P., Paulin, D., & Agbulut, O. (2011).
585 Desmin mutations in the terminal consensus motif prevent synemin-desmin heteropolymer
586 filament assembly. Experimental Cell Research, 317(6), 886–897.
587 https://doi.org/10.1016/j.yexcr.2011.01.013

588 Clemen, C. S., Stöckigt, F., Strucksberg, K.-H., Chevessier, F., Winter, L., Schütz, J., Bauer,
589 R., Thorweihe, J.-M., Wenzel, D., Schlötzer-Schrehardt, U., Rasche, V., Krsmanovic, P., Katus,
590 H. A., Rottbauer, W., Just, S., Müller, O. J., Friedrich, O., Meyer, R., Herrmann, H., …
591 Schröder, R. (2015). The toxic effect of R350P mutant desmin in striated muscle of man and
592 mouse. Acta Neuropathologica, 129(2), 297–315. https://doi.org/10.1007/s00401-014-1363-2

593 Coscarella, I. L., Landim-Vieira, M., Rastegarpouyani, H., Chase, P. B., Irianto, J., & Pinto, J.
594 R. (2023). Nucleus Mechanosensing in Cardiomyocytes. International Journal of Molecular
595 Sciences, 24(17), 13341. https://doi.org/10.3390/ijms241713341

596 Cunningham, F., Allen, J. E., Allen, J., Alvarez-Jarreta, J., Amode, M. R., Armean, I. M.,
597 Austine-Orimoloye, O., Azov, A. G., Barnes, I., Bennett, R., Berry, A., Bhai, J., Bignell, A.,
598 Billis, K., Boddu, S., Brooks, L., Charkhchi, M., Cummins, C., Da Rin Fioretto, L., … Flicek,
599 P. (2022). Ensembl 2022. Nucleic Acids Research, 50(D1), D988–D995.
600 https://doi.org/10.1093/nar/gkab1049

601 Dagvadorj, A., Goudeau, B., Hilton-Jones, D., Blancato, J. K., Shatunov, A., Simon-Casteras,
602 M., Squier, W., Nagle, J. W., Goldfarb, L. G., & Vicart, P. (2003). Respiratory insufficiency in
603 desminopathy patients caused by introduction of proline residues in desmin c-terminal α-helical
604 segment. Muscle & Nerve, 27(6), 669–675. https://doi.org/10.1002/mus.10370

605 Dagvadorj, A., Olivé, M., Urtizberea, J.-A., Halle, M., Shatunov, A., Bönnemann, C., Park, K.-
606 Y., Goebel, H. H., Ferrer, I., Vicart, P., Dalakas, M. C., & Goldfarb, L. G. (2004). A series of
607 West European patients with severe cardiac and skeletal myopathy associated with a de novo
608 R406W mutation in desmin. Journal of Neurology, 251(2), 143–149.
609 https://doi.org/10.1007/s00415-004-0289-3

610 Dalakas, M. C., Park, K. Y., Semino-Mora, C., Lee, H. S., Sivakumar, K., & Goldfarb, L. G.
611 (2000). Desmin myopathy, a skeletal myopathy with cardiomyopathy caused by mutations in
612 the desmin gene. The New England Journal of Medicine, 342(11), 770–780.
613 https://doi.org/10.1056/NEJM200003163421104

614 Diermeier, S., Iberl, J., Vetter, K., Haug, M., Pollmann, C., Reischl, B., Buttgereit, A.,
615 Schürmann, S., Spörrer, M., Goldmann, W. H., Fabry, B., Elhamine, F., Stehle, R., Pfitzer, G.,
616 Winter, L., Clemen, C. S., Herrmann, H., Schröder, R., & Friedrich, O. (2017). Early signs of
617 architectural and biomechanical failure in isolated myofibers and immortalized myoblasts from
618 desmin-mutant knock-in mice. Scientific Reports, 7(1), Article 1.
619 https://doi.org/10.1038/s41598-017-01485-x

620 Diokmetzidou, A., Soumaka, E., Kloukina, I., Tsikitis, M., Makridakis, M., Varela, A., Davos,
621 C. H., Georgopoulos, S., Anesti, V., Vlahou, A., & Capetanaki, Y. (2016). Desmin and αB-
622 crystallin interplay in maintenance of mitochondrial homeostasis and cardiomyocyte survival.
623 Journal of Cell Science, jcs.192203. https://doi.org/10.1242/jcs.192203

Djabali, K., de Nechaud, B., Landon, F., & Portier, M. M. (1997). AlphaB-crystallin interacts with intermediate filaments in response to stress. Journal of Cell Science, 110(21), 2759–2769. https://doi.org/10.1242/jcs.110.21.2759

Dutour-Provenzano, G., & Etienne-Manneville, S. (2021). Intermediate filaments. Current Biology, 31(10), R522–R529. https://doi.org/10.1016/j.cub.2021.04.011

Eldirany, S. A., Lomakin, I. B., Ho, M., & Bunick, C. G. (2021). Recent insight into intermediate filament structure. Current Opinion in Cell Biology, 68, 132–143. https://doi.org/10.1016/j.ceb.2020.10.001

Elsnicova, B., Hornikova, D., Tibenska, V., Kolar, D., Tlapakova, T., Schmid, B., Mallek, M., Eggers, B., Schlötzer-Schrehardt, U., Peeva, V., Berwanger, C., Eberhard, B., Durmuş, H., Schultheis, D., Holtzhausen, C., Schork, K., Marcus, K., Jordan, J., Lücke, T., … Zurmanova, J. M. (2022). Desmin Knock-Out Cardiomyopathy: A Heart on the Verge of Metabolic Crisis. International Journal of Molecular Sciences, 23(19), 12020. https://doi.org/10.3390/ijms231912020

Fidziańska, A., Kotowicz, J., Sadowska, M., Goudeau, B., Walczak, E., Vicart, P., & Hausmanowa-Petrusewicz, I. (2005). A novel desmin R355P mutation causes cardiac and skeletal myopathy. Neuromuscular Disorders, 15(8), 525–531. https://doi.org/10.1016/j.nmd.2005.05.006

Fischer, B., Dittmann, S., Brodehl, A., Unger, A., Stallmeyer, B., Paul, M., Seebohm, G., Kayser, A., Peischard, S., Linke, W. A., Milting, H., & Schulze-Bahr, E. (2021). Functional characterization of novel alpha-helical rod domain desmin (DES) pathogenic variants associated with dilated cardiomyopathy, atrioventricular block and a risk for sudden cardiac death. International Journal of Cardiology, 329, 167–174. https://doi.org/10.1016/j.ijcard.2020.12.050

Fischer, D., Kley, R. A., Strach, K., Meyer, C., Sommer, T., Eger, K., Rolfs, A., Meyer, W., Pou, A., Pradas, J., Heyer, C. M., Grossmann, A., Huebner, A., Kress, W., Reimann, J., Schröder, R., Eymard, B., Fardeau, M., Udd, B., … Olivé, M. (2008). Distinct muscle imaging patterns in myofibrillar myopathies. Neurology, 71(10), 758–765. https://doi.org/10.1212/01.wnl.0000324927.28817.9b

Fokstuen, S., Makrythanasis, P., Hammar, E., Guipponi, M., Ranza, E., Varvagiannis, K., Santoni, F. A., Albarca-Aguilera, M., Poleggi, M. E., Couchepin, F., Brockmann, C., Mauron, A., Hurst, S. A., Moret, C., Gehrig, C., Vannier, A., Bevillard, J., Araud, T., Gimelli, S., … Antonarakis, S. E. (2016). Experience of a multidisciplinary task force with exome sequencing for Mendelian disorders. Human Genomics, 10, 24. https://doi.org/10.1186/s40246-016-0080-4

Gard, J., Yamada, K., Green, K., Eloff, B., Rosenbaum, D., Wang, X., Robbins, J., Schuessler, R., Yamada, K., & Saffitz, J. (2005). Remodeling of gap junctions and slow conduction in a mouse model of desmin-related cardiomyopathy. Cardiovascular Research, 67(3), 539–547. https://doi.org/10.1016/j.cardiores.2005.04.004

Goldfarb, L. G., & Dalakas, M. C. (2009). Tragedy in a heartbeat: Malfunctioning desmin causes skeletal and cardiac muscle disease. Journal of Clinical Investigation, 119(7), 1806–1813. https://doi.org/10.1172/JCI38027

Goldfarb, L. G., Park, K.-Y., Cervenáková, L., Gorokhova, S., Lee, H.-S., Vasconcelos, O., Nagle, J. W., Semino-Mora, C., Sivakumar, K., & Dalakas, M. C. (1998). Missense mutations in desmin associated with familial cardiac and skeletal myopathy. Nature Genetics, 19(4), Article 4. https://doi.org/10.1038/1300

Goldfarb, L. G., Vicart, P., Goebel, H. H., & Dalakas, M. C. (2004). Desmin myopathy. Brain, 127(4), 723–734. https://doi.org/10.1093/brain/awh033

Goudeau, B., Dagvadorj, A., Rodrigues-Lima, F., Nédellec, P., Casteras-Simon, M., Perret, E., Langlois, S., Goldfarb, L., & Vicart, P. (2001). Structural and functional analysis of a new desmin variant causing desmin-related myopathy. Human Mutation, 18(5), 388–396. https://doi.org/10.1002/humu.1210

Goudeau, B., Rodrigues-Lima, F., Fischer, D., Casteras-Simon, M., Sambuughin, N., de Visser, M., Laforet, P., Ferrer, X., Chapon, F., Sjöberg, G., Kostareva, A., Sejersen, T., Dalakas, M. C., Goldfarb, L. G., & Vicart, P. (2006). Variable pathogenic potentials of mutations located in the desmin alpha-helical domain. Human Mutation, 27(9), 906–913. https://doi.org/10.1002/humu.20351

Granger, B. L., & Lazarides, E. (1979). Desmin and vimentin coexist at the periphery of the myofibril Z disc. Cell, 18(4), 1053–1063. https://doi.org/10.1016/0092-8674(79)90218-6

Harada, H., Hayashi, T., Nishi, H., Kusaba, K., Koga, Y., Koga, Y., Nonaka, I., & Kimura, A. (2018). Phenotypic expression of a novel desmin gene mutation: Hypertrophic cardiomyopathy followed by systemic myopathy. Journal of Human Genetics, 63(2), 249–254. https://doi.org/10.1038/s10038-017-0383-x

Herrmann, H., & Aebi, U. (2004). Intermediate Filaments: Molecular Structure, Assembly Mechanism, and Integration Into Functionally Distinct Intracellular Scaffolds. Annual Review of Biochemistry, 73(1), 749–789. https://doi.org/10.1146/annurev.biochem.73.011303.073823

Herrmann, H., Cabet, E., Chevalier, N. R., Moosmann, J., Schultheis, D., Haas, J., Schowalter, M., Berwanger, C., Weyerer, V., Agaimy, A., Meder, B., Müller, O. J., Katus, H. A., Schlötzer-Schrehardt, U., Vicart, P., Ferreiro, A., Dittrich, S., Clemen, C. S., Lilienbaum, A., & Schröder, R. (2020). Dual Functional States of R406W-Desmin Assembly Complexes Cause Cardiomyopathy With Severe Intercalated Disc Derangement in Humans and in Knock-In Mice. Circulation, 142(22), 2155–2171. https://doi.org/10.1161/CIRCULATIONAHA.120.050218

Herrmann, H., Strelkov, S. V., Feja, B., Rogers, K. R., Brettel, M., Lustig, A., Häner, M., Parry, D. A. D., Steinert, P. M., Burkhard, P., & Aebi, U. (2000). The intermediate filament protein consensus motif of helix 2B: Its atomic structure and contribution to assembly11Edited by W. Baumeister. Journal of Molecular Biology, 298(5), 817–832. https://doi.org/10.1006/jmbi.2000.3719

Hnia, K., Ramspacher, C., Vermot, J., & Laporte, J. (2015). Desmin in muscle and associated diseases: Beyond the structural function. Cell and Tissue Research, 360(3), 591–608. https://doi.org/10.1007/s00441-014-2016-4

Hong, D., Wang, Z., Zhang, W., Xi, J., Lu, J., Luan, X., & Yuan, Y. (2011). A series of Chinese patients with desminopathy associated with six novel and one reported mutations in the desmin

gene. Neuropathology and Applied Neurobiology, 37(3), 257–270. https://doi.org/10.1111/j.1365-2990.2010.01112.x

Hovhannisyan, Y., Li, Z., Callon, D., Suspène, R., Batoumeni, V., Canette, A., Blanc, J., Hocini, H., Lefebvre, C., El-Jahrani, N., Kitsara, M., L'honoré, A., Kordeli, E., Fornes, P., Concordet, J.-P., Tachdjian, G., Rodriguez, A.-M., Vartanian, J.-P., Béhin, A., … Agbulut, O. (2024). Critical contribution of mitochondria in the development of cardiomyopathy linked to desmin mutation. Stem Cell Research & Therapy, 15(1), 10. https://doi.org/10.1186/s13287-023-03619-7

Huang, X., Li, J., Foster, D., Lemanski, S. L., Dube, D. K., Zhang, C., & Lemanski, L. F. (2002). Protein Kinase C-Mediated Desmin Phosphorylation is Related to Myofibril Disarray in Cardiomyopathic Hamster Heart1. Experimental Biology and Medicine, 227(11), 1039–1046. https://doi.org/10.1177/153537020222701113

Kaminska, A., Strelkov, S. V., Goudeau, B., Olivé, M., Dagvadorj, A., Fidzianska, A., Simon-Casteras, M., Shatunov, A., Dalakas, M. C., Ferrer, I., Kwiecinski, H., Vicart, P., & Goldfarb, L. G. (2004). Small deletions disturb desmin architecture leading to breakdown of muscle cells and development of skeletal or cardioskeletal myopathy. Human Genetics, 114(3), 306–313. https://doi.org/10.1007/s00439-003-1057-7

Kreplak, L., & Bär, H. (2009). Severe Myopathy Mutations Modify the Nanomechanics of Desmin Intermediate Filaments. Journal of Molecular Biology, 385(4), 1043–1051. https://doi.org/10.1016/j.jmb.2008.10.095

Kubánek, M., Schimerová, T., Piherová, L., Brodehl, A., Krebsová, A., Ratnavadivel, S., Stanasiuk, C., Hansíková, H., Zeman, J., Paleček, T., Houštěk, J., Drahota, Z., Nůsková, H., Mikešová, J., Zámečník, J., Macek, M., Ridzoň, P., Malusková, J., Stránecký, V., … Kmoch, S. (2020). Desminopathy: Novel Desmin Variants, a New Cardiac Phenotype, and Further Evidence for Secondary Mitochondrial Dysfunction. Journal of Clinical Medicine, 9(4), 937. https://doi.org/10.3390/jcm9040937

Kulikova, O., Brodehl, A., Kiseleva, A., Myasnikov, R., Meshkov, A., Stanasiuk, C., Gärtner, A., Divashuk, M., Sotnikova, E., Koretskiy, S., Kharlap, M., Kozlova, V., Mershina, E., Pilus, P., Sinitsyn, V., Milting, H., Boytsov, S., & Drapkina, O. (2021). The Desmin (DES) Mutation p.A337P Is Associated with Left-Ventricular Non-Compaction Cardiomyopathy. Genes, 12(1), 121. https://doi.org/10.3390/genes12010121

Lapouge, K., Fontao, L., Champliaud, M.-F., Jaunin, F., Frias, M. A., Favre, B., Paulin, D., Green, K. J., & Borradori, L. (2006). New insights into the molecular basis of desmoplakinand desmin-related cardiomyopathies. Journal of Cell Science, 119(23), 4974–4985. https://doi.org/10.1242/jcs.03255

Lazarides, E. (1978). The distribution of desmin (100 Å) filaments in primary cultures of embryonic chick cardiac cells. Experimental Cell Research, 112(2), 265–273. https://doi.org/10.1016/0014-4827(78)90209-4

Lazarides, E. (1980). Intermediate filaments as mechanical integrators of cellular space. Nature, 283(5744), 249–255. https://doi.org/10.1038/283249a0

Li, S. C., Goto, N. K., Williams, K. A., & Deber, C. M. (1996). Alpha-helical, but not beta-sheet, propensity of proline is determined by peptide environment. Proceedings of the National Academy of Sciences of the United States of America, 93(13), 6676–6681. https://doi.org/doi: 10.1073/pnas.93.13.6676

Li, Z., Colucci-Guyon, E., Pinçon-Raymond, M., Mericskay, M., Pournin, S., Paulin, D., & Babinet, C. (1996). Cardiovascular Lesions and Skeletal Myopathy in Mice Lacking Desmin. Developmental Biology, 175(2), 362–366. https://doi.org/10.1006/dbio.1996.0122

Li, Z., Lilienbaum, A., Butler-Browne, G., & Paulin, D. (1989). Human desmin-coding gene: Complete nucleotide sequence, characterization and regulation of expression during myogenesis and development. Gene, 78(2), 243–254. https://doi.org/10.1016/0378-1119(89)90227-8

Lityagina, O., & Dobreva, G. (2021). The LINC Between Mechanical Forces and Chromatin. Frontiers in Physiology, 12, 710809. https://doi.org/10.3389/fphys.2021.710809

Luethje, L. G. C., Boennemann, C., Goldfarb, L., Goebel, H. H., & Halle, M. (2004). Prophylactic Implantable Cardioverter Defibrillator Placement in a Sporadic Desmin Related Myopathy and Cardiomyopathy. Pacing and Clinical Electrophysiology, 27(4), 559–560. https://doi.org/10.1111/j.1540-8159.2004.00484.x

Maerkens, A., Kley, R. A., Olivé, M., Theis, V., van der Ven, P. F. M., Reimann, J., Milting, H., Schreiner, A., Uszkoreit, J., Eisenacher, M., Barkovits, K., Güttsches, A. K., Tonillo, J., Kuhlmann, K., Meyer, H. E., Schröder, R., Tegenthoff, M., Fürst, D. O., Müller, T., … Marcus, K. (2013). Differential proteomic analysis of abnormal intramyoplasmic aggregates in desminopathy. Journal of Proteomics, 90, 14–27. https://doi.org/10.1016/j.jprot.2013.04.026

Maggi, L., Mavroidis, M., Psarras, S., Capetanaki, Y., & Lattanzi, G. (2021). Skeletal and Cardiac Muscle Disorders Caused by Mutations in Genes Encoding Intermediate Filament Proteins. International Journal of Molecular Sciences, 22(8), 4256. https://doi.org/10.3390/ijms22084256

Mavroidis, M., Athanasiadis, N. C., Rigas, P., Kostavasili, I., Kloukina, I., Te Rijdt, W. P., Kavantzas, N., Chaniotis, D., van Tintelen, J. P., Skaliora, I., & Davos, C. H. (2020). Desmin is essential for the structure and function of the sinoatrial node: Implications for increased arrhythmogenesis. American Journal of Physiology-Heart and Circulatory Physiology, 319(3), H557–H570. https://doi.org/10.1152/ajpheart.00594.2019

Mavroidis, M., Davos, C. H., Psarras, S., Varela, A., C Athanasiadis, N., Katsimpoulas, M., Kostavasili, I., Maasch, C., Vater, A., van Tintelen, J. P., & Capetanaki, Y. (2015). Complement system modulation as a target for treatment of arrhythmogenic cardiomyopathy. Basic Research in Cardiology, 110(3), 27. https://doi.org/10.1007/s00395-015-0485-6

Milner, D. J., Taffet, G. E., Wang, X., Pham, T., Tamura, T., Hartley, C., Gerdes, M. A., & Capetanaki, Y. (1999). The Absence of Desmin Leads to Cardiomyocyte Hypertrophy and Cardiac Dilation with Compromised Systolic Function. Journal of Molecular and Cellular Cardiology, 31(11), 2063–2076. https://doi.org/10.1006/jmcc.1999.1037

Minoche, A. E., Horvat, C., Johnson, R., Gayevskiy, V., Morton, S. U., Drew, A. P., Woo, K., Statham, A. L., Lundie, B., Bagnall, R. D., Ingles, J., Semsarian, C., Seidman, J. G., Seidman,

C. E., Dinger, M. E., Cowley, M. J., & Fatkin, D. (2019). Whole-Genome Sequencing as a First-Line Genetic Test in Familial Dilated Cardiomyopathy. Genetics in Medicine : Official Journal of the American College of Medical Genetics, 21(3), 650–662. https://doi.org/10.1038/s41436-018-0084-7

Miszalski-Jamka, K., Jefferies, J. L., Mazur, W., Głowacki, J., Hu, J., Lazar, M., Gibbs, R. A., Liczko, J., Kłyś, J., Venner, E., Muzny, D. M., Rycaj, J., Białkowski, J., Kluczewska, E., Kalarus, Z., Jhangiani, S., Al-Khalidi, H., Kukulski, T., Lupski, J. R., … Bainbridge, M. N. (2017). Novel Genetic Triggers and Genotype-Phenotype Correlations in Patients with Left Ventricular Non-Compaction. Circulation. Cardiovascular Genetics, 10(4), e001763. https://doi.org/10.1161/CIRCGENETICS.117.001763

Noureddine, M., & Gehmlich, K. (2023). Structural and signaling proteins in the Z-disk and their role in cardiomyopathies. Frontiers in Physiology, 14, 1143858. https://doi.org/10.3389/fphys.2023.1143858

Oka, H., Nakau, K., Imanishi, R., Furukawa, T., Tanabe, Y., Hirono, K., Hata, Y., Nishida, N., & Azuma, H. (2021). A Case Report of a Rare Heterozygous Variant in the Desmin Gene Associated With Hypertrophic Cardiomyopathy and Complete Atrioventricular Block. CJC Open, 3(9), 1195–1198. https://doi.org/10.1016/j.cjco.2021.05.003

Olivé, M., Armstrong, J., Miralles, F., Pou, A., Fardeau, M., Gonzalez, L., Martínez, F., Fischer, D., Matos, J. A. M., Shatunov, A., Goldfarb, L., & Ferrer, I. (2007). Phenotypic patterns of desminopathy associated with three novel mutations in the desmin gene. Neuromuscular Disorders : NMD, 17(6), 443–450. https://doi.org/10.1016/j.nmd.2007.02.009

Olivé, M., Goldfarb, L., Moreno, D., Laforet, E., Dagvadorj, A., Sambuughin, N., Martínez-Matos, J. A., Martínez, F., Alió, J., Farrero, E., Vicart, P., & Ferrer, I. (2004). Desmin-related myopathy: Clinical, electrophysiological, radiological, neuropathological and genetic studies. Journal of the Neurological Sciences, 219(1), 125–137. https://doi.org/10.1016/j.jns.2004.01.007

Olivé, M., Odgerel, Z., Martínez, A., Poza, J. J., Bragado, F. G., Zabalza, R. J., Jericó, I., Gonzalez-Mera, L., Shatunov, A., Lee, H. S., Armstrong, J., Maraví, E., Arroyo, M. R., Pascual-Calvet, J., Navarro, C., Paradas, C., Huerta, M., Marquez, F., Rivas, E. G.-, … Goldfarb, L. G. (2011). Clinical and myopathological evaluation of early- and late-onset subtypes of myofibrillar myopathy. Neuromuscular Disorders, 21(8), 533–542. https://doi.org/10.1016/j.nmd.2011.05.002

Park, K.-Y., Dalakas, M. C., Semino-Mora, C., Lee, H.-S., Litvak, S., Takeda, K., Ferrans, V. J., & Goldfarb, L. G. (2000). Sporadic cardiac and skeletal myopathy caused by a de novo desmin mutation. Clinical Genetics, 57(6), 423–429. https://doi.org/10.1034/j.1399-0004.2000.570604.x

Paulin, D., Hovhannisyan, Y., Kasakyan, S., Agbulut, O., Li, Z., & Xue, Z. (2020). Synemin-related skeletal and cardiac myopathies: An overview of pathogenic variants. American Journal of Physiology. Cell Physiology, 318(4), C709–C718. https://doi.org/10.1152/ajpcell.00485.2019

Protonotarios, A., Brodehl, A., Asimaki, A., Jager, J., Quinn, E., Stanasiuk, C., Ratnavadivel, S., Futema, M., Akhtar, M. M., Gossios, T. D., Ashworth, M., Savvatis, K., Walhorn, V.,

Anselmetti, D., Elliott, P. M., Syrris, P., Milting, H., & Lopes, L. R. (2021). The Novel Desmin Variant p.Leu115Ile Is Associated With a Unique Form of Biventricular Arrhythmogenic Cardiomyopathy. Canadian Journal of Cardiology, 37(6), 857–866. https://doi.org/10.1016/j.cjca.2020.11.017

Ramspacher, C., Steed, E., Boselli, F., Ferreira, R., Faggianelli, N., Roth, S., Spiegelhalter, C., Messaddeq, N., Trinh, L., Liebling, M., Chacko, N., Tessadori, F., Bakkers, J., Laporte, J., Hnia, K., & Vermot, J. (2015). Developmental Alterations in Heart Biomechanics and Skeletal Muscle Function in Desmin Mutants Suggest an Early Pathological Root for Desminopathies. Cell Reports, 11(10), 1564–1576. https://doi.org/10.1016/j.celrep.2015.05.010

Rapti, K., Diokmetzidou, A., Kloukina, I., Milner, D. J., Varela, A., Davos, C. H., & Capetanaki, Y. (2017). Opposite effects of catalase and MnSOD ectopic expression on stress induced defects and mortality in the desmin deficient cardiomyopathy model. Free Radical Biology & Medicine, 110, 206–218. https://doi.org/10.1016/j.freeradbiomed.2017.06.010

Ripoll-Vera, T., Zorio, E., Gámez, J. M., Molina, P., Govea, N., & Crémer, D. (2015). Phenotypic Patterns of Cardiomyopathy Caused by Mutations in the Desmin Gene. A Clinical and Genetic Study in Two Inherited Heart Disease Units. Revista Española de Cardiología (English Edition), 68(11), 1027–1029. https://doi.org/10.1016/j.rec.2015.07.007

Schrickel, J. W., Stöckigt, F., Krzyzak, W., Paulin, D., Li, Z., Lübkemeier, I., Fleischmann, B., Sasse, P., Linhart, M., Lewalter, T., Nickenig, G., Lickfett, L., Schröder, R., & Clemen, C. S. (2010). Cardiac conduction disturbances and differential effects on atrial and ventricular electrophysiological properties in desmin deficient mice. Journal of Interventional Cardiac Electrophysiology, 28(2), 71–80. https://doi.org/10.1007/s10840-010-9482-8

Segura-Rodríguez, D., Bermúdez-Jiménez, F. J., Carriel, V., López-Fernández, S., González-Molina, M., Oyonarte Ramírez, J. M., Fernández-Navarro, L., García-Roa, M. D., Cabrerizo, E. M., Durand-Herrera, D., Alaminos, M., Campos, A., Macías, R., Álvarez, M., Tercedor, L., & Jiménez-Jáimez, J. (2020). Myocardial fibrosis in arrhythmogenic cardiomyopathy: A genotype–phenotype correlation study. European Heart Journal - Cardiovascular Imaging, 21(4), 378–386. https://doi.org/10.1093/ehjci/jez277

Sharma, S., Mücke, N., Katus, H. A., Herrmann, H., & Bär, H. (2009). Disease mutations in the “head” domain of the extra-sarcomeric protein desmin distinctly alter its assembly and network-forming properties. Journal of Molecular Medicine, 87(12), 1207–1219. https://doi.org/10.1007/s00109-009-0521-9

Shy, D., Gillet, L., & Abriel, H. (2013). Cardiac sodium channel NaV1.5 distribution in myocytes via interacting proteins: The multiple pool model. Biochimica Et Biophysica Acta, 1833(4), 886–894. https://doi.org/10.1016/j.bbamcr.2012.10.026

Smolina, N., Khudiakov, A., Knyazeva, A., Zlotina, A., Sukhareva, K., Kondratov, K., Gogvadze, V., Zhivotovsky, B., Sejersen, T., & Kostareva, A. (2020). Desmin mutations result in mitochondrial dysfunction regardless of their aggregation properties. Biochimica et Biophysica Acta (BBA) - Molecular Basis of Disease, 1866(6), 165745. https://doi.org/10.1016/j.bbadis.2020.165745

Spörrer, M., Kah, D., Gerum, R. C., Reischl, B., Huraskin, D., Dessalles, C. A., Schneider, W., Goldmann, W. H., Herrmann, H., Thievessen, I., Clemen, C. S., Friedrich, O.,

Hashemolhosseini, S., Schröder, R., & Fabry, B. (2022). The desmin mutation R349P increases contractility and fragility of stem cell-generated muscle micro-tissues. Neuropathology and Applied Neurobiology, 48(3), e12784. https://doi.org/10.1111/nan.12784

Stöckigt, F., Eichhorn, L., Beiert, T., Knappe, V., Radecke, T., Steinmetz, M., Nickenig, G., Peeva, V., Kudin, A. P., Kunz, W. S., Berwanger, C., Kamm, L., Schultheis, D., Schlötzer-Schrehardt, U., Clemen, C. S., Schröder, R., & Schrickel, J. W. (2020). Heart failure after pressure overload in autosomal-dominant desminopathies: Lessons from heterozygous DES-p.R349P knock-in mice. PLoS ONE, 15(3), e0228913. https://doi.org/10.1371/journal.pone.0228913

Strach, K., Sommer, T., Grohé, C., Meyer, C., Fischer, D., Walter, M. C., Vorgerd, M., Reilich, P., Bär, H., Reimann, J., Reuner, U., Germing, A., Goebel, H. H., Lochmüller, H., Wintersperger, B., & Schröder, R. (2008). Clinical, genetic, and cardiac magnetic resonance imaging findings in primary desminopathies. Neuromuscular Disorders, 18(6), 475–482. https://doi.org/10.1016/j.nmd.2008.03.012

Strelkov, S. V., Herrmann, H., Geisler, N., Wedig, T., Zimbelmann, R., Aebi, U., & Burkhard, P. (2002). Conserved segments 1A and 2B of the intermediate filament dimer: Their atomic structures and role in filament assembly. The EMBO Journal, 21(6), 1255–1266. https://doi.org/10.1093/emboj/21.6.1255

Sugawara, M., Kato, K., Komatsu, M., Wada, C., Kawamura, K., Shindo, S., Yoshioka, N., Tanaka, K., Watanabe, S., & Toyoshima, I. (2000). A novel de novo mutation in the desmin gene causes desmin myopathy with toxic aggregates. Neurology, 55(7), 986–990. https://doi.org/10.1212/WNL.55.7.986

Takegami, N., Mitsutake, A., Mano, T., Shintani-Domoto, Y., Unuma, A., Yamaguchi-Takegami, N., Ishiura, H., Sakuishi, K., Ando, M., Yamauchi, H., Ono, M., Morishita, S., Mitsui, J., Shimizu, J., Tsuji, S., & Toda, T. (2023). The Myocardial Accumulation of Aggregated Desmin Protein in a Case of Desminopathy with a de novo DES p.R406W Mutation. Internal Medicine, 0992–22. https://doi.org/10.2169/internalmedicine.0992-22

Taylor, M. R. G., Slavov, D., Ku, L., Di Lenarda, A., Sinagra, G., Carniel, E., Haubold, K., Boucek, M. M., Ferguson, D., Graw, S. L., Zhu, X., Cavanaugh, J., Sucharov, C. C., Long, C. S., Bristow, M. R., Lavori, P., & Mestroni, L. (2007). Prevalence of Desmin Mutations in Dilated Cardiomyopathy. Circulation, 115(10), 1244–1251. https://doi.org/10.1161/CIRCULATIONAHA.106.646778

Thornell, L.-E., Carlsson, L., Li, Z., Mericskay, M., & Paulin, D. (1997). Null Mutation in the Desmin Gene Gives Rise to a Cardiomyopathy. Journal of Molecular and Cellular Cardiology, 29(8), 2107–2124. https://doi.org/10.1006/jmcc.1997.0446

Tse, H.-F., Ho, J. C. Y., Choi, S.-W., Lee, Y.-K., Butler, A. W., Ng, K.-M., Siu, C.-W., Simpson, M. A., Lai, W.-H., Chan, Y.-C., Au, K.-W., Zhang, J., Lay, K. W. J., Esteban, M. A., Nicholls, J. M., Colman, A., & Sham, P. C. (2013). Patient-specific induced-pluripotent stem cells-derived cardiomyocytes recapitulate the pathogenic phenotypes of dilated cardiomyopathy due to a novel DES mutation identified by whole exome sequencing. Human Molecular Genetics, 22(7), 1395–1403. https://doi.org/10.1093/hmg/dds556

Tsikitis, M., Galata, Z., Mavroidis, M., Psarras, S., & Capetanaki, Y. (2018). Intermediate filaments in cardiomyopathy. Biophysical Reviews, 10(4), 1007–1031. https://doi.org/10.1007/s12551-018-0443-2

van Spaendonck-Zwarts, K. Y., van Hessem, L., Jongbloed, J. D. H., de Walle, H. E. K., Capetanaki, Y., van der Kooi, A. J., van Langen, I. M., van den Berg, M. P., & van Tintelen, J. P. (2011). Desmin-related myopathy. Clinical Genetics, 80(4), 354–366. https://doi.org/10.1111/j.1399-0004.2010.01512.x

Van Waning, J. I., Caliskan, K., Hoedemaekers, Y. M., Van Spaendonck-Zwarts, K. Y., Baas, A. F., Boekholdt, S. M., Van Melle, J. P., Teske, A. J., Asselbergs, F. W., Backx, A. P. C. M., Du Marchie Sarvaas, G. J., Dalinghaus, M., Breur, J. M. P. J., Linschoten, M. P. M., Verlooij, L. A., Kardys, I., Dooijes, D., Lekanne Deprez, R. H., IJpma, A. S., … Majoor-Krakauer, D. (2018). Genetics, Clinical Features, and Long-Term Outcome of Noncompaction Cardiomyopathy. Journal of the American College of Cardiology, 71(7), 711–722. https://doi.org/10.1016/j.jacc.2017.12.019

Vermij, S. H., Abriel, H., & van Veen, T. A. B. (2017). Refining the molecular organization of the cardiac intercalated disc. Cardiovascular Research, cvw259. https://doi.org/10.1093/cvr/cvw259

Vogel, B., Meder, B., Just, S., Laufer, C., Berger, I., Weber, S., Katus, H. A., & Rottbauer, W. (2009). In-vivo characterization of human dilated cardiomyopathy genes in zebrafish. Biochemical and Biophysical Research Communications, 390(3), 516–522. https://doi.org/10.1016/j.bbrc.2009.09.129

Wahbi, K., Béhin, A., Charron, P., Dunand, M., Richard, P., Meune, C., Vicart, P., Laforêt, P., Stojkovic, T., Bécane, H. M., Kuntzer, T., & Duboc, D. (2012). High cardiovascular morbidity and mortality in myofibrillar myopathies due to DES gene mutations: A 10-year longitudinal study. Neuromuscular Disorders, 22(3), 211–218. https://doi.org/10.1016/j.nmd.2011.10.019

Walter, M. C., Reilich, P., Huebner, A., Fischer, D., Schröder, R., Vorgerd, M., Kress, W., Born, C., Schoser, B. G., Krause, K. H., Klutzny, U., Bulst, S., Frey, J. R., & Lochmüller, H. (2007). Scapuloperoneal syndrome type Kaeser and a wide phenotypic spectrum of adult-onset, dominant myopathies are associated with the desmin mutation R350P. Brain, 130(6), 1485–1496. https://doi.org/10.1093/brain/awm039

Weihl, C. C., Iyadurai, S., Baloh, R. H., Pittman, S. K., Schmidt, R. E., Lopate, G., Pestronk, A., & Harms, M. B. (2015). Autophagic Vacuolar Pathology in Desminopathies. Neuromuscular Disorders : NMD, 25(3), 199–206. https://doi.org/10.1016/j.nmd.2014.12.002

Weisleder, N., Taffet, G. E., & Capetanaki, Y. (2004). Bcl-2 overexpression corrects mitochondrial defects and ameliorates inherited desmin null cardiomyopathy. Proceedings of the National Academy of Sciences of the United States of America, 101(3), 769–774. https://doi.org/10.1073/pnas.0303202101

West, G., Sedighi, S., Agnetti, G., & Taimen, P. (2023). Intermediate filaments in the heart: The dynamic duo of desmin and lamins orchestrates mechanical force transmission. Current Opinion in Cell Biology, 85, 102280. https://doi.org/10.1016/j.ceb.2023.102280

953 Yu, M., Zheng, Y., Jin, S., Gang, Q., Wang, Q., Yu, P., Lv, H., Zhang, W., Yuan, Y., & Wang,
954 Z. (2017). Mutational spectrum of Chinese LGMD patients by targeted next-generation
955 sequencing. PloS One, 12(4), e0175343. https://doi.org/10.1371/journal.pone.0175343

956 Zhao, Y., Feng, Y., Zhang, Y.-M., Ding, X.-X., Song, Y.-Z., Zhang, A.-M., Liu, L., Zhang, H.,
957 Ding, J.-H., & Xia, X.-S. (2015). Targeted next-generation sequencing of candidate genes
958 reveals novel mutations in patients with dilated cardiomyopathy. International Journal of
959 Molecular Medicine, 36(6), 1479–1486. https://doi.org/10.3892/ijmm.2015.2361

960

Chapter IV

Objectives

ST-segment depression syndrome (STDS) is a recently described cardiac disease with an unknown genetic cause (Bundgaard et al., 2018). Patient ECGs have a characteristic nonischemic and persistent concave ST-depression on the antero-lateral leads of the ECG (Christensen et al., 2021, 2022). Up until now, sequencing of gene panels associated with heart diseases has failed to identify morbid genetic variants in patients diagnosed with STDS, making it difficult to investigate and model the disease but also to treat it, since no potential drug targets have been identified.

Desmin, a type III IF, has been studied since the late seventies and many mutations have since been identified along the desmin (*DES*) coding gene. Desmin-related cardiomyopathy or myopathy (desminopathy) is frequently associated with RCM, HCM, LVNC, DCM and ACM (Maggi et al., 2021) and most notably results in intracytoplasmic aggregate formation. Various models and in vitro approaches have been used to study consequences of desmin mutations on filament formation, yet the exact role of desmin within cardiomyocytes has still not been completely elucidated.

A young female patient presented at the hospital with ventricular fibrillation-induced SCD. Her ECG revealed a persistent depression of the ST-segment and genetic testing confirmed a *de novo* p.R406W mutation in *DES.* In this context, our objective was to determine the causal relationships between the mutation and the patient's cardiac phenotype. The interest of this study was to use the patients reprogrammed hiPSCs carrying the *DES* genetic variant and differentiate them into hiPSC-CMs. To better understand the role of desmin in cardiomyocytes, hiPSC-CMs were studied using multiple approaches to elucidate the structural and functional role of desmin in control and mutant cardiomyocytes.

Chapter V
Materials and Methods

5.1 Case Study

A 9-year-old female patient was admitted to the intensive care unit of l'institut du thorax (Nantes University Hospital) after her mother successfully resuscitated her from SCD. Her medical history was uneventful and with no family history of SCD. The patient's ECG revealed a generalized ST-segment depression (Figure 21; top panel) with no remarkable cardiac structural defects. An exercise test did not trigger arrhythmias and this ECG pattern was persistent over time. She received an implantable cardiac defibrillator (ICD) and was treated with hydroquinidine for the suspicion of Brugada Syndrome (BrS). BrS is often associated with mutations in the $Na_V1.5$ channel coded for by the *SCN5A* gene, but genetic testing was negative for mutations in this channel, both in the patient and her parents.

The patient's condition rapidly deteriorated from two episodes of ventricular fibrillation over the span of one and a half years, to at least one episode per month. She was hereby treated with amiodarone and beta-blockers. Nevertheless, her condition worsened to several episodes of ventricular fibrillation per day that were initiated from polymorphic premature ventricular beats mainly originating from the left ventricle (LV). The severity of her condition led to multiple catheter ablations at various locations but these were not enough to prevent the electrical storms as she was eventually placed on extracorporeal membrane oxygenation (ECMO) (Zhang et al., 2023) to help with her weakened LV function. Finally, the patient was successfully transplanted with a new heart at the age of 12.

Genetic testing of the patient identified a *de novo* p.R406W mutation in the *DES* gene which was not found in either of her parents (Figure 21; bottom panel). This mutation is located in exon 6 that codes for segment 2B of the desmin protein. Desmin mutations have been identified at multiple sites throughout the filament including the N-terminal head and C-terminal tail (Chapter III: Review). The p.R406W mutation has been previously described in some patients and has also been studied using various models.

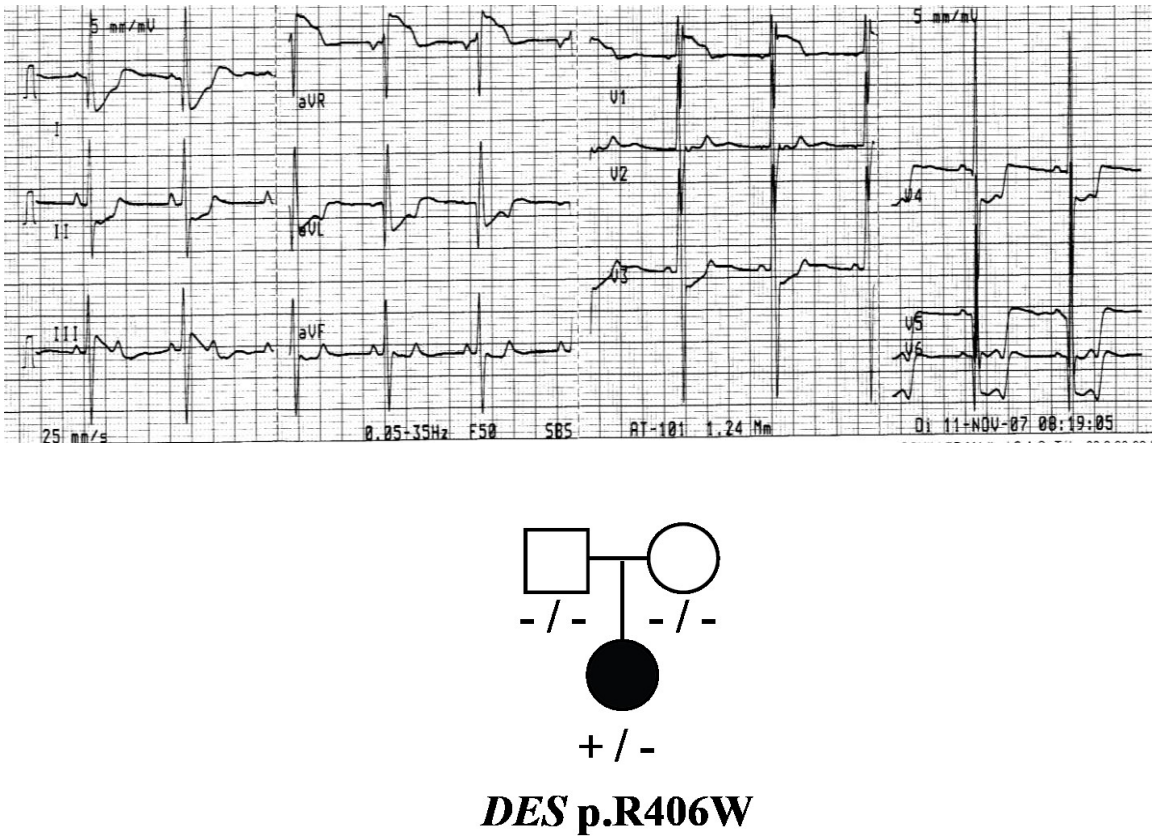

Figure 21. Patient case of ST-segment depression.

Electrocardiogram of patient that showed a depression in the ST-segment (top panel). Genetic testing of the family revealed a *de novo* mutation in the desmin (*DES*) gene at position c.1216 C > T (R406W) in the patient but was absent in the parents (bottom panel).

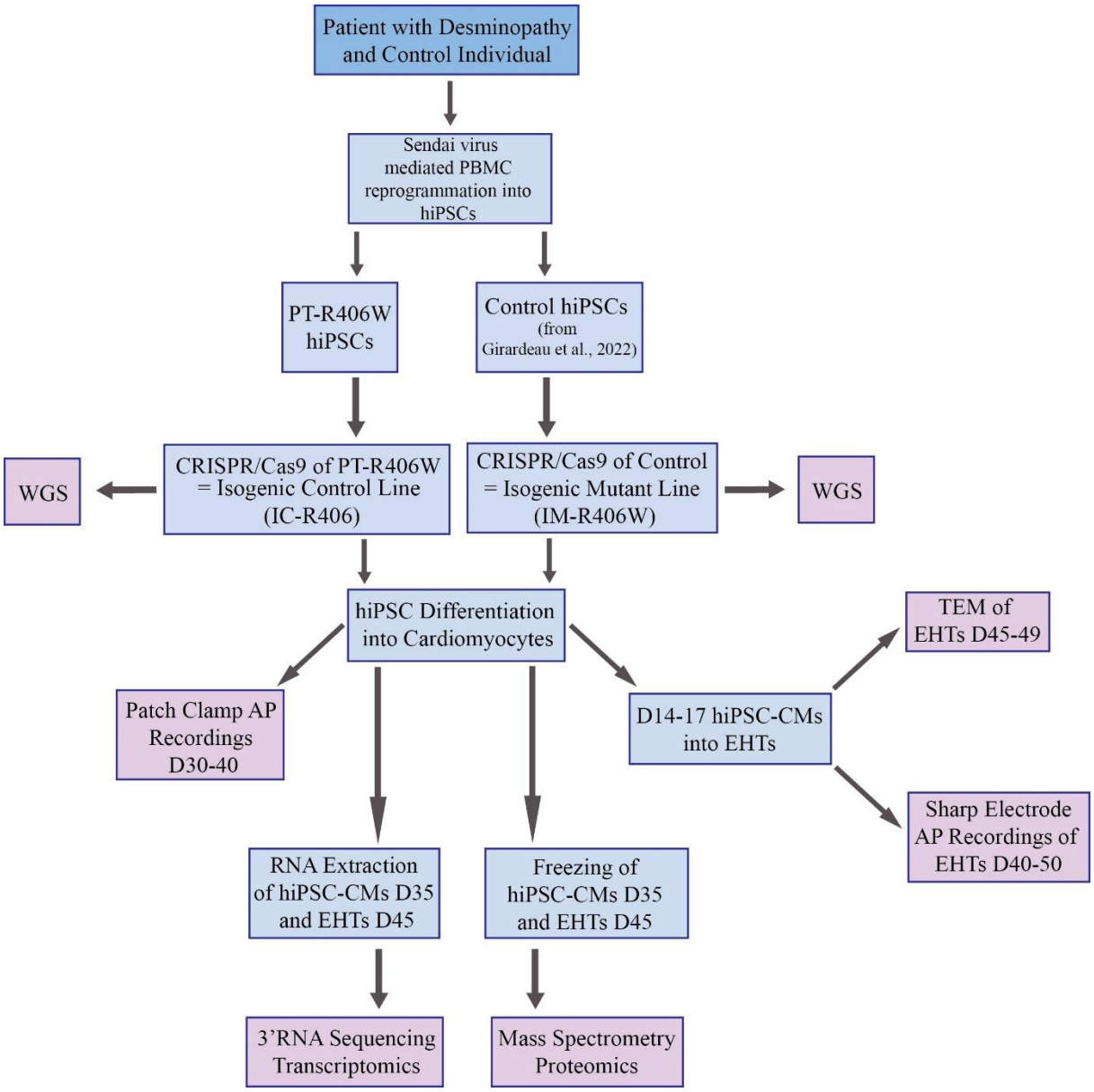

Figure 22. Workflow chart of methods.

5.2 Reprogramming and Maintenance of hiPSCs

The two hiPSC lines, Control (WT8288 was previously described (Girardeau et al., 2022)) and patient, were reprogrammed using Sendai viruses expressing Oct4, Sox2, Klf4, and c-Myc at the iPSC platform in Nantes, France. The patient line (PT-R406W) was derived from the patient's peripheral blood mononuclear cells (PBMC). All hiPSC lines were cultured on Matrigel® hESC-Qualified Matrix (0.05 mg/mL, Corning) coated plates and maintained at 37°C, 5% CO_2 and 21% O_2 in StemMACS^{TM} iPS Brew XF (Miltenyi Biotec). At 80% confluency, the cells were washed with DPBS without Ca^{2+}/Mg^{+} (Thermo Fisher Scientific),

dissociated using Gentle Cell Dissociation Reagent (STEMCELL™ Technologies) and re-plated as small clusters into new Matrigel coated plates.

5.3 Differentiation Protocol

The protocol for cardiac differentiation of hiPSCs was modified from previously described protocols (Calloe et al., 2022; Treat et al., 2019). Briefly, hiPSCs were cultured in Matrigel coated 12-well plates. When hiPSCs reached 80-90% confluency, cardiac differentiation was initiated with RPMI1640 (Life Technologies) supplemented with B27 (minus insulin, Life Technologies) (RPMI1640 + B27), 6 µM CHIR99021 (a Wnt pathway activator; Tocris), 10 ng/mL Activin A (R&D Systems) and 50 µg/mL L-ascorbic acid (Sigma) (D0; Figure 23). The next day (D1), the same medium was applied. On days 2,4, and 6, the medium was changed with RPMI1640 + B27 (minus insulin), 5 µM XAV 939 (a Wnt/β-catenin pathway inhibitor; Hello Bio), and 10 µM KY 02111 (a Wnt canonical pathway inhibitor; Hello Bio). On D8, medium was changed using RPMI1640 + B27 (plus insulin) and L-ascorbic acid. The cells underwent glucose starvation between days 10-14 using RPMI1640 without glucose (Life Technologies) + B27 (plus insulin) and containing 4mM sodium L-lactate (Sigma). From D14 to 30, the medium was changed every other day with RPMI1640 + B27 (plus insulin), 20 ng/mL thyroid hormone (3,3′,5-Triiodo-L-thyronine sodium salt, T_3, Sigma), and 1 µM dexamethasone (Cayman Chemical). Cells were dissociated on D16 and re-plated into new, Matrigel coated, 12-well plates using TrypLE 10x (Life Technologies). From D30 onward, hiPSC-CMs were maintained in RPMI1640 + B27 (plus insulin), which was changed every other day.

5.3.1 Freezing and Thawing of hiPSC-CMs

The desired wells containing beating hiPSC-CMs were washed with DPBS without Ca^{2+}/Mg^{+} and incubated at 37°C for 5 minutes with TrypLE 10x. Following incubation, the dissociation reagent was deactivated with RPMI1640 + B27 (with insulin) + 20% FBS (Eurobio®), the contents of the wells were collected into a tube, and centrifuged for 5 minutes at 200g. The supernatant was aspirated and the pellet was resuspended in CellBambanker (BAMBANKER™ - Fujifilm WAKO, SOBIODA, W1W302-14681). The cells were frozen at -150°C in cryogenic vials (Thermo Fisher Scientific).

To thaw hiPSC-CMs, the vial was incubated for 2-5 minutes at 37°C. The cells were then resuspended using DMEM-F12 (Life Technologies) + 20% FBS and centrifuged for 5 minutes at 200g. Following centrifugation, the pellet was resuspended in RPMI1640 + B27

(with insulin) + 1/1000 Y-27632 ROCK inhibitor (Tocris) and plated onto the desired Matrigel coated plates. The following day, the medium was changed according to the differentiation protocol.

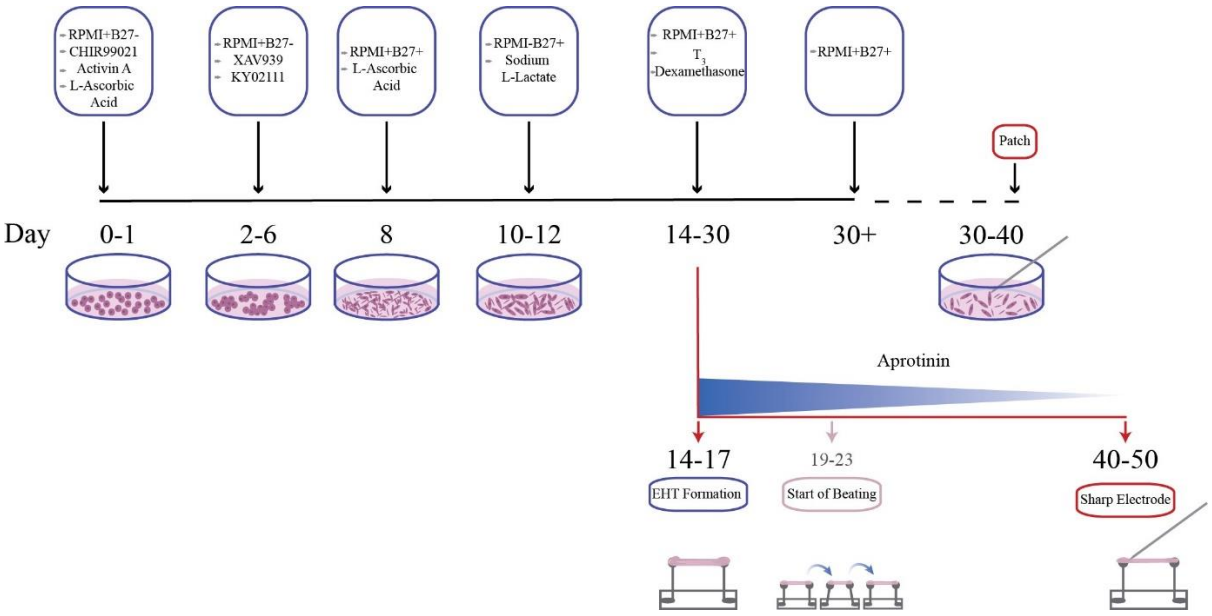

Figure 23. Differentiation protocol of hiPSCs into hiPSC-CMs and EHTs.

5.4 Generation of Isogenic Mutant and Control Lines from hiPSCs using CRISPR/Cas9

An isogenic control (IC-R406) was generated from the PT-R406W hiPSCs by correcting the mutation located on the *DES* gene at c.1216 C > T (p.R406W) to c.1216 T > C (p.R406). Likewise, an isogenic mutant line (IM-R406W) was created from the Control hiPSCs by introducing the mutation (experiments performed by Virginie Forest). To do so, CRISPR/Cas9 technology (Table 5) was employed according to the previously described protocol (Caillaud et al., 2022). The detailed description of these experiments and their validation is described in Article 1.

In order to genotype the cells, DNA was extracted from confluent colonies using the NucleoSpin® Tissue kit (MACHEREY-NAGEL) according to manufacturer's instructions, followed by PCR to genotype the region (Caillaud et al., 2022), and later sent for Sanger sequencing (Eurofins genomics) for sequence verification (Figure 24). Furthermore, the isogenic clones with the desired modification were sent for validation with whole genome sequencing (WGS) that was

performed by the Human Genetics team at *L'unité de recherche de l'institut du thorax* in Nantes, France (Estelle Baron, Julien Barc, and Pierre Lindenbaum) to confirm the presence or absence of the point mutation.

Table 5. Primers, guide RNA, and oligo DNA used for CRISPR/Cas9 experiments.

Product	Sequence
Alexa Fluor® 660 single strand oligo DNA (ssODN, IDT)	5'-AGGACCTGCTCAACGTGAAGATGGC CCTGGATGTGGAGATTGCCACCTAC**C**G GAAGCTGCTGGAGGGAGAGGAGAGCC GGTGAGGGGCCAGGCAGGAGCC -3'
gRNA (IDT)	ATG TGG AGA TTG CCA CCT AC
Alexa Fluor® 660 single strand oligo DNA (ssODN, IDT)	5'-AGGACCTGCTCAACGTGAAGATGGC CCTGGATGTGGAGATTGCCACCTAC**T**G GAAGCTGCTGGAGGGAGAGGAGAGCC GGTGAGGGGCCAGGCAGGAGCC -3'
Forward Primer 1 (Eurofins genomics)	5'- GAA ATC CGG CAC CTC AAG - 3'
Reverse Primer 1 (Eurofins genomics)	5'- CAG GTG GCC TTG GTT AAT TC - 3'
Forward Primer 2 (Eurofins genomics)	5'- CAG TGG CTA CCA GGA CAA CA - 3'
Reverse Primer 2 (Eurofins genomics)	5'- CCT GGG GAC AGA AAT GGA C - 3'

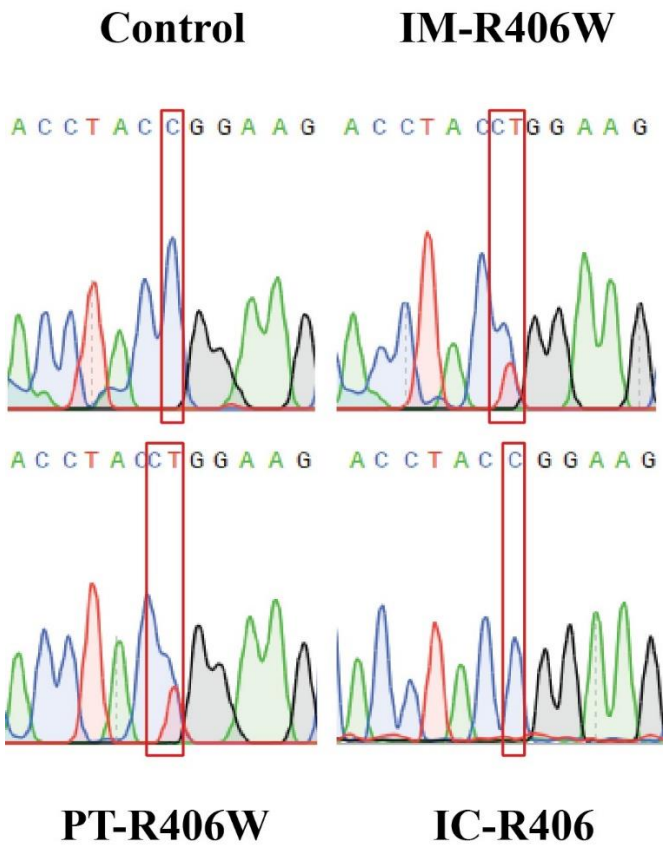

Figure 24. Results from Sanger sequencing of isogenic control and mutant clones.
To generate an isogenic control (IC-R406) from the PT-R406W hiPSCs, a nucleotide was changed at position c.1216 T > C on exon 6 of *DES*. Similarly, the isogenic mutant clone (IM-R406W) was generated from the Control hiPSCs (c.1216 C > T). The red boxes highlight the targeted nucleotides.

5.5 Generation of Engineered Heart Tissue from hiPSC-CMs

HiPSC-CMs were used to create EHTs that were matured into adult-like cardiomyocytes/tissues by culturing them in a 3D tissue form, as opposed to the standard 2D model. The technique was adapted from previously described protocols (Lam et al., 2019; Mannhardt et al., 2017; Ronaldson-Bouchard et al., 2019). Briefly, cardiomyocytes derived from hiPSCs were differentiated according to the protocol described above (refer to section 5.3 Differentiation Protocol). Multiple wells containing spontaneously beating cells (3 wells from a 12-well plate, with at least $1x10^6$ cells/ EHT) were dissociated between D14-17 using TrypLE 1x (Life Technologies) for 7 minutes at 37°C. The dissociation solution was deactivated with DMEM-F12 + 20% FBS, cells were collected into a tube and centrifuged for 3 minutes at 200 g. The supernatant was removed and the cells were washed with an extra 5 mL of deactivation solution and centrifuged for a second time. Following the washing step, supernatant was

aspirated and an EHT matrix (77 µl matrix + 10 µl/EHT Matrigel® Basement Membrane Matrix, Corning) was gently added on top of the cells, mixed, and incubated on ice for 3 minutes. The EHT matrix is a combination of 147 µl sterile filtered 2x DMEM solution (2 mL of heat-inactivated horse serum (Life Technologies), 6 mL of sterile water, 2 mL of 10x DMEM (134 mg/mL dissolved in sterile water, Life Technologies)) and 2640 µl of NKM solution (8.9 mL DMEM (Life Technologies) combined with 1 mL FBS and 100 µl L-glutamine (Life Technologies)) with 1/1000 of ROCK inhibitor. Next, for every EHT, 10 µl of fibrinogen (200 mg/mL, Sigma) was added to the tube and mixed gently by pipetting, while the tube was kept on ice. For every EHT, 100 µl of the cell-containing mixture was added to 3 µl of thrombin (100 U/mL, Sigma) in a separate 1.5 mL Eppendorf and added to the pre-set 2% agarose mold (Life Technologies, Figure 25A and C) in a 24-well plate containing a silicone rack (DiNAQOR, Figure 25B, D). The EHTs were incubated for two hours at 37°C (Figure 25E). Following incubation, the silicone racks were removed gently and place into a new 24-well plate containing warm EHT Medium 1 (50% RPMI1640 + B27 (with insulin), 50% EBM-2 + EGM-2 (Lonza), 1% penicillin/streptomycin (Life Technologies), 13.2 mg/L aprotinin (Sigma), 20 ng/mL of T_3, and 1 µM of dexamethasone) and left untouched in the incubator for 3 days (Figure 25F). EHTs started beating after three days and the medium was changed every day using EHT Medium 1 until D30. From D30 onward, EHT Medium 2 (50% RPMI1640 + B27 (with insulin), 50% DMEM F-12 + B27 (with insulin), 1% penicillin/streptomycin, and 6.6 mg/L of aprotinin) was changed every day (Figure 25G).

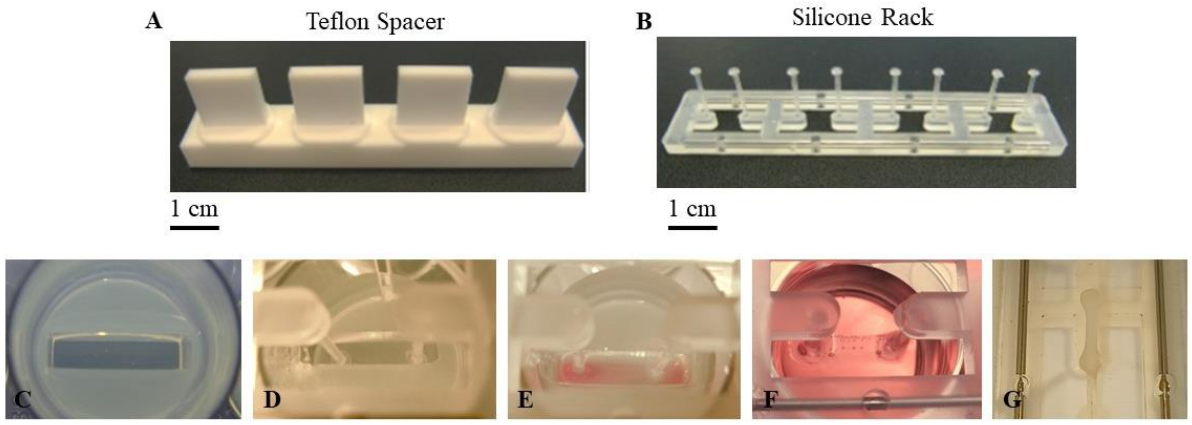

Figure 25. EHT formation and maturation.
EHTs are created using hiPSC-CMs by setting them into a 2% agarose mold (C) created using a Teflon spacer (A) onto a silicone rack (B). The hiPSC-CMs are incubated in the mold (D-E) and then the silicone rack is removed and added to a new well (F) containing appropriate culture medium. EHTs start to contract spontaneously after 3 days and thin overtime (G) (images modified from DiNAQOR and (Mannhardt et al., 2017)).

5.6 Transmission Electron Microscopy

Collaboration with Rodolphe Perrot from Service Commun d'Imageries et d'Analyses Microscopiques (SCIAM), Université d'Angers, France

EHTs were fixed on Day 47 (± 2 days) in 2.5% glutaraldehyde diluted in a phosphate buffer (DPBS without Ca^{2+} and Mg^{+}) at pH 7.4, for 24-hours at 4°C. The next day, the EHTs were removed from the silicone pillars (Figure 25G) and transferred to a phosphate buffer containing 67.04 mM Na_2HPO_4 (81%) and 65.2 mM NaH_2PO_4 (19%) at pH 7.4 and stored at 4°C and sent to the SCIAM facility in Angers, France. Afterward, samples were post-fixed in 1% osmium tetroxide/1% potassium ferrocyanide in water for 1h30 at room temperature. Then, the samples were washed three times by deionized water and subsequently dehydrated in a graded series of 35% (2x15 min), 50% (2x15 min), 70% (2x15 min), 95% (2x15 min) and 100% ethanol (2x30 min), followed by propylene oxide (2x15 min). After infiltration at 1:1 propylene oxide and epoxy resin (Epon™ 812) overnight, samples were embedded in 100% epoxy resin which was then left to polymerize for 24 h at 37°C, 24 h at 45°C and 48 h at 60°C. Ultra-thin sections (60 nm) were cut from each sample using Leica UC7 ultramicrotome (Leica microsystems, Wetzlar, Germany) and deposited onto copper grids. Sections were stained with 3% uranyl acetate in 50% ethanol for 15 min, washed three times with deionized water, stained with 3% lead citrate and washed again three times with deionized water. The samples were left to dry and then examined using the JEOL JEM-1400 electron microscope (JEOL, Tokyo, Japan) under 120 keV.

5.7 Micropatterning

Collaboration with Jean-Sébastien Hulot and Charlène Jouve from PARCC, Université Paris Cité, Paris, France

Frozen hiPSC-CMs were thawed on D29 and plated onto Matrigel coated 12-well plates with 1/1000 ROCK inhibitor. The culture medium was changed every other day using RPMI1640 + B27 (plus insulin). Seven days later (D36), cells were dissociated and 250 000 hiPSC-CMs were seeded onto custom designed micropatterened 18 mm coverslips (4D Cell, Montreuil, France). The micropatterned lines were 30 µm wide and 100 µm apart. Similarly, the following days, the medium was changed every other day using RPMI1640 + B27 (plus insulin). One-week later (D42), the seeded hiPSC-CMs were fixed with 4% paraformaldehyde for 10 min at RT, permeabilized with 0.5% Triton X-100 in PBS for 15 min and blocked with 2% BSA in PBS for 1 hour. Cells were incubated overnight at 4°C with primary antibodies diluted in

1% BSA in PBS, washed three times with PBS and incubated with suitable secondary antibodies and DAPI for 1 hour at room temperature. Desmin primary antibody (REF: HPA018803, Sigma) and the desmoplakin primary antibody (REF: 61024, Thermo Fisher Scientific) were both diluted at 1:100. Secondary antibodies were diluted at 1:1000 (goat anti-rabbit 546 REF: A11010, Thermo Fisher Scientific; goat anti-mouse 488 REF: A10680, Thermo Fisher Scientific). Immunostainings were examined using an inverted Eclipse Ti2 fluorescence microscope (Nikon) using Nikon Standard software.

5.8 Electrophysiology

5.8.1 Dissociation of hiPSC-CMs for Patch Clamp

On D28 or D30 of the differentiation protocol, the wells containing beating hiPSC-CMs were washed with DPBS and enzymatically dissociated using TrypLE 10x for 5 minutes at 37°C. The dissociation medium was deactivated using PRMI1640 + B27 (plus insulin) and 20% FBS. Cells were collected into a tube and centrifuged for 5 minutes at 200g. The supernatant was discarded and fresh culture medium containing 1/1000 ROCK inhibitor was added. Cells were re-plated onto Matrigel-coated 35-mm dishes (Thermo Fisher Scientific). Twenty-four hours later, the medium was changed to wash out the ROCK inhibitor. The following days the medium was changed every other day according to the differentiation protocol.

5.8.2 AP Recordings in hiPSC-CMs

The APs of all hiPSC-CM lines were acquired between D30-40 of differentiation using an amphotericin-B perforated-patch configuration with an Alembic VE-2 (Alembic Instruments, Montreal, QC, Canada) or Axopatch 200A amplifier controlled by Axon pClamp 10.6 software through an A/D converter (Digidata 1440A Molecular Devices, San Jose, CA, USA). The hiPSC-CMs were superfused with a HEPES-Tyrode solution containing (in mM): 130 NaCl, 4 KCl, 10 HEPES, 5 glucose, 1.2 $MgSO_4$, 1.2 NaH_2PO_4 and 1 $CaCl_2$; pH 7.4 (with NaOH). Borosilicate glass pipettes (Sutter Instruments, Novato, CA, USA) were pulled on a horizontal puller (Sutter Instruments; 1.5-3 MΩ of tip resistance) and filled with an intracellular solution containing (in mM): 5 NaCl, 20 KCl, 5 HEPES, and 125 K-Gluconate; pH 7.2 (with KOH). Amphotericin-B (Sigma) was added extemporarily to the intracellular solution (0.2 to 0.4 µg/mL). All measurements were conducted at 35-37°C. Single, spontaneously beating hiPSC-CMs were studied and the spontaneous APs were recorded first. Since hiPSC-CMs have limited I_{K1}, artificial I_{K1} was injected using dynamic patch-clamp (Meijer van Putten et al., 2015; Wilders, 2006). A custom-made software that runs on RT-Linux allows injection of I_{K1}

through an A/D converter (PCI-6221, National Instrument, Austin, TX, USA) connected to the voltage output and the current command of the patch-clamp amplifier. By controlling I_{K1} amplitude, the membrane potential was set between -85 to -90 mV. Cells were paced using a 1-ms square depolarizing current pulsed at a pacing cycle length (PCL) of 1000 ms and 700 ms. The cell capacitance (C_m) was entered to adapt the currents (I_{K1} and stimulation) to each cell. Since it is usually not possible to measure C_m at the beginning of the experiment, due to the poor permeabilization of the patch membrane beneath the pipette, we set its value to 33 pF. At the end of the recording, when the access resistance was low, C_m was measured. The correct current amplitude could be calculated afterward during analysis. APs were analyzed using an R script created by Jérôme Montnach, that analyzed individual APs from files created in Clampfit 10.6 during acquisition of either spontaneous or paced APs. The interval between APs, overshoot, MDP, dV/dt_{max}, AP duration (APD) at different levels of full repolarization (20% - 90%), and the amplitude of APs were measured. Data from five consecutive APs were averaged. Frozen as well as non-frozen hiPSC-CMs were used to record APs.

5.8.3 AP Recordings in EHTs

APs were recorded from spontaneously beating EHTs by impalement using high resistance glass microelectrodes (40-60 MΩ tip resistance; Harvard Apparatus) pulled using a horizontal puller (Sutter Instruments) and filled with 3 M KCl. The EHTs were superfused in a custom, 3D printed chamber (Figure 26) with the same HEPES-Tyrode solution as was used for patch-clamp experiments, and bubbled with 100% O_2. Electrodes were connected to a dual microelectrode amplifier (VF-102, BioLogicm Seyssinet-Pariset, France) and voltage traces were visualized on an oscilloscope (Tektronix, Beaverton, OR, USA) and digitized with an analogic/digital converter (PowerLab C, AD Instruments, Dunedin, New Zealand) at a sampling rate of 20 kHz for recording and further analyzed with LabChart 8 Pro software (AD Instruments). All AP recordings were performed at 36-37°C. Similarly, APs were analyzed using an R script written by Jérôme Montnach to measure the APDs, MDP, AP amplitude, interval between APs, dV/dt_{max}, and the overshoot. Data from five consecutive APs were averaged.

Figure 26. A custom 3D printed chamber used to measure action potentials in EHTs. (Photo by: Flavien Charpentier)

5.9 Transcriptomics and Proteomics

5.9.1 RNA Extraction

The four hiPSC lines were differentiated into cardiomyocytes until D35 of the protocol (Figure 23). Samples were collected from spontaneously beating wells from 7-9 independent differentiations. Likewise, independent EHTs (between 4-8 tissues per cell line) were cultured until D45. For every EHT, half of the tissue was flash frozen in a Cryotube (Thermo Fisher Scientific) with liquid nitrogen and stored at -80°C for proteomic applications and the other half was resuspended in RA1 and frozen at -80°C, prior to RNA extraction. RNA was extracted from EHTs and hiPSC-CMs using the NucleoSpin® RNA extraction kit (MACHEREY-NAGEL, Hoerdt, France), according to manufacturer's instructions. The RNA quality was evaluated by NanoDrop™ 1000 spectrophotometer (Thermo Fisher Scientific).

5.9.2 3'Sequencing RNA Profiling

Collaboration with the Genomics Core Facility GenoA and the Bioinformatics Core Facility BiRD, Nantes, France

3'Sequencing RNA Profiling (3'SRP) was performed according to the previously published protocol (Charpentier et al., 2021). Libraries were created by the GenoBiRD platform in Nantes, France from the hiPSC-CM and EHT RNA samples and sequenced using the NovaSeq 6000 sequencer (Illumina, San Diego, CA, USA).

5.9.3 Proteomics

Collaboration with François Guillonneau at the Prot'ICO proteomics facility, from the *Institut de Cancérologie de l'Ouest,* Angers, France

Protein extraction was performed on the same differentiations that were used for the 3'SRP; for every differentiation, half of the wells were used to extract RNA while cells from the others wells were pelleted for proteomic experiments. Similarly, for every EHT made, a part was used for RNA extraction and the other for proteomics. This was done to ensure that the same differentiation was represented in both techniques.

To create a dry pellet of hiPSC-CMs, the wells were washed with cold (4°C) DPBS without Ca^{2+}/Mg^{+}. Next, the cells were detached by flushing the well with 1000 µl DPBS using a pipette, collected into a tube and centrifuged at 200 g for 4 minutes. The supernatant was removed and the cells were washed with an extra 1000 µl DPBS and centrifuged again. The cells were washed a total of four times. Finally, the supernatant was aspirated, and the remaining dry pellet was frozen at -80°C.

The EHTs were washed four times with cold (4°C) DPBS without Ca^{2+}/Mg^{+}. Next, they were removed from the silicone pillars and cut into two, while kept on ice. The EHT sample was then placed in a Cryotube and flash frozen in liquid nitrogen and stored at -80°C.

Proteome Analysis by Prot'ICO

Liquid Chromatography-Mass Spectrometry (LC-MS/MS):

The pelleted EHT/hiPSC-CMs were thawed quickly and proteins were concomitantly extracted and denatured using 200 µL of 0.1% Rapigest SF acid-labile detergent (Waters), 5 mM DTT and 50 mM ammonium bicarbonate, at 95°C for 30 min. Thiol residues were thus chemically reduced and subsequently protected by alkylation in 10 mM MMTS (Sigma) for 10 minutes at 37°C. Samples were cooled to room temperature before adding trypsin (Porcine, sequencing grade from ABSciex), incubated at 37°C overnight (1 µg trypsin for 50 µg of protein). Peptides were then cleared by centrifugation, desalted on microcolumns and eluted. Eluates were dried in a vacuum centrifuge concentrator (Thermo Fisher Scientific), resuspended in 25 µL of 10% Acetonitrile (ACN) and 0.1% Formic Acid (FA). The equivalent of 200 ng of peptides were injected after microBCA peptide assay.

Each sample was injected and separated on a C18 reverse phase column (Aurora series 1.6 µm particles size, 75 µm inner diameter and 25 cm length from IonOptics) using a

NanoElute LC system (Bruker). Eluate flow was electrosprayed into a timsTOF Pro 2 mass spectrometer (Bruker) for the 60-minute duration of the hydrophobicity gradient ranging from 99% of solvent A containing 0.1% FA in milliQ-grade H_2O to 40% of solvent B containing 80% ACN plus 0.1% FA in mQ-H_2O. The mass spectrometer acquired data throughout the elution process and operated in data-independent analysis (DIA) with PASEF-enabled method using the TIMS-Control software (Bruker). Samples were injected in batch replicate order to circumvent possible technical biases.

LC-MS/MS Raw Data Analysis:

The raw data were extracted, normalized and analyzed using Spectronaut 18.0.23 (Biognosys) in DirectDIA+ mode, which modelized elution behavior, mobility and MS/MS events based on the Uniprot/Swissprot sequence 2022 database of human proteins. Protein identification false discovery rate (FDR) was restricted to 1% maximum, with a match between runs option enabled, and inter-injection data normalization. The enzyme's specificity was trypsin's. The precursor and fragment mass tolerances were set to 15 ppm. Oxidation of methionines was set as variable modifications while thiol groups from cysteines were considered completely alkylated by methylation. A minimum of two ratios of peptides was required for relative quantification between groups. Protein quantification analysis was performed using Label-Free Quantification (LFQ) intensities. The resulting proteins LFQ values were log2-transformed and stored in a matrix

5.9.4 Data Analysis

Data analysis for proteomics and transcriptomics was performed in collaboration with Bastien Cimarosti at L'Institut du Thorax, Nantes, France

5.10 Ethical Statement

The study was conducted according to the principles set forth under the Declaration of Helsinki (1989) and European guidelines for clinical and genetic research. Institutional review board approvals of the study were obtained before the initiation of patient enrolment. Informed written consent was obtained from each individual who agreed to participate in the clinical and genetic study. Authorization has been obtained from competent ethics review board (CPP Ouest II n◦ 2010-33) and approval authority (MESR n◦DC2011–1399) to generate the iPS lines.

Chapter VI

Results

Article 1

Generation of a patient-specific induced pluripotent stem cell line carrying the DES p.R406W mutation, an isogenic control and a DES p.R406W knock-in line

Michelle Geryk, Robin Canac, Virginie Forest, Pierre Lindenbaum, Aurore Girardeau, Manon Baudic, Estelle Baron, Anne Bibonne, Caroline Chariau, Florence Kyndt, Richard Redon, Jean-Jacques Schott, Jean-Baptiste Gourraud, Julien Barc, Flavien Charpentier

Published in *Stem Cell Research*

DOI: 10.1016/j.scr.2024.103396

Lab Resource: Genetically-Modified Cell Line

Title: Generation of a patient-specific induced pluripotent stem cell line carrying the DES p.R406W mutation, an isogenic control and a DES p.R406W knock-in line

Authors: Michelle Geryk[1], Robin Canac[1], Virginie Forest[1], Pierre Lindenbaum[1], Aurore Girardeau[1], Manon Baudic[1], Estelle Baron[1], Anne Bibonne[1], Caroline Chariau[2], Florence Kyndt[1], Richard Redon[1], Jean-Jacques Schott[1], Jean-Baptiste Gourraud[1], Julien Barc[1], Flavien Charpentier[1]

Affiliations: [1] Nantes Université, CHU Nantes, CNRS, Inserm, l'institut du thorax, F-44000 Nantes, France
[2] Nantes Université, CHU Nantes, Inserm, CNRS, BioCore, F-44000 Nantes, France

Abstract:
Mutations in the *DES* gene, which encodes the intermediate filament desmin, lead to desminopathy, a rare disease characterized by skeletal muscle weakness and different forms of cardiomyopathies associated with cardiac conduction defects and arrhythmias. We generated induced pluripotent stem cells (iPSC) from a patient carrying the DES p.R406W mutation, and employed CRISPR/Cas9 to rectify the mutation in the patient's iPSC line and introduced the mutation in an iPSC line from a control individual unrelated to the patient. These iPSC lines represent useful models for delving into the mechanisms of desminopathy and developing new therapeutic approaches.

Resource Table:

Unique stem cell line identifier	1. ITXi013-A 2. ITXi013-B 3. ITXi006-A-1
Alternative name(s) of stem cell line	PT-R406W (ITXi013-A) IC-R406 (ITXi013-B) IM-R406W (ITXi006-A-1)
Institution	L'institut du thorax (INSERM UMR1087, CNRS UMR6291, Nantes, France)
Contact information of the reported cell line distributor	Flavien Charpentier, Flavien.charpentier@univ-nantes.fr
Type of cell line	Induced pluripotent stem cells (iPSCs)
Origin	Human
Additional origin info ***(applicable for human ESC or iPSC)***	Age: 22 Sex: Female Ethnicity: European

Cell Source	Peripheral blood mononuclear cells (PBMCs)
Method of reprogramming	Integration-free Sendai virus expressing human *OCT4*, *SOX2*, *KLF4*, and c-*MYC*
Clonality	Clonal
Evidence of the reprogramming transgene loss (including genomic copy if applicable)	RT-qPCR
The cell culture system used	StemMACS™ iPS Brew XF Medium on Matrigel® hESC-Qualified Matrix
Type of the Genetic Modification	PT-R406W: spontaneous/naturally occurred mutation IC-R406: mutation correction of PT-R406W iPSCs by CRISPR/Cas9 IM-R406W: induced mutation by CRISPR/Cas9 in control iPSCs
Associated disease	Cardiomyopathy associated with desmin (*DES*) mutation OMIM: 601419 / 125660
Gene/locus modified in the reported transgenic line	PT-R406W and IM-R406W: *DES* (GRCh38 2q35: 219418377-219426734) exon 6, NM_001927.4(DES):c.1216C>T (p.R406W) IC-R406: *DES* (GRCh38 2q35: 219418377-219426734) exon 6, NM_001927.4(DES):c.1216 T>C (p.R406W)
Method of modification / user-customisable nucleases (UCN) used, the resource used for design optimisation	HiFi-CRISPR/Cas9 endonuclease
User-customisable nuclease (UCN) delivery method	Electroporation of Cas9-RNP
All double-stranded DNA genetic material molecules introduced into the cells	Single-stranded oligo DNA nucleotide (ssODN) CRISPR/Cas9
Evidence of the absence of random integration of any plasmids or DS DNA introduced into the cells.	Whole genome sequencing (WGS)
Analysis of the nuclease-targeted allele status	WGS
Homozygous allele status validation	Sanger sequencing and WGS
Method of the off-target nuclease activity prediction and surveillance	WGS
Descriptive name of the transgene	N/A

Eukaryotic selective agent resistance cassettes (including inducible, gene/cell type-specific)	N/A
Inducible/constitutive expression system details	N/A
Date archived/stock creation date	2020/01/03
Cell line repository/bank	PT-R406W: https://hpscreg.eu/cell-line/ITXi013-A IC-R406: https://hpscreg.eu/cell-line/ITXi013-B IM-R406W: https://hpscreg.eu/cell-line/ITXi006-A-1
Ethical/GMO work approvals	A signed informed consent has been received.
Addgene/public access repository recombinant DNA sources' disclaimers (if applicable)	N/A

Resource utility

The patient generated iPSC line harbouring the desmin gene (*DES*) p.R406W mutation, along with the isogenic control and isogenic mutant lines are a useful resource for investigating the function of the desmin protein in derived cardiomyocytes. Desmin mutations have previously been linked to cardiac and skeletal disorders.

Resource Details

Desmin is a type Ⅲ intermediate filament that is encoded by *DES* and is found in smooth, skeletal and cardiac muscle cells. Desmin is important for interconnecting essential organelles to one another as well as to the cell membrane in order to provide support and maintain the structural integrity of the cells. Mutations in *DES* have been shown to cause skeletal and/or cardiac myopathies (Capetanaki et al., 2007). Histology experiments that have been performed on patient skeletal and cardiac muscle samples most often reveal dense cytoplasmic aggregates (Tsikitis et al., 2018). *In vitro* studies have shown that mutations in *DES* impact the formation of proper filaments (Bär et al., 2005).

A nine-year old female patient presented with sudden cardiac death (SCD) and a persistent ST-segment depression on her electrocardiogram (ECG). Genetic testing revealed a *de novo* mutation in *DES* at c.1216C>T (p.R406W), while the patients parents were negative for the mutation (Fig. 1A). The mutation (c.1216C>T) is located in exon 6 that codes for the highly conserved segment 2B of the desmin filament (Fig.1B) and has been previously reported in patient cases with cardiac disorders (Brodehl et al., 2018).

At the age of 22, the patient's peripheral blood mononuclear cells (PBMCs) were collected and hiPSC lines were generated using the Sendai virus method. We generated an isogenic control line (IC-R406) from the patients hiPSC line (PT-R406W) as well as an isogenic mutant line (IM-R406W) from the

WT8288 (ITXi006-A) line that was published previously (Girardeau et al., 2022). Both isogenic lines were created using the CRISPR/Cas9 technology as previously published (Caillaud et al., 2022).

The four hiPSC lines were cultured on Matrigel® coated plates in StemMACS™ iPS-Brew XF media. Mycoplasma contamination assessment was performed by Eurofins genomics and no contamination has been identified in any of the lines (Supplementary Table 1). All hiPSC clones showed typical colony morphology that was assessed by brightfield microscopy (Fig. 1C, left panel). Expression of pluripotency markers OCT3/4 and TRA-1-60 was evaluated by immunofluorescence experiments (Fig. 1C). Pluripotency status of hiPSCs was likewise quantitatively assessed by RT-qPCR using *SOX2*, *NANOG* and *POU5F1* markers (Fig. 1D). The absence of Sendai virus persistence following reprogramming of PT-R406W clone was shown (Fig. 1E). Each cell line was differentiated into endoderm, mesoderm, and ectoderm using the Miltenyi Biotec Trilineage differentiation kit. The ability of PT-R406W, IC-R406 and IM-R406W hiPSCs to be able to differentiate into derivatives of the three germ layers was validated by RT-qPCR with *PAX6* as the ectoderm marker, *FOXA2* as the endoderm marker, and *HAND1* as the marker for the mesoderm layer (Fig. 1F). Furthermore, no major chromosomal aberrations were found between (1) the control (WT8288) and the CRISPR/Cas9 generated isogenic mutant as well as (2) the patient cells, the patient hiPSC line and the CRISPR/Cas9 generated isogenic control clone (Supplementary Fig.1) Finally, relatedness between clones was validated from the WGS data using Somalier tool (Supplementary Table 2). Detailed information for all lines is provided in Tables 1 and 2.

Materials and Methods

HiPSC Generation and Maintenance

After Sendai virus reprogramming and CRISPR/Cas9 based editing, all hiPSC lines were maintained at 37°C, 5% CO_2, 21% O_2 in StemMACS™ iPS Brew XF Medium (Miltenyi Biotec) and on Matrigel® hESC-Qualified Matrix (0.05 mg/mL, Corning). At 80% confluency, cells were passaged as clusters using Gentle Cell Dissociation Reagent (STEMCELL Technologies).

CRISPR/Cas9 Genome Editing

The gRNA, gRNA_KI_DES, was first duplexed with ATTO™ 488-tagged transactivating RNA and then complexed to the Alt-R® Hifi Cas9 Nuclease according to IDT recommendations. The complex and a specific ssODN donor (either DES_Donor_Mut or DES_Donor_c.1216C-T) was delivered into hiPSCs using the P3 Primary Cell 4D-Nucleofector™X Kit L with the Amaxa nucleofector (CA137, Lonza). hiPSCs double positive for ATTO™488 and Alexa Fluor®660, and negative for DAPI, were single-cell FACS-sorted 48 hours post-transfection (BD FACSMelody™ cell sorter, BD). Cells were maintained in iPS Brew until they reached 80% confluency and then used for cloning, amplification and duplication for banking and genotyping.

DNA Extraction, PCR, Sanger Sequencing and WGS

The genomic DNA was isolated using the NucleoSpin Tissue Purification Kit (MACHEREY-NAGEL). The DNA fragment of *DES* containing the knock-in was amplified by PCR using 10 ng/µl of genomic DNA with specific forward and reverse primers (Table 2). The PCR products were visualized on 1.5% agarose gel and sequenced by Eurofins Genomics.

To visualize any large CNVs that would have occurred in our cell lines, CRAM files were filtered for primary reads having a mapping quality greater than 30 and were reindexed. The resulting BAM files were processed with indexcov (https://pubmed.ncbi.nlm.nih.gov/29048539/). The relatedness

between cell lines was validated using Somalier (https://pubmed.ncbi.nlm.nih.gov/32664994/). Analysis was processed using Nextflow (https://pubmed.ncbi.nlm.nih.gov/28398311/) and our local pipeline (https://github.com/lindenb/gazoduc-nf/).

Trilineage Differentiation

HiPSC lines were differentiated into the 3 germ layers using the STEMdiff™ Trilineage Differentiation Kit (Miltenyi Biotech) according to the manufacturer's instructions. RNA was extracted using NucleoSpin RNA kit (MACHEREYNAGEL). The three differentiation-markers-Taqman™ probes that were used are listed in Table 2.

RT-qPCR

RNA was extracted from samples as described above and reverse transcribed using High-Capacity cDNA Reverse Transcription kit (Applied Biosystems™). PCR amplification was per formed using FAM-labeled TaqMan probes (Applied Biosystems) for pluripotency and trilineage differentiation (Table 2). Data was normalized to ACTB or GAPDH.

Immunofluorescence

Cells were washed three times using PBS and fixed with 4% paraformaldehyde (Sigma-Aldrich) for 20 mins at room temperature (RT). Cells were washed another three times with PBS and permeabilized with 0.5% Triton X-100 (Sigma-Aldrich) for 15 mins at RT and then blocked with 3% BSA at RT for 30 mins. Primary antibodies in 1% BSA were applied to cells and incubated for 2 hours at RT. Following three washing steps with PBS, cells were incubated for 1 hour at RT with secondary antibodies and then washed again three times with PBS and kept in 0.5% paraformaldehyde at 4°C. The next day, cells were imaged using Eclipse Ti2 fluorescence microscope (Nikon) using the Nikon Standard software. Antibody information is listed in Table 2.

Mycoplasma Detection

Mycoplasma contamination assessment was performed by Eurofins genomics (Supplementary Table 1).

Acknowledgements

We thank the iPSC core facility of Nantes (funded by Biogenouest, IBiSA). We are most grateful to the Genomics Core Facility GenoA, member of Biogenouest and France Genomique and to the Bioinformatics Core Facility BiRD, member of Biogenouest and *Institut Français de Bioinformatique* (IFB; ANR-11-INBS-0013) for the use of their resources and their technical support. We thank Lise Bray (l'institut du thorax) for her help and support. This work was funded by grants for the INSERM cross-cutting program GOLD (Genomic variability in health and disease to R.R.), the Fondation Genavie (JB.G.), and the French National Research Agency (ANR-19-CE14-0031-02 to F.C.).

References

Bär, H., Mucke, N., Kostareva, A., Sjoberg, G., Aebi, U., & Herrmann, H. (2005). Severe muscle disease-causing desmin mutations interfere with in vitro filament assembly at distinct stages. *Proceedings of the National Academy of Sciences*, *102*(42), 15099–15104. https://doi.org/10.1073/pnas.0504568102

Brodehl, A., Gaertner-Rommel, A., & Milting, H. (2018). Molecular insights into cardiomyopathies associated with desmin (DES) mutations. *Biophysical Reviews*, *10*(4), 983–1006. https://doi.org/10.1007/s12551-018-0429-0

Caillaud, A., Lévêque, A., Thédrez, A., Girardeau, A., Canac, R., Bray, L., Baudic, M., Barc, J., Gaborit, N., Lamirault, G., Gardie, B., Idriss, S., Rimbert, A., Le May, C., Cariou, B., & Si-Tayeb, K. (2022). FACS-assisted CRISPR-Cas9 genome editing of human induced pluripotent stem cells. *STAR Protocols*, *3*(4), 101680. https://doi.org/10.1016/j.xpro.2022.101680

Capetanaki, Y., Bloch, R. J., Kouloumenta, A., Mavroidis, M., & Psarras, S. (2007). Muscle intermediate filaments and their links to membranes and membranous organelles. *Experimental Cell Research*, *313*(10), 2063–2076. https://doi.org/10.1016/j.yexcr.2007.03.033

Girardeau, A., Atticus, D., Canac, R., Cimarosti, B., Caillaud, A., Chariau, C., Simonet, F., Cariou, B., Charpentier, F., Gourraud, J.-B., Probst, V., Belbachir, N., Jesel, L., Lemarchand, P., Barc, J., Redon, R., Gaborit, N., & Lamirault, G. (2022). Generation of human induced pluripotent stem cell lines from four unrelated healthy control donors carrying European genetic background. *Stem Cell Research*, *59*, 102647. https://doi.org/10.1016/j.scr.2021.102647

Tsikitis, M., Galata, Z., Mavroidis, M., Psarras, S., & Capetanaki, Y. (2018). Intermediate filaments in cardiomyopathy. *Biophysical Reviews*, *10*(4), 1007–1031. https://doi.org/10.1007/s12551-018-0443-2

Table 1: Characterization and validation

Classification	Output type	Result	Data
Schematic of a transgene/genetic modification	Schematic representation	Visual representation of the desmin protein structure and the location of the mutation on segment 2B. The c1216 C>T or c.1216T>C transition causes a change in amino acids p.R406 to R406W and vice versa.	Fig.1B
Morphology	Photography	Normal	Brightfield images Fig.1C Scale bar= 100µm
Pluripotency status evidence for the described cell line	Qualitative analysis (Immunofluorescence)	Positive expression of pluripotency markers: OCT3/4 and TRA-1-60	Fig. 1C Scale bar= 100µm
	Quantitative analysis (RT-qPCR)	Stable expression of pluripotency markers throughout cell lines: *SOX2, POU5F1*, and *NANOG*	Fig. 1D
Karyotype	WGS, copy number variations (CNV)	No evidence for CNVs	Supplementary Fig.1
Genotyping for the desired genomic alteration/allelic status of the gene of interest	PCR, Sanger sequencing and WGS (BAM files)	Presence of desired genomic alteration in *DES* c.1216 C>T or c.1216 T>C	Fig.1G
	PCR, Sanger sequencing and WGS (BAM files)	Successful knock-in of desired nucleotide in the desmin gene	Fig.1G
	Transgene-specific PCR (when applicable)	N/A	N/A
Verification of the absence of random plasmid integration events	N/A	N/A	N/A
Parental and modified cell line genetic identity evidence	WGS (relatedness based on common variants along the genome)	Edited cell lines matched (100%) their parental cell line	Supplementary Table 2

		N/A	N/A
Mutagenesis / genetic modification outcome analysis	PCR, Sanger sequencing	Sanger sequencing of alteration: *DES* (GRCh38 2q35: 219418377-219426734) exon 6, c.1216 C>T (p.R406W) and *DES* (GRCh38 2q35: 219418377-219426734) exon 6, c.1216 T>C (p.R406)	Fig. 1G
	PCR-based analyses	N/A	N/A
	Southern Blot or WGS; western blotting (for knock-outs, KOs)	N/A	N/A
Off-target nuclease activity analysis	WGS	N/A	N/A
Specific pathogen-free status	Mycoplasma	No contamination was detected in any of the cell lines	Supplementary Table 1
Multilineage differentiation potential	Directed trilineage differentiation	Miltenyi Biotec Trilineage differentiation kit and RNA analysis by RT-qPCR. Cell lines were positive for: Mesoderm: *HAND1* Endoderm: *FOXA2* Ectoderm: *PAX6*	Fig. 1F
List of recommended germ layer markers	N/A	N/A	N/A
Outcomes of gene editing experiment (OPTIONAL)	N/A	N/A	N/A
Donor screening (OPTIONAL)	N/A	N/A	N/A
Genotype - additional histocompatibility info (OPTIONAL)	N/A	N/A	N/A
	N/A	N/A	N/A

Table 2: Reagents details

Antibodies and stains used for immunocytochemistry/flow-cytometry			
	Antibody	**Dilution**	**Company Cat # and RRID**
Pluripotency Markers	Mouse anti-TRA-1-60	1:200	Thermo Fisher Scientific Cat# 14-8863-82, RRID: AB_891610
	Rat anti-OCT3/4	1:200	Thermo Fisher Scientific Cat# 14-5841-82, RRID: AB_914301
Nuclear Stain	Hoechst 33342	1:500	Thermo Fisher Scientific Cat# 62249
Secondary antibodies	Goat anti-rat 488nm	1:1000	Invitrogen Cat# A11006, RRID: AB_2534074
	Donkey anti-mouse 568nm	1:1000	Invitrogen Cat# A10037, RRID: AB_2534013
Site-specific nuclease			
Nuclease information	Alt-R® S.p. HiFi Cas9 Nuclease V3	Integrated DNA Technologies (IDT) Cat# 1081061	
Delivery method	Nucleofection	P3 Primary Cell 4D-Nucleofector™ X Kit L, Lonza, Cat# V4XP-3024	
Selection/enrichment strategy	FACS sorting using transactivator-associated fluorescence	Transactivator: Alt-R® CRISPR-Cas9 tracrRNA ATTO™ 488, IDT ssODN: Single-stranded DNA oligo Alexa Fluor® 660, IDT	
Primers and Oligonucleotides used in this study			
	Target	**Forward/Reverse primer (5'-3')**	
Differentiation markers (qPCR)	*PAX6*	Thermo Fisher Scientific TaqMan®probe ID: Hs01088114_m1	
	FOXA2	Thermo Fisher Scientific TaqMan®probe ID: Hs00232764_m1	
	HAND1	Thermo Fisher Scientific TaqMan®probe ID: Hs02330376_s1	
Pluripotency Markers (qPCR)	*SOX2*	Thermo Fisher Scientific TaqMan®probe ID: Hs01053049_s1	
	POU5F1	Thermo Fisher Scientific TaqMan®probe ID: Hs04260367_gH	
	NANOG	Thermo Fisher Scientific TaqMan®probe ID: Hs02387400_g1	
House-Keeping Genes (qPCR)	*ACTB*	Thermo Fisher Scientific TaqMan®probe ID: Hs99999903_m1	
	GAPDH	Forward: 5'-AAT CCC ATC ACC ATC TTC CA-3' Reverse: 5'TGG ACT CCA CGA CGT ACT CA-3'	
Primers for PCR and Sanger sequencing	Desmin	Forward 1: 5'-GAA ATC CGG CAC CTC AAG-3'	
		Reverse 1: 5'-CAG GTG GCC TTG GTT AAT TC-3'	
		Forward 2: 5'-CAG TGG CTA CCA GGA CAA CA-3'	
		Reverse 2: 5'-CCT GGG GAC AGA AAT GGA C-3'	
Potential random	N/A	N/A	

integration-detecting PCRs		
Sendai Virus Detection (primer)	SeV	Forward: 5'-GGA TCA CTA GGT GAT ATC GAG C-3' Reverse: 5'-ACC AGA CAA GAG TTT AAG AGA TAT GTA TC-3'
gRNA oligonucleotide	gRNA_KI_DES	5'-ATG TGG AGA TTG CCA CCT AC-3'
Genomic target sequence(s)	N/A	N/A
Bioinformatic gRNA on- and -off-target binding prediction tool used, specific sequence/outputs link(s)	IDT	https://eu.idtdna.com/site/order/designtool/index/CRISPR_CUSTOM
Primers for top off-target mutagenesis predicted site sequencing (for all CRISPR/Cas9, ZFN and TALENs)	N/A	N/A
ssODN guides for HDR-mediated mutagenesis	DES_Donor_Mut (induction of the mutation)	5'-AGGACCTGCTCAACGTGAAGATGGCCCTGGATGTGGAGATT GCCACCTAC**T**GGAAGCTGCTGGAGGGAGAGGAGAGCCGGTGAGGGGCCAGGCAGGAGCC -3'
	DES_Donor_c.1216C-T (correction of the mutation)	5'-AGGACCTGCTCAACGTGAAGATGGCCCTGGATGTGGAGATTG CCACCTAC**C**GGAAGCTGCTGGAGGGAGAGGAGAGCCGGTGAGGGGCCAGGCAGGAGCC -3'

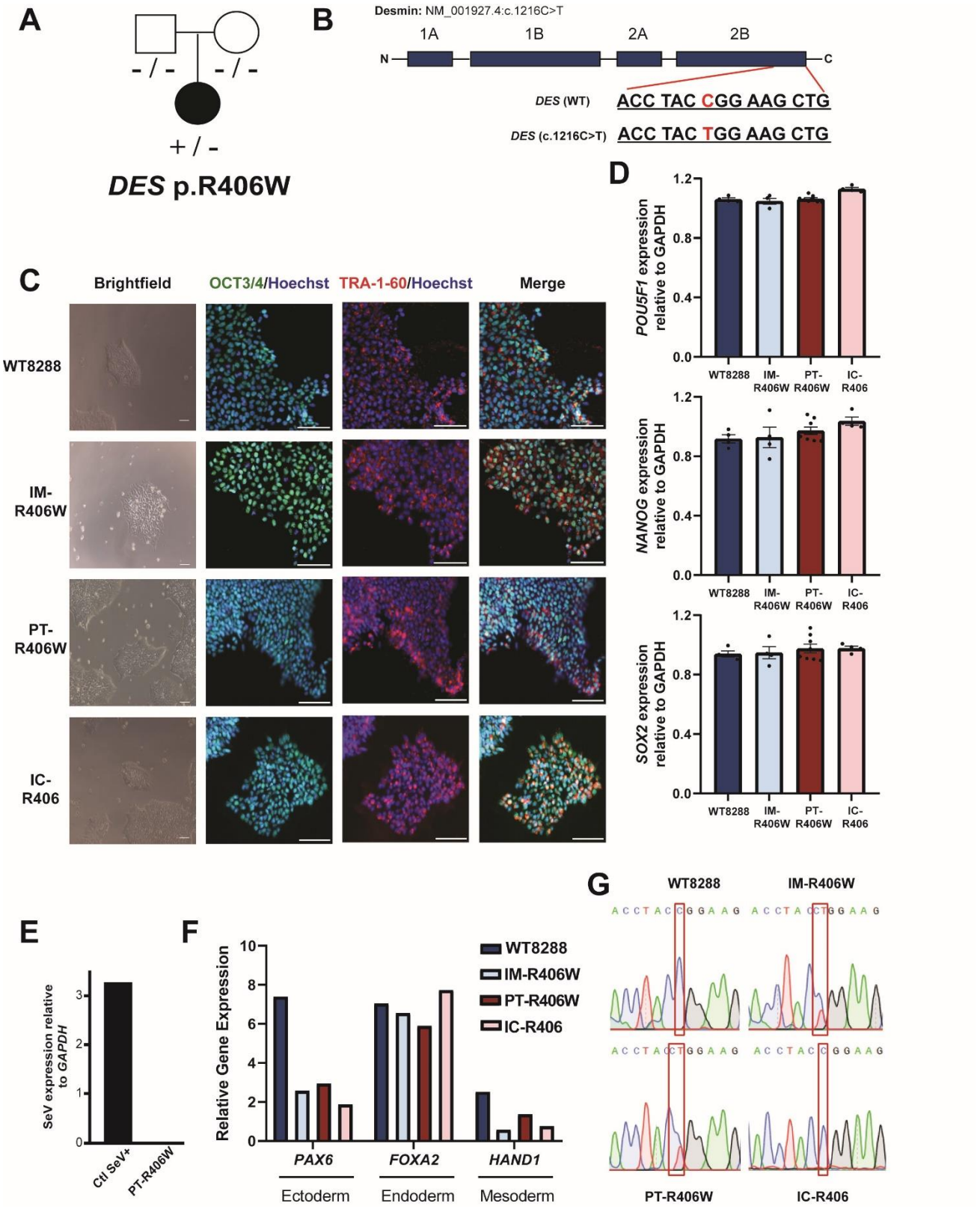
A
- / -
- / -
+ / -
DES p.R406W
B
Desmin: NM_001927.4:c.1216C>T
1A
1B
2A
2B
N
C
DES (WT) ACC TAC CGG AAG CTG
DES (c.1216C>T) ACC TAC TGG AAG CTG
C
Brightfield
OCT3/4/Hoechst
TRA-1-60/Hoechst
Merge
WT8288
IM-R406W
PT-R406W
IC-R406
D
POU5F1 expression relative to GAPDH
NANOG expression relative to GAPDH
SOX2 expression relative to GAPDH
1.2
0.8
0.4
0.0
WT8288
IM-R406W
PT-R406W
IC-R406
E
SeV expression relative to GAPDH
Ctl SeV+
PT-R406W
F
Relative Gene Expression
WT8288
IM-R406W
PT-R406W
IC-R406
PAX6
FOXA2
HAND1
Ectoderm
Endoderm
Mesoderm
G
WT8288
IM-R406W
PT-R406W
IC-R406

Figure 1.

Supplementary

Table 1. Mycoplasma assessment performed by Eurofins Genomics. No contamination was detected.

Barcode	Cell Line Name	Testing Date	PCR Inhibition	Mycoplasma	Summary
MP00093406	Negative control	31/01/2023	Absent	Absent	Clean
MP00093412	PT-R406W	31/01/2023	Absent	Absent	Clean
MP00093411	IM-R406W	31/01/2023	Absent	Absent	Clean
MP00093413	IC-R406	31/01/2023	Absent	Absent	Clean
MP00093415	WT8288	31/01/2023	Absent	Absent	Clean

Table 2. Comparison of the relatedness two by two between the patient (B00I9FS), the patient-derived hiPSCs (PT-R406W), isogenic control (IC-R406), and the isogenic mutant (IM-R406W) generated from the control line (WT8288) was validated using WGS data with the Somalier tool. Cells originating from the patient are in blue. Cells originating from the control individual are in black.

Sample A	Sample B	Relatedness	Conclusion
Isogenic Control IC-R406	Isogenic Mutant- IM-R406W	0.144	Not related
Isogenic Control IC-R406	Patient PT-R406W	1.000	Related
Isogenic Control IC-R406	Patient Cells-B00I9FS	1.000	Related
Isogenic Control IC-R406	WT8288	0.126	Not related
Isogenic Mutant- IM-R406W	Patient PT-R406W	0.134	Not related
Isogenic Mutant- IM-R406W	Patient Cells-B00I9FS	0.083	Not related
Isogenic Mutant- IM-R406W	WT8288	1.000	Related
Patient PT-R406W	Patient Cells-B00I9FS	1.000	Related
Patient PT-R406W	WT8288	0.115	Not related
Patient Cells-B00I9FS	WT8288	0.068	Not related

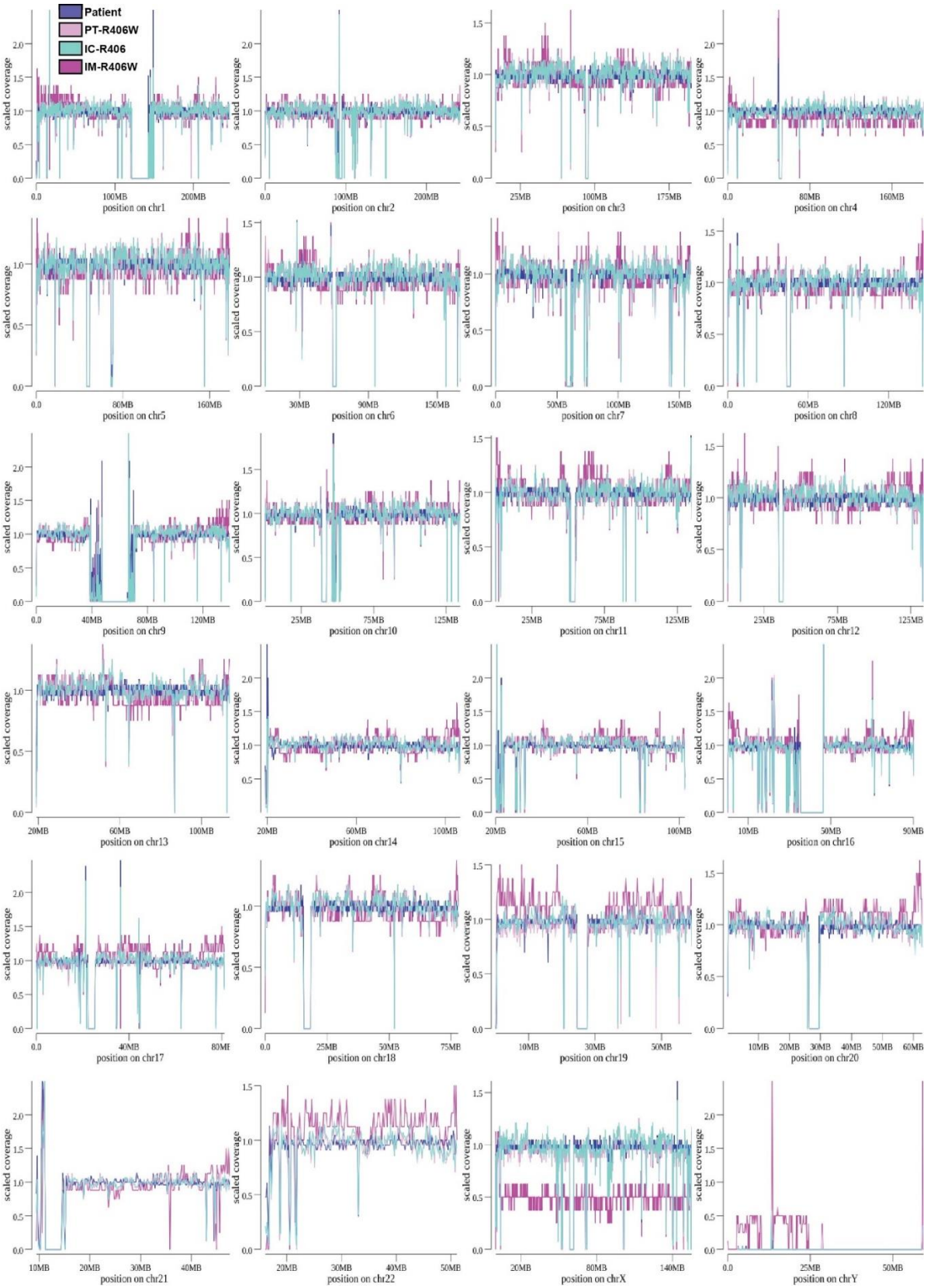

Figure 1. Indexcov output that estimates the genome-wide coverage of samples (patient in dark blue, PT-R406W in pink, IC-R406 in green, and IM-R406W in purple) along the genome to identify any copy number variation (CNV). The plots show the normalized coverage of each samples in the genome for each chromosome. There is no evidence for new or large CNVs.

Table 3. Passage number of hiPSC lines tested for trilineage and immunostaining.

Clone	Passage Number
WT8288	p. 52
IM-R406W	p.49
PT-R406W	p.45
IC-R406	p.62

Article 2

DES p.R406W mutation causing cardiac arrhythmias impacts gene expression and electrical properties of hiPSC derived cardiomyocytes

Michelle Geryk, Bastien Cimarosti, Isabelle Baró, Pierre Lindenbaum, Florence Kyndt, Alice Boissard, Cécile Henry, Catherine Guette, Mélèze Hocini, Michel Haissaguerre, Guillaume Lamirault, Francois Guillonneau, Michel Haissaguerre, Hervé le Marec, Jean-Jacques Schott, Jean-Baptiste Gourraud, Flavien Charpentier

In Preparation

DES p.R406W mutation causing cardiac arrhythmias impacts gene expression and electrical properties of hiPSC derived cardiomyocytes

Michelle Geryk[1], Bastien Cimarosti[1], Isabelle Baró[1], Pierre Lindenbaum[1], Florence Kyndt[1], Alice Boissard[2], Cécile Henry[2], Catherine Guette[3], Mélèze Hocini[4], Michel Haissaguerre[4], Guillaume Lamirault[1], Francois Guillonneau[3], Michel Haissaguerre[4], Hervé le Marec[1], Jean-Jacques Schott[1], Jean-Baptiste Gourraud[1], Flavien Charpentier[1]*

1. Nantes Université, CHU Nantes, CNRS, INSERM, l'institut du thorax, F-44000 Nantes, France
2. Institut de Cancérologie de l'Ouest, F-49055 Angers, France
3. Nantes Université, Univ Angers, INSERM, CNRS, CRCI2NA, F-44000 Nantes, France
4. IHU LIRYC, Electrophysiology and Heart Modeling Institute, and Bordeaux University Hospital, Bordeaux, France.

*** Correspondence:**

L'institut du thorax, Inserm UMR1087, CNRS UMR6291

IRS-UN, 8 quai Moncousu

44007 Nantes cedex 1, France

E-mail: flavien.charpentier@univ-nantes.fr

Tel. + 33 2 28 08 01 64

Abstract

Background and aims: Cardiomyopathy has been linked to mutations in the desmin intermediate filament. The aim of this study was to illustrate the structural and functional consequences of the desmin p.R406W mutation *(DES*^{R406W}) involved in a patient-specific case of severe cardiomyopathy.

Methods: We report a patient in her first decade of life presenting with sudden cardiac death (SCD) and severe arrhythmias, caused by a heterozygous *DES*^{R406W} mutation, leading to heart transplantation. The patient's reprogrammed human induced pluripotent stem cells (hiPSC) were differentiated into cardiomyocytes (hiPSC-CMs). Subsequently, an isogenic mutant and control (*DES*^{R406}) hiPSC lines were generated by CRISPR/Cas9 gene editing. Action potentials (AP) of hiPSC-CMs were measured using the dynamic-clamp method. Subsequently, engineered heart tissues (EHT) were generated from the hiPSC-CMs and their APs were recorded by impalement with sharp electrodes. Effects of the *DES*^{R406W} mutation on cellular function were addressed by proteomic and transcriptomic analysis. Structural effects of the mutation were observed using transmission electron microscopy (TEM).

Results: Patch-clamp analysis of hiPSC-CMs revealed longer action potential durations (APD) in *DES*^{R406W} lines compared to *DES*^{R406} hiPSC-CMs. Similarly, longer APDs were observed in *DES*^{R406W}-EHTs compared to control tissues. Mutant EHTs displayed a large remodeling of genes and proteins expression, including an up-regulation of proteins involved in metabolism and cardiac contraction. TEM analysis of the EHTs revealed changes in Z-disc architecture.

Conclusion: This work highlights the disruptive effects of the *DES*^{R406W} variant on electrophysiological properties and biological processes related to cardiac contraction and metabolism.

Key words: cardiomyopathies, desminopathy, arrhythmia, human induced pluripotent stem cell-derived cardiomyocytes, engineered heart tissue.

Introduction

Desmin, a type III muscle-specific intermediate filament (IF) (OMIM # 125660), is found in cardiac, smooth and skeletal muscle cells and is the most abundant IF in cardiomyocytes (1,2). Desmin filaments traverse the cell forming a web that interconnects various parts of the cardiomyocyte including organelles, such as the mitochondria and the nucleus, insuring their correct location and position within the cell (1). Similarly, desmin attaches at the Z-discs and interconnects them laterally; anchoring the contractile apparatus to the cell membrane at the level of the intercalated discs (IDs) and costameres (2–4). These complex connections contribute to the structural and functional integrity of cardiomyocytes in order for them to perform their highly demanding function.

Mutations in desmin have been identified at different positions along the desmin gene (*DES)*. Desmin has a non-alpha helical N-terminal head and C-terminal tail, and four alpha helical segments (1A, 1B, 2A, 2B) separated by linkers (L1, L12, L2) (4). Patients with *DES* mutations have been reported to have skeletal and/or cardiac myopathy, so called desminopathy (OMIM# 601419). Cardiomyopathy ranges from hypertrophic (HCM), restrictive (RCM), dilated (DCM) with reports of left ventricle non-compaction (LVNC), and arrhythmogenic cardiomyopathy (ACM), with ranging symptoms (2). Unrelated patients with the same mutation do not all have the same age of onset or progression of disease, nor do they present with the same symptoms or cardiomyopathy, adding to the complexity of desminopathy. Consequences of desmin mutations have been studied to uncover the underlying mechanism of disease progression in various *in vivo* and *in vitro* models (5–7). It has been reported that mitochondria (8–11), intercalated discs (5), and Z-discs (12,13) are largely affected by desmin mutations. The effect of desmin mutations on the electrophysiology of cardiomyocytes remains uncharacterized, although desminopathies have been associated with cardiac conduction blocks and arrhythmias.

In the present study, we investigated the electrophysiological, transcriptomic and proteomic consequences of the *DES* mutation p.R406W (c.1216C>T), DES^{R406W}, identified in a female patient with persistent, non-ischemic ST depression on her ECG, severe ventricular arrhythmias, and sudden cardiac death (SCD). The DES^{R406W} variant is located in a highly conserved region among species (14). To address this, we used two and three-dimensional models generated from human (patient and control individual) induced pluripotent stem cell-derived cardiomyocytes (hiPSC-CMs) and engineered heart tissues (EHT).

Methods

The study was conducted according to the principles set forth under the Declaration of Helsinki (1989) and European guidelines for clinical and genetic research. Institutional review board approvals of the study were obtained before the initiation of patient enrolment. Informed written consent was obtained from each individual who agreed to participate in the clinical and genetic study.

Maintenance of hiPSCs

The four hiPSC lines (PT-R406W, IC-R406, Control, and IM-R406W) used in the current study have been previously described ((15) (Article 1)). Briefly, both PT-R406W and Control lines were generated from peripheral blood mononuclear cells (PBMC) of the patient and an unrelated healthy donor, respectively. Two isogenic lines, IC-R406 and IM-R406W lines, were created using CRISPR/Cas9 technology to correct the mutation in the PT-R406W line and introduce the mutation in the Control line, respectively. The success of gene modification was verified using Sanger sequencing and whole genome sequencing (WGS).

All hiPSC lines were maintained at 37°C, 5% CO_2, 21% O_2 in StemMACS™ iPS Brew XF Medium (Miltenyi Biotec, Bergisch Gladbach, Germany) on culture plates coated with Matrigel® hESC-Qualified Matrix (0.05 mg/mL, Corning, NY, USA). At 80% confluency, the

hiPSCs were passaged using Gentle Cell Dissociation Reagent (STEMCELL™ Technologies, Vancouver, Canada).

Cardiac Differentiation of hiPSCs

Step specific directed cardiac differentiation of hiPSCs was performed using a modified version of the previously described protocol (16). Briefly, differentiation was initiated once hiPSCs reached 90% confluency by culturing the cells in RPMI1640 medium (Thermo Fisher Scientific, Waltham, MA, USA) supplemented with B27 (without insulin, Thermo Fisher Scientific), 6 µM CHIR99021 (Tocris Bioscience, Bristol, UK), 10 ng/mL recombinant human/mouse/rat activin A protein (R&D Systems, Minneapolis, MN, USA), 50 µg/ml L-ascorbic acid (Sigma-Aldrich), and changed the next day using the same media. On days 2, 4, and 6, the culture medium was changed using RPMI1640 + B27 (without insulin), 5 µM XAV 939 (Hello Bio, Bristol, UK), and 10 µM KY 02111 (Hello Bio). The medium was replaced with RPMI1640 + B27 (with insulin) and L-ascorbic acid on days 8 and 10 followed by a glucose depletion medium containing RPMI1640 medium without glucose (Thermo Fisher Scientific) + B27 (with insulin) and 4 mM sodium L-lactate (Sigma-Aldrich). Cells were kept in depletion medium from day 10-14 and were subsequently changed to maturation medium RPMI1640 + B27 (with insulin) containing 1 µM dexamethasone (Cayman Chemical Co, Ann Arbor, MI) and 20 ng/ml 3,3′,5′-Triiodo-L-thyronine sodium salt (T_3, Sigma-Aldrich). Maturation medium was changed every other day until day 30 and RPMI1640 + B27 (with insulin) was used after that. Spontaneously beating cardiomyocytes were observed between days 8 and 10.

Generation of engineered heart tissues (EHTs) from hiPSC-CMs

EHTs were made from hiPSC-CMs (at least $1x10^6$ cells/EHT) between days 14-17 of differentiation as described previously (17–19). Briefly, hiPSC-CMs were dissociated using TrypLE 1x (7 minutes, 37°C, Thermo Fisher Scientific) and centrifuged twice for 3 minutes at

200 g before being resuspended in an EHT mastermix, fibrinogen (200 mg/mL, Sigma-Aldrich) and 10 µl Matrigel® Basement Membrane Matrix (Corning). The EHT mastermix was a combination of sterile filtered 2x DMEM solution [2 mL heat-inactivated horse serum (Thermo Fisher Scientific), 6 mL sterile water, and 2 mL of 10x DMEM (134 mg/mL, Thermo Fisher Scientific) and NKM solution (8.9 mL DMEM (Thermo Fisher Scientific) combined with 1 mL FBS and 100 µl L-glutamine (Thermo Fisher Scientific)]. For every EHT, 100 µl of the cell-containing solution was briefly mixed with 3 µl thrombin (100 U/mL, Sigma-Aldrich) and pipetted into a pre-set 2% agarose mold created using a teflon spacer (DiNAQOR, Hamburg, Germany) in a 24-well plate containing a silicone rack (DiNAQOR). After a 2-hour incubation at 37°C, the silicone racks were removed gently from the molds and added to a new 24-well plate containing a culture medium composed of 50% RPMI1640 + B27 (with insulin), 50% EBM-2 + EGM-2 (Lonza, Basel, Switzerland), 1% penicillin/streptomycin (Thermo Fisher Scientific) with 13.2 mg/L aprotinin (Sigma-Aldrich), 20 ng/mL of T_3 hormone, and 1 µM of dexamethasone. This medium was changed every day until day 30. Subsequently, EHTs were switched to a medium containing 50% RPMI1640 + B27 (with insulin), 50% DMEM F-12 + B27 (with insulin), 1% penicillin/streptomycin, and 6.6 mg/L aprotinin.

Action Potential Recordings Using hiPSC-CMs

The APs of single hiPSC-CMs were acquired at 35-37°C using the amphotericin-B perforated patch method as previously described (20) with an Alembic VE-2 (Alembic Instruments, Montreal, QC, Canada) or Axopatch 200A amplifier controlled by Axon pClamp 10.6 software through an A/D converter (Digidata 1440A Molecular Devices, San Jose, CA, USA). hiPSC-CMs were superfused with a modified Tyrode solution containing (in mM): 130 NaCl, 4 KCl, 10 HEPES, 5 glucose, 1.2 $MgSO_4$, 1.2 NaH_2PO_4 and 1 $CaCl_2$; pH 7.4 (with NaOH). Borosilicate glass pipettes (1.5-3 MΩ of tip resistance, Sutter Instrument, Novato, CA, USA) were pulled on a horizontal puller (P97, Sutter Instruments) and filled with an

intracellular solution containing (in mM): 5 NaCl, 20 KCl, 5 HEPES, and 125 K-Gluconate; pH 7.2 (with KOH). Amphotericin-B (Sigma) was added extemporarily to the intracellular solution (0.2 to 0.4 μg/mL). APs of spontaneously beating hiPSC-CMs were recorded first. Since hiPSC-CMs have a limited I_{K1}, artificial I_{K1} was injected using dynamic patch-clamp (21,22). A custom-made software that runs on RT-Linux allows injection of I_{K1} through an A/D converter (PCI-6221, National Instruments, Austin, TX, USA) connected to the voltage output and the current command of the patch-clamp amplifier. By controlling I_{K1} amplitude, the membrane potential was set between -85 to -90 mV. Cells were paced using a 1-ms square depolarizing current pulsed at a pacing cycle length (PCL) of 1000 ms and 700 ms. APs were analyzed using an R script that analyzed individual APs from files created in Clampfit 10.6 during acquisition of either spontaneous or paced APs. The interval between APs, the AP maximum diastolic potential (MDP), overshoot, amplitude, maximum upstroke velocity (dV/dt_{max}), and duration (APD) at different levels (20%, 30%, 50%, 70%, 80%, 90%) of full repolarization were measured. Data from four to five consecutive APs were averaged. Part of the AP recordings have been performed on hiPSC-CMs frozen on day 28 and thawed at day 29. There was no statistical difference in AP parameters between frozen and non-frozen cells.

Action Potential Recordings Using EHTs

APs were recorded from spontaneously beating EHTs by impalement using high resistance glass microelectrodes (40-60 MΩ tip resistance; Harvard Apparatus) pulled using a horizontal puller (P97, Sutter Instrument) and filled with 3 M KCl. The EHTs were superfused in a custom, 3D printed chamber, with the same Tyrode solution as was used for patch-clamp experiments, and bubbled with 100% O_2. Microelectrodes were connected to an amplifier (VF-102, BioLogic, Seyssinet-Pariset, France) and voltage traces were visualized on an oscilloscope (Tektronix, Beaverton, OR, USA) and digitized with an analogic/digital converter (PowerLab C, ADInstruments, Dunedin, New Zealand) at a sampling rate of 20 kHz for recording with

LabChart 8 Pro software (AD Instruments). All AP recordings were performed at 36-37°C. Intervals between APs, MDP, AP amplitude, overshoot, dV/dt_{max} and APDs were analyzed using an R script. Data from five consecutive APs were averaged.

Omics analyses

Sample Collection

For all four hiPSC lines, samples were collected from 5 to 8 independent EHTs at day 45 of differentiation. EHTs were washed four times with DPBS without $Ca^{2+}$and Mg^{2+} at 4°C, removed from the silicone rack and then cut into two. For every EHT, one half was flash frozen in a Cryotube (Thermo Fisher Scientific) in liquid nitrogen and stored at -80°C for proteomic applications and the second half was resuspended in RA1 (MACHEREY-NAGEL) and stored at -80°c for transcriptomic applications.

Data generation

Transcriptomics (3'RNA-Sequencing). Total RNA was extracted using the NucleoSpin RNA kit (MACHEREY-NAGEL) according to manufacturer's instructions and their quality assessed by NanoDropTM 1000 Spectrophotometer (Thermo Fisher Scientific). 3'RNA libraries were prepared by GenoBiRD core facility according to their published method (23) and sequenced on a NovaSeq 6000 Sequencing System (Illumina, San Diego, CA, USA).

Proteomics (LC-MS/MS). EHTs were quickly thawed and proteins were concomitantly extracted and denatured using 200 µL of 0.1% Rapigest SF acid-labile detergent (Waters), 5 mM DTT and 50 mM ammonium bicarbonate, at 95°C for 30 min. Thiol residues were thus chemically reduced and subsequently protected by alkylation in 10 mM MMTS (Sigma) for 10 min at 37°C. Samples were cooled to room temperature before adding trypsin (Porcine, sequencing grade from ABSciex), incubated at 37°C overnight (1 µg trypsin for 50 µg of protein). Peptides were then cleared by centrifugation, desalted on microcolumns and eluted.

Eluates were dried in a vacuum centrifuge concentrator (Thermo), resuspended in 25 µL of 10% Acetonitrile (ACN) and 0.1% Formic Acid (FA). The equivalent of 200 ng of peptides were injected after microBCA peptide assay.

Each sample was injected and separated on a C18 reverse phase column (Aurora series 1.6-µm particles size, 75-µm inner diameter and 25-cm length from IonOptics) using a NanoElute LC system (Bruker). Eluate flow was electrosprayed into a timsTOF Pro 2 mass spectrometer (Bruker) for the 60 min duration of the hydrophobicity gradient ranging from 99% of solvent A containing 0.1% FA in milliQ-grade H_2O to 40% of solvent B containing 80% ACN plus 0.1% FA in mQ-H_2O. The mass spectrometer acquired data throughout the elution process and operated in data-independent analysis (DIA) with PASEF-enabled method using the TIMS-Control software (Bruker). Samples were injected in batch replicate order to circumvent possible technical biases.

Data analysis

Transcriptomics. Demultiplexing, alignment on GRCh38 reference genome, counting steps, normalization and log-transformation of expression matrices were conducted with the Snakemake pipeline developed by the GenoBiRD core facility (23). Genes with significant expression variation between *DES*^{R406}-EHTs (Control and IC-R406 lines) and *DES*^{R406W}-EHT (PT and IM-R406W lines) were identified with DESeq2 (RRID:SCR_015687) (24) and a Benjamini-Hochberg-corrected p-value < 0.05. Principal Component Analysis (PCA) was performed with the R package FactoMineR (RRID:SCR_014602) (25) on the entire mean-centered and log-transformed matrix.

Proteomics. The raw data were extracted, normalized and analyzed using Spectronaut 18.0.23 (Biognosys) in DirectDIA+ mode, which modelized elution behavior, mobility and MS/MS events based on the Uniprot/Swissprot sequence 2022 database of human proteins. Protein identification false discovery rate (FDR) was restricted to 1% maximum, with a match

between runs option enabled, and inter-injection data normalization. The enzyme's specificity was trypsin's. The precursor and fragment mass tolerances were set to 15 ppm. Oxidation of methionines was set as variable modifications while thiol groups from cysteines were considered completely alkylated by methylation. A minimum of two ratios of peptides was required for relative quantification between groups. Protein quantification analysis was performed using Label-Free Quantification (LFQ) intensities. The resulting proteins LFQ values were then log2-transformed and stored in a matrix.

PCA was performed with the R package FactoMineR (RRID:SCR_014602) (25) on the entire mean-centered and log-transformed matrix. Proteins with significant expression variation between *DES*^{R406}-EHTs and *DES*^{R406W}-EHTs were identified with a Limma test from the R package limma (26) and a Benjamini-Hochberg-corrected p-value < 0.05 based on a log2-transformed matrix with missing values imputed. Missing values were imputed separately for each hiPSC lines. A minimum of 50% of values was required to impute data with the R package missForest (RRID:SCR_018543) (27), else missing values were imputed as 0.

Multi-omic analysis. Differentially expressed genes and proteins were grouped into 4 clusters based on their expression fold-change in both transcriptomic and proteomic studies. Row and column dendrograms were calculated using Euclidean distance and Ward.D2 method on transcriptomic and proteomic data for row dendrogram and on all 4 clusters for column dendrogram. Data were then visualized with the R package ComplexHeatmap (RRID:SCR_017270) (28). When necessary, gene SYMBOL and UNIPROT ID were matched using the R package ClusterProfiler (RRID:SCR_016884) (29) and org.Hs.eg.db_3.18.0 database.

Over-Representation Analysis was performed using either the R package DOSE (30) for disease ontology annotation or the R package ClusterProfiler (RRID:SCR_016884) (29) and the org.Hs.eg.db_3.18.0 database for GO biological process and GO cellular component

annotations. Significantly enriched (Benjamini-Hochberg-corrected p-value < 0.05) annotation, as compared to reference proteome, and with a Gene Set Size (GSSize) between 10 and 500, were considered for further analysis. The 30 GO or disease terms with the lowest corrected p-value were visualized with treeplot.

Transmission Electron Microscopy

EHTs were fixed on day 47 (+/- 2 days) in 2.5% glutaraldehyde in phosphate buffer (DPBS without Ca^{2+} and Mg^{+}) at pH 7.4 for 24 h at 4°C. The next day, the EHTs were removed from the silicone pillars and transferred to a phosphate buffer containing 81% 67.04 mM Na_2HPO_4 and 19% 65.2 mM NaH_2PO_4 at a pH 7.4 and stored at 4°C and sent to the SCIAM facility in Angers. Afterward, samples were post-fixed in 1% osmium tetroxide/1% potassium ferrocyanide in water for 1h30 at room temperature. Then, the samples were washed three times by deionized water and subsequently dehydrated in a graded series of 35% (2x15 min), 50% (2x15 min), 70% (2x15 min), 95% (2x15 min) and 100% ethanol (2x30 min), followed by propylene oxide (2x15 min). After infiltration at 1:1 propylene oxide and epoxy resin (Epon™ 812) overnight, samples were embedded in 100% epoxy resin which was then left to polymerize 24 h at 37°C, 24 h at 45°C and 48 h at 60°C. Ultra-thin sections (60 nm) were cut from each sample using Leica UC7 ultramicrotome (Leica microsystems, Wetzlar, Germany) and deposited onto copper grids. Sections were stained with 3% uranyl acetate in 50% ethanol for 15 min, washed three times with deionized water, stained with 3% lead citrate and washed again three times with deionized water. The samples were left to dry and then examined using the JEOL JEM-1400 electron microscope (JEOL, Tokyo, Japan) under 120 keV.

Statistical analysis of electrophysiological data

Statistical analysis was performed using Prism8 v8.3.0 software (GraphPad) using the non-parametric Mann-Whitney test to compare two groups. P-values <0.05 were considered significant.

Results

Case Study

A 9-year-old female patient was admitted to the Hospital after she was successfully resuscitated from SCD. Her medical history was uneventful with no family history of SCD. A complete clinical evaluation including echocardiography and cardiac computed tomography did not reveal any structural heart disease, including abnormalities of the coronary arteries. In contrast, the patient's electrocardiogram (ECG) revealed a deep and persistent ST-segment depression in leads I, II, aVL, and V3 through V6 and a mirror image in leads III, aVR and V1 (Figure 1A). An exercise test did not trigger any arrhythmia. This ECG pattern persisted over time. She received an implantable cardioverter-defibrillator and was treated with hydroquinidine. Familial screening was performed in all the first-degree relatives of the patient and did not reveal any abnormalities.

After an initial 18-month period with 2 recurrences of ventricular fibrillation (VF), the patient's condition deteriorated to at least one VF episode per month. Several antiarrhythmic drugs (including beta-blocker therapy and amiodarone) were tried and finally combined without efficacy. Her condition eventually worsened to several episodes of VF per day during several days leading to an alteration of her hemodynamic status. VF episodes were initiated from polymorphic premature ventricular beats (PVB) mainly originating from the left ventricle (LV; Figure 1A). The severity of her condition prompted an electrophysiological investigation during which few Purkinje potentials were detected, thus explaining the conduction defects observed on the ECG. Multiple catheter ablations at various locations, namely the left interventricular septum, the right ventricular outflow track, and the left ventricular apex and anterior wall did not stop the onset of arrhythmias, as new electrical storms emerged from different PVBs, ultimately leading to cardiogenic shock. The patient was placed on extracorporeal membrane oxygenation because of her weakened LV function, and finally successfully transplanted. She

has since remained healthy, with a follow-up period of 15 years.

Anatomo-histopathological examination showed that both the right ventricle and focally the LV exhibited increased amounts of epicardial adipose tissue but no overt evidence of fibro-fatty replacement. In the LV, small areas of fibrosis and scarring, which may represent ischemic changes possibly caused by VF, were noted, in addition to ablation. A clear substrate for the clinical presentation of the patient was not evident on histology. Evidence for myocarditis, pericarditis, endocarditis or vasculitis was not noted.

Genetic investigation

Whole genome sequencing was performed on the patient and her siblings, leading to the identification of a *de novo* variant (c.1216C>T) on the *DES* gene (Figure 1B), resulting in a substitution of the arginine at position 406 by a tryptophan (p.R406W) in desmin.

Electrophysiological Characterization of hiPSC-CMs

To investigate the electrophysiological consequences of the heterozygous DES^{R406W} mutation, we differentiated the four lines into hiPSC-CMs (Figure 1D). The electrophysiological phenotype was evaluated by recording spontaneous (Figure 2 A, left panels) and paced APs (Figure 2A, right panels). The beat-to-beat interval of the spontaneously beating hiPSC-CMs was not significantly different between the cell lines (Figure 2B). There was a significant difference in the MDPs between the two compared groups. The MDP was less negative in IM-R406W (-52.4 ± 1.3 mV) compared to the Control (-56.8 ± 1.6 mV, p=0.03) (Figure 2C). The MDP of PT-R406W hiPSCs (-49.3 ± 1.2 mV) was also significantly less negative than the IC-R406 hiPSC-CMs (-54.2 ± 1.5 mV, p=0.008). There were no significant differences in amplitude between the four lines (Figure 2E).

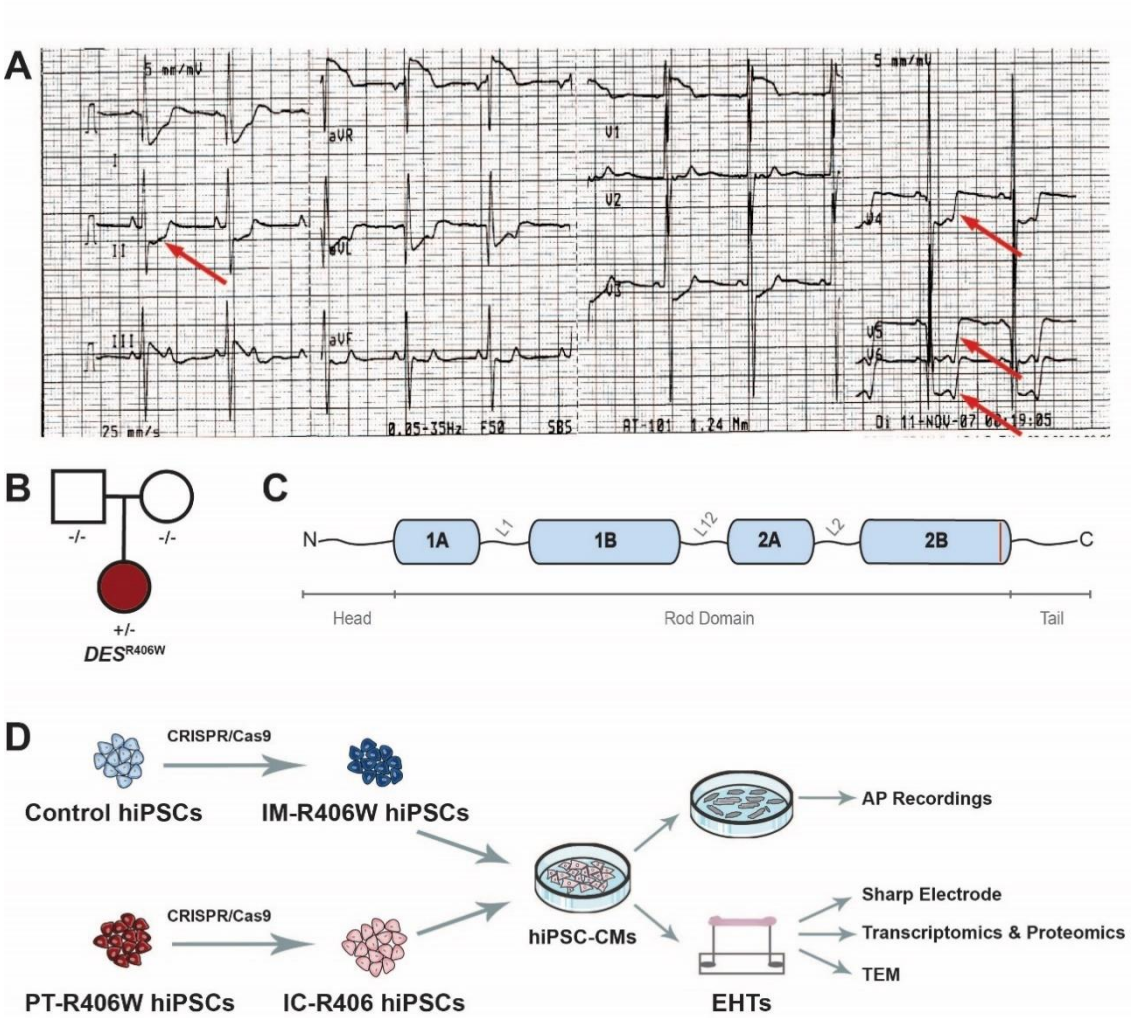

Figure 1. ***De novo*** **heterozygous** ***DES*^{R406W} **variant**. **A**. Representative ECG of the patient demonstrating ST-segment depression (red arrows; leads II, and V4-6). **B**. Family pedigree; circles and squares represent female and male patients, respectively. Empty symbols represent unaffected family members. The dark red circle represents the affected patient and indicates that PBMCs were collected to generate a patient hiPSC line. **C**. Schematic representation of a desmin monomer that is composed of non-helical N-terminal head and C-terminal tail and a rod domain composed of four segments (in blue: 1A, 1B, 2A, 2B) that are separated by three linkers (L1, L12, L2). The *DES*^{R406W} variant is located in the terminal part of segment 2B (dark red line). **D.** Schematic overview of the hiPSC lines and techniques used. **Top left.** Control hiPSCs (unrelated to the patient; light blue) were used to generate an isogenic mutant line (IM-R406W; dark blue) containing the *DES*^{R406W} variant using CRISPR/Cas9. **Bottom.** Likewise, an isogenic control line (IC-R406; light pink) was generated from the patients hiPSCs (PT-R406W; dark red) using CRISPR/Cas9. **Middle.** All four cell lines were differentiated into hiPSC derived cardiomyocytes (hiPSC-CMs). **Top right.** HiPSC-CMs from all clones were used for action potential (AP) recordings using the patch clamp technique. **Bottom right.** Engineered heart tissues (EHTs) of all clones were generated from hiPSC-CMs, and were used for transcriptomic and proteomic studies, transmission electron microscopy (TEM), and AP measurements using sharp electrodes. Figure 1D was drawn by using pictures from Servier Medical Art, which is licensed under a Creative Commons Attribution 3.0 Unported License (https://creativecommons.org/licenses/by/3.0/).

When comparing the duration of the spontaneous APs (Figure 2D), the APD_{30} and APD_{50} were significantly longer in IC-R406 hiPSC-CMs (103.8 ± 8.5 mV and 131.0 ± 11.2 mV, respectively) than in PT-R406W hiPSC-CMs (76.4 ± 5.6 mV, p=0.03, and 98.4 ± 6.9 mV, p=0.04). There were no significant differences between the APDs of Control and IM-R406W lines (Supplementary Table 1).

Due to the lack of intrinsic I_{K1} in hiPSC-CMs, we used the dynamic patch-clamp to inject computed I_{K1} and impose an MDP around -90 mV. The cells were paced at cycle lengths of 1000 and 700 ms. The APD_{30}, APD_{50} and APD_{90} was significantly longer in IM-R406W hiPSC-CMs (149.5 ± 18.4 mV, 198.5 ± 25.6 mV, and 217.6 ± 26.8 mV, respectively) than in Control hiPSC-CMs (92.2 ± 11.0 mV, 112.3 ± 15.9 mV, and 138.9 ± 18.1 mV, respectively) when paced at 1000 ms (Figure 2F). The same pattern was observed between the two lines at a PCL of 700 ms (Figure 2G): IM-R406W hiPSC-CMs had longer APDs (APD_{30}: 128.5 ± 16.2 mV, APD_{50}: 168.6 ± 21.3 mV, and APD_{90}: 189.8 ± 21.6 mV) than Control hiPSC-CMs (APD_{30}: 85.5 ± 10.9 mV, APD_{50}: 112.8 ± 14.5 mV, and APD_{90}: 129.2 ± 16.2 mV). In contrast, there were no significant differences in APD between PT-R406W and IC-R406 hiPSC-CMs (Supplementary Table 1). Furthermore, the PT-R406W APDs were longer than the Control and the IM-R406W APDs were longer than those of IC-R406 at both PCLs (Supplementary Table 1).

Electrophysiological Characterization of EHTs

To assess the properties of the *DES*^{R406W} mutation in a three-dimensional model, we generated EHTs from the hiPSC-CM lines (Figure 1D) and measured their electrophysiological properties by impaling with sharp microelectrodes. The beat-to-beat interval of spontaneously contracting EHTs did not differ significantly between the four lines (Figure 3B). However, the IM-R406W and PT-R406W intervals were shorter (1.4 ± 0.2 s and 0.8 ± 0.0 s, respectively)

than those of Control and IC-R406 EHTs (1.7 ± 0.1 s and 1.0 ± 0.2 s, respectively). Similarly, there were no significant differences in the overshoot (Figure 3C) and MDP (Figure 3E) between the different EHTs. Representative APs of the four EHT types are shown in Figure 3A.

Similar to the patch-clamp results obtained from hiPSC-CMs, the IM-R406W EHTs had significantly longer APD_{30}, APD_{50} and APD_{80} (244.0 ± 33.1 ms, 284.3 ± 37.1 ms, 308.0 ± 38.3 ms, respectively) than Control EHTs (149.0 ± 6.6 ms, 177.8 ± 8.7 ms, 205.0 ± 11.1 ms, respectively). A similar trend was observed between the PT-R406W EHTs (APD_{30}: 254.6 ± 20.3 ms; APD_{50}: 310.1 ± 22.8 ms; APD_{80}: 342.3 ± 24.2 ms) and the IC-R406 EHTs (APD_{30}: 193.8 ± 16.8 ms; APD_{50}: 243.8 ± 32.7 ms; APD_{80}: 282.9 ± 43.6 ms), although the differences did not reach significance (Supplementary Table 2). Taken together, the EHTs containing the *DES*^{R406W} variant displayed prolonged APDs.

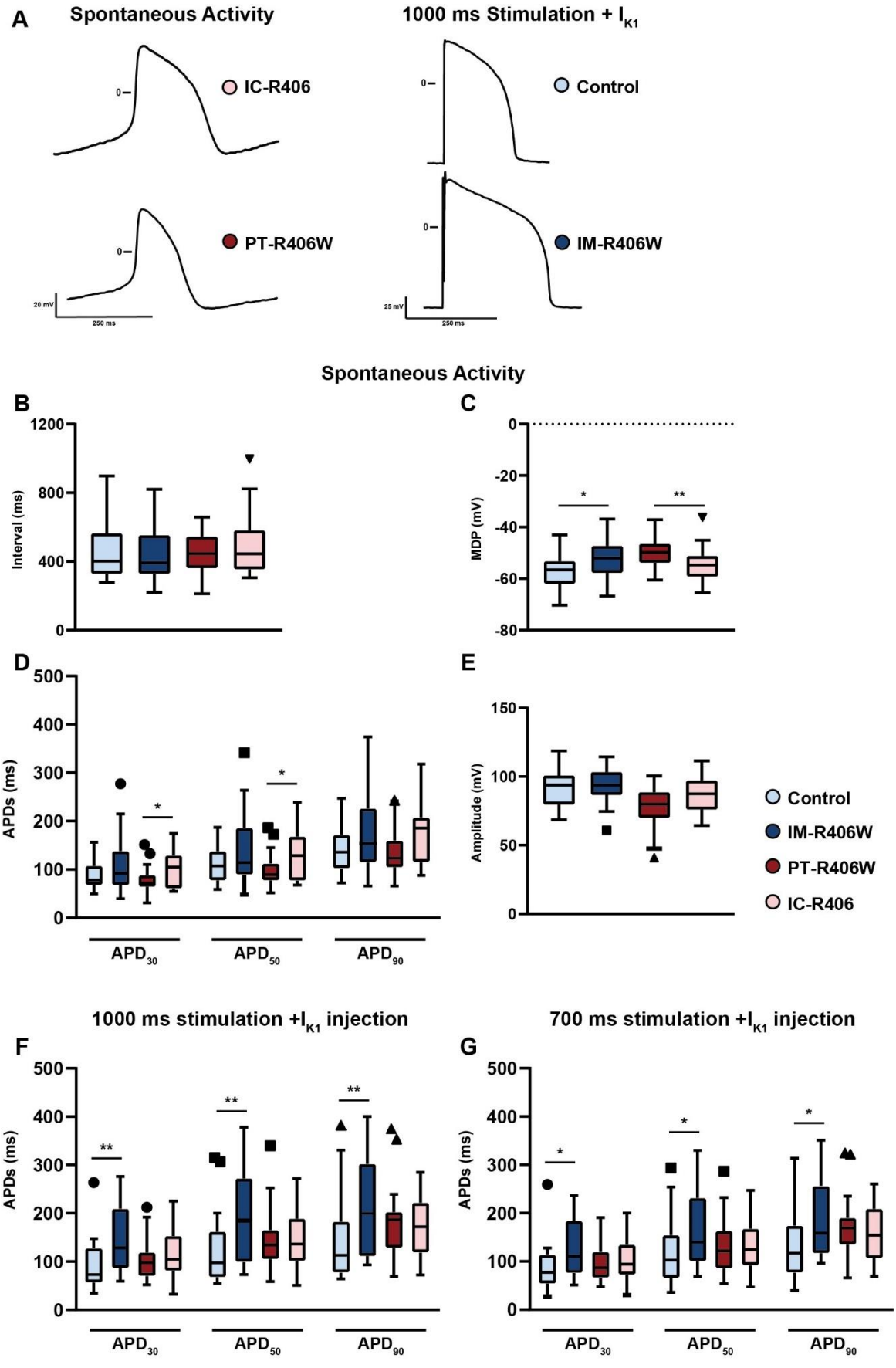
A
Spontaneous Activity
1000 ms Stimulation + I_{K1}
IC-R406
Control
PT-R406W
IM-R406W
0
20 mV
25 mV
250 ms
Spontaneous Activity
B
Interval (ms)
C
MDP (mV)
D
APDs (ms)
E
Amplitude (mV)
Control
IM-R406W
PT-R406W
IC-R406
APD_{30}
APD_{50}
APD_{90}
1000 ms stimulation +I_{K1} injection
700 ms stimulation +I_{K1} injection
F
G

375

376

Figure 2. ***DES*^{R406W} variant leads to changes in hiPSC-CM action potentials (APs).** Dynamic clamp experiments comparing various AP parameters of Control, patient (PT-R406W), and isogenic (mutant; IM-R406W, control; IC-R406) hiPSC-CMs. **A**. Representative APs of spontaneously beating (left) and stimulated (pacing cycle length = 1000 ms) hiPSC-CMs with I_{K1} injected using dynamic clamp (right). Beat-to-beat interval (**B**), maximum diastolic potential (MDP; **C**), AP duration (APD) at 30, 50, and 90% of repolarization (APD_{30}, APD_{50}, APD_{90}, respectively; **D**), and amplitude (**E**) of spontaneously beating Control (n=19), IM-R406W (n=25), PT-R406W (n=24), and IC-R406 (n=20) hiPSC-CMs. APD_{30}, APD_{50}, APD_{90} (**F**) of Control (n=22), IM-R406W (n=15), PT-R406W (n=30), and IC-R406 (n=28) hiPSC-CM clones stimulated at 1000 ms with injected I_{K1}. APD_{30}, APD_{50}, APD_{90} (**G**) of Control (n=21), IM-R406W (n=15), PT-R406W (n=27), and IC-R406 (n=25) hiPSC-CM clones stimulated at a cycle length of 700 ms with injected I_{K1}. Mann-Whitney test was used to assess significance between Control versus IM-R406W and PT-R406W versus IC-R406 (*: $p < 0.05$, **: $p < 0.01$). Data represented as Tukey box plots.

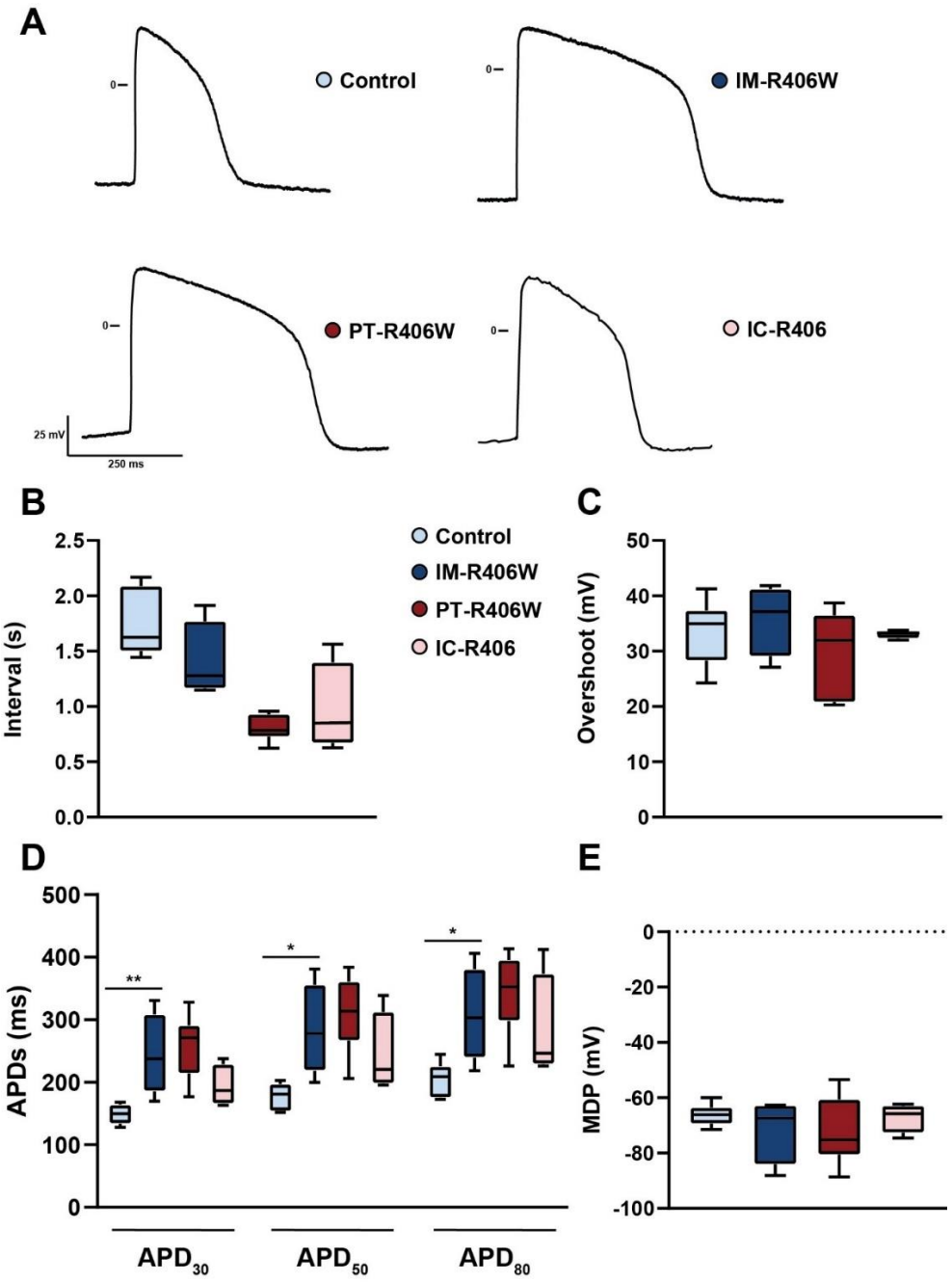

Figure 3. Effects of the *DES*^{R406W} variant on action potential (AP) parameters of engineered heart tissues (EHTs). A. Representative APs of spontaneously beating EHTs. Beat-to-beat interval (**B**), overshoot (**C**), AP duration at 30, 50, and 80% of repolarization (APD_{30}, APD_{50}, APD_{80}, respectively; **D**), and maximum diastolic potential (MDP) **(E**), of spontaneously beating control (n=6), IM-R406W (n=4), PT-R406W (n=7), and IC-R406 (n=4) EHTs. Mann-Whitney test was used to assess significance between Control versus IM-R406W and PT-R406W versus IC-R406 (*$p < 0.05$, **$p < 0.01$). Data represented as Tukey box plots.

Omics study

To investigate how the *DES*^{R406W} mutation affects cell biology, transcriptomic and proteomic data were generated from 5 to 8 independent EHTs for all four hiPSC lines. Principal Component Analyses (PCA) highlight that the principal factor in gene/protein expression variations, represented by PC1 (23% of gene expression variation and 24% of protein expression variation), reflects differences between the 2 original hiPSCs lines (Control and PT-R406W background, Figure 4A and B). The PC2, on the other hand, displays a gene/protein expression variation related to whether or not the *DES*^{R406W} mutation is present.

To further explore molecular alterations associated with the *DES*^{R406W} mutation, genes/proteins with significant expression variations in EHTs carrying the mutation (PT-R406W and IM-R406W) in comparison to those who did not (Control and IC-R406) were identified in transcriptomic and proteomic datasets independently. A total of 882 genes had their RNA or protein expression dysregulated, with only 55 (6.23%) reaching the significance threshold in both transcriptomic and proteomic analyses (Figure 4C, Supplementary Table 3). Disease Ontology analysis identified a significantly enriched set of genes/proteins associated with a range of cardiomyopathies among the 882 differentially expressed genes/proteins (Figure 4D, Supplementary Table 4).

Among the 882 differential genes/proteins, the expression of the 641 genes covered by both transcriptomics and proteomics datasets was displayed as a heatmap (Figure 4E). Genes/proteins were sorted into 4 clusters based on their expression fold change between *DES*^{R406W}-EHTs and *DES*^{R406}-EHTs in both transcriptomics and proteomics datasets. Up-regulated proteins were enriched in biological processes related to cardiac development and contraction, as well as cellular respiration, whereas down-regulated proteins seem enriched in biological processes related to stress response (Figure 4F, Supplementary Tables 5 & 7). Interestingly, among the biological processes enriched in up-regulated proteins, there are

several cardiac action potential-related functions consistent with the above described electrophysiological phenotype (Supplementary Table 5). When considering which cellular components up-regulated proteins are part of, significant enrichment is restricted to contractile apparatus and mitochondria (Figure 4G, Supplementary Table 6). Together, these omics analyses suggest that the *DES*^{R406W} mutation may lead to altered mitochondrial function and cardiac cell structural defects.

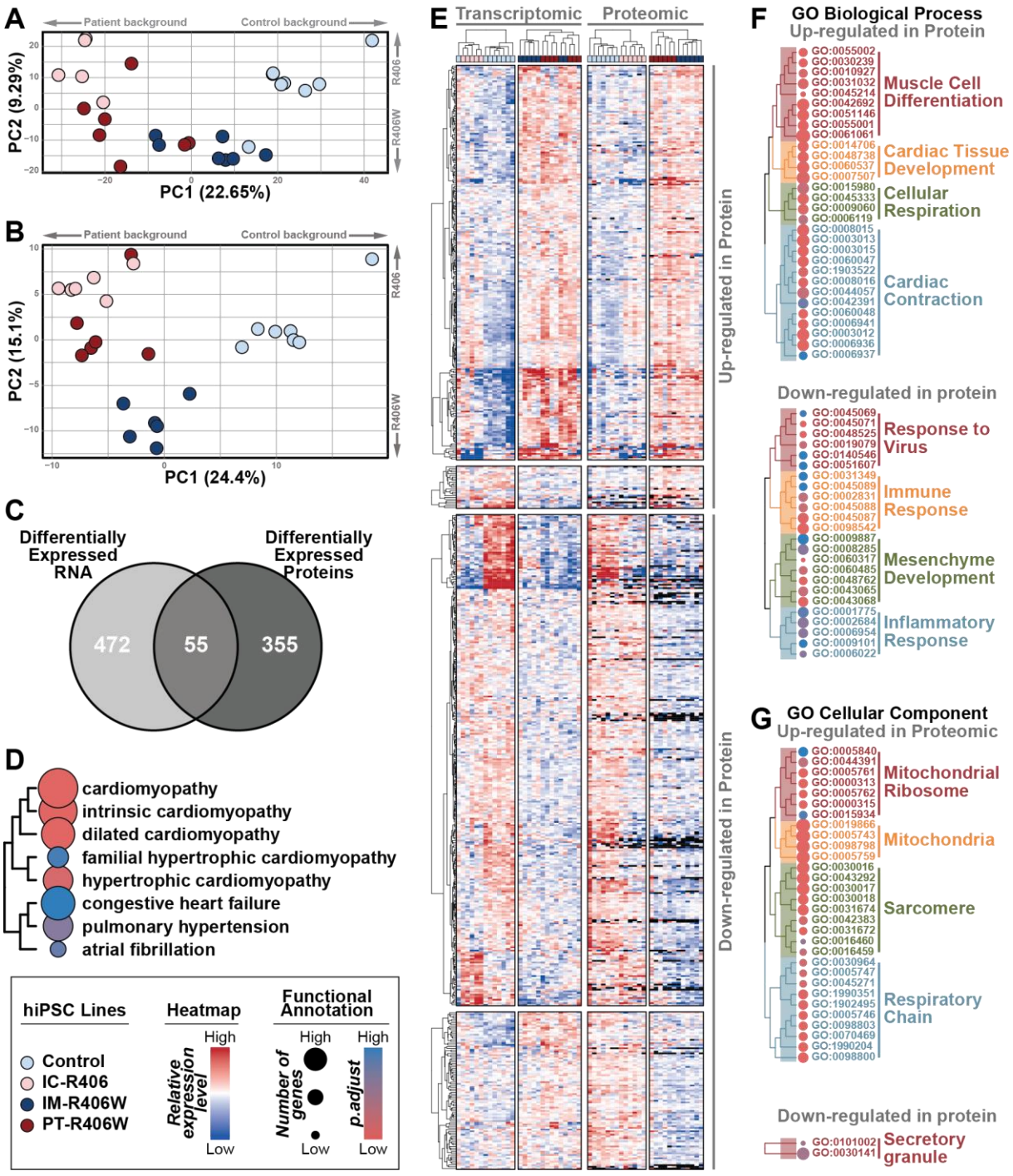

Figure 4. Transcriptomic and proteomic analyses point towards mitochondrial and structural defects in *DES*^{R406W}-EHTs. Global transcriptomic (**A**) or proteomic (**B**) variations of EHTs displayed with the first two components of the Principal Component Analysis. Five to eight EHTs were studied for each of the four hiPSC lines. **C.** Comparison of differentially expressed genes and proteins identified between *DES*^{R406}-EHTs and *DES*^{R406W}-EHTs. **D.** Disease Ontology annotation of the union of differentially genes and proteins. **E.** Heatmap displaying the expression levels of all differentially expressed genes and proteins identified. RNA and protein expression levels are shown on the left and on the right, respectively. **F.** Gene Ontology Biological Process annotation of up- and down-regulated proteins on the top and on the bottom, respectively. **G.** Gene Ontology Cellular Component annotation of up- and down-regulated proteins on the top and on the bottom, respectively.

Transmission Electron Microscopy

To investigate how the *DES*^{R406W} mutation affects the intracellular structure of EHTs, we imaged the tissues using transmission electron microscopy (TEM). We observed sarcomeres with prominent contractile filaments aligned at the Z-discs in both Control and IC-R406 EHTs (Figure 5, top panels) where the Z-discs were visible and distinguishable (black asterisks). For the EHTs carrying the *DES*^{R406W} mutation, PT-R406W and IM-R406W, the opposite was true (Figure 5, bottom panels). Although the sarcomeres were visible, the tissues exhibited Z-disc that were wider and "fuzzy" in appearance, making them almost indistinguishable from the filaments (black asterisks). These results align with previous studies that used mutant mice (5).

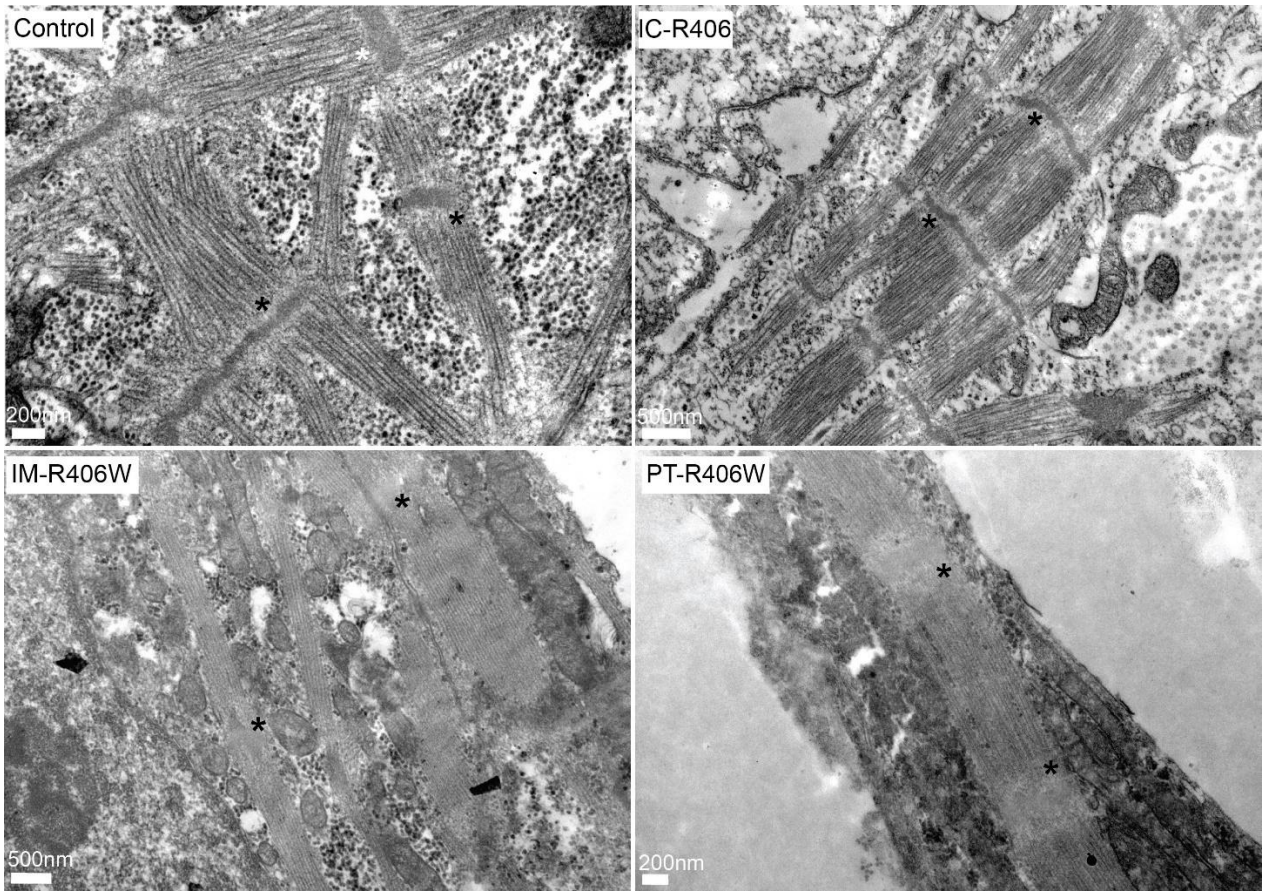

Figure 5. Transmission electron microscopy images of EHTs illustrate Z-disc abnormalities. The two control clones (Control and IC-R406; top panels) have visible Z-discs and filaments. The two clones carrying the DES^{R406W} variant (IM-R406W and PT-R406W; bottom panels) have wider Z-discs with a fuzzy appearance. The asterisks (black) point to the Z-discs.

Discussion

In this study, we showed that the *DES*^{R406W} mutation (1) can lead to the occurrence of severe ventricular arrhythmias and SCD in young patients, during their first decade of life; (2) induces electrophysiological and structural abnormalities in hiPSC-CMs carrying the mutation; (3) leads to significant remodeling of the expression of genes and proteins involved, among other processes, in cardiac electrical activity and contractility, as well as mitochondrial function. More generally, this study highlights the value of the hiPSC-CM model and EHTs for analyzing the cellular and subcellular consequences in the heart of mutations leading to desminopathies.

The *DES*^{R406W} mutation is usually described as a *de novo* mutation, *i.e.*, not found in index cases' parents and other relatives (31) – although there are some exceptions (32) – which manifests early in life. One other case study has reported this variant in a 8-year-old patient presenting with HCM and atrioventricular conduction block (33), highlighting the early onset and strong pathogenicity of this variant. Most *DES*^{R406W} carriers present with cardiac involvement first, followed by gradual skeletal muscle degeneration throughout life (31,33,34). Most patients are diagnosed with RCM (5,14,32,35), although HCM (33,36) and DCM (31) have also been reported. The absence of an obvious structural cardiomyopathy in our patient might be linked to the early onset of her numerous VF episodes that ultimately led to early transplantation. Almost all patients with this mutation have cardiac conduction disorders (5,14,31–35), sometimes associated with ventricular tachyarrhythmias (5). Interestingly, the electrocardiographic pattern of the patient described in the present study resembles that observed in a recently identified inherited cardiac arrhythmia, the familial ST-segment depression syndrome, which is characterized by persistent, non-ischemic ST-segment depression and increased risk of ventricular arrhythmias and SCD (37–39). The pathophysiological mechanisms underlying this syndrome have not been established and, to our

knowledge, no causal gene has yet been identified. A similar ECG pattern has also been found in a 15-year-old female patient with a homozygous deletion of 7 amino acids in the 1B helix domain of desmin (40). This suggests that familial ST-segment depression syndrome might have common pathogenic mechanisms with cardiac arrhythmias observed in some desminopathies. A knock-in mouse model carrying the p.R405W mutation, the orthologous counterpart to the human p.R406W mutation, has been generated (5) but no *in vivo* or *ex vivo* electrophysiological investigations have been published. This mouse, however, exhibits abnormal intercalated discs that might partly explain conduction defects and arrhythmias observed in patients carrying the DES^{R406W} mutation. Investigating this model further could help decipher the pathogenic mechanisms of this mutation.

Our study is the first to highlight the cardiac cellular electrophysiological consequences of the DES^{R406W} variant. Our results suggest that the mutation affects the repolarization process, which could contribute to the occurrence of arrhythmias. Surprisingly, we did not observe any electrophysiological abnormalities that could explain conduction defects. For example, no change in AP upstroke velocity was observed. However, on the basis of previous studies of this variant showing desmosome alterations (5), it would be useful to carry out experiments more specifically designed to measure the speed of electrical impulse conduction in EHTs.

Our multi-omics study of EHTs is the first of its kind to investigate the pathogenic mechanisms of desminopathies. It provides a global overview of the altered functions in the cells. The transcriptomic data does not always represent the protein expression profiles, especially in pathology (41–43). Therefore, studying protein expression provides a more accurate view of the functions altered in desminopathy. Conversely, with the technology available today, transcriptomic sequencing technology enables better coverage of gene expression (41), as opposed to proteomic techniques. This difference can be observed by the coverage in our study, with close to 8 000 proteins compared to almost 15 000 genes; which

demonstrates a smaller coverage of the proteins. Therefore, we decided to combine both techniques. As it turns out, for some genes, mRNA expression varied inversely to protein expression, suggesting a feedback mechanism. If we had studied mRNA alone, we would have misinterpreted the variations in expression for these genes. The transcriptomic and proteomic data generated in this study suggest that the hiPSC-CM-derived EHT model carrying the *DES*^{R406W} mutation recapitulates a number of features characteristic of desminopathies. First using the Disease Ontology database, the analysis of genes and proteins whose expression is significantly altered by the presence of the *DES*^{R406W} mutation provides an accurate portrait of major clinical features of desminopathies. Second, the analysis of biological processes and cellular components affected by *DES*^{R406W} mutation highlights the damage to cardiomyocyte ultrastructure and mitochondrial function. Concerning cardiomyocyte ultrastructure, analysis of our TEM images revealed a faint appearance of the Z-discs in the mutant tissues. This is intriguing since the biological process GO terms revealed an up-regulation of proteins related to cardiac contraction. Decreased levels of desmin at the Z-discs have been reported in desmin knock-in R405W mice (5) further supporting the notion that the interplay between desmin and its cell-spanning connections is critical for proper cardiac function. As for mitochondria, alterations in their structure and function have already been shown. Changes in respiratory chain complex activity and quantity have been observed in a patient carrying the *DES*^{R406W} variant (11), which is in accordance with our omics data that depict a disturbance in mitochondria function. Our multi-omics study also suggests that the mutation may lead to abnormalities in intracellular calcium handling. These could explain, at least in part, the repolarization defects observed in hiPSC-CMs and slower automaticity of *DES*^{R406W}-EHTs. More generally, it might also contribute to the cardiac contractile defects in patients. Increased cytosolic calcium has been reported in desmin mutant myotubes (10). Furthermore, cardiac and skeletal cells have been shown to have a higher uptake of calcium by the mitochondria when stimulated (44).

Overall, our multi-omics study shows that changes in the structure of desmin filaments lead not only to structural alterations in the cell – desmin being responsible for the correct positioning and shape of organelles, including mitochondria – but also to a complex remodeling of the expression of a large number of proteins, thus affecting many cardiomyocyte functions.

Finally, we demonstrated for the first time that EHTs could be a relevant model for studying the cardiac consequences of desminopathy. Our study demonstrates that hiPSC-CMs are a relevant model to investigate desmin mutations. In parallel, EHTs generated from these CMs are a valuable three-dimensional model that can recapitulate certain aspects of the disease. To date, studies that have investigated desmin used different cell lines that are typically desmin- and vimentin-free, such as the human adrenocortical carcinoma (SW13) cells (6,7,45). These studies provided insight into the structural consequences of mutant desmin filaments. It was established that the *DES*^{R406W} variant forms aggregates and prevents proper filament formation (6,7). The aggregate phenotype has also been observed in biopsy samples from patients with the *DES*^{R406W} mutation (14,32,34,36). Nevertheless, hiPSC-CMs transfected with the *DES*^{R406W} variant has demonstrated aggregate deposits in these cells (11), providing support for modeling desminopathy with hiPSC-CMs. Mutations located in different parts of *DES* have likewise been transfected into hiPSC-CMs, where aggregates were observed(46–49), demonstrating pathogenicity of the variants. However, few studies have used patient hiPSCs to investigate the molecular mechanisms of desminopathies (8,49). One limitation of the hiPSC-CMs is their immaturity since they have a fetal-like metabolic, structural and electrophysiological phenotype that differs from that of adult cardiomyocytes (50–53). However, this limitation might represent an advantage if one is interested in the developmental consequences of gene mutations leading to early-onset diseases, such as the *DES*^{R406W} mutation. From an electrophysiological point of view, for the purpose of this study we have been able to recapitulate certain aspects of mature cardiac AP with the dynamic clamp technique in order to compare pertinent

electrophysiological parameters. We also found that the electrical maturity of EHTs could allow better identification of electrophysiological abnormalities, although our study would require more in-depth exploitation of this model.

Acknowledgements

We are most grateful to the *Centre National de Recherche en Génomique Humaine, Institut de Génomique, CEA, Evry, France*, for whole genome sequencing, and to the Genomics Core Facility GenoA, member of Biogenouest and *France Génomique* and to the Bioinformatics Core Facility BiRD, member of Biogenouest and *Institut Français de Bioinformatique* (IFB) (ANR-11-INBS-0013) for the use of their resources and their technical support. We would like to thank Rodolphe Perrot from SCIAM (Common Service for Imaging and Microscopy Analysis, University of Angers, France) for TEM sample preparation and observation.

Funding

This work was supported by the *Agence Nationale de la Recherche* (ANR-19-CE14-0031-02; FC) and the *Fondation Genavie* (JBG).

References

1. Capetanaki Y, Bloch RJ, Kouloumenta A, Mavroidis M, Psarras S. Muscle intermediate filaments and their links to membranes and membranous organelles. Exp Cell Res. 2007 Jun 10;313(10):2063–76.

2. Tsikitis M, Galata Z, Mavroidis M, Psarras S, Capetanaki Y. Intermediate filaments in cardiomyopathy. Biophys Rev. 2018 Aug;10(4):1007–31.

3. Agnetti G, Herrmann H, Cohen S. New roles for desmin in the maintenance of muscle homeostasis. FEBS J. 2022 May;289(10):2755–70.

4. Hol EM, Capetanaki Y. Type III Intermediate Filaments Desmin, Glial Fibrillary Acidic Protein (GFAP), Vimentin, and Peripherin. Cold Spring Harb Perspect Biol. 2017 Dec;9(12):a021642.

5. Herrmann H, Cabet E, Chevalier NR, Moosmann J, Schultheis D, Haas J, et al. Dual Functional States of R406W-Desmin Assembly Complexes Cause Cardiomyopathy With Severe Intercalated Disc Derangement in Humans and in Knock-In Mice. Circulation. 2020 Dec 1;142(22):2155–71.

6. Goudeau B, Rodrigues-Lima F, Fischer D, Casteras-Simon M, Sambuughin N, de Visser M, et al. Variable pathogenic potentials of mutations located in the desmin alpha-helical domain. Hum Mutat. 2006;27(9):906–13.

7. Bär H, Mucke N, Kostareva A, Sjoberg G, Aebi U, Herrmann H. Severe muscle disease-causing desmin mutations interfere with in vitro filament assembly at distinct stages. Proc Natl Acad Sci. 2005 Oct 18;102(42):15099–104.

8. Hovhannisyan Y, Li Z, Callon D, Suspène R, Batoumeni V, Canette A, et al. Critical contribution of mitochondria in the development of cardiomyopathy linked to desmin mutation. Stem Cell Res Ther. 2024 Jan 2;15(1):10.

9. Smolina N, Khudiakov A, Knyazeva A, Zlotina A, Sukhareva K, Kondratov K, et al. Desmin mutations result in mitochondrial dysfunction regardless of their aggregation properties. Biochim Biophys Acta BBA - Mol Basis Dis. 2020 Jun;1866(6):165745.

10. Smolina N, Bruton J, Sjoberg G, Kostareva A, Sejersen T. Aggregate-prone desmin mutations impair mitochondrial calcium uptake in primary myotubes. Cell Calcium. 2014 Oct 1;56(4):269–75.

11. Kubánek M, Schimerová T, Piherová L, Brodehl A, Krebsová A, Ratnavadivel S, et al. Desminopathy: Novel Desmin Variants, a New Cardiac Phenotype, and Further Evidence for Secondary Mitochondrial Dysfunction. J Clin Med. 2020 Mar 29;9(4):937.

12. Milner DJ, Weitzer G, Tran D, Bradley A, Capetanaki Y. Disruption of muscle architecture and myocardial degeneration in mice lacking desmin. J Cell Biol. 1996 Sep;134(5):1255–70.

13. Mavroidis M, Panagopoulou P, Kostavasili I, Weisleder N, Capetanaki Y. A missense mutation in desmin tail domain linked to human dilated cardiomyopathy promotes cleavage of the head domain and abolishes its Z-disc localization. FASEB J. 2008;22(9):3318–27.

14. Olivé M, Goldfarb L, Moreno D, Laforet E, Dagvadorj A, Sambuughin N, et al. Desmin-related myopathy: clinical, electrophysiological, radiological, neuropathological and genetic studies. J Neurol Sci. 2004 Apr 15;219(1):125–37.

15. Girardeau A, Atticus D, Canac R, Cimarosti B, Caillaud A, Chariau C, et al. Generation of human induced pluripotent stem cell lines from four unrelated healthy control donors carrying European genetic background. Stem Cell Res. 2022 Mar;59:102647.

16. Treat JA, Goodrow RJ, Bot CT, Haedo RJ, Cordeiro JM. Pharmacological enhancement of repolarization reserve in human induced pluripotent stem cells derived cardiomyocytes. Biochem Pharmacol. 2019 Nov 1;169:113608.

17. Lam CK, Tian L, Belbachir N, Wnorowski A, Shrestha R, Ma N, et al. Identifying the Transcriptome Signatures of Calcium Channel Blockers in Human Induced Pluripotent Stem Cell-Derived Cardiomyocytes. Circ Res. 2019 Jul 5;125(2):212–22.

18. Mannhardt I, Saleem U, Benzin A, Schulze T, Klampe B, Eschenhagen T, et al. Automated Contraction Analysis of Human Engineered Heart Tissue for Cardiac Drug Safety Screening. J Vis Exp. 2017 Apr 15;(122):55461.

19. Ronaldson-Bouchard K, Yeager K, Teles D, Chen T, Ma S, Song L, et al. Engineering of human cardiac muscle electromechanically matured to an adult-like phenotype. Nat Protoc. 2019 Oct;14(10):2781–817.

20. Al Sayed ZR, Jouni M, Gourraud JB, Belbachir N, Barc J, Girardeau A, et al. A consistent arrhythmogenic trait in Brugada syndrome cellular phenotype. Clin Transl Med. 2021;11(6):e413.

21. Meijer van Putten RME, Mengarelli I, Guan K, Zegers JG, van Ginneken ACG, Verkerk AO, et al. Ion channelopathies in human induced pluripotent stem cell derived cardiomyocytes: a dynamic clamp study with virtual IK1. Front Physiol [Internet]. 2015 Feb 3 [cited 2021 Apr 7];6. Available from: http://journal.frontiersin.org/Article/10.3389/fphys.2015.00007/abstract

22. Wilders R. Dynamic clamp: a powerful tool in cardiac electrophysiology: Dynamic clamp: a powerful tool in cardiac electrophysiology. J Physiol. 2006 Oct 15;576(2):349–59.

23. Charpentier E, Cornec M, Dumont S, Meistermann D, Bordron P, David L, et al. 3’ RNA sequencing for robust and low-cost gene expression profiling [Internet]. Protocol Exchange; 2021 Jan [cited 2023 Nov 14]. Available from: https://protocolexchange.researchsquare.com/article/pex-1336/v1

24. Love MI, Huber W, Anders S. Moderated estimation of fold change and dispersion for RNA-seq data with DESeq2. Genome Biol. 2014 Dec 5;15(12):550.

25. Lê S, Josse J, Husson F. FactoMineR: An R Package for Multivariate Analysis. J Stat Softw. 2008 Mar 18;25:1–18.

26. Ritchie ME, Phipson B, Wu D, Hu Y, Law CW, Shi W, et al. limma powers differential expression analyses for RNA-sequencing and microarray studies. Nucleic Acids Res. 2015 Apr 20;43(7):e47.

27. Stekhoven DJ, Bühlmann P. MissForest—non-parametric missing value imputation for mixed-type data. Bioinformatics. 2012 Jan 1;28(1):112–8.

28. Gu Z, Eils R, Schlesner M. Complex heatmaps reveal patterns and correlations in multidimensional genomic data. Bioinformatics. 2016 Sep 15;32(18):2847–9.

29. Wu T, Hu E, Xu S, Chen M, Guo P, Dai Z, et al. clusterProfiler 4.0: A universal enrichment tool for interpreting omics data. Innov Camb Mass. 2021 Aug 28;2(3):100141.

30. Yu G, Wang LG, Yan GR, He QY. DOSE: an R/Bioconductor package for disease ontology semantic and enrichment analysis. Bioinforma Oxf Engl. 2015 Feb 15;31(4):608–9.

31. Dagvadorj A, Olivé M, Urtizberea JA, Halle M, Shatunov A, Bönnemann C, et al. A series of West European patients with severe cardiac and skeletal myopathy associated with a de novo R406W mutation in desmin. J Neurol. 2004 Feb 1;251(2):143–9.

32. Arbustini E, Pasotti M, Pilotto A, Pellegrini C, Grasso M, Previtali S, et al. Desmin accumulation restrictive cardiomyopathy and atrioventricular block associated with desmin gene defects. Eur J Heart Fail. 2006;8(5):477–83.

33. Oka H, Nakau K, Imanishi R, Furukawa T, Tanabe Y, Hirono K, et al. A Case Report of a Rare Heterozygous Variant in the Desmin Gene Associated With Hypertrophic Cardiomyopathy and Complete Atrioventricular Block. CJC Open. 2021 May 12;3(9):1195–8.

34. Park KY, Dalakas MC, Semino-Mora C, Lee HS, Litvak S, Takeda K, et al. Sporadic cardiac and skeletal myopathy caused by a de novo desmin mutation. Clin Genet. 2000;57(6):423–9.

35. Chen Z, Li R, Wang Y, Cao L, Lin C, Liu F, et al. Features of myocardial injury detected by cardiac magnetic resonance in a patient with desmin-related restrictive cardiomyopathy. ESC Heart Fail. 2021 Oct 5;8(6):5560–4.

36. Takegami N, Mitsutake A, Mano T, Shintani-Domoto Y, Unuma A, Yamaguchi-Takegami N, et al. The Myocardial Accumulation of Aggregated Desmin Protein in a Case of Desminopathy with a *de novo DES* p.R406W Mutation. Intern Med. 2023;0992–22.

37. Bundgaard H, Jøns C, Lodder EM, Izarzugaza JMG, Romero Herrera JA, Pehrson S, et al. A Novel Familial Cardiac Arrhythmia Syndrome with Widespread ST-Segment Depression. N Engl J Med. 2018 Nov;379(18):1780–1.

38. Christensen AH, Nyholm BC, Vissing CR, Pietersen A, Tfelt-Hansen J, Olesen MS, et al. Natural History and Clinical Characteristics of the First 10 Danish Families With Familial ST-Depression Syndrome. J Am Coll Cardiol. 2021 May;77(20):2617–9.

39. Christensen AH, Vissing CR, Pietersen A, Tfelt-Hansen J, Hartvig Lindkær Jensen T, Pehrson S, et al. Electrocardiographic Findings, Arrhythmias, and Left Ventricular Involvement in Familial ST-Depression Syndrome. Circ Arrhythm Electrophysiol. 2022 Apr;15(4):e010688.

40. Piñol-Ripoll G, Shatunov A, Cabello A, Larrodé P, de la Puerta I, Pelegrín J, et al. Severe infantile-onset cardiomyopathy associated with a homozygous deletion in desmin. Neuromuscul Disord. 2009 Jun;19(6):418–22.

41. Haider S, Pal R. Integrated analysis of transcriptomic and proteomic data. Curr Genomics. 2013 Apr;14(2):91–110.

42. Du Y, Clair GC, Al Alam D, Danopoulos S, Schnell D, Kitzmiller JA, et al. Integration of transcriptomic and proteomic data identifies biological functions in cell populations from human infant lung. Am J Physiol Lung Cell Mol Physiol. 2019 Sep 1;317(3):L347–60.

43. Liu Y, Beyer A, Aebersold R. On the Dependency of Cellular Protein Levels on mRNA Abundance. Cell. 2016 Apr 21;165(3):535–50.

44. Kostareva A, Sjöberg G, Bruton J, Zhang SJ, Balogh J, Gudkova A, et al. Mice expressing L345P mutant desmin exhibit morphological and functional changes of skeletal and cardiac mitochondria. J Muscle Res Cell Motil. 2008 Jan 1;29(1):25–36.

45. Chourbagi O, Bruston F, Carinci M, Xue Z, Vicart P, Paulin D, et al. Desmin mutations in the terminal consensus motif prevent synemin-desmin heteropolymer filament assembly. Exp Cell Res. 2011 Apr 1;317(6):886–97.

46. Kulikova O, Brodehl A, Kiseleva A, Myasnikov R, Meshkov A, Stanasiuk C, et al. The Desmin (DES) Mutation p.A337P Is Associated with Left-Ventricular Non-Compaction Cardiomyopathy. Genes. 2021 Jan 19;12(1):121.

47. Protonotarios A, Brodehl A, Asimaki A, Jager J, Quinn E, Stanasiuk C, et al. The Novel Desmin Variant p.Leu115Ile Is Associated With a Unique Form of Biventricular Arrhythmogenic Cardiomyopathy. Can J Cardiol. 2021 Jun 1;37(6):857–66.

48. Brodehl A, Hakimi SAP, Stanasiuk C, Ratnavadivel S, Hendig D, Gaertner A, et al. Restrictive Cardiomyopathy is Caused by a Novel Homozygous Desmin (DES) Mutation p.Y122H Leading to a Severe Filament Assembly Defect. Genes. 2019 Nov 11;10(11):918.

49. Tse HF, Ho JCY, Choi SW, Lee YK, Butler AW, Ng KM, et al. Patient-specific induced-pluripotent stem cells-derived cardiomyocytes recapitulate the pathogenic phenotypes of dilated cardiomyopathy due to a novel DES mutation identified by whole exome sequencing. Hum Mol Genet. 2013 Apr 1;22(7):1395–403.

50. Ronaldson-Bouchard K, Ma SP, Yeager K, Chen T, Song L, Sirabella D, et al. Advanced maturation of human cardiac tissue grown from pluripotent stem cells. Nature. 2018 Apr;556(7700):239–43.

51. Karbassi E, Fenix A, Marchiano S, Muraoka N, Nakamura K, Yang X, et al. Cardiomyocyte maturation: advances in knowledge and implications for regenerative medicine. Nat Rev Cardiol. 2020 Jun;17(6):341–59.

52. Bekhite MM, Schulze PC. Human Induced Pluripotent Stem Cell as a Disease Modeling and Drug Development Platform—A Cardiac Perspective. Cells. 2021 Dec;10(12):3483.

53. Wu P, Deng G, Sai X, Guo H, Huang H, Zhu P. Maturation strategies and limitations of induced pluripotent stem cell-derived cardiomyocytes. Biosci Rep. 2021 Jun 16;41(6):BSR20200833.

Supplementary Data

Supplementary Table 1. Action potential parameters of hiPSC-CMs

Spontaneous

	Control			IM-R406W			Mann-Whitney	
	Mean	± sem	n	Mean	± sem	n	Sign	p-value
Interval (ms)	456.0	39.0	19	436.4	33.0	25	ns	0.7784
MDP (mV)	-56.8	1.6	19	-52.4	1.3	25	*	0.0335
Overshoot (mV)	34.2	2.1	19	41.4	1.9	25	*	0.0127
Amplitude (mV)	91.2	3.1	19	93.9	2.5	25	ns	0.4811
dV/dt_{max} (V/s)	23.2	5.3	19	18.5	2.3	25	ns	0.3811
APD_{20} (ms)	70.0	5.2	19	83.5	7.9	25	ns	0.3232
APD_{30} (ms)	88.1	6.9	19	111.5	11.3	25	ns	0.2412
APD_{50} (ms)	109.4	8.7	19	145.0	14.4	25	ns	0.1244
APD_{70} (ms)	123.1	9.7	19	162.3	15.5	25	ns	0.1077
APD_{80} (ms)	130.2	10.1	19	170.4	15.9	25	ns	0.1186
APD_{90} (ms)	139.3	10.8	19	180.5	16.3	25	ns	0.1077

	PT-R406W			IC-R406			Mann-Whitney	
	Mean	± sem	n	Mean	± sem	n	Sign	p-value
Interval (ms)	450.3	23.9	24	488.6	39.7	20	ns	0.7885
MDP (mV)	-49.3	1.2	24	-54.2	1.5	20	**	0.0089
Overshoot (mV)	27.7	2.4	24	32.4	1.9	20	ns	0.2461
Amplitude (mV)	77.0	3.3	24	86.6	2.8	20	ns	0.0750
dV/dt_{max} (V/s)	9.6	1.5	24	10.5	1.9	20	ns	0.3403
APD_{20} (ms)	62.2	4.4	24	80.4	5.9	20	*	0.0383
APD_{30} (ms)	76.4	5.6	24	103.8	8.5	20	*	0.0339
APD_{50} (ms)	98.4	6.9	24	131.0	11.2	20	*	0.0431
APD_{70} (ms)	114.6	8.5	24	149.3	12.5	20	ns	0.0674
APD_{80} (ms)	124.4	9.1	24	158.6	13.1	20	ns	0.0921
APD_{90} (ms)	137.7	9.9	24	170.8	13.9	20	ns	0.1018

PCL1000

	Control			IM-R406W			Mann-Whitney	
	Mean	± sem	n	Mean	± sem	n	Sign	p-value
Interval (ms)	1000.0	0.0	22	1000.0	0.0	15	ns	0.8115
MDP (mV)	-91.5	0.1	22	-91.8	0.4	15	ns	0.9452
Overshoot (mV)	46.0	3.1	22	52.3	3.1	15	ns	0.2132
Amplitude (mV)	137.5	3.1	22	144.1	3.0	15	ns	0.1612
dV/dt_{max} (V/s)	88.1	15.5	22	77.2	10.8	15	ns	0.9149
APD_{20} (ms)	65.3	7.9	22	96.5	11.3	15	*	0.0104
APD_{30} (ms)	92.2	11.0	22	149.5	18.4	15	**	0.0063
APD_{50} (ms)	122.3	15.9	22	198.5	25.6	15	**	0.0063
APD_{70} (ms)	134.2	17.8	22	212.7	26.7	15	**	0.0078
APD_{80} (ms)	136.7	18.0	22	215.4	26.8	15	**	0.0086
APD_{90} (ms)	138.9	18.1	22	217.6	26.8	15	**	0.0086

	PT-R406W			IC-R406			Mann-Whitney	
	Mean	± sem	n	Mean	± sem	n	Sign	p-value
Interval (ms)	1000.0	0.0	30	1000.0	0.1	28	ns	0.0994
MDP (mV)	-91.3	0.2	30	-91.2	0.2	28	ns	0.9109
Overshoot (mV)	40.8	1.5	30	40.4	1.6	28	ns	0.7486
Amplitude (mV)	132.1	1.5	30	131.6	1.7	28	ns	0.787
dV/dt_{max} (V/s)	65.6	13.9	30	57.3	7.8	28	ns	0.96
APD_{20} (ms)	77.1	5.9	30	88.7	7.3	28	ns	0.2749
APD_{30} (ms)	102.7	7.3	30	115.6	9.3	28	ns	0.3492
APD_{50} (ms)	140.4	10.4	30	144.3	10.8	28	ns	0.7167
APD_{70} (ms)	161.5	11.4	30	159.7	11.2	28	ns	0.9692
APD_{80} (ms)	170.0	11.8	30	165.8	11.5	28	ns	0.9537
APD_{90} (ms)	179.7	12.2	30	174.0	12.4	28	ns	0.9323

PCL700

	Control			IM-R406W			Mann-Whitney	
	Mean	± sem	n	Mean	± sem	n	Sign	p-value
Interval (ms)	700.0	0.0	21	700.0	0.0	15	ns	0.582
MDP (mV)	-91.4	0.2	21	-91.4	0.3	15	ns	0.9243
Overshoot (mV)	46.2	2.9	21	51.7	3.0	15	ns	0.2651
Amplitude (mV)	137.5	2.8	21	143.1	2.8	15	ns	0.2937
dV/dt_{max} (V/s)	96.3	17.9	21	80.0	11.2	15	ns	>0.9999
APD_{20} (ms)	61.2	8.8	21	87.4	11.1	15	*	0.026
APD_{30} (ms)	85.5	10.9	21	128.5	16.2	15	*	0.0389
APD_{50} (ms)	112.8	14.5	21	168.6	21.3	15	*	0.0303
APD_{70} (ms)	124.3	15.9	21	184.0	21.7	15	*	0.0255
APD_{80} (ms)	126.9	16.1	21	187.2	21.7	15	*	0.0233
APD_{90} (ms)	129.2	16.2	21	189.8	21.6	15	*	0.0233

	PT-R406W			IC-R406			Mann-Whitney	
	Mean	± sem	n	Mean	± sem	n	Sign	p-value
Interval (ms)	699.9	0.1	27	700.0	0.1	25	ns	0.28
MDP (mV)	-91.1	0.1	27	-91.3	0.2	25	ns	0.2236
Overshoot (mV)	40.8	1.6	27	39.7	1.7	25	ns	0.6238
Amplitude (mV)	131.9	1.6	27	131.0	1.8	25	ns	0.7029
dV/dt_{max} (V/s)	62.4	10.6	27	61.1	10.1	25	ns	0.8881
APD_{20} (ms)	73.0	6.1	27	79.2	7.1	25	ns	0.467
APD_{30} (ms)	96.3	7.4	27	102.3	8.5	25	ns	0.611
APD_{50} (ms)	130.8	10.0	27	129.0	9.7	25	ns	0.9566
APD_{70} (ms)	152.0	11.1	27	144.2	10.3	25	ns	0.7889
APD_{80} (ms)	160.4	11.4	27	150.1	10.8	25	ns	0.5983
APD_{90} (ms)	170.7	11.9	27	158.2	12.0	25	ns	0.5012

Test: Unpaired non-parametric t-test (Mann-Whitney)
Control vs IM-R406W
PT-R406W vs IC-R406

ns = not significant
*: $p < 0.05$
**: $p < 0.01$

Supplementary Table 2. Action potential parameters of impaled EHTs

Spontaneous

	Control			IM-R406W				PT-R406W			IC-R406			
	Mean	± sem	n	Mean	± sem	n	Sign	Mean	± sem	n	Mean	± sem	n	Sign
Interval (s)	1.7	0.1	6	1.4	0.2	4	ns	0.8	0.0	7	1.0	0.2	4	ns
MDP (mV)	-66.2	1.6	6	-71.4	5.9	4	ns	-73.3	4.6	7	-67.1	2.7	4	ns
Overshoot (mV)	33.5	2.4	6	35.8	3.2	4	ns	30.5	2.8	7	33.1	0.4	4	ns
Amplitude (mV)	100.3	4.1	6	106.1	2.5	4	ns	100.6	5.0	7	102.1	2.3	4	ns
dV/dt_{max} (V/s)	77.6	18.1	6	116.5	27.6	4	ns	36.8	9.5	7	14.6	1.8	4	ns
APD_{20} (ms)	118.8	5.7	6	192.7	25.0	4	*	196.7	15.7	7	150.8	9.6	4	ns
APD_{30} (ms)	149.0	6.6	6	244.0	33.1	4	**	254.6	20.3	7	193.8	16.8	4	ns
APD_{50} (ms)	177.8	8.7	6	284.3	37.1	4	*	310.1	22.8	7	243.8	32.7	4	ns
APD_{70} (ms)	194.6	10.5	6	299.9	38.0	4	*	332.5	23.8	7	269.8	40.6	4	ns
APD_{80} (ms)	205.0	11.1	6	308.0	38.3	4	*	342.3	24.2	7	282.9	43.6	4	ns
APD_{90} (ms)	229.8	12.3	6	323.4	37.6	4	ns	355.0	25.0	7	302.6	48.9	4	ns

Test: Unpaired non-parametric t-test (Mann-V
Control vs IM-R406W
PT-R406W vs IC-R406

ns = not significant
*: $p < 0.05$
**: $p < 0.01$

Complementary Results

Differences Between 2D and 3D Models

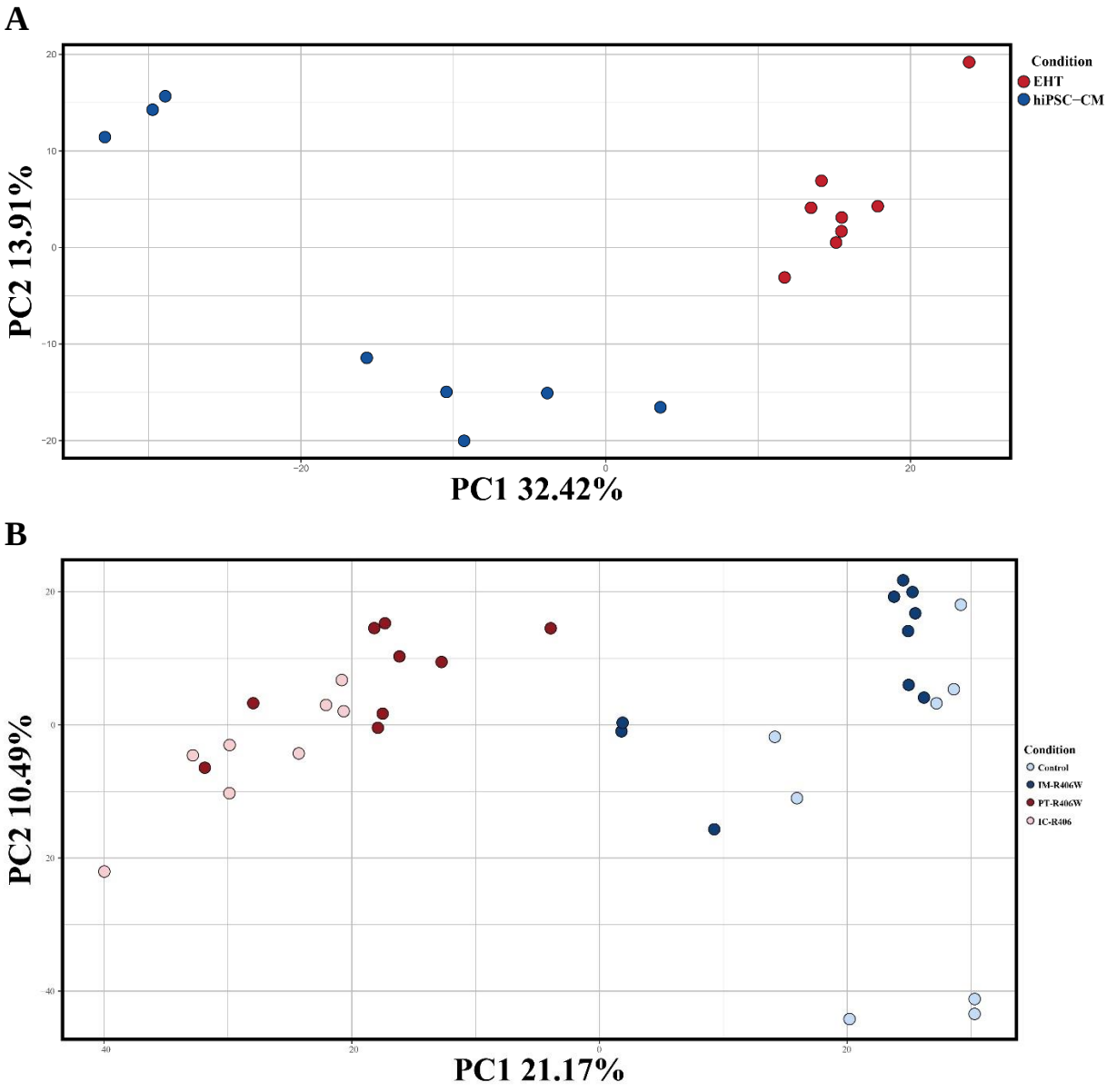

Figure 27. Transcriptomic differences between 2D and 3D cultures.
Principal component analysis (PCA) plots depicting the variation between Control hiPSC-CMs and EHTs (A) and the variability among the different hiPSC-CM lines (B).

The variation of the transcriptomic data are represented in Figure 27. The top panel (Figure 27A) elucidates the variability between the transcriptome of the Control hiPSC-CMs and EHT. Here, we observe that the EHT samples group together more than the hiPSC-CMs, which in contrast form two groups. This depicts that there is less variability between the Control EHT data, making them more reproducible. The bottom panel (Figure 27B) represents the variability among the different hiPSC-CM lines. Principal component analysis fails to separate hiPSC lines carrying the desmin p.R406W mutation from those without it. This suggests that, from a transcriptomic perspective, the hiPSC cardiac differentiation model is not adapted to the study of the desmin p.R406W mutation.

Electrophysiological Differences Between hiPSC-CMs and EHTs

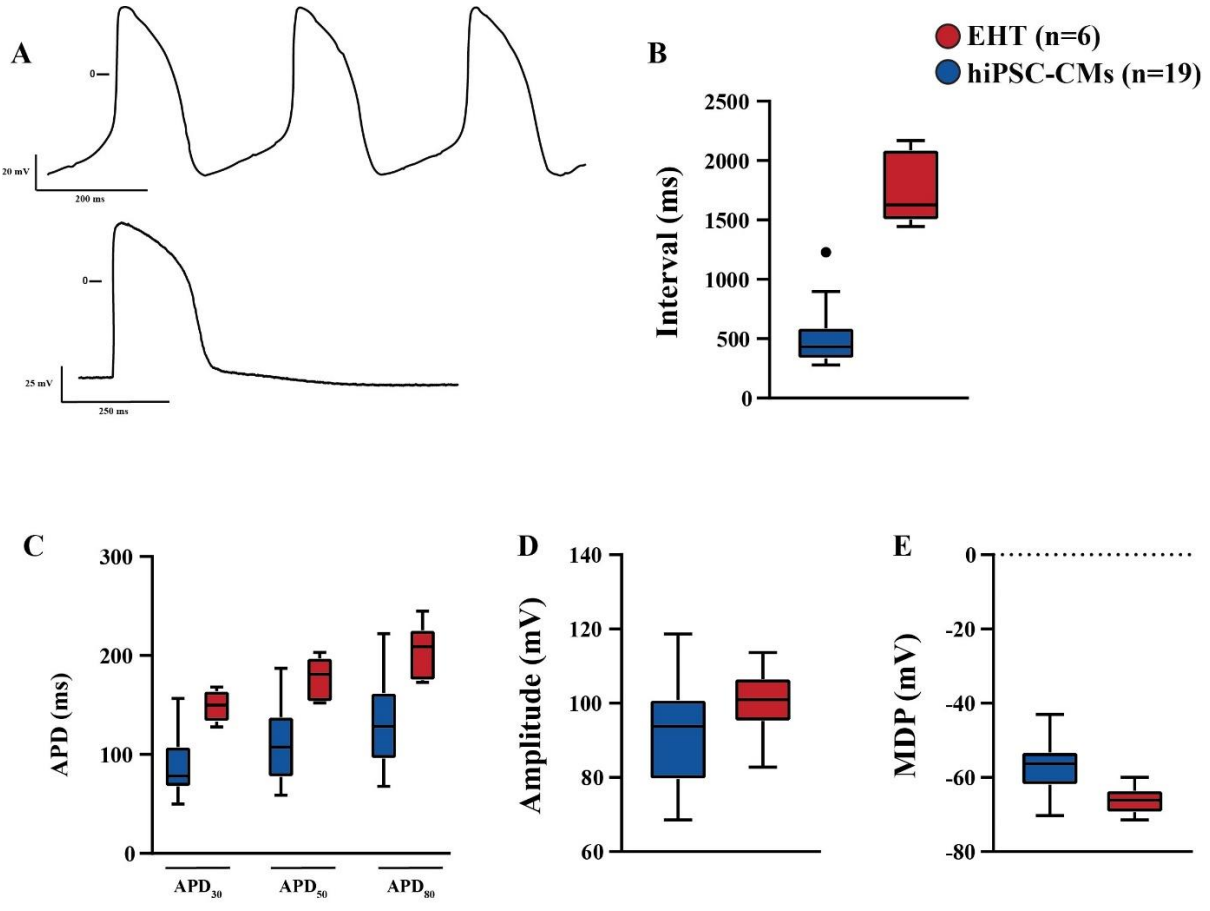

Figure 28. Action Potentials of Control hiPSC-CMs compared to Control EHTs.
Spontaneous recordings of hiPSC-CMs (A; top) compared to EHT (A: bottom). The beat-to-beat interval (B) differences demonstrated a faster beating rate of hiPSC-CMs. The APDs (C), amplitude (D), and MDP (E), are distinctly different between the 2D and 3D model.

There are several differences that exist between different models of study, such as hiPSC-CMs and EHTs, including differences in their electrical properties. A graphical representation of the electrical differences that exist between the two models, using Control cell line as means of comparison, are depicted in Figure 28. It is important to keep in mind that the hiPSC-CMs were measured individually using the patch-clamp technique, whereas the EHTs were impaled using sharp electrodes and remained as intact tissues throughout the experiments. Furthermore, the number of hiPSC-CMs (n= 19) that were patched is far greater than impaled EHTs (n=6).

Future perspectives:

There are many intriguing differences between hiPSC-CMs and EHTs. The next steps would be to investigate the differences further, especially the transcriptomic data. Furthermore, it would be of high interest to explore the proteomics data. Together, we would be able to show the differences that exist between 2D and 3D models. This could benefit many research groups that are deciding on a pertinant model of study.

Desmin at the Intercalated Disc

Desmin interacts with desmoplakin (*DSP*) at the desmosomes. To identify the extent of the desmin-ID interaction, we took advantage of the micropatterning technique, and seeded hiPSC-CMs in a single file to promote their attachment at the IDs. First, we can observe the expected striated pattern of desmin in Control and IC-R406 cells (Figure 28; bottom panels in red). Next, we can observe a dense DSP signal (Figure 28; green) at the ID. Compared to the two control lines (Control and IC-R406), the PT-R406W and IM-R406W lines have a less striated desmin pattern and the DSP signal is not as concentrated at the ID and is more dispersed. Taken together, there appears to be a variable connection between desmin and desmoplakin at the IDs of cell lines with the DES^{R406W} mutation.

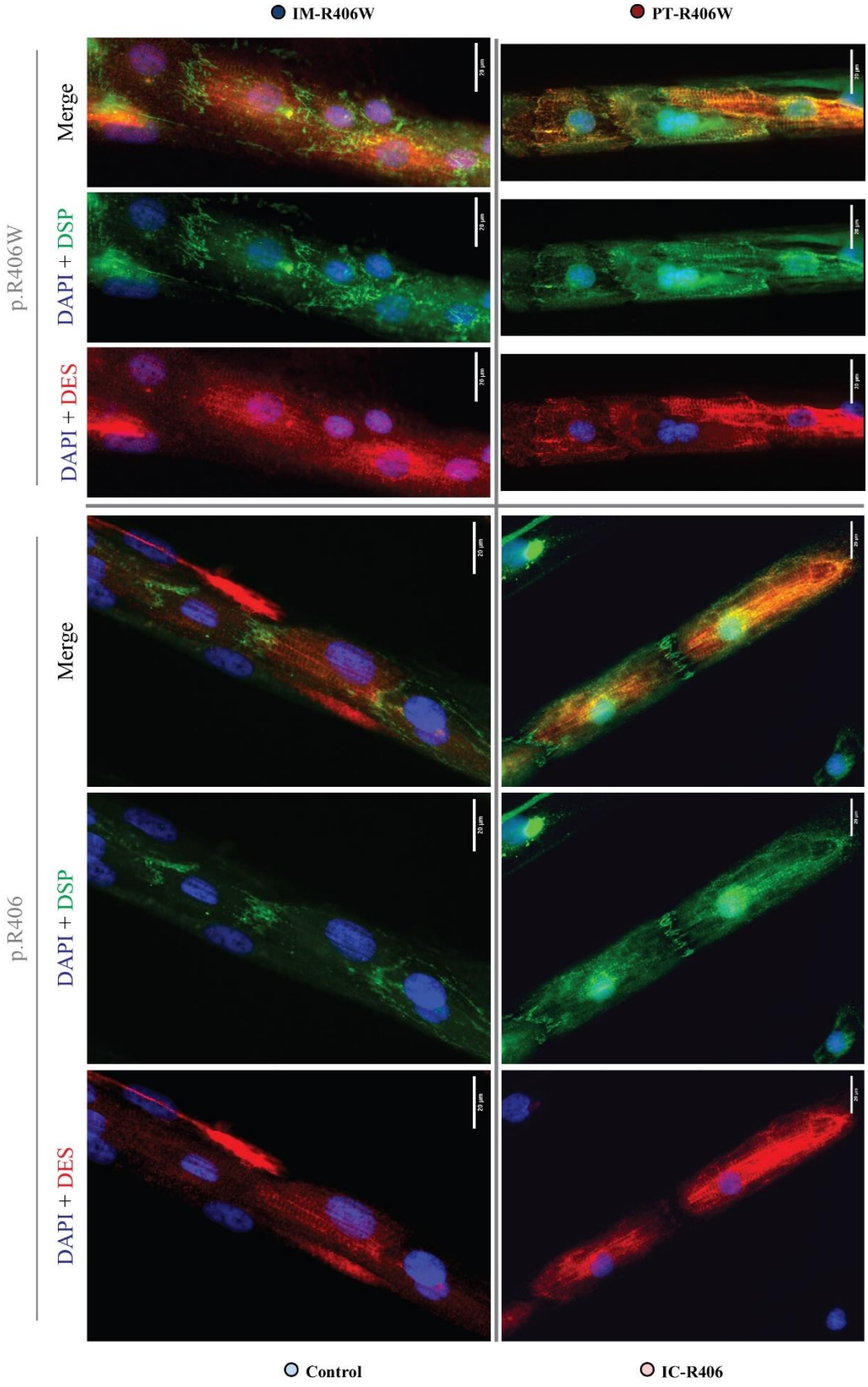

Figure 29. Micropatterned hiPSC-CMs depict the co-localization of desmin and desmoplakin at the IDs.

Chapter VII

Discussion

Characterizing unknown, underlying mechanisms of cardiac diseases to understand the structure-function relationships that exist in the heart has been one of the central themes of this study. Desmin exerts a highly demanding function within muscle cells, and mutations within *DES* have been linked to skeletal and cardiac myopathy, yet the precise role of the IF remains poorly understood. Likewise, the mechanism of onset and progression of disease is still unclear, demanding us to wonder what comes first: aggregate formation, mitochondrial disturbances or a novel unidentified mechanism? Research groups have largely focused on identifying the structural consequences of desmin mutations, *i*.e., is there aggregate formation or not (Bär et al., 2005). In recent years, the idea that desmin mutations are associated with mitochondrial dysfunction, irrespective of aggregate formation, has introduced a novel way of viewing desminopathies as potentially being a mitochondrial disease (Smolina et al., 2020). Studies have suggested that one scenario does not exclude the other, but no consensus has been reached as there is a lack of direct evidence explaining the genotype-phenotype relationships (as reviewed in Chapter III: Review). Consequently, considering that there have been numerous studies describing cardiac diseases in patients with desmin mutations, to the best of my knowledge, little has been investigated in different models of study regarding the electrophysiological consequences, using the patch-clamp technique, for example.

Here, we were presented with a unique opportunity to investigate a complex patient phenotype in order to decipher some of the cardiac ramifications of the desmin p.R406W mutation, using patient hiPSC-CMs as a model. Additionally, we used EHTs to model the disease, an approach that has not been used to study desminopathy, to the best of my knowledge. We used a combination of electrophysiology, proteomic and transcriptomic approaches to get a better understanding of the genotype-phenotype relationship. The results demonstrate a prolongation of the different APDs in hiPSC-CMs and EHTs containing the *DES* p.R406W variant. Moreover, we studied the transcriptomic and proteomic changes in control and mutant EHTs; another poorly explored field in desmin research. The multi-omics results demonstrated a significant change in cellular respiration, and functions related to mitochondria as well as changes in genes related to cardiac contraction.

hiPSC-CMs as a Model for Desminopathy?

HiPSCs have become a prominent model in many branches of research, including cardiology, mainly because of their potential to use patient cells to model and study their disease, thanks to different methods of reprogramming (Teshigawara et al., 2017). Another

advantage of hiPSCs is their ability to differentiate into the three germ layers, with emerging protocols for different cell types such as hepatocytes (endoderm), cardiomyocytes (mesoderm), neural cells (ectoderm), to name a few (Poorna et al., 2021; Zhao et al., 2019). The scope of this technique has broadened to where we are capable of modelling frequent, but also rare diseases. Furthermore, with the rise of CRISPR/Cas9 technology, we are able to modify desired locations of the genome and create isogenic models (Bassett, 2017). For this study, we had the advantage of using the patient's reprogrammed hiPSCs that we differentiated into CMs. To the best of my knowledge, we are the first group to use patient derived hiPSCs from a patient with the desmin p.R406W mutation, although a different research group has transfected this mutation into hiPSCs (Kubánek et al., 2020). Similarly, we employed CRISPR/Cas9 technology to modify *DES* and targeted a desired locus within the patient's and Control hiPSCs. Using isogenic control model, we were able to highlight the effects of the desmin mutation in the cells that could not be attributed to the patient's genetic background. For example, the IM-R406W cell line had a significantly prolonged APD_{90} as opposed to the Control cells, when we measured APs of hiPSC-CMs. Cell reprogramming and genetic modification hold great promise, but these approaches are limited in their efficacy. Further improvements need to happen to increase the success and precision of these approaches.

A common disadvantage that is often pointed out and associated with hiPSC-CMs, is their immaturity, which is readily noticeable by their spontaneous beating. Although strong efforts are being made to establish protocols that can improve maturity and prompt the cells into forming the mesodermal layer using cytokines (Zhao et al., 2019), they continue to lack certain properties. Furthermore, the heart is electrically heterogeneous so there is a need to differentiate the hiPSCs into a specific cell type, whether they are nodal, atrial or ventricular CMs, typically through a combination of hormones and cytokines. To circumvent these issues and promote the differentiation into ventricle-like hiPSC-CMs, we chose a differentiation protocol that used T_3 hormone, which was shown to increase sarcomere length and improve cellular respiratory capacity (Chirico et al., 2022; X. Yang et al., 2014). We also combined the T_3 with dexamethasone, which has been shown to enhance development of T-tubules and improve excitation-contraction coupling (Parikh et al., 2017). Despite our efforts, the MDP of spontaneously beating hiPSC-CMs did not reach the potential of adult cells and CM heterogeneity persisted in our culture conditions, meaning that there is still ample room for improvement of differentiation techniques.

Subsequently, the electrophysiological properties of hiPSC-CMs are not representative of adult CMs, due to their faint expression or lack of certain ionic currents such as, I_{K1} and I_{Na} (J. Liu et al., 2016). The dynamic-clamp technique allows for the injection of synthetic I_{K1}, bringing the MDP to more negative, physiological values similar to adult CMs (Wilders, 2006). With the use of the dynamic-clamp system, we were able to inject synthetic I_{K1} (Verkerk et al., 2017; Verkerk & Wilders, 2020) to obtain an MDP around -90 mV and pace the cells at 1000 and 700 ms. This approach allowed us to measure various AP parameters with cells subjected to similar sampling conditions. Thanks to this method, we were able to show that there is a significant prolongation of APD_{30}, APD_{50}, and APD_{90} in the IM-R406W cells when compared to Control hiPSC-CMs. A slightly longer APD_{90} was observed in PT-R406W cells as opposed to IC-R406. This needs to be explored further to identify the channels responsible for the lengthening by measuring different currents such as the sodium, calcium and potassium currents. To the best of my knowledge, there is an overall lack of electrophysiology studies exploring the implications of desmin mutations. This makes it difficult to compare if all mutations result in prolongation of the APD or if effects are mutation and patient specific, similar to the onset and outcome of cardiomyopathy that varies among patients with the same mutation (Yeow et al., 2023).

The downfall of the patch-clamp technique is the limited number of cells that can be measured on a given day. To measure the channels implicated in the AP prolongation, for example, a high throughput technique such as the automated patch-clamp which can measure up to 384 cells per run (Seibertz & Voigt, 2024), could be used instead. The advantage is of course the number of cells that can be recorded and the relative speed at which results can be obtained. The different currents that are potentially at play, whether it be calcium, sodium or potassium, could be measured in a timely manner and open new avenues that need to be explored. The great disadvantage of this technique is the relative low success rate of proper seal formation of cardiomyocytes and the relatively high numbers, around 400 000 (with 50% success of attachment), that are required per plate (Seibertz & Voigt, 2024). Another limit is that the technique is not well adapted to measuring APs of hiPSC-CMs and therefore we need to rely on the manual patch-clamp method (Seibertz & Voigt, 2024). Therefore, the question of quality versus quantity arises when choosing the proper electrophysiology techniques but the choice is dependent on the scientific question at hand.

The limit of the electrophysiology side of this study is the absence of patch-clamp recordings of the various currents that could help us decipher the mechanism that drives the

disease, genotype-phenotype relationships, and the underlying causes of the AP differences. These recordings would likewise complement our current data and knowledge. The voltage-clamp has been previously applied to record I_{Na} in hiPSC-CMs (Calloe et al., 2022) along with others (Ismaili et al., 2023) making the technique available and feasible for future experiments.

Going 3D

Considering that desmin holds a highly dynamic role by interconnecting various parts of the cardiomyocyte and participates in mechanotransduction and mechanosensation, 3D modelling of desminopathy is more appropriate. Mice are a highly used model in research, including desminopathies (Herrmann et al., 2020), but do not necessarily model the human disease accurately (Boheler et al., 2021) and are not always accessible. As mentioned in Chapter III: Review, hiPSCs and 3D structures generated from these cells, are not commonly used for studying consequences of desmin mutations. The PCA in Figure 27A demonstrates the variability between Control hiPSC-CM samples whereas Control EHTs demonstrated less heterogeneity, suggesting that the 3D model is more representative of the differences.

Multiple EHT conformations have been described, whether they are ring shaped, patches, cylinders, or columns held between two posts (Ormrod & Ehler, 2023; Querdel et al., 2021). Different cardiac diseases have been modelled using 3D tissues, for example ACM (Tsui et al., 2023) and DCM (Ito et al., 2020; Miura et al., 2022). The cell-cell interactions are preserved in organoids and EHTs, and are therefore more representative of the electromechanical connections and the role of desmin at the intercalated discs (Andrysiak et al., 2021; Chua et al., 2023) making them interesting to investigate. Engineered tissues provide an opportunity to perform functional studies to inspect the desmin-protein interactions, especially at the desmosomes (Chua et al., 2023). Mannhardt and colleagues used video-optical recordings to analyze the force of contraction of EHTs (Mannhardt et al., 2016) that can be useful for understanding effects of desmin mutations, especially since patients often present with different cardiomyopathies. Desmin mutations alter the structural integrity of CMs by weakening of its bonds that span the cells (Agnetti et al., 2022), which can result in less effective and weakened force of contraction. Loss of force could potentially be linked to the Z-disc remodeling that we observed in our TEM images. Histology evaluation of the left ventricle of a patient carrying the *DES* p.R406W mutation, confirmed the absence of desmin at the IDs (Herrmann et al., 2020). Therefore, studying the contractile force can help us gain insight into possible cell-cell interaction disturbances, especially at the IDs. If the IDs and cellular integrity are compromised

by desmin mutations, then remodeling of ion channels could also take place (Y. Wang & Hill, 2010). If we combine the loss of desmin at the IDs and the compromised Z-disc structure, we can imagine this as a recipe for disaster. Studies that integrate different fields of research and techniques are lacking in the desmin research field and it is imperative that we take advantage of the new and promising techniques.

In parallel, Tsui and colleagues examined the behavior of a plakophilin-2 (PKP2) pathogenic mutation resulting in ACM. ACM patients often carry mutations in proteins associated with the desmosomes (*JUP*, *DSG*, *DSP*, *PKP2*, and *DSC*). To study the link between desmosomes and ACM, they applied different models including hiPSC-CMs, mice, human heart samples, and microtissues (Tsui et al., 2023). They performed patch-clamp experiments of hiPSC-CM single cells where they demonstrated a decreased I_{Na}. Subsequently, the researchers paced the microtissues and discovered the inability of mutant tissues to respond to higher pacing frequencies (>2 Hz), and thus demonstrating arrhythmic behavior. Their knock-in mice and hiPSC-CMs revealed a decrease in the PKP2 protein and mRNA, in the mutant models. Here, proteomic studies using control and mutant mice exposed a downregulation of the desmosomal proteins in *PKP2* mutant mice (Tsui et al., 2023). The results from this study could be extended to our data, where we can imagine that pacing cells/tissues at faster rates may likewise result in their inability to respond to pacing. Ultimately, this study emphasizes the need for integrative research combining molecular and functional data. Furthermore, they were able to demonstrate the importance of the desmosomal proteins and their association with ACM, by combining different experimental models and methods. Unfortunately, they did not report any results pertaining to desmin. The limit of our study is the absence of histology data from our patient making it difficult to assess the structural consequences of the mutation. Combining patient samples and hiPSC-CM/EHTs for multi-omics would enforce the results that we obtained.

It has been reported that three dimensional models created using hiPSC-CMs have an improved metabolic maturity, ameliorate sarcomere positioning and structure, improvements in the release and storage of calcium, increased Cx43, and presence of T-tubules (Ormrod & Ehler, 2023). Several groups have also demonstrated that the 3D tissue maturity can also be improved with the help of electrical stimulation (Radisic et al., 2004; Ronaldson-Bouchard et al., 2018; Sun & Nunes, 2016). Ronaldson-Bouchard and colleagues tested different stimulation frequencies, either by constant stimulation (at 2 Hz) or increasing the intensity of stimulation (starting at 2 Hz and finishing at 6 Hz with 0.33 Hz increments/day) to assess maturity. They

demonstrated that intensity training of EHTs were comparable to adult tissue on a structural level with adult-like sarcomere length and organization; and also on a functional level with a metabolic switch to oxidative metabolism (Ronaldson-Bouchard et al., 2018). Furthermore, stimulated EHTs showed molecular maturity by means of their improved gene expression for example, increased *MYH7*, *GJA1*, and *RYR2* expression (Ronaldson-Bouchard et al., 2018). Taken together, modelling patient specific mutations using EHTs and with electrical stimulation would allow us to compare the inter/intracellular connections of patient versus control tissues. Subjecting EHTs to electrical stress would give insight as to how the cells adapt to stressful conditions. It would be of special interest to observe these tissues using TEM images to expose the organization of mitochondria relative to Z-discs, when subject to extreme conditions. If the model is as mature as the research suggests, the field of IF research could strongly benefit from it and unveil the missing fundamental gaps of knowledge about the precise role of desmin in CMs.

Taking the 2D model and making it 3D, proposes certain benefits that are intriguing especially for cardiac research. Furthermore, it has been suggested that during the formation of 3D tissues, co-culture of hiPSC-CMs with fibroblasts has positive effects on EHT formation most probably because the cells aid in forming the extracellular matrix and can also secrete certain growth factors (Ormrod & Ehler, 2023). With improved structural and functional maturity, the 3D model holds promise for research of diseases that are less frequent. On this note, research concerning patient specific desmin mutations could largely benefit from this model, especially if we consider using the patient's hiPSCs.

Can we do better?

As shown in this study, sharp electrode data from EHTs complement the patch-clamp experiments. They too showed longer APDs in cell lines containing the mutation. Considering that desmin mutations often result in cardiac myopathy, we have demonstrated some first-hand consequences of this genetic variant, that could be pertinent to some, if not all, other desmin mutations. We demonstrate the importance of broadening our scope beyond aggregate investigation and studying the underlying electrical disturbances that occur in desminopathy patients.

To fully take advantage of the 3D model and fill the gaps of knowledge, there are techniques that would greatly complement our data. Seeing as there is a prolongation of the APD in EHTs (also in hiPSC-CMs) with the *DES* p.R406W mutation, investigating the

excitation-contraction coupling is of high relevance (Eisner et al., 2017). One approach for monitoring calcium is to implement optical mapping using Ca^{2+}-sensitive and voltage-sensitive dyes (Djemai et al., 2023). This strategy was used in a hypertrophy mouse model to analyze the coupling between voltage and calcium handling. The research group of He *et al*. demonstrated a delay between the AP and the peak of calcium transient, which they attributed as the driving factor of arrhythmias in hypertrophied hearts (He et al., 2021). Furthermore, optical mapping has been applied to EHTs where it was possible to capture the coupling of calcium and contraction (Baines et al., 2024; Woodhams et al., 2023). Moreover, optical mapping of hiPSC-CM monolayers has given insight into conduction velocity (Pierre et al., 2021) which is beneficial to comprehend the relationship of desmin-causing cardiac diseases and the hindered of signal propagation. Understanding if electrical remodeling occurs will be the next step to unwrap any conduction disturbances (Han et al., 2021).

With that being said, we have tried optical mapping of hiPSC-CMs as well as EHTs. Unfortunately, the experiments were not successful. The primary issue with the EHTs was the lack of penetration of the voltage-sensitive dyes into the tissue. We were unable to see the conduction velocity of the AP, nor the calcium transient. This is unfortunate since we expected to see how the signal propagates throughout the tissue, which would have been a novel result in the field. Furthermore, this data could have helped confirm our suspicions about the actions of calcium in the tissues and could have complemented our AP data. Optical mapping of the 2D hiPSC-CMs did allow us to observe the fluctuation of the Rhod-2AM (calcium) and Rh237 (voltage) signal, but it was not uniform. The downfall of the 2D culture is that the signal did not spread evenly throughout the dish. There were several loci from where the signal originated, with some of them being very close to one another. This made it extremely difficult to observe the direction and rate of conduction. Furthermore, there were several locations in the dish that did not emit a signal, and so the signal propagated unevenly. If these spots were confirmed fibroblasts, it would give us a better depiction how the electrical signal propagates in the presence of fibrosis, which is often found in patients. The next step to optimize this technique would be to adapt the optical mapping system we have in the lab for EHTs, making it more sensitive for smaller tissues, and optimize the loading of the dyes. For the hiPSC-CMs, it would be of high interest to map them in an aligned, single file fashion using micropatterning techniques, to avoid the above-mentioned problems. Subsequently, optical mapping of mouse hearts carrying the mutation are planned for the near future, and we hope to have better success in observing the consequences of the mutation.

What value do the omic studies bring to the desminopathy table?

The omics field has been pushing the boundaries of research and integrating knowledge in a new way. Proteomic studies allow us to study the proteome of a given sample (Jovanovic et al., 2015), whereas transcriptomics give us insight into the RNA transcripts of an sample (Lowe et al., 2017). By combining omic techniques, we can gather a global understanding of gene expression in an organism. Abundant mRNA expression does not necessarily reflect protein level expression, especially in diseased models (Y. Liu et al., 2016). This is therefore a limiting factor of our multi-omic study, since we cannot conclude with certainty that an increase in mRNA is correlated to an increase in protein expression.

Changes in mitochondria function have been documented in different experimental models. Kubánek and colleagues observed that the activity of the respiratory chain enzymes were decreased along with and overall downregulation of respiratory complexes in myocardial samples from desminopathy patients (Kubánek et al., 2020). Hovhannisyan and colleagues investigated mitochondrial changes in the heart, hiPSC-CMs, and 3D cardiac spheroids. Mitochondrial respiratory proteins were likewise downregulated, similar to the previous study. They attributed the lower protein levels to the mitochondria structural changes observed in their TEM imaging. RNA sequencing revealed downregulated gene expression of genes pertaining to the mitochondria in mutant hiPSC-CMs. The researchers took the study further by measuring the respiration activity of hiPSC-CMs. The results of this experiment showed a decrease of mitochondrial respiration in mutant cells (Hovhannisyan et al., 2024). Taken together with our results, mitochondria seem to be central to the problems caused by desmin mutations. Seeing as mitochondrial consequences arise in 2D and 3D models, both in our and the above-mentioned studies, the importance of proper mitochondrial positioning and function is evident, and this relationship needs to be explored further.

Nevertheless, multi-omics has opened new avenues of knowledge that are of high interest to the field. We were able to complement the published data about the mitochondria involvement in desminopathy with our data from the EHT omic studies. Taken together, desminopathy seems to mimic mitochondrial disease. A large part of our GO terms were related to mitochondria and contractile function. Ultimately, if we could complement our multi-omic studies with further mitochondria activity experiments, we would be able to get a better understanding of the link between the AP differences and the metabolism of the cell. Integrative

research would lead to our understanding of the structural and functional role of the desmin p.R406W mutation.

Multi-omic approaches are being applied to unravel the mechanisms behind human development. Within this realm, organ specific studies are taking place, including research focused on different transcription factors that are important for cardiac development (Canac et al., 2022). Transcriptomic and proteomic studies are being complemented with chromatin accessibility studies using assay for transposase-accessible chromatin with sequencing (ATAC-seq) methods (Carraro et al., 2023). With this, we have advanced our knowledge on cellular processes that occur during cardiac development. These ideas can likewise be applied to the development and progression of desmin disease. Similarly, it would be important to investigate the current desmin mutation, p.R406W, since its onset is relatively early; between the first two decades of life, as opposed to the other mutations. Subjecting samples to omic analysis on a 24-hour interval could unravel how the disease starts. In combination with imaging and functional studies, the results would bring not only value to the desmin research field, but also to the field of cardiac development. Taking our observations into account, using EHTs as a model for this type of study would be ideal since we would start on a 2D level and progress into 3D; improving maturity along the way. Seeing as desminopathy can involve skeletal muscles in combination with the heart, applying this methodology to primary myotubes would be of great importance (Smolina et al., 2014). Machine learning integrates omics data, such as proteomics and transcriptomics, and creates connections between systems using predictive algorithms (Reel et al., 2021). Advances in this field should be taken advantage of in order to bring novel biomarkers of disease to light, but also to help us find new connection we might not be aware of.

Are we missing something?

We know that desmin is the most abundant IF in the cardiomyocytes (Tsikitis et al., 2018). Moreover, what is unsettling is the lack of information regarding desmin in Purkinje fibers. It has been reported that there is a strong presence of desmin in Purkinje fibers of mammal thanks to immunohistochemistry experiments (Yoshimura et al., 2014). Considering that the Purkinje fiber cytoskeleton is primarily composed of desmin IFs (about 50-70%) (Schrickel et al., 2010), little is known about the mechanism behind desmin mutations and their effects in the cardiac conduction system. We have seen the effects of different point mutations in case studies reporting bundle branch blocks, tachyarrhythmia, AV conduction defects (Table

1 in Chapter III: Review). Electrogram recordings of the His bundle of a patient with a missense desmin mutation, p.S13F, demonstrated evidence of conduction block within the His-Purkinje conduction system (Boulé et al., 2015), implicating the cardiac conduction system in desminopathy. In addition, desmin knock-out mice have shown slower conduction velocities and longer ventricle refractory periods (Schrickel et al., 2010), providing strong evidence of cardiac conduction system involvement in desminopathies.

More often than not, studies asses pathogenicity of desmin mutations by observing the presence or absence of aggregates. The missing link in our study and the overall desmin research field pertains to Purkinje fibers. Not only that, but there is a need for human models of these fibers to assess their implication in desminopathy, for example by using hiPSC-CMs, especially since the Purkinje fiber network and their penetration varies among species (Ono et al., 2009). A recent publication applied a cocktail of small molecules in order to transform hiPSC-CMs into Purkinje fibers (Prodan et al., 2022). Although the method is still being optimized, it demonstrates a promising potential. In future studies, it would be if high interest to perform function, molecular and structural experiments on hiPSC generated Purkinje fibers containing desmin mutations. Additionally, culturing hiPSC-CMs together with hiPSC generated Purkinje fibers would allow us to have an intricate human model of the heart combined with the conduction system. Furthermore, forming a 3D model from these two cell types would allow for intricate, deep studies of desminopathy, but also of other cardiac diseases. Taken together, integrating models and techniques hold promise for deciphering several genotype-phenotype relationships in the heart.

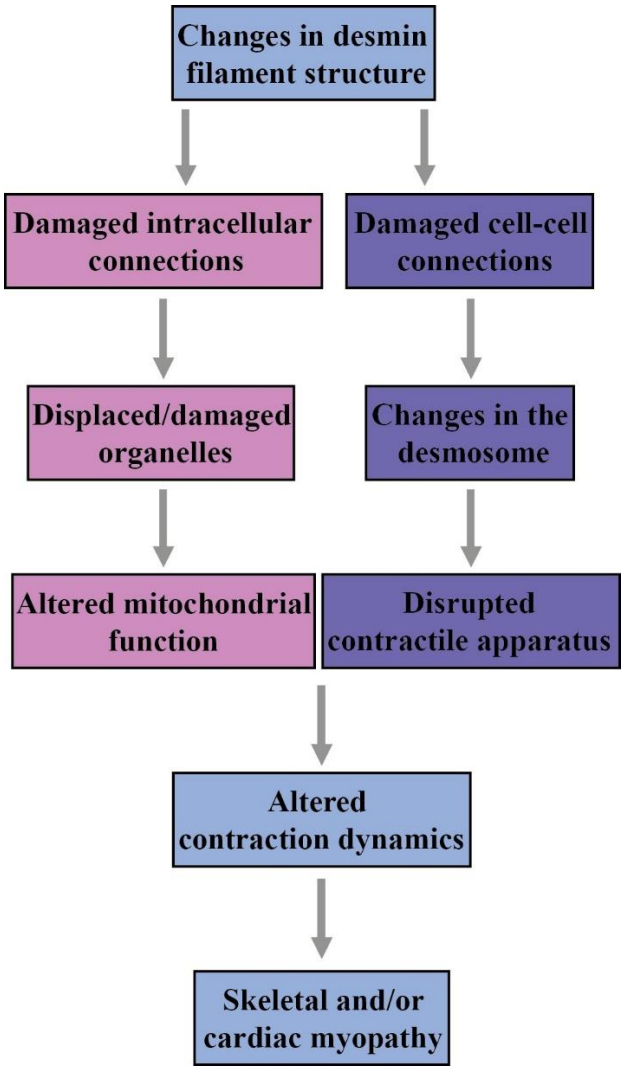

Figure 30. Proposed mechanism of desminopathy development.

Desmin can be considered as the backbone of muscle cells. It creates a cell-spanning web, interconnecting several intracellular structures together. If the filamentous structure cannot form, and instead aggregates or uncompacted filaments appear, several downstream consequences follow (Figure 30). Firstly, the loss of desmin at the IDs can result in loose connections between the ID and the rest of the intracellular structures. This can potentially decrease the number of connexin channels between cells, since a loss of mechanosensation arises. Loss of strong connections can cause the tissue to stretch and lead to cardiomyopathy such as DCM, for example. The origin of desminopathy can be hypothesized to start by the loss or weakening of cell-cell connections.

In parallel, improper cell-cell attachment also causes a loss of tensile strength within the cell, making it less responsive to the mechanosensation and mechanotransduction signals. Loss of tension inside the cell could cause the cell to lose its brick-like appearance and in turn

increase in size, which could be associated with HCM. Lack of the dynamic filaments in the cell could additionally cause the cells to stiffen and be less responsive to signals. Stiffening of the ventricles is seen in RCM, which has been described in patients with desmin mutations. Furthermore, if these intercellular connections are not stable, the myocardial tissue can be replaced by scar tissue (fibrosis), which is often seen is ACM.

Concerning the intracellular consequences, improper positioning of the mitochondria due to desmins inability to form connections and bring it to close proximity with the contractile apparatus, can have detrimental effects on the cells ability to contract. If there is not enough energy in the cell to perform its function, the contractions will be weak and unable to contribute to cardiac contraction or propagate the signal to neighbouring cells. We can also imagine that apoptosis of these cells can prevail since they are unable to perform. The collapse of the nucleus can be another detrimental effect of desmin mutations. Subsequently, if the myocardium is replaced by scar tissue, it makes it difficult for the Purkinje fibers to propagate the electrical signal throughout the heart. Taken together, structural changes of the desmin filament, whether its aggregate formation or uncompacted filaments that arise, affect the function of the heart.

The up-regulated proteins related to cardiac contraction in EHTs with the *DES* p.R406W mutation, such as *MYH7, MYL3*, *TNNC1, TNNI3,* could possibly be explained by the lack of Z-disc organization and stability. Overall, it appears that correct protein anchoring is affected that can cause a loss of intracellular tension. Therefore, the overexpression of such proteins might be a compensatory mechanism in mutant cells. Subsequently, *PKP2*, an important protein of the ID that modulates desmins connection to the ID, is up-regulated in mutant cells. This up-regulation could be taking part in a compensatory mechanism in an attempt to promote and correct the lost cell-to-cell connections, although we cannot be sure if the protein is correctly positioned and distributed within the ID. High resolution images of the desmin-desmoplakin-plakophillin-2 connection using exampsion microscopy (Agullo-Pascual et al., 2013; F. Chen et al., 2015), for example, would be helpful to elucidate how the structural bond is hindered. Furthermore, the prolongation of the APD in the isogenic mutant hiPSC-CMs and EHTs might be explained by the up-regulation of proteins that are relevant to the AP, such as *CACNB1, SLC8A1, RYR2,* and *CAMK2D.* These proteins play a role in correct calcium handling of the cell. Their up-regulation therefore, might be the primary contributor to the APD prolongation. To the contrary, afterdepolarizations were not observed in any our AP recordings. Measurements of calcium current and calcium transient are therefore imperative for further

insight into the calcium homeostasis disturbances within the cells and the contribution of these up-regulated proteins.

What's next?

The next steps in this project would be to explore the metabolomics aspect of the EHTs using techniques such as the Seahorse metabolic analyzer (Yépez et al., 2018). This would help us understand the precise changes in oxygen consumption that occur in the tissues and the rate of ATP production and it would be interesting to compare the results with our omics data to see how the metabolism fits into the equation and if the datasets are linked and comparable. Subsequently, we should test if there is aggregate formation in hiPSC-CMs and EHTs, as seen in patients. Comparing aggregate composition of our models to the previously reported human biopsy samples would further validate the model. Next, it would be of interest to perform ECGs and optical mapping studies on mice carrying the desmin mutation. Our group has started performing ECGs on mice at different ages, but we are missing data on older mice (>15 weeks) as well as young mice as old as one week.

Most notably, it would be of high interest to differentiate the hiPSCs into Purkinje fibers. This would, for the first time, allow us to explore the effects of mutant desmin in the fibers. Furthermore, optical mapping of Purkinje fibers could elucidate the electrical differences between control and mutant lines. This could help illustrate any conduction disturbances that arise and could explain some of the cardiac phenotypes seen in patients. Of course, combining a 3D model, such as the EHTs, with Purkinje fibers is an integrative approach that needs to be explored. Such an approach would benefit many cardiac research fields.

Subsequently, understanding how and if the desmin mutation affects the nucleus could help explain some of the omic differences we have observed. Understanding desmins role in maintaining nuclear shape and position could be achieved through immunofluorescence studies. Taking into account our observations (Article 2) of the transcriptomic changes, mutant desmin may cause a collapse of the nuclear envelope that could change the architecture of the nucleus (Agnetti et al., 2022) causing these effects. Lamins and desmin both play an important role in preserving the nuclear structure, therefore, investigating this relationship could give us insight into disease onset.

There are many intracellular structures that depend on desmin IFs for proper function. Exploring all of these interactions is detrimental for deciphering the role of desmin in the structure-function relationships of the heart.

References

Agnetti, G., Halperin, V. L., Kirk, J. A., Chakir, K., Guo, Y., Lund, L., Nicolini, F., Gherli, T., Guarnieri, C., Caldarera, C. M., Tomaselli, G. F., Kass, D. A., & Van Eyk, J. E. (2014). Desmin modifications associate with amyloid-like oligomers deposition in heart failure. *Cardiovascular Research*, *102*(1), 24–34. https://doi.org/10.1093/cvr/cvu003

Agnetti, G., Herrmann, H., & Cohen, S. (2022). New roles for desmin in the maintenance of muscle homeostasis. *The FEBS Journal*, *289*(10), 2755–2770. https://doi.org/10.1111/febs.15864

Agullo-Pascual, E., Reid, D. A., Keegan, S., Sidhu, M., Fenyö, D., Rothenberg, E., & Delmar, M. (2013). Super-resolution fluorescence microscopy of the cardiac connexome reveals plakophilin-2 inside the connexin43 plaque. *Cardiovascular Research*, *100*(2), 231–240. https://doi.org/10.1093/cvr/cvt191

Ahmed, R. E., Tokuyama, T., Anzai, T., Chanthra, N., & Uosaki, H. (2022). Sarcomere maturation: Function acquisition, molecular mechanism, and interplay with other organelles. *Philosophical Transactions of the Royal Society B: Biological Sciences*, *377*(1864), 20210325. https://doi.org/10.1098/rstb.2021.0325

Ai, Z., Fischer, A., Spray, D. C., Brown, A. M., & Fishman, G. I. (2000). Wnt-1 regulation of connexin43 in cardiac myocytes. *The Journal of Clinical Investigation*, *105*(2), 161–171. https://doi.org/10.1172/JCI7798

Alcalai, R., Metzger, S., Rosenheck, S., Meiner, V., & Chajek-Shaul, T. (2003). A recessive mutation in desmoplakin causes arrhythmogenic right ventricular dysplasia, skin disorder, and woolly hair. *Journal of the American College of Cardiology*, *42*(2), 319–327. https://doi.org/10.1016/S0735-1097(03)00628-4

Alcocer-Cuarón, C., Rivera, A. L., & Castaño, V. M. (2014). Hierarchical structure of biological systems. *Bioengineered*, *5*(2), 73–79. https://doi.org/10.4161/bioe.26570

Andrysiak, K., Stępniewski, J., & Dulak, J. (2021). Human-induced pluripotent stem cell-derived cardiomyocytes, 3D cardiac structures, and heart-on-a-chip as tools for drug research. *Pflügers Archiv - European Journal of Physiology*, *473*(7), 1061–1085. https://doi.org/10.1007/s00424-021-02536-z

Anumonwo, J. M. B., & Lopatin, A. N. (2010). Cardiac strong inward rectifier potassium channels. *Journal of Molecular and Cellular Cardiology*, *48*(1), 45–54. https://doi.org/10.1016/j.yjmcc.2009.08.013

Arbustini, E., Pasotti, M., Pilotto, A., Pellegrini, C., Grasso, M., Previtali, S., Repetto, A., Bellini, O., Azan, G., Scaffino, M., Campana, C., Piccolo, G., Viganò, M., & Tavazzi, L. (2006). Desmin accumulation restrictive cardiomyopathy and atrioventricular block associated with desmin gene defects. *European Journal of Heart Failure*, *8*(5), 477–483. https://doi.org/10.1016/j.ejheart.2005.11.003

Ashley, E. A., & Niebauer, J. (2004). Conquering the ECG. In *Cardiology Explained*. Remedica. https://www.ncbi.nlm.nih.gov/books/NBK2214/

Aweida, D., Rudesky, I., Volodin, A., Shimko, E., & Cohen, S. (2018). GSK3-β promotes calpain-1-mediated desmin filament depolymerization and myofibril loss in atrophy. *The Journal of Cell Biology*, *217*(10), 3698–3714. https://doi.org/10.1083/jcb.201802018

Baines, O., Sha, R., Kalla, M., Holmes, A. P., Efimov, I. R., Pavlovic, D., & O'Shea, C. (2024). Optical mapping and optogenetics in cardiac electrophysiology research and therapy: A state-of-the-art review. *Europace*, *26*(2), euae017. https://doi.org/10.1093/europace/euae017

Bär, H., Mucke, N., Kostareva, A., Sjoberg, G., Aebi, U., & Herrmann, H. (2005). Severe muscle disease-causing desmin mutations interfere with in vitro filament assembly at distinct stages. *Proceedings of the National Academy of Sciences*, *102*(42), 15099–15104. https://doi.org/10.1073/pnas.0504568102

Bär, H., Strelkov, S. V., Sjöberg, G., Aebi, U., & Herrmann, H. (2004). The biology of desmin filaments: How do mutations affect their structure, assembly, and organisation? *Journal of Structural Biology*, *148*(2), 137–152. https://doi.org/10.1016/j.jsb.2004.04.003

Bassett, A. R. (2017). Editing the genome of hiPSC with CRISPR/Cas9: Disease models. *Mammalian Genome*, *28*(7), 348–364. https://doi.org/10.1007/s00335-017-9684-9

Becker, D. E. (2006). Fundamentals of Electrocardiography Interpretation. *Anesthesia Progress*, *53*(2), 53–64. https://doi.org/10.2344/0003-3006(2006)53[53:FOEI]2.0.CO;2

Bekhite, M. M., & Schulze, P. C. (2021). Human Induced Pluripotent Stem Cell as a Disease Modeling and Drug Development Platform—A Cardiac Perspective. *Cells*, *10*(12), Article 12. https://doi.org/10.3390/cells10123483

Benitah, J.-P., Perrier, R., Mercadier, J.-J., Pereira, L., & Gómez, A. M. (2021). RyR2 and Calcium Release in Heart Failure. *Frontiers in Physiology*, *12*, 734210. https://doi.org/10.3389/fphys.2021.734210

Bers, D. M. (2002). Cardiac excitation–contraction coupling. *Nature*, *415*(6868), Article 6868. https://doi.org/10.1038/415198a

Bishop, S. P., Zhang, J., & Ye, L. (2022). Cardiomyocyte Proliferation from Fetal- to Adult- and from Normal- to Hypertrophy and Failing Hearts. *Biology*, *11*(6), 880. https://doi.org/10.3390/biology11060880

Boheler, K. R., Meli, A. C., & Yang, H.-T. (2021). Special issue on recent progress with hPSC-derived cardiovascular cells for organoids, engineered myocardium, drug discovery, disease models, and therapy. *Pflügers Archiv - European Journal of Physiology*, *473*(7), 983–988. https://doi.org/10.1007/s00424-021-02594-3

Boulé, S., Richard, P., de Groote, P., Renaud, F., & Charron, P. (2015). Recurrent suspected myocarditis combined with infrahisian conduction disturbances revealing a desminopathy. *HeartRhythm Case Reports*, *1*(5), 305–309. https://doi.org/10.1016/j.hrcr.2015.04.002

Bouvet, M., Dubois-Deruy, E., Turkieh, A., Mulder, P., Peugnet, V., Chwastyniak, M., Beseme, O., Dechaumes, A., Amouyel, P., Richard, V., Lamblin, N., & Pinet, F. (2021). Desmin aggrephagy in rat and human ischemic heart failure through PKCζ and GSK3β as upstream signaling pathways. *Cell Death Discovery*, *7*(1), 153. https://doi.org/10.1038/s41420-021-00549-2

Brayson, D., & Shanahan, C. M. (2017). Current insights into LMNA cardiomyopathies: Existing models and missing LINCs. *Nucleus*, *8*(1), 17–33. https://doi.org/10.1080/19491034.2016.1260798

Brodehl, A., Gaertner-Rommel, A., & Milting, H. (2018). Molecular insights into cardiomyopathies associated with desmin (DES) mutations. *Biophysical Reviews*, *10*(4), 983–1006. https://doi.org/10.1007/s12551-018-0429-0

Bundgaard, H., Jøns, C., Lodder, E. M., Izarzugaza, J. M. G., Romero Herrera, J. A., Pehrson, S., Tfelt-Hansen, J., Ahlberg, G., Olesen, M. S., Holst, A. G., Wellens, H., de Villiers, C., Hastings, R., Stuart, G., Brunak, S., Wilde, A. A. M., Watkins, H., & Christensen, A. H. (2018). A Novel Familial Cardiac Arrhythmia Syndrome with Widespread ST-Segment Depression. *New England Journal of Medicine*, *379*(18), 1780–1781. https://doi.org/10.1056/NEJMc1807668

Burkett, E. L., & Hershberger, R. E. (2005). Clinical and genetic issues in familial dilated cardiomyopathy. *Journal of the American College of Cardiology*, *45*(7), 969–981. https://doi.org/10.1016/j.jacc.2004.11.066

Caillaud, A., Lévêque, A., Thédrez, A., Girardeau, A., Canac, R., Bray, L., Baudic, M., Barc, J., Gaborit, N., Lamirault, G., Gardie, B., Idriss, S., Rimbert, A., Le May, C., Cariou, B., & Si-Tayeb, K. (2022). FACS-assisted CRISPR-Cas9 genome editing of human induced pluripotent stem cells. *STAR Protocols*, *3*(4), 101680. https://doi.org/10.1016/j.xpro.2022.101680

Calloe, K., Broendberg, A. K., Christensen, A. H., Pedersen, L. N., Olesen, M. S., de los Angeles Tejada, M., Friis, S., Thomsen, M. B., Bundgaard, H., & Jensen, H. K. (2018). Multifocal atrial and ventricular premature contractions with an increased risk of dilated cardiomyopathy caused by a Nav1.5 gain-of-function mutation (G213D). *International Journal of Cardiology*, *257*, 160–167. https://doi.org/10.1016/j.ijcard.2017.11.095

Calloe, K., Geryk, M., Freude, K., Treat, J. A., Vold, V. A., Frederiksen, H. R. S., Broendberg, A. K., Frederiksen, T. C., Jensen, H. K., & Cordeiro, J. M. (2022). The G213D variant in Nav1.5 alters sodium current and causes an arrhythmogenic phenotype resulting in a multifocal ectopic Purkinje-related premature contraction phenotype in human-induced pluripotent stem cell-derived cardiomyocytes. *EP Europace*, *24*(12), 2015–2027. https://doi.org/10.1093/europace/euac090

Canac, R., Cimarosti, B., Girardeau, A., Forest, V., Olchesqui, P., Poschmann, J., Redon, R., Lemarchand, P., Gaborit, N., & Lamirault, G. (2022). Deciphering Transcriptional Networks during Human Cardiac Development. *Cells*, *11*(23), 3915. https://doi.org/10.3390/cells11233915

Cao, J., Gao, Q., Chen, H., Zhang, Q., Wang, Z., & Li, Y. (2021). Desmin Correlated with Cx43 May Facilitate Intercellular Electrical Coupling during Chronic Heart Failure. *Evidence-Based Complementary and Alternative Medicine*, *2021*, 1–9. https://doi.org/10.1155/2021/6621132

Capetanaki, Y., Bloch, R. J., Kouloumenta, A., Mavroidis, M., & Psarras, S. (2007). Muscle intermediate filaments and their links to membranes and membranous organelles. *Experimental Cell Research*, *313*(10), 2063–2076. https://doi.org/10.1016/j.yexcr.2007.03.033

Capetanaki, Y., Papathanasiou, S., Diokmetzidou, A., Vatsellas, G., & Tsikitis, M. (2015). Desmin related disease: A matter of cell survival failure. *Current Opinion in Cell Biology*, *32*, 113–120. https://doi.org/10.1016/j.ceb.2015.01.004

Caporizzo, M. A., & Prosser, B. L. (2022). The microtubule cytoskeleton in cardiac mechanics and heart failure. *Nature Reviews Cardiology*, *19*(6), Article 6. https://doi.org/10.1038/s41569-022-00692-y

Carraro, C., Bonaguro, L., Srinivasa, R., van Uelft, M., Isakzai, V., Schulte-Schrepping, J., Gambhir, P., Elmzzahi, T., Montgomery, J. V., Hayer, H., Li, Y., Theis, H., Kraut, M., Mahbubani, K. T., Aschenbrenner, A. C., König, I., Fava, E., Fried, H.-U., De Domenico, E., … Schultze, J. L. (2023). Chromatin accessibility profiling of targeted cell populations with laser capture microdissection coupled to ATAC-seq. *Cell Reports Methods*, *3*(10), 100598. https://doi.org/10.1016/j.crmeth.2023.100598

Chakraborty, P., Aggarwal, A. K., Nair, M. K. K., Massé, S., Riazi, S., & Nanthakumar, K. (2023). Restoration of calcium release synchrony: A novel target for heart failure and ventricular arrhythmia. *Heart Rhythm*, *20*(12), 1773–1781. https://doi.org/10.1016/j.hrthm.2023.08.040

Charpentier, E., Cornec, M., Dumont, S., Meistermann, D., Bordron, P., David, L., Redon, R., Bonnaud, S., & Bihouée, A. (2021). *3' RNA sequencing for robust and low-cost gene expression profiling* [Preprint]. Protocol Exchange. https://doi.org/10.21203/rs.3.pex-1336/v1

Chen, F., Tillberg, P. W., & Boyden, E. S. (2015). Expansion microscopy. *Science*, *347*(6221), 543–548. https://doi.org/10.1126/science.1260088

Chen, Z., Li, R., Wang, Y., Cao, L., Lin, C., Liu, F., Hu, R., Nan, J., Zhuang, X., Lu, X., Nan, G., Hu, G., Xue, J., Zhang, Y., Xiao, J., Yao, Y., Guo, S., & Lei, J. (2021). Features of myocardial injury detected by cardiac magnetic resonance in a patient with desmin-related restrictive cardiomyopathy. *ESC Heart Failure*, *8*(6), 5560–5564. https://doi.org/10.1002/ehf2.13624

Chintanaphol, M., Orgil, B.-O., Alberson, N. R., Towbin, J. A., & Purevjav, E. (2022). Restrictive cardiomyopathy: From genetics and clinical overview to animal modeling. *Reviews in Cardiovascular Medicine*, *23*(3), 108. https://doi.org/10.31083/j.rcm2303108

Chirico, N., Kessler, E. L., Maas, R. G. C., Fang, J., Qin, J., Dokter, I., Daniels, M., Šarić, T., Neef, K., Buikema, J.-W., Lei, Z., Doevendans, P. A., Sluijter, J. P. G., & van Mil, A. (2022). Small molecule-mediated rapid maturation of human induced pluripotent stem cell-derived cardiomyocytes. *Stem Cell Research & Therapy*, *13*(1), 531. https://doi.org/10.1186/s13287-022-03209-z

Chopra, A., Tabdanov, E., Patel, H., Janmey, P. A., & Kresh, J. Y. (2011). Cardiac myocyte remodeling mediated by N-cadherin-dependent mechanosensing. *American Journal of Physiology-Heart and Circulatory Physiology*, *300*(4), H1252–H1266. https://doi.org/10.1152/ajpheart.00515.2010

Chourbagi, O., Bruston, F., Carinci, M., Xue, Z., Vicart, P., Paulin, D., & Agbulut, O. (2011). Desmin mutations in the terminal consensus motif prevent synemin-desmin heteropolymer filament assembly. *Experimental Cell Research*, *317*(6), 886–897. https://doi.org/10.1016/j.yexcr.2011.01.013

Christensen, A. H., Nyholm, B. C., Vissing, C. R., Pietersen, A., Tfelt-Hansen, J., Olesen, M. S., Pehrson, S., Iversen, K. K., Jensene, H. K., & Bundgaard, H. (2021). Natural History and

Clinical Characteristics of the First 10 Danish Families With Familial ST-Depression Syndrome. *Journal of the American College of Cardiology*, *77*(20), 2617–2619. https://doi.org/10.1016/j.jacc.2021.03.313

Christensen, A. H., Vissing, C. R., Pietersen, A., Tfelt-Hansen, J., Hartvig Lindkær Jensen, T., Pehrson, S., Henriksen, F. L., Sandgaard, N. C. F., Iversen, K. K., Jensen, H. K., Olesen, M. S., & Bundgaard, H. (2022). Electrocardiographic Findings, Arrhythmias, and Left Ventricular Involvement in Familial ST-Depression Syndrome. *Circulation: Arrhythmia and Electrophysiology*, *15*(4), e010688. https://doi.org/10.1161/CIRCEP.121.010688

Chua, C. J., Morrissette-McAlmon, J., Tung, L., & Boheler, K. R. (2023). Understanding Arrhythmogenic Cardiomyopathy: Advances through the Use of Human Pluripotent Stem Cell Models. *Genes*, *14*(10), 1864. https://doi.org/10.3390/genes14101864

Chun, Y. W., Durbin, M. D., & Hong, C. C. (2018). Genome Editing and Induced Pluripotent Stem Cell Technologies for Personalized Study of Cardiovascular Diseases. *Current Cardiology Reports*, *20*(6), 38. https://doi.org/10.1007/s11886-018-0984-9

Cingolani, E., Goldhaber, J. I., & Marbán, E. (2018). Next-generation pacemakers: From small devices to biological pacemakers. *Nature Reviews Cardiology*, *15*(3), Article 3. https://doi.org/10.1038/nrcardio.2017.165

Claeyssen, C., Bulangalire, N., Bastide, B., Agbulut, O., & Cieniewski-Bernard, C. (2023). Desmin and its molecular chaperone, the αB-crystallin: How post-translational modifications modulate their functions in heart and skeletal muscles? *Biochimie*. https://doi.org/10.1016/j.biochi.2023.10.002

Clemen, C. S., Herrmann, H., Strelkov, S. V., & Schröder, R. (2013). Desminopathies: Pathology and mechanisms. *Acta Neuropathologica*, *125*(1), 47–75. https://doi.org/10.1007/s00401-012-1057-6

Contreras, J. E., Sáez, J. C., Bukauskas, F. F., & Bennett, M. V. L. (2003). Functioning of Cx43 Hemichannels Demonstrated by Single Channel Properties. *Cell Communication & Adhesion*, *10*(4–6), 245–249. https://doi.org/10.1080/cac.10.4-6.245.249

Corrado, D., Basso, C., & Judge, D. P. (2017). Arrhythmogenic Cardiomyopathy. *Circulation Research*, *121*(7), 784–802. https://doi.org/10.1161/CIRCRESAHA.117.309345

Costa, M. L., Escaleira, R., Cataldo, A., Oliveira, F., & Mermelstein, C. S. (2004). Desmin: Molecular interactions and putative functions of the muscle intermediate filament protein. *Brazilian Journal of Medical and Biological Research*, *37*(12), 1819–1830. https://doi.org/10.1590/S0100-879X2004001200007

Dagvadorj, A., Olivé, M., Urtizberea, J.-A., Halle, M., Shatunov, A., Bönnemann, C., Park, K.-Y., Goebel, H. H., Ferrer, I., Vicart, P., Dalakas, M. C., & Goldfarb, L. G. (2004). A series of West European patients with severe cardiac and skeletal myopathy associated with a de novo R406W mutation in desmin. *Journal of Neurology*, *251*(2), 143–149. https://doi.org/10.1007/s00415-004-0289-3

Dalakas, M. C., Park, K. Y., Semino-Mora, C., Lee, H. S., Sivakumar, K., & Goldfarb, L. G. (2000). Desmin myopathy, a skeletal myopathy with cardiomyopathy caused by mutations in

the desmin gene. *The New England Journal of Medicine*, *342*(11), 770–780. https://doi.org/10.1056/NEJM200003163421104

Daly, N., Meleady, P., Walsh, D., & Clynes, M. (1998). Regulation of keratin and integrin gene expression in cancer and drug resistance. In M. Clynes (Ed.), *Multiple Drug Resistance in Cancer 2* (pp. 321–344). Springer Netherlands. https://doi.org/10.1007/978-94-017-2374-9_22

Dayal, A. A., Medvedeva, N. V., Nekrasova, T. M., Duhalin, S. D., Surin, A. K., & Minin, A. A. (2020). Desmin Interacts Directly with Mitochondria. *International Journal of Molecular Sciences*, *21*(21), 8122. https://doi.org/10.3390/ijms21218122

de Lange, W. J., Farrell, E. T., Kreitzer, C. R., Jacobs, D. R., Lang, D., Glukhov, A. V., & Ralphe, J. C. (2021). Human iPSC-engineered cardiac tissue platform faithfully models important cardiac physiology. *American Journal of Physiology. Heart and Circulatory Physiology*, *320*(4), H1670–H1686. https://doi.org/10.1152/ajpheart.00941.2020

del Monte, F., & Agnetti, G. (2014). Protein Post-Translational Modifications and Misfolding: New Concepts in Heart Failure. *Proteomics. Clinical Applications*, *8*(0), 534–542. https://doi.org/10.1002/prca.201400037

Dellefave, L., & McNally, E. M. (2010). The genetics of dilated cardiomyopathy. *Current Opinion in Cardiology*, *25*(3), 198–204. https://doi.org/10.1097/HCO.0b013e328337ba52

Diokmetzidou, A., Soumaka, E., Kloukina, I., Tsikitis, M., Makridakis, M., Varela, A., Davos, C. H., Georgopoulos, S., Anesti, V., Vlahou, A., & Capetanaki, Y. (2016). Desmin and αB-crystallin interplay in maintenance of mitochondrial homeostasis and cardiomyocyte survival. *Journal of Cell Science*, jcs.192203. https://doi.org/10.1242/jcs.192203

Djemai, M., Cupelli, M., Boutjdir, M., & Chahine, M. (2023). Optical Mapping of Cardiomyocytes in Monolayer Derived from Induced Pluripotent Stem Cells. *Cells*, *12*(17), 2168. https://doi.org/10.3390/cells12172168

Eisner, D. A., Caldwell, J. L., Kistamás, K., & Trafford, A. W. (2017). Calcium and Excitation-Contraction Coupling in the Heart. *Circulation Research*, *121*(2), 181–195. https://doi.org/10.1161/CIRCRESAHA.117.310230

Eldemire, R., Mestroni, L., & Taylor, M. R. G. (2023). *Genetics of Dilated Cardiomyopathy*.

Electronic “expression” of the inward rectifier in cardiocytes derived from human-induced pluripotent stem cells. (2013). *Heart Rhythm*, *10*(12), 1903–1910. https://doi.org/10.1016/j.hrthm.2013.09.061

Elliott, J. L., Der Perng, M., Prescott, A. R., Jansen, K. A., Koenderink, G. H., & Quinlan, R. A. (2013). The specificity of the interaction between αB-crystallin and desmin filaments and its impact on filament aggregation and cell viability. *Philosophical Transactions of the Royal Society B: Biological Sciences*, *368*(1617), 20120375. https://doi.org/10.1098/rstb.2012.0375

Elliott, P., Andersson, B., Arbustini, E., Bilinska, Z., Cecchi, F., Charron, P., Dubourg, O., Kühl, U., Maisch, B., McKenna, W. J., Monserrat, L., Pankuweit, S., Rapezzi, C., Seferovic, P., Tavazzi, L., & Keren, A. (2008). Classification of the cardiomyopathies: A position statement from the european society of cardiology working group on myocardial and pericardial diseases. *European Heart Journal*, *29*(2), 270–276. https://doi.org/10.1093/eurheartj/ehm342

Elsnicova, B., Hornikova, D., Tibenska, V., Kolar, D., Tlapakova, T., Schmid, B., Mallek, M., Eggers, B., Schlötzer-Schrehardt, U., Peeva, V., Berwanger, C., Eberhard, B., Durmuş, H., Schultheis, D., Holtzhausen, C., Schork, K., Marcus, K., Jordan, J., Lücke, T., … Zurmanova, J. M. (2022). Desmin Knock-Out Cardiomyopathy: A Heart on the Verge of Metabolic Crisis. *International Journal of Molecular Sciences*, *23*(19), 12020. https://doi.org/10.3390/ijms231912020

Eriksson, J. E., Dechat, T., Grin, B., Helfand, B., Mendez, M., Pallari, H.-M., & Goldman, R. D. (2009). Introducing intermediate filaments: From discovery to disease. *The Journal of Clinical Investigation*, *119*(7), 1763–1771. https://doi.org/10.1172/JCI38339

Eschenhagen, T., Eder, A., Vollert, I., & Hansen, A. (2012). Physiological aspects of cardiac tissue engineering. *American Journal of Physiology-Heart and Circulatory Physiology*, *303*(2), H133–H143. https://doi.org/10.1152/ajpheart.00007.2012

Estigoy, C. B., Pontén, F., Odeberg, J., Herbert, B., Guilhaus, M., Charleston, M., Ho, J. W. K., Cameron, D., & dos Remedios, C. G. (2009). Intercalated discs: Multiple proteins perform multiple functions in non-failing and failing human hearts. *Biophysical Reviews*, *1*(1), 43. https://doi.org/10.1007/s12551-008-0007-y

Femia, G., Semsarian, C., Ross, S. B., Celermajer, D., & Puranik, R. (2020). Left Ventricular Non-Compaction: Review of the Current Diagnostic Challenges and Consequences in Athletes. *Medicina*, *56*(12), 697. https://doi.org/10.3390/medicina56120697

Foglia, M. J., & Poss, K. D. (2016). Building and re-building the heart by cardiomyocyte proliferation. *Development (Cambridge, England)*, *143*(5), 729–740. https://doi.org/10.1242/dev.132910

Fountoulakis, M., Soumaka, E., Rapti, K., Mavroidis, M., Tsangaris, G., Maris, A., Weisleder, N., & Capetanaki, Y. (2005). Alterations in the heart mitochondrial proteome in a desmin null heart failure model. *Journal of Molecular and Cellular Cardiology*, *38*(3), 461–474. https://doi.org/10.1016/j.yjmcc.2004.12.008

Frangogiannis, N. G. (2021). Cardiac fibrosis. *Cardiovascular Research*, *117*(6), 1450–1488. https://doi.org/10.1093/cvr/cvaa324

Frank, D., & Frey, N. (2011). Cardiac Z-disc Signaling Network. *The Journal of Biological Chemistry*, *286*(12), 9897–9904. https://doi.org/10.1074/jbc.R110.174268

Galou, M., Gao, J., Humbert, J., Mericskay, M., Li, Z., Paulin, D., & Vicart, P. (1997). The importance of intermediate filaments in the adaptation of tissues to mechanical stress: Evidence from gene knockout studies. *Biology of the Cell*, *89*(2), 85–97. https://doi.org/10.1111/j.1768-322X.1997.tb00997.x

Gard, J., Yamada, K., Green, K., Eloff, B., Rosenbaum, D., Wang, X., Robbins, J., Schuessler, R., Yamada, K., & Saffitz, J. (2005). Remodeling of gap junctions and slow conduction in a mouse model of desmin-related cardiomyopathy. *Cardiovascular Research*, *67*(3), 539–547. https://doi.org/10.1016/j.cardiores.2005.04.004

Girardeau, A., Atticus, D., Canac, R., Cimarosti, B., Caillaud, A., Chariau, C., Simonet, F., Cariou, B., Charpentier, F., Gourraud, J.-B., Probst, V., Belbachir, N., Jesel, L., Lemarchand, P., Barc, J., Redon, R., Gaborit, N., & Lamirault, G. (2022). Generation of human induced

pluripotent stem cell lines from four unrelated healthy control donors carrying European genetic background. *Stem Cell Research*, *59*, 102647. https://doi.org/10.1016/j.scr.2021.102647

Godsel, L. M., Hobbs, R. P., & Green, K. J. (2008). Intermediate filament assembly: Dynamics to disease. *Trends in Cell Biology*, *18*(1), 28–37. https://doi.org/10.1016/j.tcb.2007.11.004

Goldfarb, L. G., & Dalakas, M. C. (2009). Tragedy in a heartbeat: Malfunctioning desmin causes skeletal and cardiac muscle disease. *Journal of Clinical Investigation*, *119*(7), 1806–1813. https://doi.org/10.1172/JCI38027

Gomes, R. N., Manuel, F., & Nascimento, D. S. (2021). The bright side of fibroblasts: Molecular signature and regenerative cues in major organs. *Npj Regenerative Medicine*, *6*(1), Article 1. https://doi.org/10.1038/s41536-021-00153-z

Goudeau, B., Dagvadorj, A., Rodrigues-Lima, F., Nédellec, P., Casteras-Simon, M., Perret, E., Langlois, S., Goldfarb, L., & Vicart, P. (2001). Structural and functional analysis of a new desmin variant causing desmin-related myopathy. *Human Mutation*, *18*(5), 388–396. https://doi.org/10.1002/humu.1210

Goudeau, B., Rodrigues-Lima, F., Fischer, D., Casteras-Simon, M., Sambuughin, N., de Visser, M., Laforet, P., Ferrer, X., Chapon, F., Sjöberg, G., Kostareva, A., Sejersen, T., Dalakas, M. C., Goldfarb, L. G., & Vicart, P. (2006). Variable pathogenic potentials of mutations located in the desmin alpha-helical domain. *Human Mutation*, *27*(9), 906–913. https://doi.org/10.1002/humu.20351

Grant, A. O. (2009). Cardiac Ion Channels. *Circulation: Arrhythmia and Electrophysiology*, *2*(2), 185–194. https://doi.org/10.1161/CIRCEP.108.789081

Grimes, K. M., Prasad, V., & McNamara, J. W. (2019). Supporting the heart: Functions of the cardiomyocyte's non-sarcomeric cytoskeleton. *Journal of Molecular and Cellular Cardiology*, *131*, 187–196. https://doi.org/10.1016/j.yjmcc.2019.04.002

Guo, Y., & Pu, W. T. (2020). Cardiomyocyte Maturation. *Circulation Research*, *126*(8), 1086–1106. https://doi.org/10.1161/CIRCRESAHA.119.315862

Hall, C., Gehmlich, K., Denning, C., & Pavlovic, D. (2021). Complex Relationship Between Cardiac Fibroblasts and Cardiomyocytes in Health and Disease. *Journal of the American Heart Association*, *10*(5), e019338. https://doi.org/10.1161/JAHA.120.019338

Han, B., Trew, M. L., & Zgierski-Johnston, C. M. (2021). Cardiac Conduction Velocity, Remodeling and Arrhythmogenesis. *Cells*, *10*(11), 2923. https://doi.org/10.3390/cells10112923

He, S., Kou, K., O'Shea, C., Chen, T., Mu-u-min, R., Dong, R., Ren, H., Zhou, X., Fan, Z., Tan, X., Pavlovic, D., Ou, X., & Lei, M. (2021). A dataset of dual calcium and voltage optical mapping in healthy and hypertrophied murine hearts. *Scientific Data*, *8*, 314. https://doi.org/10.1038/s41597-021-01085-5

Heffler, J., Shah, P. P., Robison, P., Phyo, S., Veliz, K., Uchida, K., Bogush, A., Rhoades, J., Jain, R., & Prosser, B. L. (2020). A Balance Between Intermediate Filaments and Microtubules Maintains Nuclear Architecture in the Cardiomyocyte. *Circulation Research*, *126*(3), e10–e26. https://doi.org/10.1161/CIRCRESAHA.119.315582

Herrmann, H., & Aebi, U. (2004). Intermediate Filaments: Molecular Structure, Assembly Mechanism, and Integration Into Functionally Distinct Intracellular Scaffolds. *Annual Review of Biochemistry*, *73*(1), 749–789. https://doi.org/10.1146/annurev.biochem.73.011303.073823

Herrmann, H., Cabet, E., Chevalier, N. R., Moosmann, J., Schultheis, D., Haas, J., Schowalter, M., Berwanger, C., Weyerer, V., Agaimy, A., Meder, B., Müller, O. J., Katus, H. A., Schlötzer-Schrehardt, U., Vicart, P., Ferreiro, A., Dittrich, S., Clemen, C. S., Lilienbaum, A., & Schröder, R. (2020). Dual Functional States of R406W-Desmin Assembly Complexes Cause Cardiomyopathy With Severe Intercalated Disc Derangement in Humans and in Knock-In Mice. *Circulation*, *142*(22), 2155–2171. https://doi.org/10.1161/CIRCULATIONAHA.120.050218

Herrmann, H., Häner, M., Brettel, M., Müller, S. A., Goldie, K. N., Fedtke, B., Lustig, A., Franke, W. W., & Aebi, U. (1996). Structure and Assembly Properties of the Intermediate Filament Protein Vimentin: The Role of its Head, Rod and Tail Domains. *Journal of Molecular Biology*, *264*(5), 933–953. https://doi.org/10.1006/jmbi.1996.0688

Herrmann, H., Strelkov, S. V., Feja, B., Rogers, K. R., Brettel, M., Lustig, A., Häner, M., Parry, D. A. D., Steinert, P. M., Burkhard, P., & Aebi, U. (2000). The intermediate filament protein consensus motif of helix 2B: Its atomic structure and contribution to assembly11Edited by W. Baumeister. *Journal of Molecular Biology*, *298*(5), 817–832. https://doi.org/10.1006/jmbi.2000.3719

Hershberger, R. E., & Jordan, E. (2022). Dilated Cardiomyopathy Overview. In M. P. Adam, D. B. Everman, G. M. Mirzaa, R. A. Pagon, S. E. Wallace, L. J. Bean, K. W. Gripp, & A. Amemiya (Eds.), *GeneReviews®*. University of Washington, Seattle. http://www.ncbi.nlm.nih.gov/books/NBK1309/

Hnia, K., Ramspacher, C., Vermot, J., & Laporte, J. (2015). Desmin in muscle and associated diseases: Beyond the structural function. *Cell and Tissue Research*, *360*(3), 591–608. https://doi.org/10.1007/s00441-014-2016-4

Hofner, M., Höllrigl, A., Puz, S., Stary, M., & Weitzer, G. (2007). Desmin stimulates differentiation of cardiomyocytes and up-regulation of brachyury and nkx2.5. *Differentiation; Research in Biological Diversity*, *75*(7), 605–615. https://doi.org/10.1111/j.1432-0436.2007.00162.x

Hol, E. M., & Capetanaki, Y. (2017). Type III Intermediate Filaments Desmin, Glial Fibrillary Acidic Protein (GFAP), Vimentin, and Peripherin. *Cold Spring Harbor Perspectives in Biology*, *9*(12), a021642. https://doi.org/10.1101/cshperspect.a021642

Höllrigl, A., Hofner, M., Stary, M., & Weitzer, G. (2007). Differentiation of cardiomyocytes requires functional serine residues within the amino-terminal domain of desmin. *Differentiation; Research in Biological Diversity*, *75*(7), 616–626. https://doi.org/10.1111/j.1432-0436.2007.00163.x

Höllrigl, A., Puz, S., Al-Dubai, H., Kim, J. U., Capetanaki, Y., & Weitzer, G. (2002). Amino-terminally truncated desmin rescues fusion of des −/− myoblasts but negatively affects cardiomyogenesis and smooth muscle development. *FEBS Letters*, *523*(1–3), 229–233. https://doi.org/10.1016/S0014-5793(02)02995-2

Homberg, M., & Magin, T. M. (2014). Chapter Six - Beyond Expectations: Novel Insights into Epidermal Keratin Function and Regulation. In K. W. Jeon (Ed.), *International Review of Cell and Molecular Biology* (Vol. 311, pp. 265–306). Academic Press. https://doi.org/10.1016/B978-0-12-800179-0.00007-6

Hovhannisyan, Y., Li, Z., Callon, D., Suspène, R., Batoumeni, V., Canette, A., Blanc, J., Hocini, H., Lefebvre, C., El-Jahrani, N., Kitsara, M., L'honoré, A., Kordeli, E., Fornes, P., Concordet, J.-P., Tachdjian, G., Rodriguez, A.-M., Vartanian, J.-P., Béhin, A., … Agbulut, O. (2024). Critical contribution of mitochondria in the development of cardiomyopathy linked to desmin mutation. *Stem Cell Research & Therapy*, *15*(1), 10. https://doi.org/10.1186/s13287-023-03619-7

Ismaili, D., Schulz, C., Horváth, A., Koivumäki, J. T., Mika, D., Hansen, A., Eschenhagen, T., & Christ, T. (2023). Human induced pluripotent stem cell-derived cardiomyocytes as an electrophysiological model: Opportunities and challenges—The Hamburg perspective. *Frontiers in Physiology*, *14*, 1132165. https://doi.org/10.3389/fphys.2023.1132165

Ito, M., Nomura, S., Morita, H., & Komuro, I. (2020). Trends and Limitations in the Assessment of the Contractile Properties of Human Induced Pluripotent Stem Cell-Derived Cardiomyocytes From Patients With Dilated Cardiomyopathy. *Frontiers in Cardiovascular Medicine*, *7*, 154. https://doi.org/10.3389/fcvm.2020.00154

Izant, J. G., & Lazarides, E. (1977). Invariance and heterogeneity in the major structural and regulatory proteins of chick muscle cells revealed by two-dimensional gel electrophoresis. *Proceedings of the National Academy of Sciences of the United States of America*, *74*(4), 1450–1454. https://doi.org/10.1073/pnas.74.4.1450

Jacob, J. T., Coulombe, P. A., Kwan, R., & Omary, M. B. (2018). Types I and II Keratin Intermediate Filaments. *Cold Spring Harbor Perspectives in Biology*, *10*(4), a018275. https://doi.org/10.1101/cshperspect.a018275

Jansen, J. A., Noorman, M., Musa, H., Stein, M., de Jong, S., van der Nagel, R., Hund, T. J., Mohler, P. J., Vos, M. A., van Veen, T. A., de Bakker, J. M., Delmar, M., & van Rijen, H. V. (2012). Reduced Heterogeneous Expression Of Cx43 Results In Decreased Nav1.5 Expression And Reduced Sodium Current Which Accounts For Arrhythmia Vulnerability In Conditional Cx43 Knockout Mice. *Heart Rhythm*, *9*(4), 600–607. https://doi.org/10.1016/j.hrthm.2011.11.025

Jovanovic, M., Rooney, M. S., Mertins, P., Przybylski, D., Chevrier, N., Satija, R., Rodriguez, E. H., Fields, A. P., Schwartz, S., Raychowdhury, R., Mumbach, M. R., Eisenhaure, T., Rabani, M., Gennert, D., Lu, D., Delorey, T., Weissman, J. S., Carr, S. A., Hacohen, N., & Regev, A. (2015). Dynamic profiling of the protein life cycle in response to pathogens. *Science*, *347*(6226), 1259038. https://doi.org/10.1126/science.1259038

Kaminska, A., Strelkov, S. V., Goudeau, B., Olivé, M., Dagvadorj, A., Fidzianska, A., Simon-Casteras, M., Shatunov, A., Dalakas, M. C., Ferrer, I., Kwiecinski, H., Vicart, P., & Goldfarb, L. G. (2004). Small deletions disturb desmin architecture leading to breakdown of muscle cells and development of skeletal or cardioskeletal myopathy. *Human Genetics*, *114*(3), 306–313. https://doi.org/10.1007/s00439-003-1057-7

Karbassi, E., Fenix, A., Marchiano, S., Muraoka, N., Nakamura, K., Yang, X., & Murry, C. E. (2020). Cardiomyocyte maturation: Advances in knowledge and implications for regenerative medicine. *Nature Reviews Cardiology*, *17*(6), Article 6. https://doi.org/10.1038/s41569-019-0331-x

Kennedy, A., Finlay, D. D., Guldenring, D., Bond, R., Moran, K., & McLaughlin, J. (2016). The Cardiac Conduction System: Generation and Conduction of the Cardiac Impulse. *Critical Care Nursing Clinics*, *28*(3), 269–279. https://doi.org/10.1016/j.cnc.2016.04.001

Klabunde, R. E. (2017). Cardiac electrophysiology: Normal and ischemic ionic currents and the ECG. *Advances in Physiology Education*, *41*(1), 29–37. https://doi.org/10.1152/advan.00105.2016

Kléber, A. G., & Jin, Q. (2021). Coupling between cardiac cells-An important determinant of electrical impulse propagation and arrhythmogenesis. *Biophysics Reviews*, *2*(3), 031301. https://doi.org/10.1063/5.0050192

Kléber, A. G., & Rudy, Y. (2004). Basic Mechanisms of Cardiac Impulse Propagation and Associated Arrhythmias. *Physiological Reviews*, *84*(2), 431–488. https://doi.org/10.1152/physrev.00025.2003

Konieczny, P., Fuchs, P., Reipert, S., Kunz, W. S., Zeöld, A., Fischer, I., Paulin, D., Schröder, R., & Wiche, G. (2008). Myofiber integrity depends on desmin network targeting to Z-disks and costameres via distinct plectin isoforms. *Journal of Cell Biology*, *181*(4), 667–681. https://doi.org/10.1083/jcb.200711058

Kostetskii, I., Li, J., Xiong, Y., Zhou, R., Ferrari, V. A., Patel, V. V., Molkentin, J. D., & Radice, G. L. (2005). Induced Deletion of the N-Cadherin Gene in the Heart Leads to Dissolution of the Intercalated Disc Structure. *Circulation Research*, *96*(3), 346–354. https://doi.org/10.1161/01.RES.0000156274.72390.2c

Kouloumenta, A., Mavroidis, M., & Capetanaki, Y. (2007). Proper Perinuclear Localization of the TRIM-like Protein Myospryn Requires Its Binding Partner Desmin. *Journal of Biological Chemistry*, *282*(48), 35211–35221. https://doi.org/10.1074/jbc.M704733200

Kubánek, M., Schimerová, T., Piherová, L., Brodehl, A., Krebsová, A., Ratnavadivel, S., Stanasiuk, C., Hansíková, H., Zeman, J., Paleček, T., Houštěk, J., Drahota, Z., Nůsková, H., Mikešová, J., Zámečník, J., Macek, M., Ridzoň, P., Malusková, J., Stránecký, V., … Kmoch, S. (2020). Desminopathy: Novel Desmin Variants, a New Cardiac Phenotype, and Further Evidence for Secondary Mitochondrial Dysfunction. *Journal of Clinical Medicine*, *9*(4), 937. https://doi.org/10.3390/jcm9040937

Kucera, J. P., Rohr, S., & Rudy, Y. (2002). Localization of sodium channels in intercalated disks modulates cardiac conduction. *Circulation Research*, *91*(12), 1176–1182. https://doi.org/10.1161/01.res.0000046237.54156.0a

Lam, C. K., Tian, L., Belbachir, N., Wnorowski, A., Shrestha, R., Ma, N., Kitani, T., Rhee, J. W., & Wu, J. C. (2019). Identifying the Transcriptome Signatures of Calcium Channel Blockers in Human Induced Pluripotent Stem Cell-Derived Cardiomyocytes. *Circulation Research*, *125*(2), 212–222. https://doi.org/10.1161/CIRCRESAHA.118.314202

Lazarides, E., & Hubbard, B. D. (1976). Immunological characterization of the subunit of the 100 A filaments from muscle cells. *Proceedings of the National Academy of Sciences*, *73*(12), 4344–4348. https://doi.org/10.1073/pnas.73.12.4344

Lemoine, M. D., Mannhardt, I., Breckwoldt, K., Prondzynski, M., Flenner, F., Ulmer, B., Hirt, M. N., Neuber, C., Horváth, A., Kloth, B., Reichenspurner, H., Willems, S., Hansen, A., Eschenhagen, T., & Christ, T. (2017). Human iPSC-derived cardiomyocytes cultured in 3D engineered heart tissue show physiological upstroke velocity and sodium current density. *Scientific Reports*, *7*, 5464. https://doi.org/10.1038/s41598-017-05600-w

Lerman, B. B., Markowitz, S. M., Cheung, J. W., Thomas, G., & Ip, J. E. (2024). Ventricular Tachycardia Due to Triggered Activity: Role of Early and Delayed Afterdepolarizations. *JACC: Clinical Electrophysiology*, *10*(2), 379–401. https://doi.org/10.1016/j.jacep.2023.10.033

Li, Z., Lilienbaum, A., Butler-Browne, G., & Paulin, D. (1989). Human desmin-coding gene: Complete nucleotide sequence, characterization and regulation of expression during myogenesis and development. *Gene*, *78*(2), 243–254. https://doi.org/10.1016/0378-1119(89)90227-8

Liew, A. C., Vassiliou, V. S., Cooper, R., & Raphael, C. E. (2017). Hypertrophic Cardiomyopathy—Past, Present and Future. *Journal of Clinical Medicine*, *6*(12), Article 12. https://doi.org/10.3390/jcm6120118

Lin, J., & Keener, J. P. (2010). Modeling electrical activity of myocardial cells incorporating the effects of ephaptic coupling. *Proceedings of the National Academy of Sciences of the United States of America*, *107*(49), 20935–20940. https://doi.org/10.1073/pnas.1010154107

Lin, J., & Keener, J. P. (2013). Ephaptic coupling in cardiac myocytes. *IEEE Transactions on Bio-Medical Engineering*, *60*(2), 576–582. https://doi.org/10.1109/TBME.2012.2226720

Litviňuková, M., Talavera-López, C., Maatz, H., Reichart, D., Worth, C. L., Lindberg, E. L., Kanda, M., Polanski, K., Heinig, M., Lee, M., Nadelmann, E. R., Roberts, K., Tuck, L., Fasouli, E. S., DeLaughter, D. M., McDonough, B., Wakimoto, H., Gorham, J. M., Samari, S., … Teichmann, S. A. (2020). Cells of the adult human heart. *Nature*, *588*(7838), Article 7838. https://doi.org/10.1038/s41586-020-2797-4

Liu, H.-X., Jing, Y.-X., Wang, J.-J., Yang, Y.-P., Wang, Y.-X., Li, H.-R., Song, L., Li, A.-H., Cui, H.-L., & Jing, Y. (2020). Expression patterns of intermediate filament proteins desmin and lamin A in the developing conduction system of early human embryonic hearts. *Journal of Anatomy*, *236*(3), 540–548. https://doi.org/10.1111/joa.13108

Liu, J., Laksman, Z., & Backx, P. H. (2016). The electrophysiological development of cardiomyocytes. *Advanced Drug Delivery Reviews*, *96*, 253–273. https://doi.org/10.1016/j.addr.2015.12.023

Liu, J., Miller, K., Ma, X., Dewan, S., Lawrence, N., Whang, G., Chung, P., McCulloch, A. D., & Chen, S. (2020). Direct 3D bioprinting of cardiac micro-tissues mimicking native myocardium. *Biomaterials*, *256*, 120204. https://doi.org/10.1016/j.biomaterials.2020.120204

Liu, Y., Beyer, A., & Aebersold, R. (2016). On the Dependency of Cellular Protein Levels on mRNA Abundance. *Cell*, *165*(3), 535–550. https://doi.org/10.1016/j.cell.2016.03.014

Lowe, R., Shirley, N., Bleackley, M., Dolan, S., & Shafee, T. (2017). Transcriptomics technologies. *PLoS Computational Biology*, *13*(5), e1005457. https://doi.org/10.1371/journal.pcbi.1005457

Luethje, L. G. C., Boennemann, C., Goldfarb, L., Goebel, H. H., & Halle, M. (2004). Prophylactic Implantable Cardioverter Defibrillator Placement in a Sporadic Desmin Related Myopathy and Cardiomyopathy. *Pacing and Clinical Electrophysiology*, *27*(4), 559–560. https://doi.org/10.1111/j.1540-8159.2004.00484.x

MacTaggart, B., & Kashina, A. (2021). Posttranslational modifications of the cytoskeleton. *Cytoskeleton (Hoboken, N.J.)*, *78*(4), 142–173. https://doi.org/10.1002/cm.21679

Maloyan, A., Sanbe, A., Osinska, H., Westfall, M., Robinson, D., Imahashi, K., Murphy, E., & Robbins, J. (2005). Mitochondrial Dysfunction and Apoptosis Underlie the Pathogenic Process in Alpha-B-Crystallin Desmin Related Cardiomyopathy. *Circulation*, *112*(22), 3451–3461. https://doi.org/10.1161/CIRCULATIONAHA.105.572552

Mangoni, M. E., & Nargeot, J. (2008). Genesis and Regulation of the Heart Automaticity. *Physiological Reviews*, *88*(3), 919–982. https://doi.org/10.1152/physrev.00018.2007

Mannhardt, I., Breckwoldt, K., Letuffe-Brenière, D., Schaaf, S., Schulz, H., Neuber, C., Benzin, A., Werner, T., Eder, A., Schulze, T., Klampe, B., Christ, T., Hirt, M. N., Huebner, N., Moretti, A., Eschenhagen, T., & Hansen, A. (2016). Human Engineered Heart Tissue: Analysis of Contractile Force. *Stem Cell Reports*, *7*(1), 29–42. https://doi.org/10.1016/j.stemcr.2016.04.011

Mannhardt, I., Saleem, U., Benzin, A., Schulze, T., Klampe, B., Eschenhagen, T., & Hansen, A. (2017). Automated Contraction Analysis of Human Engineered Heart Tissue for Cardiac Drug Safety Screening. *Journal of Visualized Experiments*, *122*, 55461. https://doi.org/10.3791/55461

Marakhonov, A. V., Brodehl, A., Myasnikov, R. P., Sparber, P. A., Kiseleva, A. V., Kulikova, O. V., Meshkov, A. N., Zharikova, A. A., Koretsky, S. N., Kharlap, M. S., Stanasiuk, C., Mershina, E. A., Sinitsyn, V. E., Shevchenko, A. O., Mozheyko, N. P., Drapkina, O. M., Boytsov, S. A., Milting, H., & Skoblov, M. Yu. (2019). Noncompaction cardiomyopathy is caused by a novel in-frame desmin (DES) deletion mutation within the 1A coiled-coil rod segment leading to a severe filament assembly defect. *Human Mutation*, *40*(6), 734–741. https://doi.org/10.1002/humu.23747

Marks, A. R. (2013). Calcium cycling proteins and heart failure: Mechanisms and therapeutics. *The Journal of Clinical Investigation*, *123*(1), 46–52. https://doi.org/10.1172/JCI62834

Maron, B. J., Towbin, J. A., Thiene, G., Antzelevitch, C., Corrado, D., Arnett, D., Moss, A. J., Seidman, C. E., Young, J. B., American Heart Association, Council on Clinical Cardiology, Heart Failure and Transplantation Committee, Quality of Care and Outcomes Research and Functional Genomics and Translational Biology Interdisciplinary Working Groups, & Council on Epidemiology and Prevention. (2006). Contemporary definitions and classification of the cardiomyopathies: An American Heart Association Scientific Statement from the Council on Clinical Cardiology, Heart Failure and Transplantation Committee; Quality of Care and Outcomes Research and Functional Genomics and Translational Biology Interdisciplinary

Working Groups; and Council on Epidemiology and Prevention. *Circulation*, *113*(14), 1807–1816. https://doi.org/10.1161/CIRCULATIONAHA.106.174287

Martin, T. G., & Kirk, J. A. (2020). Under construction: The dynamic assembly, maintenance, and degradation of the cardiac sarcomere. *Journal of Molecular and Cellular Cardiology*, *148*, 89–102. https://doi.org/10.1016/j.yjmcc.2020.08.018

Mason, A. B., Tardiff, J. C., & Schwartz, S. D. (2022). Free-Energy Surfaces of Two Cardiac Thin Filament Conformational Changes during Muscle Contraction. *The Journal of Physical Chemistry. B*, *126*(21), 3844–3851. https://doi.org/10.1021/acs.jpcb.2c01337

McCormick, E. M., Kenyon, L., & Falk, M. J. (2015). Desmin common mutation is associated with multi-systemic disease manifestations and depletion of mitochondria and mitochondrial DNA. *Frontiers in Genetics*, *6*. https://www.frontiersin.org/articles/10.3389/fgene.2015.00199

McKoy, G., Protonotarios, N., Crosby, A., Tsatsopoulou, A., Anastasakis, A., Coonar, A., Norman, M., Baboonian, C., Jeffery, S., & McKenna, W. J. (2000). Identification of a deletion in plakoglobin in arrhythmogenic right ventricular cardiomyopathy with palmoplantar keratoderma and woolly hair (Naxos disease). *The Lancet*, *355*(9221), 2119–2124. https://doi.org/10.1016/S0140-6736(00)02379-5

McLendon, P. M., & Robbins, J. (2011). Desmin-related cardiomyopathy: An unfolding story. *American Journal of Physiology - Heart and Circulatory Physiology*, *301*(4), H1220–H1228. https://doi.org/10.1152/ajpheart.00601.2011

Meijer van Putten, R. M. E., Mengarelli, I., Guan, K., Zegers, J. G., van Ginneken, A. C. G., Verkerk, A. O., & Wilders, R. (2015). Ion channelopathies in human induced pluripotent stem cell derived cardiomyocytes: A dynamic clamp study with virtual IK1. *Frontiers in Physiology*, *6*. https://doi.org/10.3389/fphys.2015.00007

Mestroni, L., & Sbaizero, O. (2018). ARRHYTHMOGENIC CARDIOMYOPATHY: MECHANOTRANSDUCTION GOING WRONG. *Circulation*, *137*(15), 1611–1613. https://doi.org/10.1161/CIRCULATIONAHA.118.033558

Milner, D. J., Mavroidis, M., Weisleder, N., & Capetanaki, Y. (2000). Desmin Cytoskeleton Linked to Muscle Mitochondrial Distribution and Respiratory Function. *The Journal of Cell Biology*, *150*(6), 1283–1298.

Milner, D. J., Taffet, G. E., Wang, X., Pham, T., Tamura, T., Hartley, C., Gerdes, M. A., & Capetanaki, Y. (1999). The Absence of Desmin Leads to Cardiomyocyte Hypertrophy and Cardiac Dilation with Compromised Systolic Function. *Journal of Molecular and Cellular Cardiology*, *31*(11), 2063–2076. https://doi.org/10.1006/jmcc.1999.1037

Milner, D. J., Weitzer, G., Tran, D., Bradley, A., & Capetanaki, Y. (1996). Disruption of muscle architecture and myocardial degeneration in mice lacking desmin. *The Journal of Cell Biology*, *134*(5), 1255–1270. https://doi.org/10.1083/jcb.134.5.1255

Miquerol, L., & Kelly, R. G. (2013). Organogenesis of the vertebrate heart. *WIREs Developmental Biology*, *2*(1), 17–29. https://doi.org/10.1002/wdev.68

Mirza, H., Mohan, G., Khan, W., Alkhatib, A., Kaur, I., Asif, M., Shah, A., & Mughal, M. S. (2022). A Review of Left Ventricular Non-compaction Cardiomyopathy (LVNC). *Journal of*

Community Hospital Internal Medicine Perspectives, *12*(6), 51–63. https://doi.org/10.55729/2000-9666.1120

Miura, K., Matsuura, K., Yamasaki Itoyama, Y., Sasaki, D., Takada, T., Furutani, Y., Hayama, E., Ito, M., Nomura, S., Morita, H., Toyoda, M., Umezawa, A., Onoue, K., Saito, Y., Aburatani, H., Nakanishi, T., Hagiwara, N., Komuro, I., & Shimizu, T. (2022). Functional Evaluation of Human Bioengineered Cardiac Tissue Using iPS Cells Derived from a Patient with Lamin Variant Dilated Cardiomyopathy. *International Heart Journal*, *63*(2), 338–346. https://doi.org/10.1536/ihj.21-790

Moazzen, H., Bolaji, M. D., & Leube, R. E. (2023). Desmosomes in Cell Fate Determination: From Cardiogenesis to Cardiomyopathy. *Cells*, *12*(17), 2122. https://doi.org/10.3390/cells12172122

Monteiro, L. M., Vasques-Nóvoa, F., Ferreira, L., Pinto-do-Ó, P., & Nascimento, D. S. (2017). Restoring heart function and electrical integrity: Closing the circuit. *Npj Regenerative Medicine*, *2*(1), Article 1. https://doi.org/10.1038/s41536-017-0015-2

Moorman, A. F. M., de Jong, F., Denyn, M. M. F. J., & Lamers, W. H. (1998). Development of the Cardiac Conduction System. *Circulation Research*, *82*(6), 629–644. https://doi.org/10.1161/01.RES.82.6.629

Murphy, A. C. H., & Young, P. W. (2015). The actinin family of actin cross-linking proteins – a genetic perspective. *Cell & Bioscience*, *5*(1), 49. https://doi.org/10.1186/s13578-015-0029-7

Nerbonne, J. M., & Kass, R. S. (2005). Molecular Physiology of Cardiac Repolarization. *Physiological Reviews*, *85*(4), 1205–1253. https://doi.org/10.1152/physrev.00002.2005

Nicholl, I. D., & Quinlan, R. A. (1994). Chaperone activity of alpha-crystallins modulates intermediate filament assembly. *The EMBO Journal*, *13*(4), 945–953.

Nicin, L., Wagner, J. U. G., Luxán, G., & Dimmeler, S. (2022). Fibroblast-mediated intercellular crosstalk in the healthy and diseased heart. *FEBS Letters*, *596*(5), 638–654. https://doi.org/10.1002/1873-3468.14234

Nielsen, M. S., van Opbergen, C. J. M., van Veen, T. A. B., & Delmar, M. (2023). The intercalated disc: A unique organelle for electromechanical synchrony in cardiomyocytes. *Physiological Reviews*. https://doi.org/10.1152/physrev.00021.2022

Nikolova, V., Leimena, C., McMahon, A. C., Tan, J. C., Chandar, S., Jogia, D., Kesteven, S. H., Michalicek, J., Otway, R., Verheyen, F., Rainer, S., Stewart, C. L., Martin, D., Feneley, M. P., & Fatkin, D. (2004). Defects in nuclear structure and function promote dilated cardiomyopathy in lamin A/C-deficient mice. *The Journal of Clinical Investigation*, *113*(3), 357–369. https://doi.org/10.1172/JCI19448

Noorman, M., van der Heyden, M. A. G., van Veen, T. A. B., Cox, M. G. P. J., Hauer, R. N. W., de Bakker, J. M. T., & van Rijen, H. V. M. (2009). Cardiac cell–cell junctions in health and disease: Electrical versus mechanical coupling. *Journal of Molecular and Cellular Cardiology*, *47*(1), 23–31. https://doi.org/10.1016/j.yjmcc.2009.03.016

Oh, J. G., Kho, C., Hajjar, R. J., & Ishikawa, K. (2019). Experimental models of cardiac physiology and pathology. *Heart Failure Reviews*, *24*(4), 601–615. https://doi.org/10.1007/s10741-019-09769-2

Oka, H., Nakau, K., Imanishi, R., Furukawa, T., Tanabe, Y., Hirono, K., Hata, Y., Nishida, N., & Azuma, H. (2021). A Case Report of a Rare Heterozygous Variant in the Desmin Gene Associated With Hypertrophic Cardiomyopathy and Complete Atrioventricular Block. *CJC Open*, *3*(9), 1195–1198. https://doi.org/10.1016/j.cjco.2021.05.003

Olivé, M., Goldfarb, L., Moreno, D., Laforet, E., Dagvadorj, A., Sambuughin, N., Martínez-Matos, J. A., Martínez, F., Alió, J., Farrero, E., Vicart, P., & Ferrer, I. (2004). Desmin-related myopathy: Clinical, electrophysiological, radiological, neuropathological and genetic studies. *Journal of the Neurological Sciences*, *219*(1), 125–137. https://doi.org/10.1016/j.jns.2004.01.007

Omary, M. B. (2009). "IF-pathies": A broad spectrum of intermediate filament–associated diseases. *The Journal of Clinical Investigation*, *119*(7), 1756–1762. https://doi.org/10.1172/JCI39894

Ono, N., Yamaguchi, T., Ishikawa, H., Arakawa, M., Takahashi, N., Saikawa, T., & Shimada, T. (2009). Morphological varieties of the Purkinje fiber network in mammalian hearts, as revealed by light and electron microscopy. *Archives of Histology and Cytology*, *72*(3), 139–149. https://doi.org/10.1679/aohc.72.139

Ormrod, B., & Ehler, E. (2023). Induced pluripotent stem cell-derived cardiomyocytes—More show than substance? *Biophysical Reviews*, *15*(6), 1941–1950. https://doi.org/10.1007/s12551-023-01099-w

Panagopoulou, P., Davos, C. H., Milner, D. J., Varela, E., Cameron, J., Mann, D. L., & Capetanaki, Y. (2008). Desmin mediates TNF-α–induced aggregate formation and intercalated disk reorganization in heart failure. *Journal of Cell Biology*, *181*(5), 761–775. https://doi.org/10.1083/jcb.200710049

Parikh, S. S., Blackwell, D. J., Gomez-Hurtado, N., Frisk, M., Wang, L., Kim, K., Dahl, C. P., Fiane, A., Tønnessen, T., Kryshtal, D. O., Louch, W. E., & Knollmann, B. C. (2017). Thyroid and Glucocorticoid Hormones Promote Functional T-tubule Development in Human-Induced Pluripotent Stem Cell Derived Cardiomyocytes. *Circulation Research*, *121*(12), 1323–1330. https://doi.org/10.1161/CIRCRESAHA.117.311920

Park, D. S., & Fishman, G. I. (2017). Development and Function of the Cardiac Conduction System in Health and Disease. *Journal of Cardiovascular Development and Disease*, *4*(2), Article 2. https://doi.org/10.3390/jcdd4020007

Park, K.-Y., Dalakas, M. C., Semino-Mora, C., Lee, H.-S., Litvak, S., Takeda, K., Ferrans, V. J., & Goldfarb, L. G. (2000). Sporadic cardiac and skeletal myopathy caused by a de novo desmin mutation. *Clinical Genetics*, *57*(6), 423–429. https://doi.org/10.1034/j.1399-0004.2000.570604.x

Patel, D. M., & Green, K. J. (2014). Desmosomes in the Heart: A Review of Clinical and Mechanistic Analyses. *Cell Communication & Adhesion*, *21*(3), 109–128. https://doi.org/10.3109/15419061.2014.906533

Paulin, D., & Li, Z. (2004). Desmin: A major intermediate filament protein essential for the structural integrity and function of muscle. *Experimental Cell Research*, *301*(1), 1–7. https://doi.org/10.1016/j.yexcr.2004.08.004

Pérez-Pomares, J. M., Kelly, R. G., & European Society of Cardiology (Eds.). (2018). *The ESC textbook of cardiovascular development* (First edition). Oxford University Press.

Perriard, J.-C., Hirschy, A., & Ehler, E. (2003). Dilated Cardiomyopathy: A Disease of the Intercalated Disc? *Trends in Cardiovascular Medicine*, *13*(1), 30–38. https://doi.org/10.1016/S1050-1738(02)00209-8

Pfeiffer, E. R., Tangney, J. R., Omens, J. H., & McCulloch, A. D. (2014). Biomechanics of Cardiac Electromechanical Coupling and Mechanoelectric Feedback. *Journal of Biomechanical Engineering*, *136*(2), 0210071–02100711. https://doi.org/10.1115/1.4026221

Pieperhoff, S., & Franke, W. W. (2007). The area composita of adhering junctions connecting heart muscle cells of vertebrates – IV: Coalescence and amalgamation of desmosomal and adhaerens junction components – Late processes in mammalian heart development. *European Journal of Cell Biology*, *86*(7), 377–391. https://doi.org/10.1016/j.ejcb.2007.04.001

Pierre, M., Djemai, M., Poulin, H., & Chahine, M. (2021). NaV1.5 knockout in iPSCs: A novel approach to study NaV1.5 variants in a human cardiomyocyte environment. *Scientific Reports*, *11*(1), Article 1. https://doi.org/10.1038/s41598-021-96474-6

Poorna, M. R., Jayakumar, R., Chen, J.-P., & Mony, U. (2021). Hydrogels: A potential platform for induced pluripotent stem cell culture and differentiation. *Colloids and Surfaces B: Biointerfaces*, *207*, 111991. https://doi.org/10.1016/j.colsurfb.2021.111991

Prajapati, C., Koivumäki, J., Pekkanen-Mattila, M., & Aalto-Setälä, K. (2022). Sex differences in heart: From basics to clinics. *European Journal of Medical Research*, *27*, 241. https://doi.org/10.1186/s40001-022-00880-z

Prodan, N., Ershad, F., Reyes-Alcaraz, A., Li, L., Mistretta, B., Gonzalez, L., Rao, Z., Yu, C., Gunaratne, P. H., Li, N., Schwartz, R. J., & McConnell, B. K. (2022). Direct reprogramming of cardiomyocytes into cardiac Purkinje-like cells. *iScience*, *25*(11), 105402. https://doi.org/10.1016/j.isci.2022.105402

Pruna, M., & Ehler, E. (2020). The intercalated disc: A mechanosensing signalling node in cardiomyopathy. *Biophysical Reviews*, *12*(4), 931–946. https://doi.org/10.1007/s12551-020-00737-x

Purevjav, E. (2019). Animal Models of Cardiomyopathies. In *Animal Models in Medicine and Biology*. IntechOpen. https://doi.org/10.5772/intechopen.89033

Querdel, E., Reinsch, M., Castro, L., Köse, D., Bähr, A., Reich, S., Geertz, B., Ulmer, B., Schulze, M., Lemoine, M. D., Krause, T., Lemme, M., Sani, J., Shibamiya, A., Stüdemann, T., Köhne, M., Bibra, C. von, Hornaschewitz, N., Pecha, S., … Weinberger, F. (2021). Human Engineered Heart Tissue Patches Remuscularize the Injured Heart in a Dose-Dependent Manner. *Circulation*, *143*(20), 1991–2006. https://doi.org/10.1161/CIRCULATIONAHA.120.047904

Radisic, M., Park, H., Shing, H., Consi, T., Schoen, F. J., Langer, R., Freed, L. E., & Vunjak-Novakovic, G. (2004). Functional assembly of engineered myocardium by electrical stimulation of cardiac myocytes cultured on scaffolds. *Proceedings of the National Academy of Sciences*, *101*(52), 18129–18134. https://doi.org/10.1073/pnas.0407817101

Rainer, P. P., Dong, P., Sorge, M., Fert-Bober, J., Holewinski, R. J., Wang, Y., Foss, C. A., An, S. S., Baracca, A., Solaini, G., Glabe, C. G., Pomper, M. G., Van Eyk, J. E., Tomaselli, G. F., Paolocci, N., & Agnetti, G. (2018). Desmin Phosphorylation Triggers Preamyloid Oligomers Formation and Myocyte Dysfunction in Acquired Heart Failure. *Circulation Research*, *122*(10), e75–e83. https://doi.org/10.1161/CIRCRESAHA.117.312082

Rajasekaran, N. S., Connell, P., Christians, E. S., Yan, L.-J., Taylor, R. P., Orosz, A., Zhang, X. Q., Stevenson, T. J., Peshock, R. M., Leopold, J. A., Barry, W. H., Loscalzo, J., Odelberg, S. J., & Benjamin, I. J. (2007). Dysregulation of Glutathione Homeostasis Causes Oxido-reductive Stress and Cardiomyopathy in R120GCryAB Mice. *Cell*, *130*(3), 427–439. https://doi.org/10.1016/j.cell.2007.06.044

Ramspacher, C., Steed, E., Boselli, F., Ferreira, R., Faggianelli, N., Roth, S., Spiegelhalter, C., Messaddeq, N., Trinh, L., Liebling, M., Chacko, N., Tessadori, F., Bakkers, J., Laporte, J., Hnia, K., & Vermot, J. (2015). Developmental Alterations in Heart Biomechanics and Skeletal Muscle Function in Desmin Mutants Suggest an Early Pathological Root for Desminopathies. *Cell Reports*, *11*(10), 1564–1576. https://doi.org/10.1016/j.celrep.2015.05.010

Reel, P. S., Reel, S., Pearson, E., Trucco, E., & Jefferson, E. (2021). Using machine learning approaches for multi-omics data analysis: A review. *Biotechnology Advances*, *49*, 107739. https://doi.org/10.1016/j.biotechadv.2021.107739

Roberts, W., Salandy, S., Mandal, G., Holda, M. K., Tomaszewksi, K. A., Gielecki, J., Tubbs, R. S., & Loukas, M. (2019). Across the centuries: Piecing together the anatomy of the heart. *Translational Research in Anatomy*, *17*, 100051. https://doi.org/10.1016/j.tria.2019.100051

Rodríguez-Sinovas, A., Sánchez, J. A., Valls-Lacalle, L., Consegal, M., & Ferreira-González, I. (2021). Connexins in the Heart: Regulation, Function and Involvement in Cardiac Disease. *International Journal of Molecular Sciences*, *22*(9), 4413. https://doi.org/10.3390/ijms22094413

Ronaldson-Bouchard, K., Ma, S. P., Yeager, K., Chen, T., Song, L., Sirabella, D., Morikawa, K., Teles, D., Yazawa, M., & Vunjak-Novakovic, G. (2018). Advanced maturation of human cardiac tissue grown from pluripotent stem cells. *Nature*, *556*(7700), Article 7700. https://doi.org/10.1038/s41586-018-0016-3

Ronaldson-Bouchard, K., Yeager, K., Teles, D., Chen, T., Ma, S., Song, L., Morikawa, K., Wobma, H. M., Vasciaveo, A., Ruiz, E. C., Yazawa, M., & Vunjak-Novakovic, G. (2019). Engineering of human cardiac muscle electromechanically matured to an adult-like phenotype. *Nature Protocols*, *14*(10), 2781–2817. https://doi.org/10.1038/s41596-019-0189-8

Schmitt, N., Grunnet, M., & Olesen, S.-P. (2014). Cardiac Potassium Channel Subtypes: New Roles in Repolarization and Arrhythmia. *Physiological Reviews*, *94*(2), 609–653. https://doi.org/10.1152/physrev.00022.2013

Schrickel, J. W., Stöckigt, F., Krzyzak, W., Paulin, D., Li, Z., Lübkemeier, I., Fleischmann, B., Sasse, P., Linhart, M., Lewalter, T., Nickenig, G., Lickfett, L., Schröder, R., & Clemen, C. S. (2010). Cardiac conduction disturbances and differential effects on atrial and ventricular electrophysiological properties in desmin deficient mice. *Journal of Interventional Cardiac Electrophysiology*, *28*(2), 71–80. https://doi.org/10.1007/s10840-010-9482-8

Schwarz, N., & Leube, R. E. (2016). Intermediate Filaments as Organizers of Cellular Space: How They Affect Mitochondrial Structure and Function. *Cells*, *5*(3), 30. https://doi.org/10.3390/cells5030030

Seibertz, F., & Voigt, N. (2024). High throughput methods for cardiac cellular electrophysiology studies: The road to personalized medicine. *American Journal of Physiology-Heart and Circulatory Physiology*. https://doi.org/10.1152/ajpheart.00599.2023

Severs, N. J., Bruce, A. F., Dupont, E., & Rothery, S. (2008). Remodelling of gap junctions and connexin expression in diseased myocardium. *Cardiovascular Research*, *80*(1), 9–19. https://doi.org/10.1093/cvr/cvn133

Singh, S. R., Kadioglu, H., Patel, K., Carrier, L., & Agnetti, G. (2020). Is Desmin Propensity to Aggregate Part of its Protective Function? *Cells*, *9*(2), 491. https://doi.org/10.3390/cells9020491

Sleiman, Y., Lacampagne, A., & Meli, A. C. (2021). "Ryanopathies" and RyR2 dysfunctions: Can we further decipher them using in vitro human disease models? *Cell Death & Disease*, *12*(11), 1–19. https://doi.org/10.1038/s41419-021-04337-9

Smolina, N., Bruton, J., Sjoberg, G., Kostareva, A., & Sejersen, T. (2014). Aggregate-prone desmin mutations impair mitochondrial calcium uptake in primary myotubes. *Cell Calcium*, *56*(4), 269–275. https://doi.org/10.1016/j.ceca.2014.08.001

Smolina, N., Khudiakov, A., Knyazeva, A., Zlotina, A., Sukhareva, K., Kondratov, K., Gogvadze, V., Zhivotovsky, B., Sejersen, T., & Kostareva, A. (2020). Desmin mutations result in mitochondrial dysfunction regardless of their aggregation properties. *Biochimica et Biophysica Acta (BBA) - Molecular Basis of Disease*, *1866*(6), 165745. https://doi.org/10.1016/j.bbadis.2020.165745

Snider, N. T., & Omary, M. B. (2014). Post-translational modifications of intermediate filament proteins: Mechanisms and functions. *Nature Reviews. Molecular Cell Biology*, *15*(3), 163–177. https://doi.org/10.1038/nrm3753

Strelkov, S. V., Herrmann, H., & Aebi, U. (2003). Molecular architecture of intermediate filaments. *BioEssays*, *25*(3), 243–251. https://doi.org/10.1002/bies.10246

Strelkov, S. V., Herrmann, H., Geisler, N., Wedig, T., Zimbelmann, R., Aebi, U., & Burkhard, P. (2002). Conserved segments 1A and 2B of the intermediate filament dimer: Their atomic structures and role in filament assembly. *The EMBO Journal*, *21*(6), 1255–1266. https://doi.org/10.1093/emboj/21.6.1255

Sun, X., & Nunes, S. S. (2016). Biowire platform for maturation of human pluripotent stem cell-derived cardiomyocytes. *Methods*, *101*, 21–26. https://doi.org/10.1016/j.ymeth.2015.11.005

Sutanto, H., Lyon, A., Lumens, J., Schotten, U., Dobrev, D., & Heijman, J. (2020). Cardiomyocyte calcium handling in health and disease: Insights from *in vitro* and *in silico* studies. *Progress in Biophysics and Molecular Biology*, *157*, 54–75. https://doi.org/10.1016/j.pbiomolbio.2020.02.008

Szeverenyi, I., Cassidy, A. J., Chung, C. W., Lee, B. T. K., Common, J. E. A., Ogg, S. C., Chen, H., Sim, S. Y., Goh, W. L. P., Ng, K. W., Simpson, J. A., Chee, L. L., Eng, G. H., Li, B., Lunny, D. P., Chuon, D., Venkatesh, A., Khoo, K. H., McLean, W. H. I., … Lane, E. B. (2008). The Human Intermediate Filament Database: Comprehensive information on a gene family involved in many human diseases. *Human Mutation*, *29*(3), 351–360. https://doi.org/10.1002/humu.20652

Tani, H., & Tohyama, S. (2022). Human Engineered Heart Tissue Models for Disease Modeling and Drug Discovery. *Frontiers in Cell and Developmental Biology*, *10*, 855763. https://doi.org/10.3389/fcell.2022.855763

Teshigawara, R., Cho, J., Kameda, M., & Tada, T. (2017). Mechanism of human somatic reprogramming to iPS cell. *Laboratory Investigation*, *97*(10), Article 10. https://doi.org/10.1038/labinvest.2017.56

Treat, J. A., Goodrow, R. J., Bot, C. T., Haedo, R. J., & Cordeiro, J. M. (2019). Pharmacological enhancement of repolarization reserve in human induced pluripotent stem cells derived cardiomyocytes. *Biochemical Pharmacology*, *169*, 113608. https://doi.org/10.1016/j.bcp.2019.08.010

Tsikitis, M., Galata, Z., Mavroidis, M., Psarras, S., & Capetanaki, Y. (2018). Intermediate filaments in cardiomyopathy. *Biophysical Reviews*, *10*(4), 1007–1031. https://doi.org/10.1007/s12551-018-0443-2

Tsoupri, E., & Capetanaki, Y. (2013). Myospryn: A multifunctional desmin-associated protein. *Histochemistry and Cell Biology*, *140*(1), 55–63. https://doi.org/10.1007/s00418-013-1103-z

Tsui, H., Kampen, S. J. van, Ji Han, S., Meraviglia, V., Ham, W. B. van, Casini, S., Kraak, P. van der, Vink, A., Yin, X., Mayr, M., Bossu, A., A. Marchal, G., Monshouwer-Kloots, J., Eding, J., Versteeg, D., Ruiter, H. de, Bezstarosti, K., Groeneweg, J., J. Klaasen, S., … Rooij, E. van. (2023). Desmosomal protein degradation as an underlying cause of arrhythmogenic cardiomyopathy. *Science Translational Medicine*. https://doi.org/10.1126/scitranslmed.add4248

Tucker, N. R., Chaffin, M., Fleming, S. J., Hall, A. W., Parsons, V. A., Bedi, K. C., Akkad, A.-D., Herndon, C. N., Arduini, A., Papangeli, I., Roselli, C., Aguet, F., Choi, S. H., Ardlie, K. G., Babadi, M., Margulies, K. B., Stegmann, C. M., & Ellinor, P. T. (2020). Transcriptional and Cellular Diversity of the Human Heart. *Circulation*, *142*(5), 466–482. https://doi.org/10.1161/CIRCULATIONAHA.119.045401

Uhlén, M., Fagerberg, L., Hallström, B. M., Lindskog, C., Oksvold, P., Mardinoglu, A., Sivertsson, Å., Kampf, C., Sjöstedt, E., Asplund, A., Olsson, I., Edlund, K., Lundberg, E., Navani, S., Szigyarto, C. A.-K., Odeberg, J., Djureinovic, D., Takanen, J. O., Hober, S., … Pontén, F. (2015). Proteomics. Tissue-based map of the human proteome. *Science (New York, N.Y.)*, *347*(6220), 1260419. https://doi.org/10.1126/science.1260419

Ulmer, B. M., Stoehr, A., Schulze, M. L., Patel, S., Gucek, M., Mannhardt, I., Funcke, S., Murphy, E., Eschenhagen, T., & Hansen, A. (2018). Contractile Work Contributes to Maturation of Energy Metabolism in hiPSC-Derived Cardiomyocytes. *Stem Cell Reports*, *10*(3), 834–847. https://doi.org/10.1016/j.stemcr.2018.01.039

van Eif, V. W. W., Devalla, H. D., Boink, G. J. J., & Christoffels, V. M. (2018). Transcriptional regulation of the cardiac conduction system. *Nature Reviews Cardiology*, *15*(10), Article 10. https://doi.org/10.1038/s41569-018-0031-y

Veeraraghavan, R., Poelzing, S., & Gourdie, R. G. (2014). Intercellular electrical communication in the heart: A new, active role for the intercalated disk. *Cell Communication & Adhesion*, *21*(3), 161–167. https://doi.org/10.3109/15419061.2014.905932

Verkerk, A. O., Veerman, C. C., Zegers, J. G., Mengarelli, I., Bezzina, C. R., & Wilders, R. (2017). Patch-Clamp Recording from Human Induced Pluripotent Stem Cell-Derived Cardiomyocytes: Improving Action Potential Characteristics through Dynamic Clamp. *International Journal of Molecular Sciences*, *18*(9). https://doi.org/10.3390/ijms18091873

Verkerk, A. O., & Wilders, R. (2020). *Dynamic Clamp in Electrophysiological Studies on Stem Cell–Derived Cardiomyocytes—Why and How? 77*(3), 13.

Vermij, S. H., Abriel, H., & van Veen, T. A. B. (2017). Refining the molecular organization of the cardiac intercalated disc. *Cardiovascular Research*, cvw259. https://doi.org/10.1093/cvr/cvw259

Viedma-Poyatos, Á., Pajares, M. A., & Pérez-Sala, D. (2020). Type III intermediate filaments as targets and effectors of electrophiles and oxidants. *Redox Biology*, *36*, 101582. https://doi.org/10.1016/j.redox.2020.101582

Viegas-Pequignot, E., Lin, L. Z., Dutrillaux, B., Apiou, F., & Paulin, D. (1989). Assignment of human desmin gene to band 2q35 by nonradioactive in situ hybridization. *Human Genetics*, *83*(1), 33–36. https://doi.org/10.1007/BF00274143

Wahbi, K., Béhin, A., Charron, P., Dunand, M., Richard, P., Meune, C., Vicart, P., Laforêt, P., Stojkovic, T., Bécane, H. M., Kuntzer, T., & Duboc, D. (2012). High cardiovascular morbidity and mortality in myofibrillar myopathies due to DES gene mutations: A 10-year longitudinal study. *Neuromuscular Disorders*, *22*(3), 211–218. https://doi.org/10.1016/j.nmd.2011.10.019

Wang, H.-G., Zhu, W., Kanter, R. J., Silva, J. R., Honeywell, C., Gow, R. M., & Pitt, G. S. (2016). A Novel NaV1.5 Voltage Sensor Mutation Associated with Severe Atrial and Ventricular Arrhythmias. *Journal of Molecular and Cellular Cardiology*, *92*, 52–62. https://doi.org/10.1016/j.yjmcc.2016.01.014

Wang, L., Wada, Y., Ballan, N., Schmeckpeper, J., Huang, J., Rau, C. D., Wang, Y., Gepstein, L., & Knollmann, B. C. (2021). Triiodothyronine and dexamethasone alter potassium channel expression and promote electrophysiological maturation of human-induced pluripotent stem cell-derived cardiomyocytes. *Journal of Molecular and Cellular Cardiology*, *161*, 130–138. https://doi.org/10.1016/j.yjmcc.2021.08.005

Wang, Q., Lin, J. L.-C., Wu, K.-H., Wang, D.-Z., Reiter, R. S., Sinn, H. W., Lin, C.-I., & Lin, J. J.-C. (2012). Xin proteins and intercalated disc maturation, signaling and diseases. *Frontiers in Bioscience : A Journal and Virtual Library*, *17*, 2566–2593.

Wang, Y., & Hill, J. A. (2010). Electrophysiological remodeling in heart failure. *Journal of Molecular and Cellular Cardiology*, *48*(4), 619–632. https://doi.org/10.1016/j.yjmcc.2010.01.009

Wang, Y., Jia, H., & Song, J. (2023). Accurate Classification of Non-ischemic Cardiomyopathy. *Current Cardiology Reports*. https://doi.org/10.1007/s11886-023-01944-0

Warner, E. F., Li, Y., & Li, X. (2022). Targeting Microtubules for the Treatment of Heart Disease. *Circulation Research*, *130*(11), 1723–1741. https://doi.org/10.1161/CIRCRESAHA.122.319808

Wilders, R. (2006). Dynamic clamp: A powerful tool in cardiac electrophysiology: Dynamic clamp: a powerful tool in cardiac electrophysiology. *The Journal of Physiology*, *576*(2), 349–359. https://doi.org/10.1113/jphysiol.2006.115840

Winter, D. L., Paulin, D., Mericskay, M., & Li, Z. (2014). Posttranslational modifications of desmin and their implication in biological processes and pathologies. *Histochemistry and Cell Biology*, *141*(1), 1–16. https://doi.org/10.1007/s00418-013-1148-z

Winter, L., Abrahamsberg, C., & Wiche, G. (2008). Plectin isoform 1b mediates mitochondrion–intermediate filament network linkage and controls organelle shape. *Journal of Cell Biology*, *181*(6), 903–911. https://doi.org/10.1083/jcb.200710151

Wolk, R., Cobbe, S. M., Hicks, M. N., & Kane, K. A. (1999). Functional, structural, and dynamic basis of electrical heterogeneity in healthy and diseased cardiac muscle: Implications for arrhythmogenesis and anti-arrhythmic drug therapy. *Pharmacology & Therapeutics*, *84*(2), 207–231. https://doi.org/10.1016/S0163-7258(99)00033-9

Woodcock, E. A., & Matkovich, S. J. (2005). Cardiomyocytes structure, function and associated pathologies. *The International Journal of Biochemistry & Cell Biology*, *37*(9), 1746–1751. https://doi.org/10.1016/j.biocel.2005.04.011

Woodhams, L. G., Guo, J., Schuftan, D., Boyle, J. J., Pryse, K. M., Elson, E. L., Huebsch, N., & Genin, G. M. (2023). Virtual blebbistatin: A robust and rapid software approach to motion artifact removal in optical mapping of cardiomyocytes. *Proceedings of the National Academy of Sciences*, *120*(38), e2212949120. https://doi.org/10.1073/pnas.2212949120

Wu, P., Deng, G., Sai, X., Guo, H., Huang, H., & Zhu, P. (2021). Maturation strategies and limitations of induced pluripotent stem cell-derived cardiomyocytes. *Bioscience Reports*, *41*(6), BSR20200833. https://doi.org/10.1042/BSR20200833

Ya, J., Markman, M. W. M., Wagenaar, G. T. M., Blommaart, P.-J. B., Moorman, A. F. M., & Lamers, W. H. (1997). Expression of the smooth-muscle proteins α-smooth-muscle actin and calponin, and of the intermediate filament protein desmin are parameters of cardiomyocyte maturation in the prenatal rat heart. *The Anatomical Record*, *249*(4), 495–505. https://doi.org/10.1002/(SICI)1097-0185(199712)249:4<495::AID-AR9>3.0.CO;2-Q

Yamamoto, M., Abe, S., Rodríguez-Vázquez, J. F., Fujimiya, M., Murakami, G., & Ide, Y. (2011). Immunohistochemical distribution of desmin in the human fetal heart. *Journal of Anatomy*, *219*(2), 253–258. https://doi.org/10.1111/j.1469-7580.2011.01382.x

Yang, X., Rodriguez, M., Pabon, L., Fischer, K. A., Reinecke, H., Regnier, M., Sniadecki, N. J., Ruohola-Baker, H., & Murry, C. E. (2014). Tri-iodo-L-thyronine Promotes the Maturation of Human Cardiomyocytes-Derived from Induced Pluripotent Stem Cells. *Journal of Molecular and Cellular Cardiology*, *72*, 296–304. https://doi.org/10.1016/j.yjmcc.2014.04.005

Yang, Z., Bowles, N. E., Scherer, S. E., Taylor, M. D., Kearney, D. L., Ge, S., Nadvoretskiy, V. V., DeFreitas, G., Carabello, B., Brandon, L. I., Godsel, L. M., Green, K. J., Saffitz, J. E., Li, H., Danieli, G. A., Calkins, H., Marcus, F., & Towbin, J. A. (2006). Desmosomal Dysfunction due to Mutations in Desmoplakin Causes Arrhythmogenic Right Ventricular Dysplasia/Cardiomyopathy. *Circulation Research*, *99*(6), 646–655. https://doi.org/10.1161/01.RES.0000241482.19382.c6

Yeow, D., Katz, M., Henderson, R., Prasad, S., Denman, R., Blum, S., Davis, M., Robertson, T., & McCombe, P. (2023). Phenotypic variability within the desminopathies: A case series of three patients. *Frontiers in Neurology*, *13*, 1110934. https://doi.org/10.3389/fneur.2022.1110934

Yépez, V. A., Kremer, L. S., Iuso, A., Gusic, M., Kopajtich, R., Koňaříková, E., Nadel, A., Wachutka, L., Prokisch, H., & Gagneur, J. (2018). OCR-Stats: Robust estimation and statistical testing of mitochondrial respiration activities using Seahorse XF Analyzer. *PloS One*, *13*(7), e0199938. https://doi.org/10.1371/journal.pone.0199938

Yoshida, Y., & Yamanaka, S. (2017). Induced Pluripotent Stem Cells 10 Years Later. *Circulation Research*, *120*(12), 1958–1968. https://doi.org/10.1161/CIRCRESAHA.117.311080

Yoshimura, A., Yamaguchi, T., Kawazato, H., Takahashi, N., & Shimada, T. (2014). Immuno-histochemistry and three-dimensional architecture of the intermediate filaments in Purkinje cells in mammalian hearts. *Medical Molecular Morphology*, *47*(4), 233–239. https://doi.org/10.1007/s00795-014-0069-9

Zhang, Y., Zhang, L., Huang, X., Ma, N., Wang, P., Li, L., Chen, X., & Ji, X. (2023). ECMO in adult patients with severe trauma: A systematic review and meta-analysis. *European Journal of Medical Research*, *28*, 412. https://doi.org/10.1186/s40001-023-01390-2

Zhao, M., Tang, Y., Zhou, Y., & Zhang, J. (2019). Deciphering Role of Wnt Signalling in Cardiac Mesoderm and Cardiomyocyte Differentiation from Human iPSCs: Four-dimensional control of Wnt pathway for hiPSC-CMs differentiation. *Scientific Reports*, *9*(1), Article 1. https://doi.org/10.1038/s41598-019-55620-x

Zimmermann, W.-H., Schneiderbanger, K., Schubert, P., Didié, M., Münzel, F., Heubach, J. f., Kostin, S., Neuhuber, W. l., & Eschenhagen, T. (2002). Tissue Engineering of a Differentiated Cardiac Muscle Construct. *Circulation Research*, *90*(2), 223–230. https://doi.org/10.1161/hh0202.103644

COLLEGE ED BIOLOGIE
DOCTORAL SANTE
PAYS DE LA LOIRE

Nantes Université

Titre : **Conséquences structurelles et fonctionnelles cardiaques de la mutation p.R406W de la desmine**

Mots clés: desmine, cardiomyopathie, cellules souches pluripotentes induites humaines, arythmie

La myopathie liée à la desmine, ou desminopathie, est une maladie génétique rare causée par des mutations dans le filament intermédiaire de la desmine. La desmine relie plusieurs composants de la cellule, notamment l'appareil contractile, et positionne les organites à l'intérieur des cellules, y compris le noyau et les mitochondries. La desminopathie est le plus souvent associée à une myopathie squelettique et/ou cardiaque et à la formation d'agrégats intracellulaires. Plus de 70 mutations ont été signalées le long du gène de la desmine qui code pour les 470 acides aminés des filaments de desmine. Bien que de nombreuses études se soient concentrées sur ces mutations au fil des ans, le mécanisme précis de la relation structure-fonction de la desmine dans les cardiomyocytes n'a pas encore été élucidé.

Le test génétique d'une patiente présentant des antécédents cardiaques complexes, notamment une mort subite cardiaque, une dépression persistante du segment ST sur l'ECG et des orages rythmiques, a révélé une mutation de la desmine en position p.R406W. Le défi de cette étude était d'utiliser les cellules souches pluripotentes induites de la patiente et des lignées cellulaires isogéniques pour comprendre la relation génotype-phénotype. En outre, un modèle tridimensionnel de tissu cardiaque a été réaliséLes conséquences électriques de cette mutation ont été analysées à l'aide de la technique du patch-clamp, révélant une repolarisation anormale. Simultanément, nous avons réalisé des études protéomiques et transcriptomiques pour étudier les mécanismes complexes en jeu, qui ont révélé des défauts mitochondriaux et de conduction. Par la suite, la microscopie électronique a révélé des changements structurels dans les cellules.

En conclusion, ce travail a combiné des approches fonctionnelles et moléculaires pour faciliter notre compréhension de la desminopathie.

Title: **Cardiac Structural and Functional Consequences of the Desmin p.R406W Mutation**

Keywords: desmin, cardiomyopathy, human induced pluripotent stem cells, arrhythmia

Desmin related myopathy, or desminopathy, is a rare genetic disorder caused by mutations in the intermediate filament desmin. Desmin interconnects several components of the cell including the contractile apparatus and positions organelles within cells, including the nucleus and mitochondria. Desminopathy is most often associated with skeletal and/or cardiac myopathy and is commonly associated with intracellular aggregate formation. Over 70 mutations have been reported along the desmin gene that codes for the filaments 470 amino acids. Although many studies have focused on these mutations over the years, the precise mechanism of the structure-function relationship of desmin within cardiomyocytes has yet to be elucidated.

Genetic testing of a patient presenting with a complex cardiac history, including sudden cardiac death, a persistent depression of the ST-segment on the ECG and arrhythmic storms revealed a desmin mutation at position p.R406W. The challenge of this study was to use the patient's induced pluripotent stem cells and isogenic cell lines to understand the genotype-phenotype relationship at hand. Furthermore, a 3-dimensional model of engineered heart tissue was applied.

The underlying electrical consequences of this mutation were analyzed using the patch-clamp technique, revealing abnormal repolarization. Simultaneously, we performed proteomic and transcriptomic studies to investigate the complex mechanisms at play, which revealed mitochondrial and conduction defects. Subsequently, electron microscopy revealed structural changes within cells.

In conclusion, this work combined functional and molecular approaches to facilitate our understanding of desminopathy.